EARTHQUAKE ENGINEERING TO EXTREME EVENTS

ISSN 1520-295X

Seismic Performance Evaluation of Precast Girders with Field-Cast Ultra High Performance Concrete (UHPC) Connections

by
George C. Lee, Chao Huang, Jianwei Song and
Jerome S. O'Connor


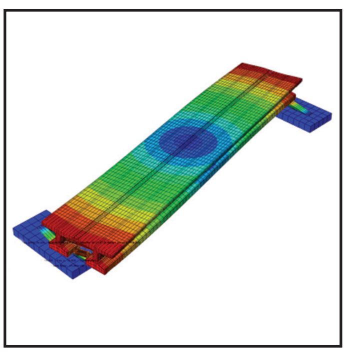

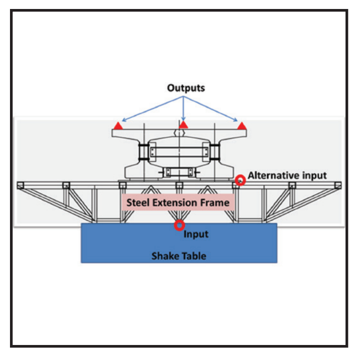

Technical Report MCEER-14-0007

July 31, 2014

This research was conducted at the University at Buffalo, State University of New York and was supported by MCEER and the Federal Highway Administration under contract number DTHF 61-07-C-00020.

Seismic Performance Evaluation of Precast Girders with Field-Cast Ultra High Performance Concrete (UHPC) Connections

by

George C. Lee,[1] Chao Huang,[2] Jianwei Song[3] and
Jerome S. O'Connor[4]

Publication Date: July 31, 2014
Submittal Date: March 30, 2014

Technical Report MCEER-14-0007

FHWA Project Contract No. DTHF 61-07-C-00020

1 Distinguished Professor, Department of Civil, Structural and Environmental Engineering, University at Buffalo, State University of New York
2 Research Scientist, Department of Civil, Structural and Environmental Engineering, University at Buffalo, State University of New York
3 Senior Research Scientist, Department of Civil, Structural and Environmental Engineering, University at Buffalo, State University of New York
4 Executive Director, Institute of Bridge Engineering, Department of Civil, Structural and Environmental Engineering, University at Buffalo, State University of New York

MCEER
University at Buffalo, State University of New York
212 Ketter Hall, Buffalo, NY 14260
E-mail: *mceer@buffalo.edu*; WWW Site: *http://mceer.buffalo.edu*

PREFACE

MCEER is a national center of excellence dedicated to the discovery and development of new knowledge, tools and technologies that equip communities to become more disaster resilient in the face of earthquakes and other extreme events. MCEER accomplishes this through a system of multidisciplinary, multi-hazard research, education and outreach initiatives.

Headquartered at the University at Buffalo, State University of New York, MCEER was originally established by the National Science Foundation (NSF) in 1986, as the first National Center for Earthquake Engineering Research (NCEER). In 1998, it became known as the Multidisciplinary Center for Earthquake Engineering Research (MCEER), from which the current name, MCEER, evolved.

Comprising a consortium of researchers and industry partners from numerous disciplines and institutions throughout the United States, MCEER's mission has expanded from its original focus on earthquake engineering to one which addresses the technical and socioeconomic impacts of a variety of hazards, both natural and man-made, on critical infrastructure, facilities, and society.

MCEER investigators derive support from the State of New York, National Science Foundation, Federal Highway Administration, National Institute of Standards and Technology, Department of Homeland Security/Federal Emergency Management Agency, other state governments, academic institutions, foreign governments and private industry.

The major objective of this study is to evaluate the seismic performance of two precast deck-bulb-tee girders with field-cast UHPC connections. A series of shake table tests were performed to analyze the seismic behavior of the girders and UHPC connections. No severe damage was found in the tests. The analyses on the maximum strain and relative displacement of the UHPC connection show that the UHPC connection remained in the elastic range and exhibited sufficient seismic performance under all tests. Based on these experimental results, it can be concluded that UHPC connections with short, straight rebar provide sufficient seismic resistance even under high-level seismic ground motions.

EXECUTIVE SUMMARY

Ultra-high performance concrete (UHPC) is an advanced cementitious composite material which provides new opportunities to significantly enhance the performance of field-cast connections. The use of UHPC in precast concrete bridge superstructure components can offer many advantages compared to conventional cast-in-place decks, especially higher quality and durability as well as ease of construction. However, the appropriate installation of connecting elements is a key challenge in completing the overall bridge system. It is recognized that the state of the practice with regard to deck-level connecting elements has been lacking in terms of resiliency and durability.

The Federal Highway Administration's ongoing research program into the use of Ultra-High Performance Concrete (UHPC) in highway bridges has recently focused on deck-level connections between modular precast components. Field-cast UHPC connections can facilitate the construction of an emulative bridge deck system whose behaviors should meet or exceed those of a conventional cast-in-place bridge deck.

However, many bridge owners may be hesitant to embrace UHPC bridge deck component technology due to a lack of knowledge of the seismic performance of field-cast UHPC connections. The seismic responses of connections under severe earthquakes need to be investigated to facilitate the wider use of these modular bridge deck systems, especially in high seismic zones. The major objective of this study is to evaluate the seismic performance of two precast deck-bulb-tee girders with field-cast UHPC connections. A series of shake table tests are performed to analyze the seismic behavior of the girders and UHPC connections.

ACKNOWLEDGEMENTS

The experiment conducted in this study is financially supported by the Federal Highway Administration (contract number DTHF 61-07-C-00020) under Dr. Philip W. Yen as the Contract Officer's Technical Representative (COTR) and Dr. Benjamin A. Graybeal as the technical advisor. The authors gratefully acknowledge the support provided. The authors would also like to acknowledge Dr. Amjad J. Aref, Dr. Salvatore Salamone, their graduate students, Mr. Mark Pitman and Ms. Myrto Anagnostopoulou from the University at Buffalo, State University of New York for support provided. The authors would also like to acknowledge Dr. Ahmed Mostafa and Mr. Mohan Rao, P.E. for their professional comments and Ms. Michelle Zuppa for her careful technical editing.

TABLE OF CONTENTS

TABLE OF CONTENTS (CONT'D)

SECTION **TITLE** **PAGE**

LIST OF FIGURES

FIGURE TITLE **PAGE**

LIST OF FIGURES (CONT'D)

FIGURE TITLE **PAGE**

LIST OF FIGURES (CONT'D)

FIGURE TITLE **PAGE**

LIST OF TABLES

SECTION 1
INTRODUCTION

1.1 UHPC Material

Precast concrete bridge components have many advantages compared to conventional cast-in-place construction. Prefabrication typically requires less time at the site due to the ease of installation. Their production in a controlled environment results in higher quality and assumed better durability. However, the appropriate installation of connecting elements is one of the most important challenges in completing the overall bridge system.

Ultra-high performance concrete (UHPC), as an advanced cementitious composite material, provides new opportunities to significantly enhance the performance of field-cast connections. The Federal Highway Administration (FHWA)'s ongoing research program into the use of Ultra-High Performance Concrete (UHPC) in highway bridges has conducted a series of experimental and analytical research on the mechanical behavior of UHPC.

Graybeal (2006; 2010; 2012) conducted a large suite of material characterization tests in order to quantify the behavior of one type of commercially available UHPC. The characteristics of the UHPC under four different curing regimes were captured. The study presented the results focused on strength-based behaviors (e.g., compressive and tensile strength), long-term stability behaviors (e.g., creep and shrinkage), and durability behaviors (e.g., chloride ion penetration and freeze-thaw). The test results showed that UHPC exhibits very high compressive strengths, great tensile strengths, and stability with durability properties significantly beyond normal concrete.

For precast bridge systems, it is recognized that the state of the practice with regard to deck-level connecting elements has been lacking in terms of resiliency and durability. Since UHPC material provides excellent mechanical behavior, FHWA has recently focused on deck-level connections between modular precast components. Graybeal (2010) investigated the structural performance of field-cast UHPC connections for modular bridge deck components using both cyclic and static loading tests. The results demonstrated that field-cast UHPC connections facilitate the construction of an emulative bridge deck system whose behaviors should meet or exceed those of a conventional cast-in-place bridge deck. Russell and Graybeal (2013) investigated over 600 references relevant to UHPC material to summarize the state of the art of research and practical applications. The results showed that over 50 bridges have been built using UHPC as the connection material in North America during the past 10 years and the trend is still growing.

However, many bridge owners may still be hesitant to embrace UHPC bridge deck component technology due to a lack of knowledge of the seismic performance of field-cast UHPC connections. The seismic responses of connections under severe earthquakes need to be investigated to facilitate the wider use of these modular bridge deck systems, especially in high seismic zones.

1.2 Shake Table Testing

Earthquakes are one of the most devastating catastrophes for human society. Lessons learned from severe earthquakes that occurred in the past two decades remind civil engineers of the importance of the seismic performance of bridge structures and direct their efforts toward the development and improvement of bridge performance.

Recently, the structural monitoring research community has endeavored to track the pre-event, during-event and post-event status of structural conditions. The collected information can be further used for the analysis, evaluation, maintenance, and retrofit of infrastructures and their components. However, because of the rare recurring rate of strong earthquakes and the small population of well-instrumented bridges, laboratory tests have to be utilized to fill this knowledge gap (Saiidi et al 2013A).

In the past, due to the limited capacity of testing equipment, shake table experiments could only be performed on single bridge components or on very small scale models of entire bridges. For example, Qu et al (2005) investigated the dynamic properties of a 1/100 scale model of the Wanzhou Yangtze River Bridge in 2005. Zaghi et al (2012) studied the nonlinear dynamic behavior of a 1/5 scale two-column bridge pier through shake table testing. Although the experimental results were analyzed and then compared with the analytical results from 3-D finite element models, the test results are questionable due to the tiny scale and use of alternative materials.

Shake tables with the capacity to generate horizontal and vertical acceleration on large scale specimens have been built in various universities and research institutes since 2000, including: the single 20 m × 15 m E-Defense shake table at the National Research Institute for Earth Science and Disaster Prevention (NIED) of Japan (Kajiwara and Nakashima 2006), the single 7.6 m × 12.2 m shake table at the University of California at San Diego (Ozcelik et al 2008); the two 7 m × 7 m shake tables at the State University of New York at Buffalo; the three 4.3 m × 4.5 m shake tables at the University of Nevada at Reno (Reitherman 2003); and the newly-built four 4 m × 6 m shake tables at Tongji University in China (Li 2013). With the rapid development of these testing facilities, large-scale full-bridge model experiments were conducted recently. In general, two types of tests were conducted: 1) full bridge models (at least two piers) seated on single table or multi-tables, and 2) one pier of bridge models seated on the shake table with the other 'abutment' parts fixed on the ground.

Park et al (2003) performed shake table tests on three scale models of a reinforced-concrete bridge column, including one based on the ductility design method (U.S.) and the others on the working stress design method (Japan). The tested column was connected to the shake table and the other supports were placed on the ground. All three specimens showed good performance; however, the ductility design specimen experienced less damage than those of working stress design.

Nakashima et al (2008) presented the US-Japan cooperative project of study on the seismic performance of bridge columns using the world's largest shake table: E-Defense. Two models were introduced: a column component model and a bridge system model. In addition, Kawashima et al (2012) presented the results of a single column test incorporating polypropylene fiber-reinforced cement composite.

Sakai and Unjoh (2006) performed a similar test to evaluate the effect of multidirectional loading on the dynamic response and seismic performance of reinforced concrete columns. A ¼ scaled RC column was tested under two horizontal and one vertical component of strong motion. Results show that the lateral force response reduced due to the bi-lateral loading effects.

Arias-Acosta and Sanders (2010) studied bridge column behavior under the combined effect of dynamic actions, including axial, shear, bending and torsion. Eight scaled cantilever-type specimens were tested on the bidirectional shake table facility at the University of Nevada, Reno (UNR). A special inertial loading system named the Bidirectional Mass Rig was developed to allow shake table testing of a single cantilever-type column under biaxial ground motions.

Saiidi et al (2013a) conducted a shake table test on a 33.6-m-long (110-ft-long), four-span, RC bridge model with a continuous posttensioned superstructure supported on three two-column bents at the University of Nevada, Reno. The variable was the pier height to introduce slight asymmetric earthquake effect. The bridge model survived and continued carrying vertical loads.

Noguez and Saiidi (2012) conducted research on the same large-scale model of the four-span bridge, incorporating several innovative plastic hinges. The research focused on the columns, which utilized different unconventional details at the bottom plastic hinges, including shape memory alloys (SMAs), engineered cementitious composites (ECCs), embedded elastomeric pads, and posttensioning tendons. Test results showed the damage was minimal for the columns with SMA/ECC and for those with built-in elastomeric pads.

Johnson et al (2008) performed shake table tests on a quarter-scale, two-span reinforced concrete bridge model at the University of Nevada, Reno. It was a part of a multi-university, multidisciplinary project utilizing the Network for Earthquake Engineering Simulation (NEES), with the objective of investigating the effects of soil-foundation-structure interaction on bridges. Results showed that detailing of the column transverse reinforcement according to NCHRP 12-49 guidelines provided sufficient column ductility to prevent collapse during a subsequent 1.4 g PGA earthquake excitation.

Saiidi et al (2013b) conducted further research on Johnson et al's model. The identical model was tested with incoherent motions that simulated fault rupture. The results were compared to Johnson et al's and it was found that fault rupture substantially affected the damage type and location in the bridge bents. The most severely damaged bent in this bridge was a relatively flexible bent near the "fault."

Chen et al (2008) conceptually justified methods that identify structural component stiffness degradation using a linear time-invariant (LTI) system based on pre- and post-event low amplitude vibration measurements. Two large-scale shake table experiments, one on a two-column reinforced concrete (RC) bridge bent specimen, and the other on a two-span, three-bent RC bridge specimen were performed. The results show that the stiffness degradation identified is consistent with the experimental hysteresis, and could be quantitatively related to the capacity residual of the components.

Ozer and Soyoz (2013) incorporated the system identification results obtained from vibration measurements with a reliability-based methodology to evaluate the safety of bridges. Tests were conducted on a three-bent reinforced concrete bridge on three-shake tables simultaneously. Test results and finite element model results were compared and damage detection and reliability estimations were carried out for these two cases using fragility curves.

Sideris (2012) introduced a hybrid sliding-rocking (HSR) precast concrete bridge pier with post-tensioned segmental members and evaluated it through the shake table testing of a large-scale (1/2.39), single-span bridge specimen incorporating a HSR-RD superstructure and two HSR-SD single-column piers at the University at Buffalo, State University of New York. Results show that the seismic performance of HSR components can fulfill the requirement for application in high-seismic regions.

As seen above, research on bridge shake table tests is emerging as a research hotspot. However, there is still very little research concerning bridge superstructures. Therefore, this report will focus on the seismic performance of a precast bridge superstructure with a UHPC connection.

1.3 Objective of the Research Project

The objective of this research report is to validate and demonstrate the seismic performance of the UHPC connection. Shake table tests for the two UHPC connected Deck-Bulb-Tee (DBT) girders were conducted to observe and analyze the seismic performances (strength) of the UHPC connection between two girders, as shown in Figure 1-1. Typical earthquake ground motion records were directly applied to two shake tables and low-amplitude white noise excitations were used to investigate the global dynamic behavior of the girder and the UHPC connection.

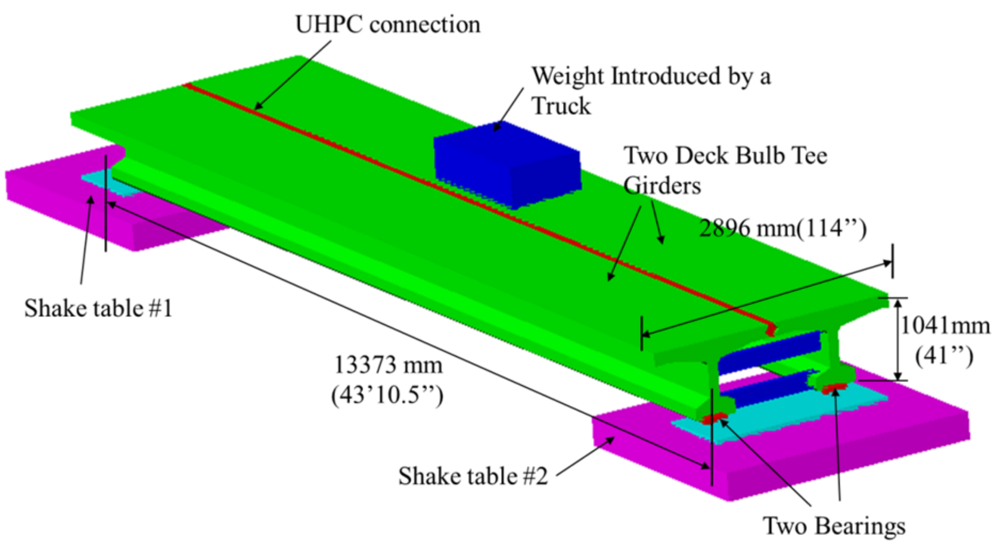

Figure 1-1 3-D Scheme of test setup

SECTION 2
DESIGN OF THE SPECIMEN

2.1 Design Considerations

To investigate the seismic behavior of the UHPC connection, two deck-bulb tee (DBT) girders with the same size and specification were designed for this project. The UHPC connection was cast between these two DBT girders in-field at the lab where shake table tests were conducted. Considering the capacity of the shake table facility and to reduce possible scaling effects, two full size DBT girders were designed based on the design of a completed project in Lyons, NY. The dimensions were in the same range but not exactly the same due to the limitation of shake table capacity. For example, the prototype girder sizes were 61 in for the deck width and 41 in for the girder depth with 6-inch wide UHPC connections, while the specimen girder sizes were 54 in for the deck width and 41 in for the girder depth.

2.2 Design of the Deck-Bulb Tee Girder

The rebar arrangement of the deck, dimensions and reinforcement of the girder are shown in Figure 2-1. Other design details and construction shop drawings can be seen in Appendix A.

Detailed notes used for manufacturing the girders were:

1) All pre-tension strands shall be ½’’ϕ AASHTO grade 270 low relaxation strands, jacked to 202.5 ksi.
2) All concrete shall be Pennsylvania (PA)’s 8,000 psi mix.
3) All strands will be cut flush with the girder ends and painted with an approved epoxy resin after the girder is cast.
4) Forms for bearing pad recess shall be constructed and fastened in such a manner as to not cause damage to the girder during the strand release operation.
5) Structural steel shapes and assemblies shall be ASTM A36. They will be painted with a primer coat in accordance with STD. SPEC 6-07.3(9).

It is noted that several extra longitudinal rebars (see details in section B-B in Figure 2-1(d)) were designed to be placed at both ends of the girder based on California Department of Transportation (Caltrans) Bridge Design Specifications. The purpose for installing these rebars was to ensure that the girders provided appropriate seismic performance so that they would not be damaged during the seismic excitations input. The other details were designed based on current AASHTO LRFD bridge design specifications.

Properties of the girder are listed in Table 2-1.

Table 2-1 Girder properties

Item	Annotation	Value	Unit
Mass	m	39	kips
Height	H	41	in
Width of deck	W_D	54	in
Span length	L	43' 10-1/2''	ft
Area	A	887	in^2
Distance from c.g. of girder to bottom	e	22	in
Moment of inertia to X-axis	I_x	196416	in^4
Moment of inertia to Y-axis	I_Y	109437	in^4

Note: c.g. = center of gravity

Calculated information about the prestressed strands is listed in Table 2-2.

Table 2-2 Girder stresses due to prestressing

Item	Value	Unit
Number of strands	26	
Distance from c.g. of strands to the bottom	4.44	in
Final prestressed force on each strand	31	kips
Total prestress force	806	kips
Compressive stress due to the presstressed strands	0.91	ksi
Negative bending moment due to total prestress force	1179	k-ft
Tension stress on the top flange	0.46	ksi
Compressive stress on the bottom flange	2.5	ksi

Note: c.g. = center of gravity

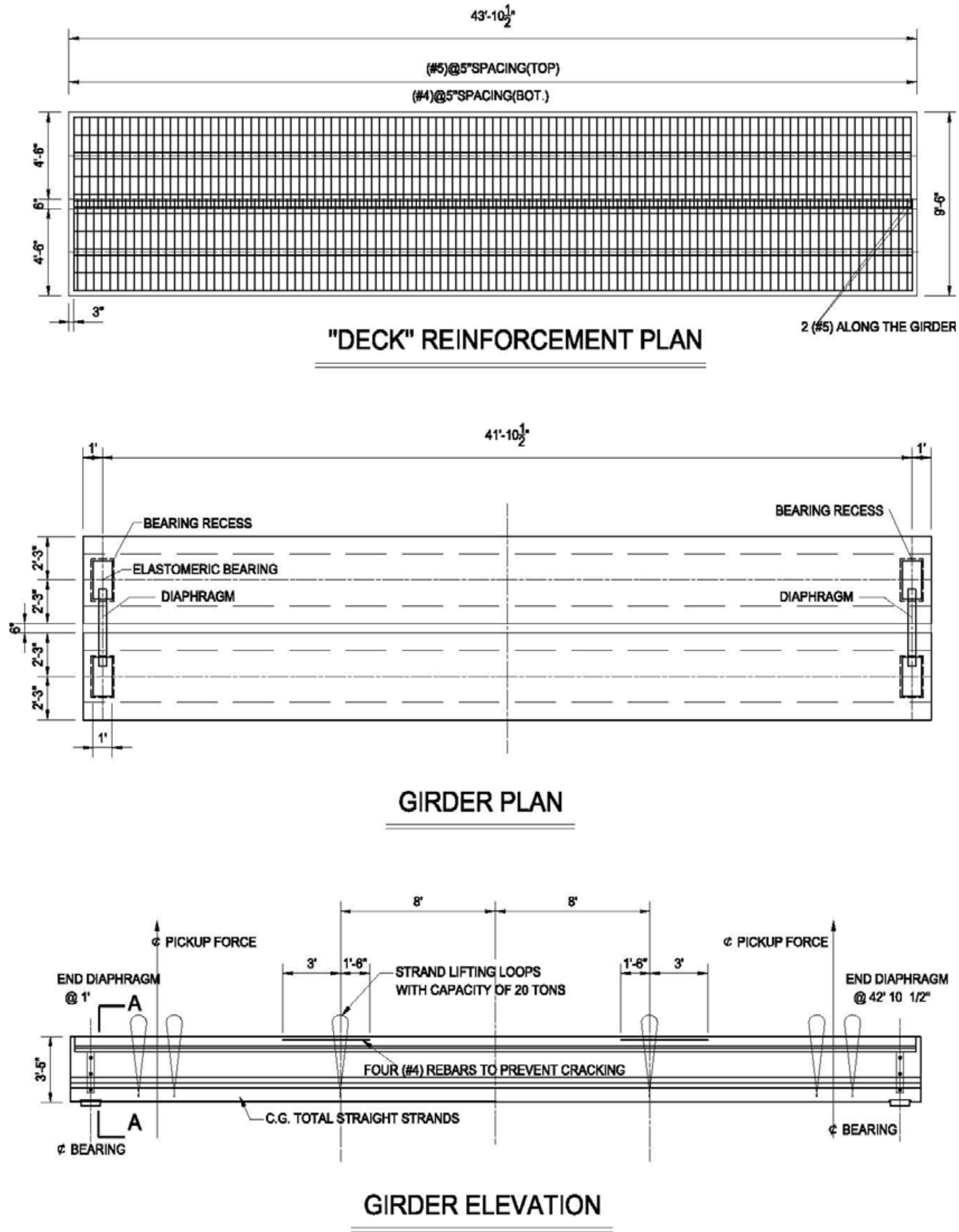

(a) Girder plan and elevation

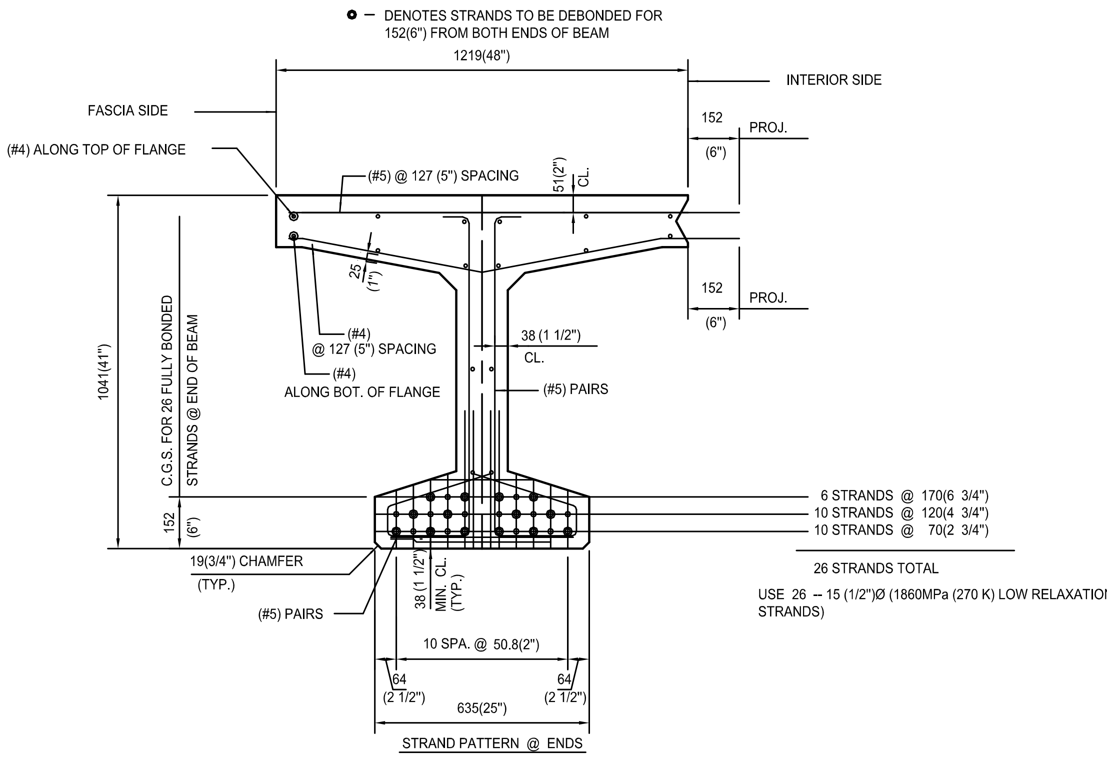

(b) Cross section at the mid-span

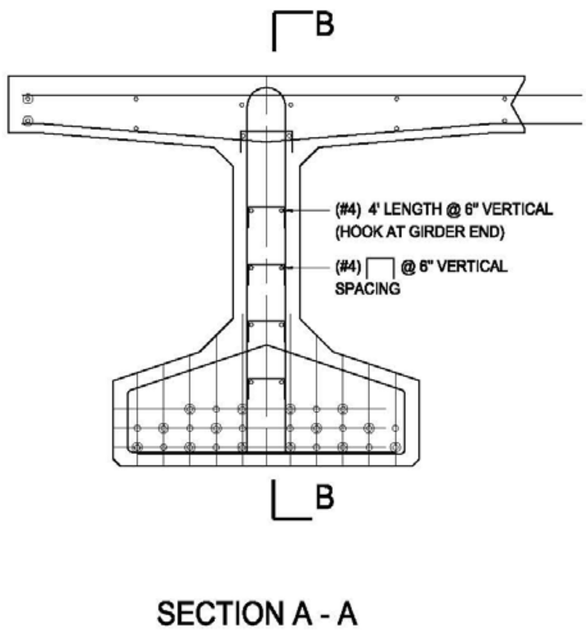

(c) Cross section at the end

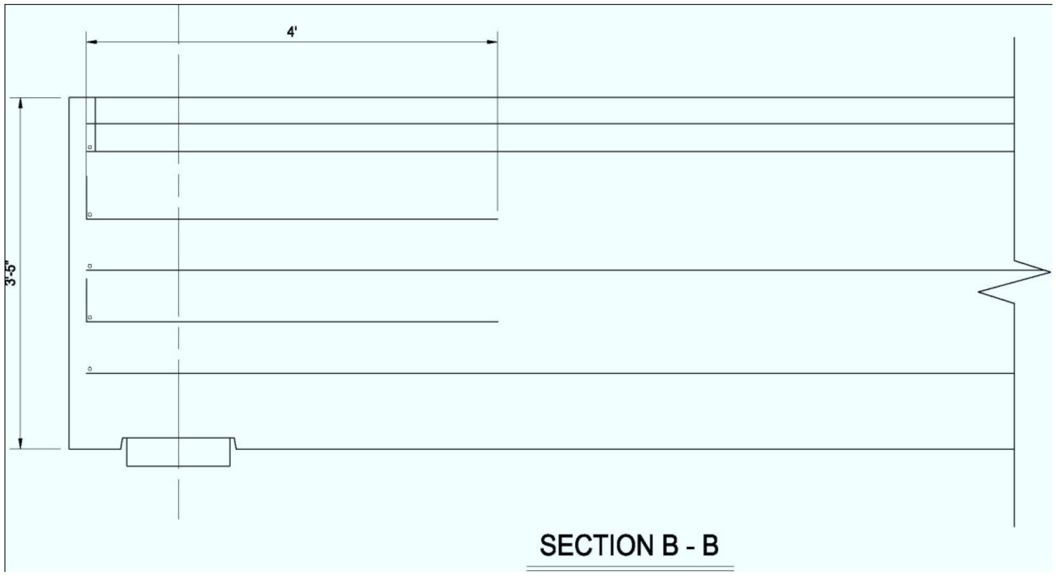

(d) Size of aseismic rebar

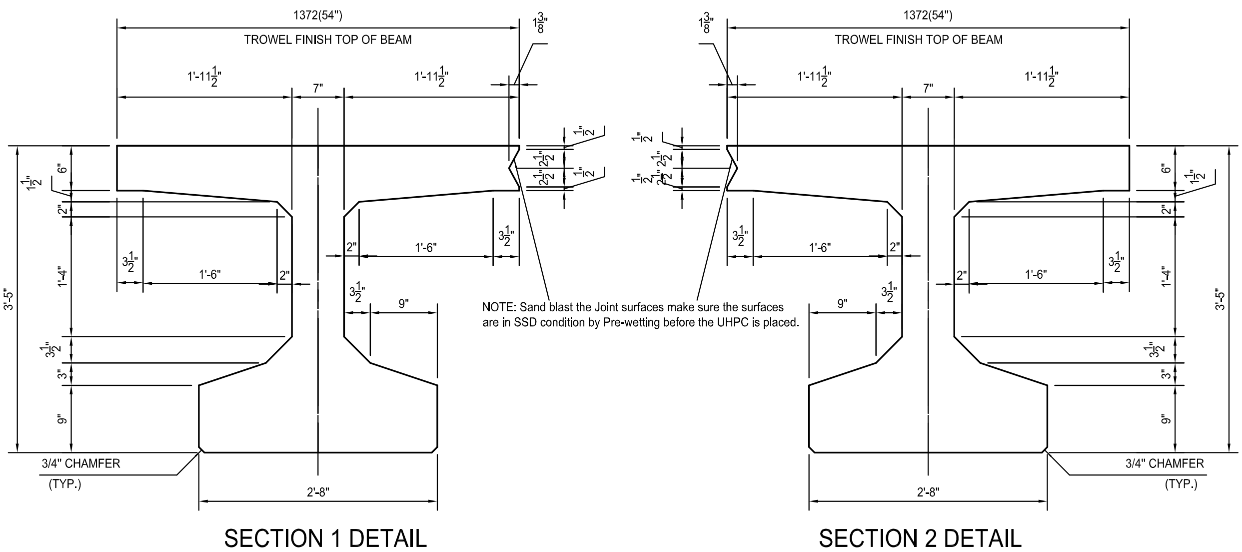

(e) Girder dimensions

Figure 2-1 Design of deck-bulb tee girder

Concrete stresses under different load cases are listed in Table 2-3.

Table 2-3 Concrete stresses due to different load cases

Case 1: Under dead load alone:		
Maximum Bending Moment (in mid-span) due to dead load	213	kip-ft
Tension Stress on the top flange	0.21	ksi
Compressive Stress on the bottom flange	-2.21	ksi
Case 2: Under dead load + live load (8 kips in the mid-span):		
Maximum Bending Moment (in mid-span) due to live load	167.5	kip-ft
Tension Stress on the top flange	0.02	ksi
Compressive Stress on the bottom flange	-1.98	ksi
Case 3: Lifting (lifting point at 8 feet apart from mid-span):		
Maximum Negative Bending Moment (at lifting point) due to live load	-95.3	kip-ft
Tension Stress on the top flange	0.57	ksi
Compressive Stress on the bottom flange	2.63	ksi

Note that the tension stress for concrete cracking is approximately 0.67 ksi. Therefore, the tension stress during lifting will not cause severe cracks on the top flange concrete.

To further verify the calculated result, a preliminary simplified model was established using SAP 2000 v 14.0. The girder flange and web were modeled using shell elements. The UHPC was defined as rigidly connected to the flange deck. The resulting stress in the girder under dead load and live load are shown in Figure 2-2 and Figure 2-3.

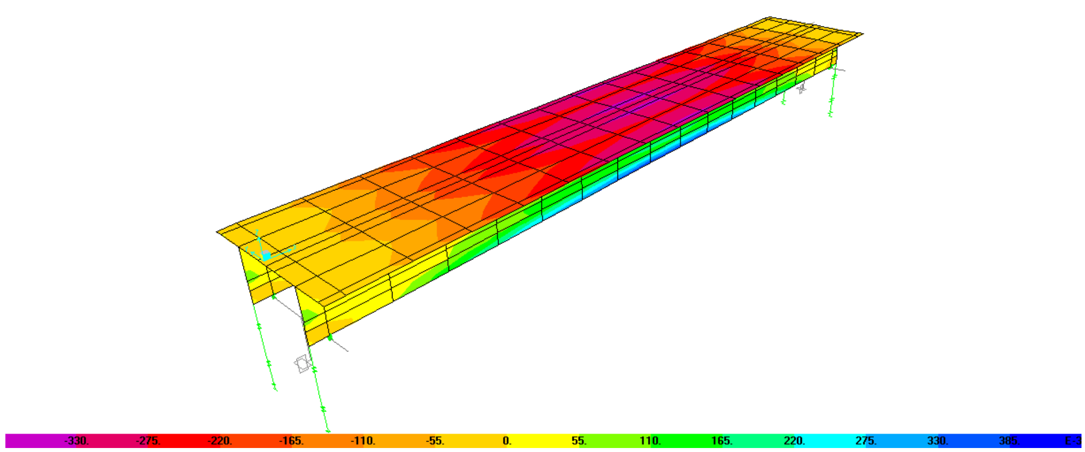

Figure 2-2 Stress under dead load from SAP2000

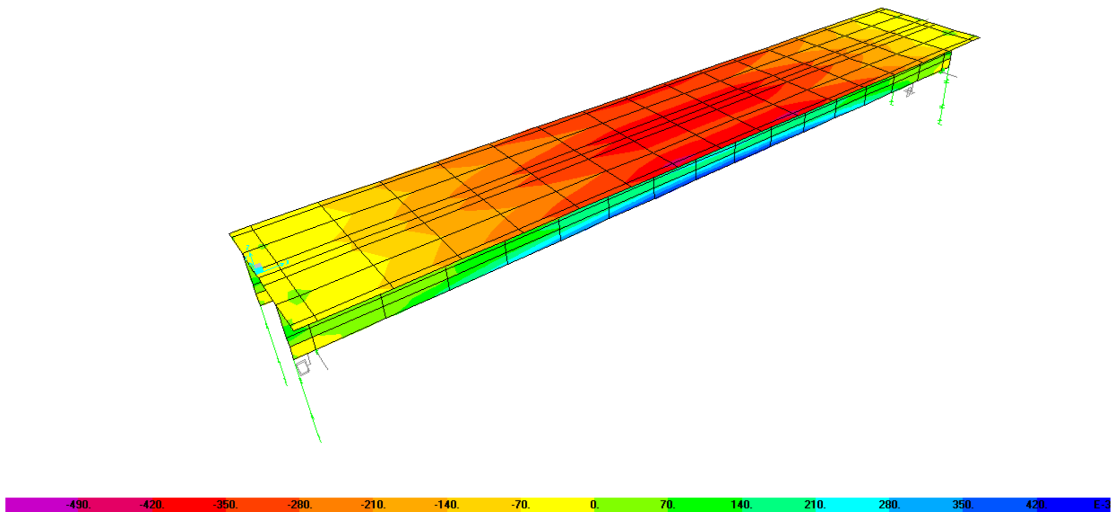

Figure 2-3 Stress under dead load + live load from SAP2000

2.3 Design of the UHPC Connection

Graybeal (2010) compared the static and cyclic behavior of six types of UHPC connection details as shown in Table 2-4**.** Test results showed no evidence of rebar debonding in any of the six types of connection specimens. The most heavily stressed specimen (6B) was subjected to a large static overload and a subsequent 11.5 million cycles of structural loading. From the standpoint of cost-saving and ease of construction, the connection with a 6-inch connection width and straight rebar details (6B in Table 2-4) was selected as the design base of the UHPC connection. Since other types of construction detail apparently provide better bond effect between rebar and UHPC, their seismic performances are considered to be better than the selected connection. The construction details of the UHPC connection used are shown in Figure 2-4.

Table 2-4 UHPC deck connections from previous research (Graybeal 2010)

Name	Orientation	Depth	Reinforcement
8H	Transverse	200 mm	Alternating 16M (#5) **headed black** reinforcement with 90 mm lap length and 450 mm (top) and 180 mm (bottom) spacing
8E	Transverse	200 mm	Alternating 13M (#4) **hairpin epoxy-coated** bars with 100 mm lap length and 55 mm spacing
8G	Transverse	200 mm	Alternating 16M (#5) **galvanized straight** bars with 150 mm lap length and 450 mm (top) and 180 mm (bottom) spacing
8B	Transverse	200 mm	Alternating 16M (#5) **black straight** bars with 150 mm lap length and 450 mm (top) and 180 mm (bottom) spacing
6H	Longitudinal	150 mm	Alternating 16M (#5) **headed black** reinforcement with 90 mm lap length and 450 mm (top) and 180 mm (bottom) spacing
6B	Longitudinal	150 mm	Alternating 16M (#5) **black straight** bars with 150 mm lap length and 450 mm (top) and 180 mm (bottom) spacing

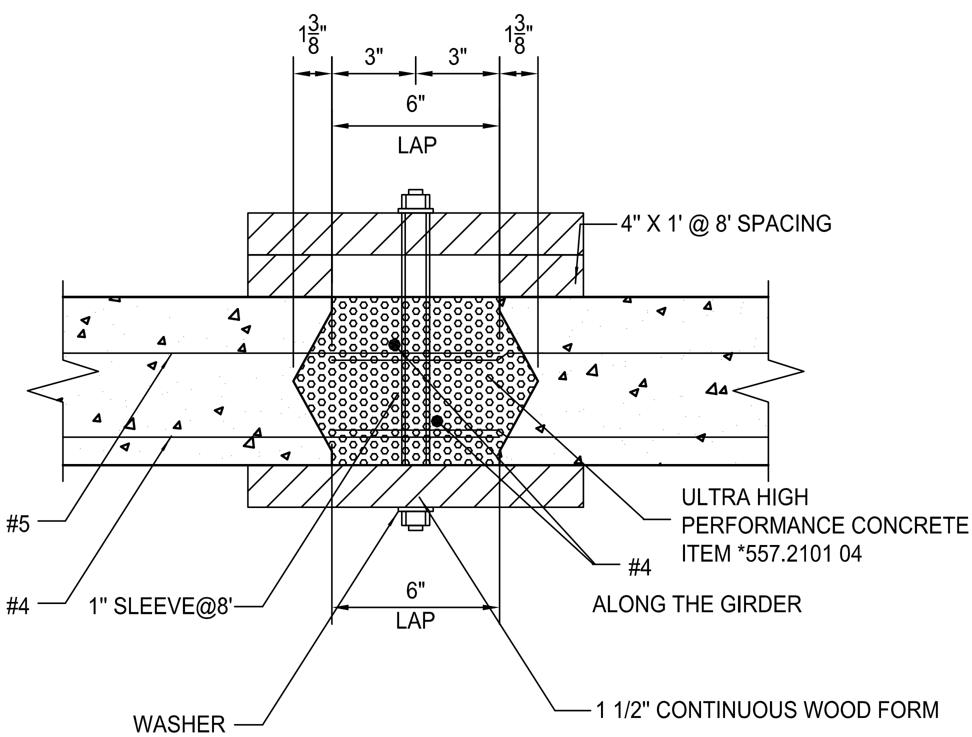

Figure 2-4 Construction details of the UHPC connection

2.4 Estimation of Loading Capacity of Shake Tables

To protect the shake table facility, the estimation of the force in the test was necessary. The weight estimate for the entire specimen and accessories are shown in Table 2-5.

Table 2-5 Weight on the shake table

Items	Weight (kips)	Amount	Total Weight (kips)	On Each Table (kips)
Deck-Bulb-Tee Girders	40	2	80	40
Diaphragm	0.4	2	0.8	0.4
Sensors, etc.	1	1	1	0.5
Foundation Plate	2.1	2	4.2	2.1
Live Load	17	1	17	8.5
Total Weight above Extension Frames	--	--	103	51.5
Extension Frames	20	2	40	20
Total Weight	--	--	**143**	**71.5**

Assuming a ground motion of 0.8 g was applied on the specimen, the shear force on each table was approximately 58.4 kips, while the bending moment was 280 kips-ft. The bending moment was less than the capacity of the table (407 kip-ft, provided by the Structural Engineering and Earthquake Simulation Laboratory at University at Buffalo); thus, the safety of the shake table facility was ensured.

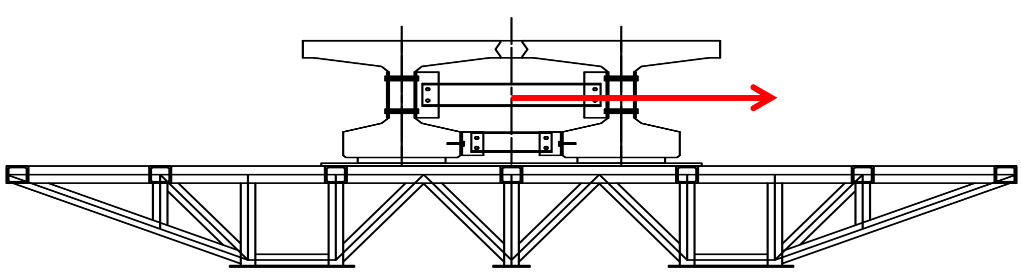

Figure 2-5 Specimen and shake table extension frame

2.5 Design of Steel Foundation Plates

To avoid collision between the girder and the shake table, one steel foundation plate needed to be installed on each extension frame. Detailed drawings are shown in Figure 2-6 and Figure 2-7.

The maximum shear stress of the steel plate during testing was approximately 3.6 ksi, as shown in Figure 2-8.

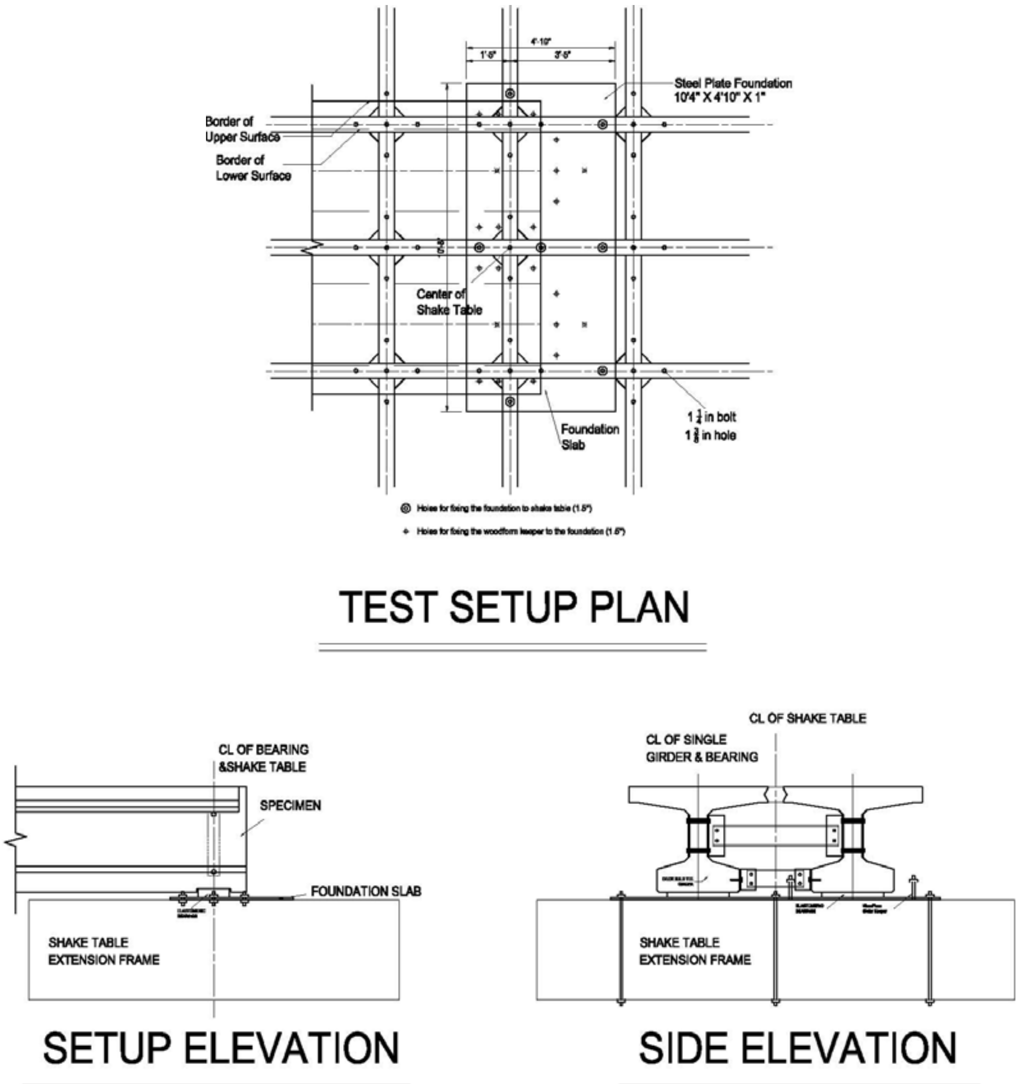

Figure 2-6 Specimen installation plan

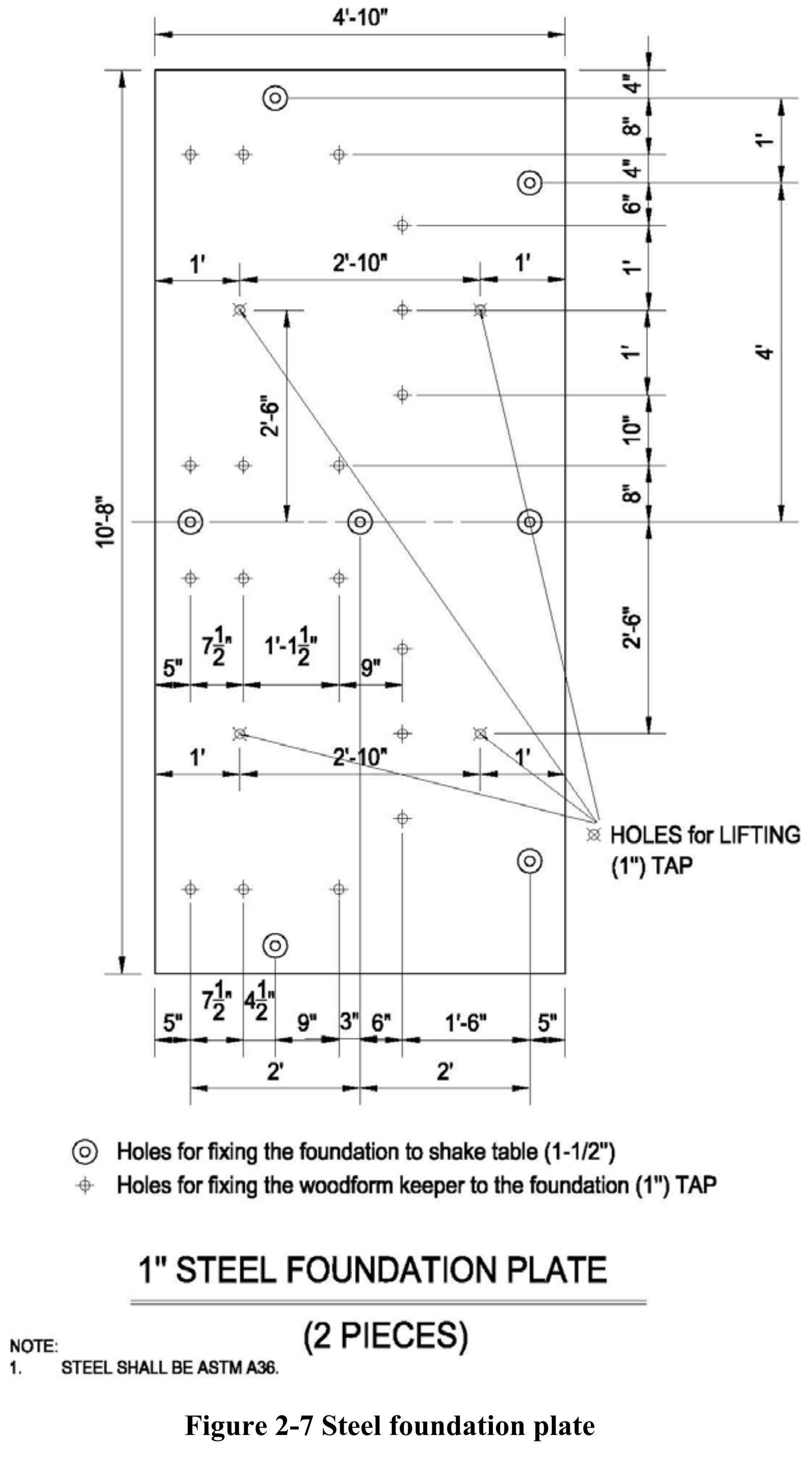

Figure 2-7 Steel foundation plate

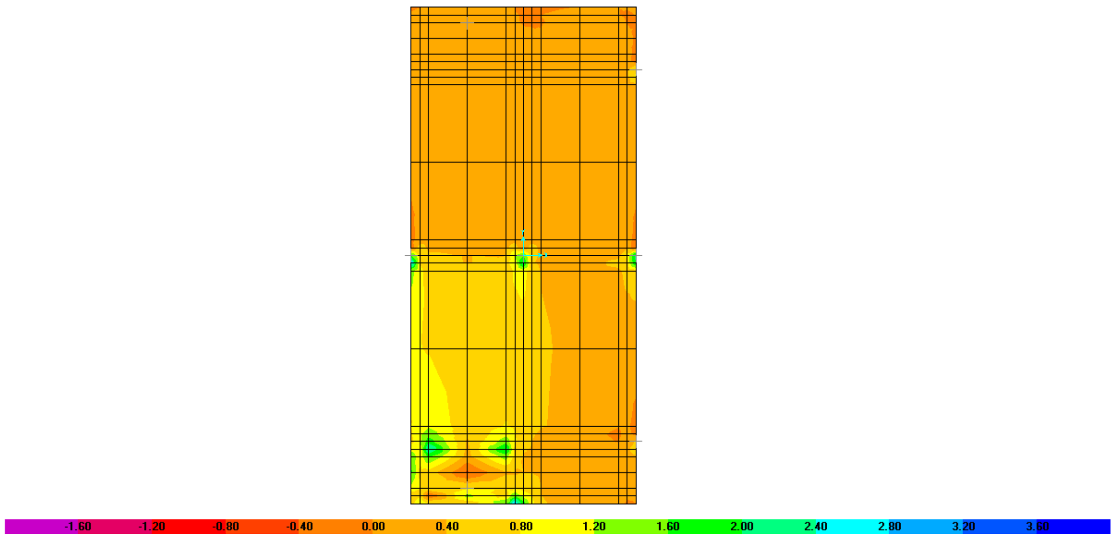

Figure 2-8 Shear stress of steel plate in the test

SECTION 3
PREPARATION OF THE SHAKE TABLE TESTS

3.1 Preparation Plan for Shake Table Tests

Two $43' - 10\frac{1}{2}''$ concrete DBT girders were prefabricated and delivered to the Structural Engineering and Earthquake Simulation Laboratory (SEESL) at the University at Buffalo, State University of New York. A concrete joint along the girder in the longitudinal direction was formed and poured using UHPC.

3.1.1 Preparation of Shake Tables

Before the delivery of these two DBT girders, the shake tables were moved to the appropriate position and tuned up with low-amplitude white noise. The two steel base plates and neoprene pads were installed in designed positions. Detailed drawings of the neoprene pads are shown in Figure 3-1. Several wood pads were used to facilitate the installation and alignment of girders.

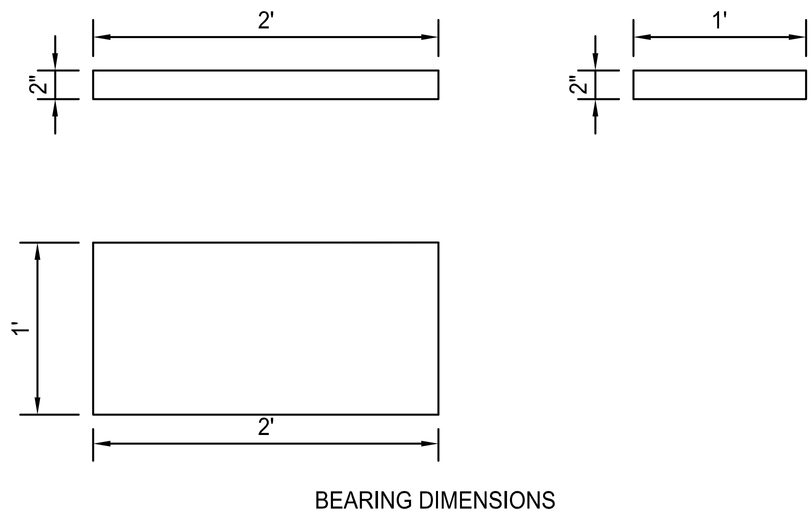

(a) Neoprene Pads

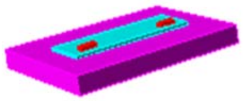

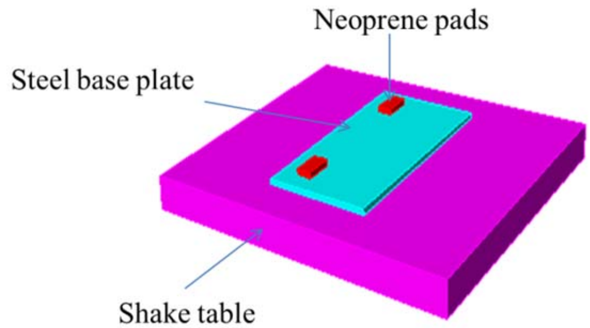

(b) 3-D Scheme

(c) Pictures

Figure 3-1 Preparation of the shake tables

3.1.2 Lifting Plan

Since the required minimum depth of the Dayton P53 lifting anchor exceeded the girder depth of 41'', a set of sophisticated loop lifters was used for lifting. The locations of these loop lifters are shown in Figure 3-2. D-rings and ropes with capacity of 20 tons were used for rigging.

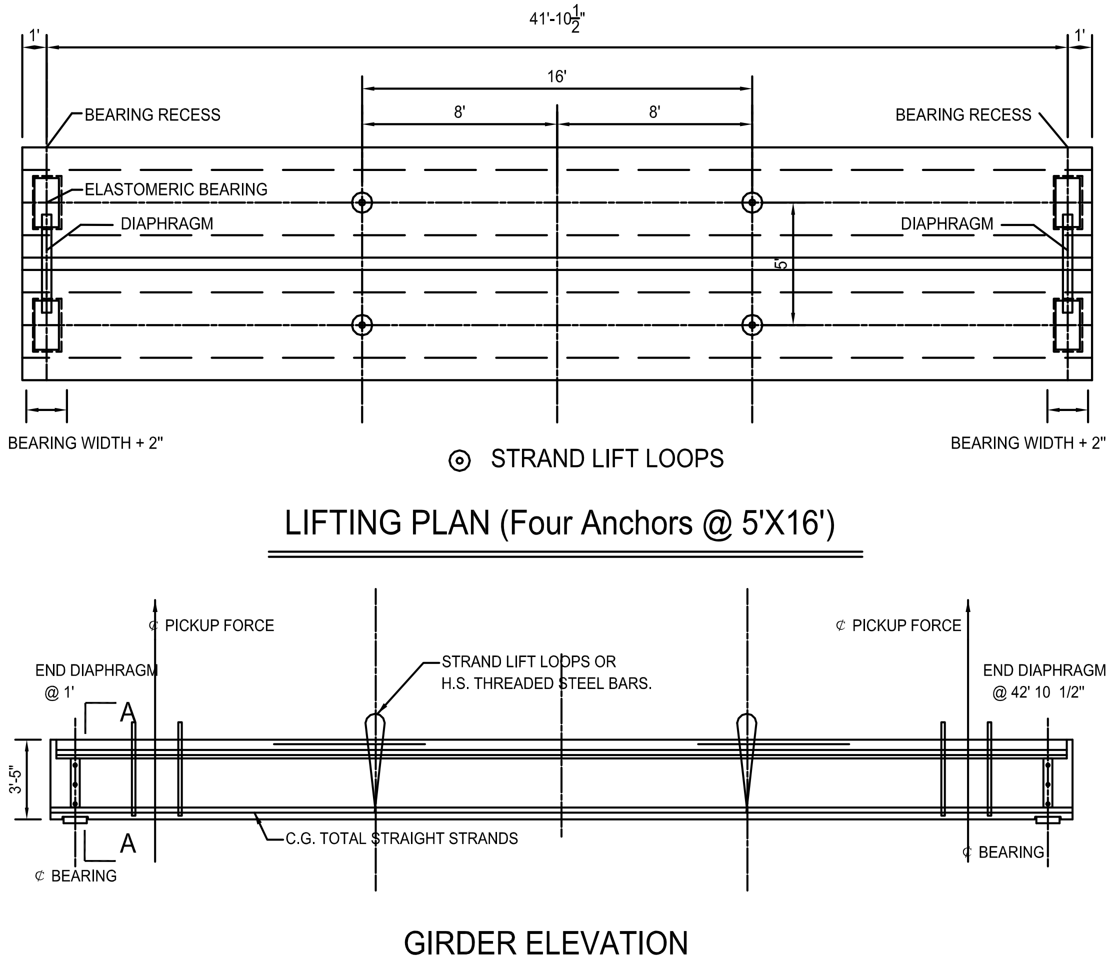

Figure 3-2 Locations of loop lifters

3.1.3 Manufacture and Installation of Girders

Two $43' - 10\frac{1}{2}''$ concrete DBT girders were prefabricated in a precast concrete shop using PA 8000 psi concrete. Figure 3-3 shows a picture of the fabrication procedure of the DBT girders.

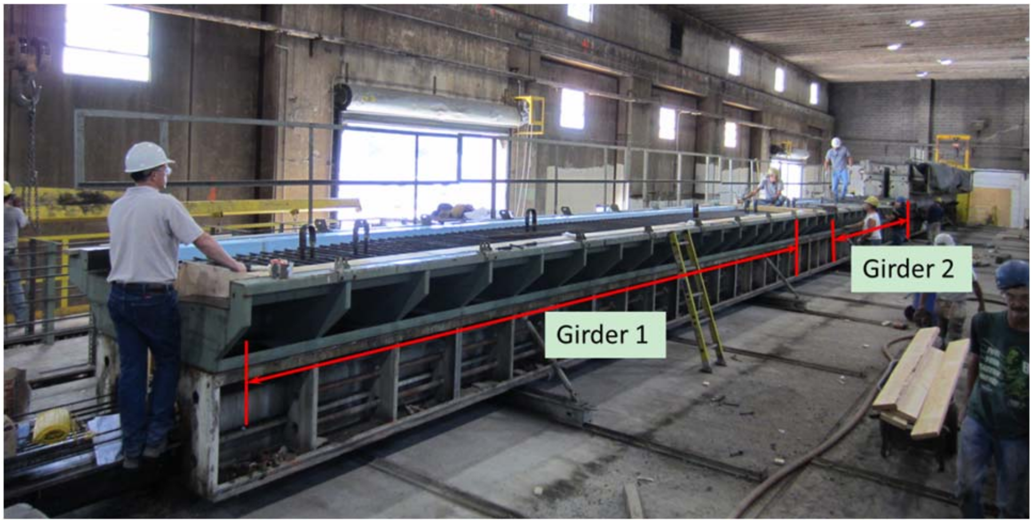

Figure 3-3 Fabrication of the DBT girders

Twenty-nine days after the fabrication, these two girders were delivered to the Structural Engineering and Earthquake Simulation Laboratory (SEESL) at the University at Buffalo, State University of New York. Each girder was delivered, lifted and installed separately (see Figure 3-4). After being aligned in the appropriate position, two sets of steel diaphragms were connected at both ends of each girder. Detailed drawings of the steel diaphragms are shown in Figure 3-5.

(a) Delivery of the DBT girder 1

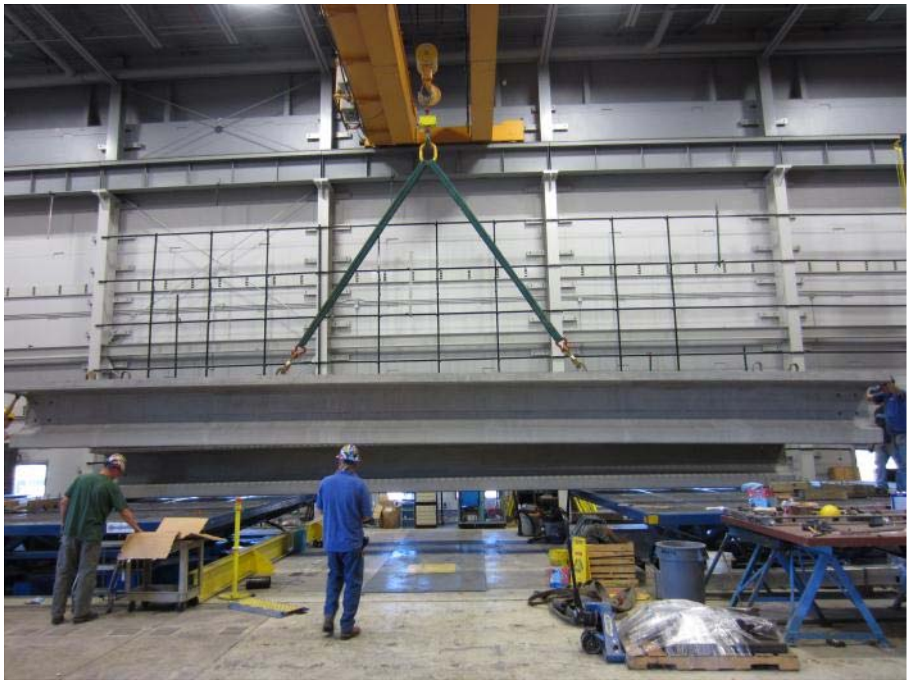

(b) Lifting of the DBT girder 2

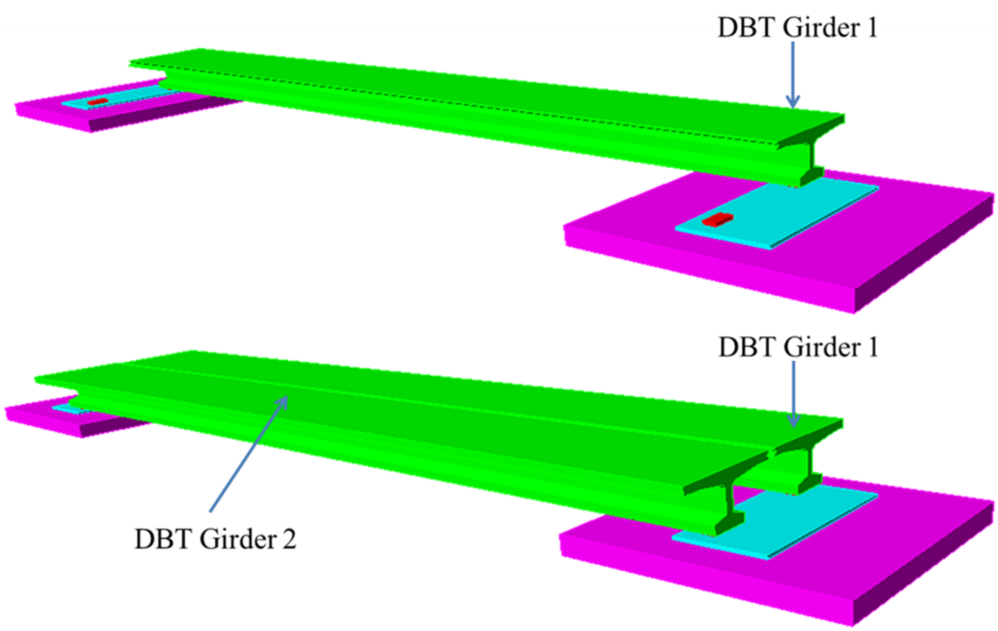

(c) 3D- scheme

Figure 3-4 Installation of the girders

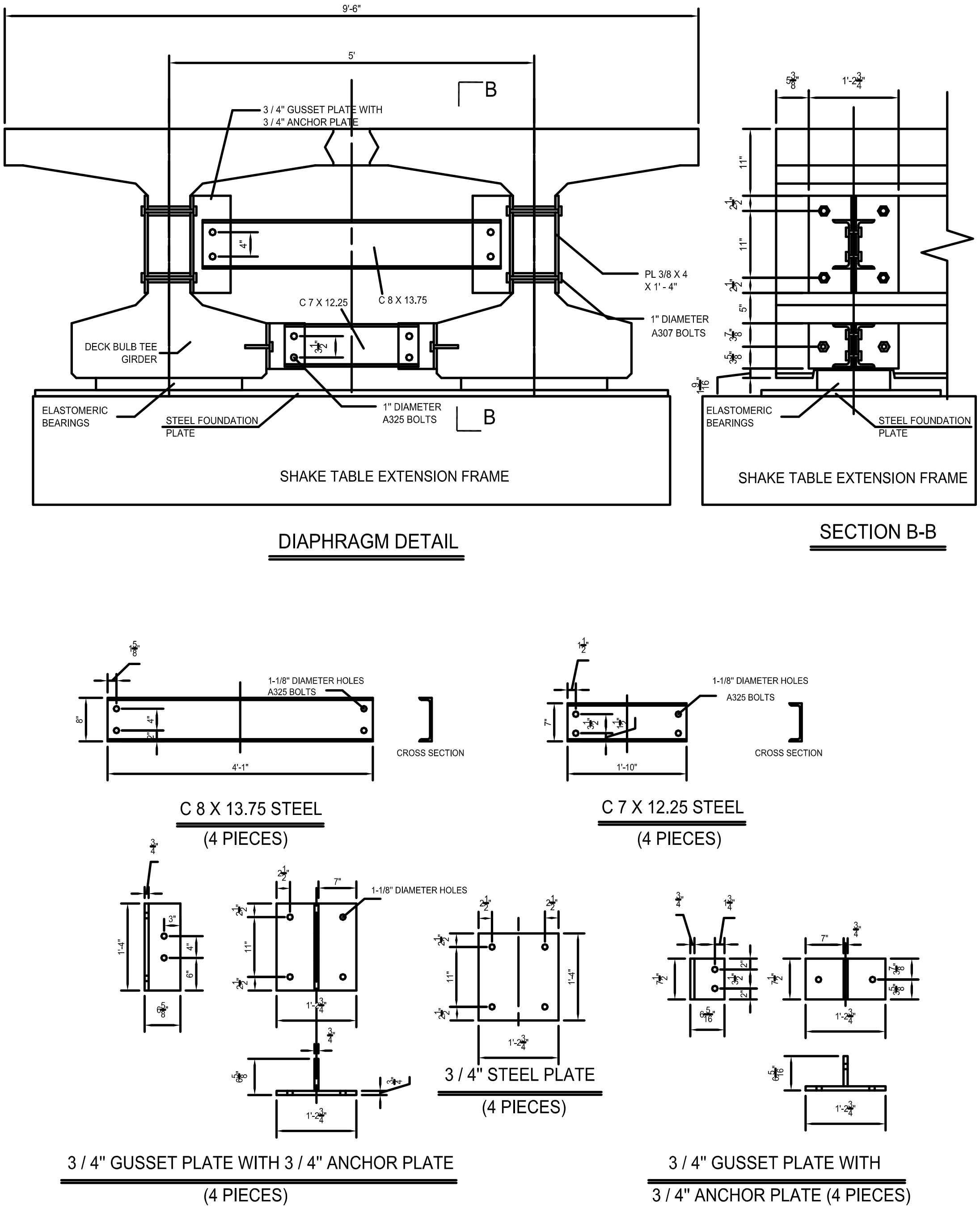

(a) Shop drawings of the diaphragms and gusset plates

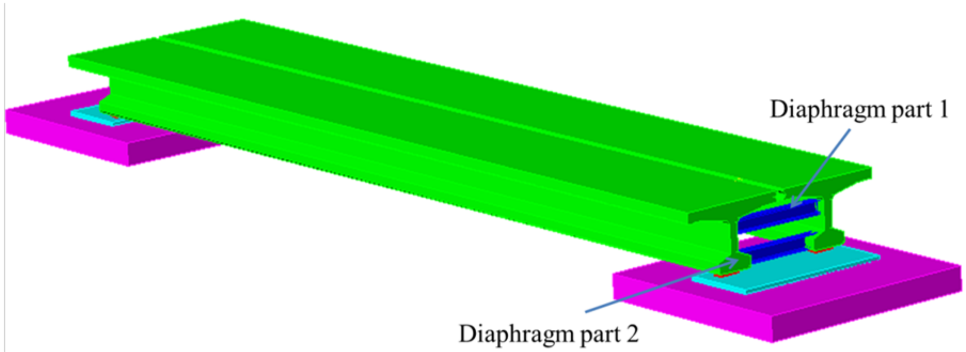

(b) 3D- scheme

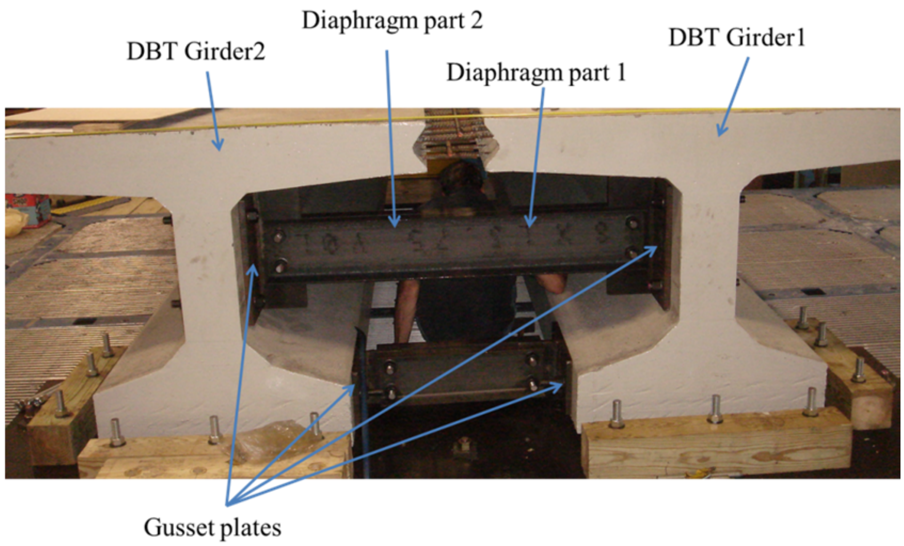

(c) Picture

Figure 3-5 Steel diaphragms and gusset plates

3.1.4 Casting of the UHPC Connection

A continuous wood form along the longitudinal direction of the girder was placed and sealed to the end of the connection. Wood forms of 4'' x 1' were connected to the lower full-length wood form using bolts at a spacing of 8', as the detailed drawing in Figure 2-4 shows. The casting procedure is shown in Figure 3-6. Due to the time limit, the joint was heated with electric blankets and covered in insulation to facilitate the curing procedure. Prior to commencing the experiment, grout cylinders were tested to ensure that the UHPC had reached a compressive strength of at least 8,000 psi, equal to that of the concrete used in the precast girder. The results will be introduced in Section 3.2.

(a) Preparation of wood form

(b) Casting UHPC

(c) UHPC Connection

(d) Under fill at the end of girder

Figure 3-6 UHPC connection casting procedure

3.2 Compressive Strength of UHPC Material

3.2.1 Early-age compressive strength (strength before and during the shake table tests)

Due to the occupation time limit for the shake table, the tests started on the fifth day after the UHPC connection was cast. To increase the accuracy of the compressive strength test results, the 3’’ x 6’’ UHPC cylinders were prepared by cutting off a half inch at each end (see Figure 3-7). Compressive tests of several UHPC cylinders were conducted using the compressive testing machine in the SEESL at UB, as shown in Figure 3-8. Table 3-1 lists the results of compressive strength tests. It can be seen that at the fifth day (the first day of the shake table testing), the compressive strength reached 16,094 psi, which is close to two times that of the concrete used in the precast girder.

Figure 3-7 Preparation of UHPC cylinders

Figure 3-8 Compressive tests of UHPC cylinders

Table 3-1 Compressive strength of UHPC at early-age (SEESL)

Batch No.	Age (days)	Break force(lb)	Compressive strength (psi)	Avg. compressive strength (psi)
UB#1	3	103674	15100	11089
		68902	10035	
		68957	10043	
		66998	9758	
		72153	10509	
UB#2	5	127121	18515	16094
		87195	12700	
		100763	14676	
		112573	16396	
		122378	17824	
		112958	16452	
UB#3	6	96075	13993	13600
		89556	13044	
		98154	14296	
UB#4	10	89722	13068	13160
		70761	10306	
		91113	13270	
		93457	13612	
		84110	12250	
		75403	10982	

Several UHPC cylinders were also sent to the manufacturer's lab for testing their compressive strength. Table 3-2 gives the results of these tests. It can be seen that the five-day compressive strength provided by the manufacturer is 21% higher than the results at UB. The difference can be attributed to the different methods of preparing the UHPC cylinders. The specimen was pre-treated by a right-angle saw; thus, the eccentricity-induced bending moment may have been much smaller than the specimen prepared at UB.

Table 3-2 Compressive strength of UHPC at 5th day (manufacturer)

Batch No.	Age (days)	Break force(lb)	Compressive strength (psi)	Avg. compressive strength (psi)
Manufacturer #1	5	132935	19362	19566
		137055	19962	
		133035	19376	

3.2.2 28-day compressive strength

Three batches of UHPC were tested for compressive strength at three individual labs. Table 3-3 gives a summary of the compressive strength results. Apparently, the tests conducted at SEESL provided a lower compressive strength. The nonparallel contact surfaces may be the main reason for the difference. The lower and upper surfaces of the cylinder were not prepared simultaneously; thus, the nonparallel surfaces may have been subject to an additional bending moment, which caused the cylinder to fail at a lower compressive force. A horizontal crack that occurred on one of the specimens indicates that the specimen was subject to tension stress due to the additional moment, as shown in Figure 3-9.

Table 3-3 Compressive strength of UHPC at 28-day

Batch No.	Age (days)	Breaking force (lb)	Compressive strength (psi)	Avg. compressive strength (psi)
UB #5	28	76355	11121	13200
		96762	14093	
		93027	13549	
		79385	11562	
		102914	14989	
		95352	13888	
Larfarge #2	32	189555	27608	27904
		193615	28199	
Turner Fairbank #1	54	167187	24350	23787
		154416	22490	
		158354	24520	

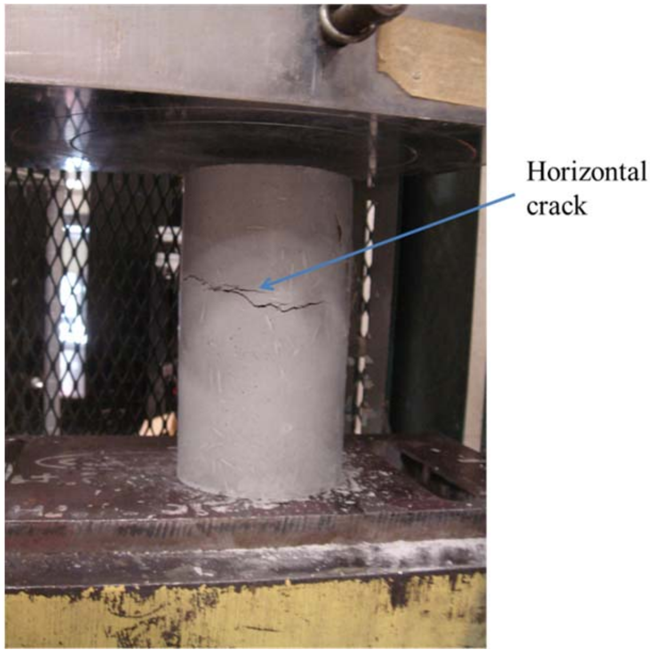

Figure 3-9 A horizontal crack in the compressive test

3.2.3 Compressive strength of plain concrete used in precast girders

Concrete compression tests were conducted on three 6'' x 12'' plain concrete (PC) specimens. The results are shown in Table 3-4. Typical failure modes of PC specimens are shown in Figure 3-10. It can be seen that, unlike the PC specimens, the UHPC specimen remained in one piece due to the existence of the steel fiber.

(a) PC (b) UHPC

Figure 3-10 Typical failure mode

Table 3-4 Material properties of PC specimens

<table>
<tr><th>Specimen</th><th>Compressive strength (psi)</th><th>Average compressive strength (psi)</th></tr>
<tr><td>1</td><td>7550</td><td rowspan="3">7819</td></tr>
<tr><td>2</td><td>7983</td></tr>
<tr><td>3</td><td>7925</td></tr>
</table>

SECTION 4
FINITE ELEMENT MODELING OF THE SPECIMEN

4.1 FEM Modeling

The FEM software ABAQUS was used for this numerical analysis. A brief description of the model is presented below.

Elements: The concrete, diaphragms, UHPC connection, steel support plates and bearings were modeled with solid elements. Eight node linear and reduced brick elements (C3D8R) were selected for these parts. All the reinforcements were modeled by linear truss elements (T3D2).

Materials: The bridge deck was modeled with concrete material. The Concrete Damage Plasticity Option was selected to model the post yield behavior of concrete. The Mander-Park Confined Concrete Model was used to calculate the plasticity properties of concrete. The structural steel shapes such as the bracings, gussets, and bolts were given simple plastic properties using the ABAQUS plasticity model. Also, the reinforcements were modeled using the same material used for the other steel parts. The prestress was applied using the initial conditions option. The bearing placed between the deck and the steel foundation was comprised of 60 durometer neoprene pads. This bearing was modeled by hyperelastic material with Neo Hooke strain energy potential.

Contact: General interaction property was used for modeling the contacts between different steel parts and the concrete deck. An appropriate frictional coefficient was applied in the contact property. The contact between the UHPC connector and the deck was tied. The prestress at the tendons was applied by editing the Initial Condition in keyword script. All the reinforcements were inserted in the concrete deck using embedded constraint.

For the frequency calculation, the implicit analysis method was used, while the seismic analyses were performed in explicit method. Figure 4-1 shows an isotropic view of the FEM bridge model.

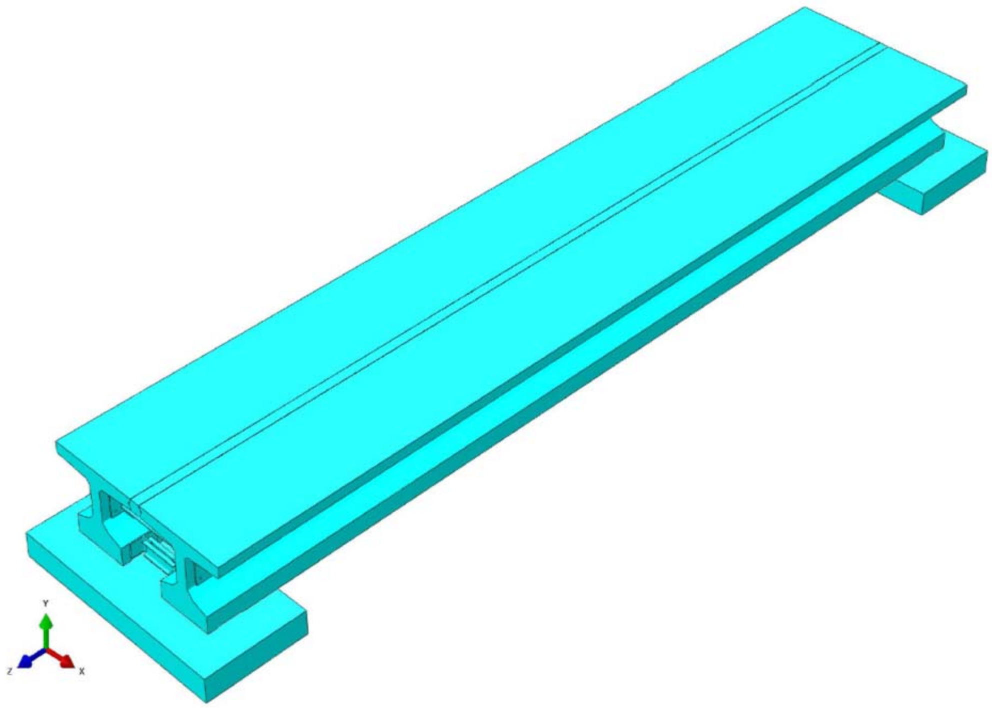

Figure 4-1 The FEM model of the bridge

4.2 Natural Frequency Calculation Results

The major frequencies obtained from the experiment closely resembled the results of numerical analysis. Two phases of the tests were simulated: the specimen without additional weight (phase 1) or with the weight (phase 2). A detailed description can be found in Section 5.3. Table 4-1 presents both values and Figure 4-2 ~ Figure 4-6 show the modes of the respective frequencies.

Table 4-1 Natural frequencies of the specimen in phase 1

Modal Orders	Mode Shapes	FEM Model Frequencies (Hz)
1	Transverse translation	6.97
2	Longitudinal translation	7.62
3	Rotation around vertical axis	11.91
4	Vertical bending	12.73
5	Combined vertical and transverse bending	16.95

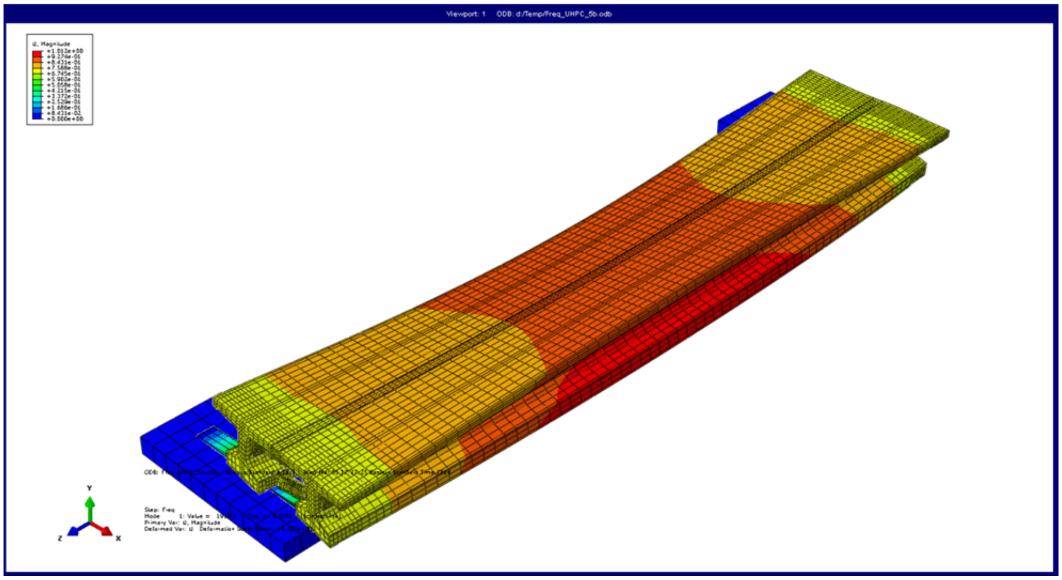

Figure 4-2 Transverse mode (frequency 6.97 Hz)

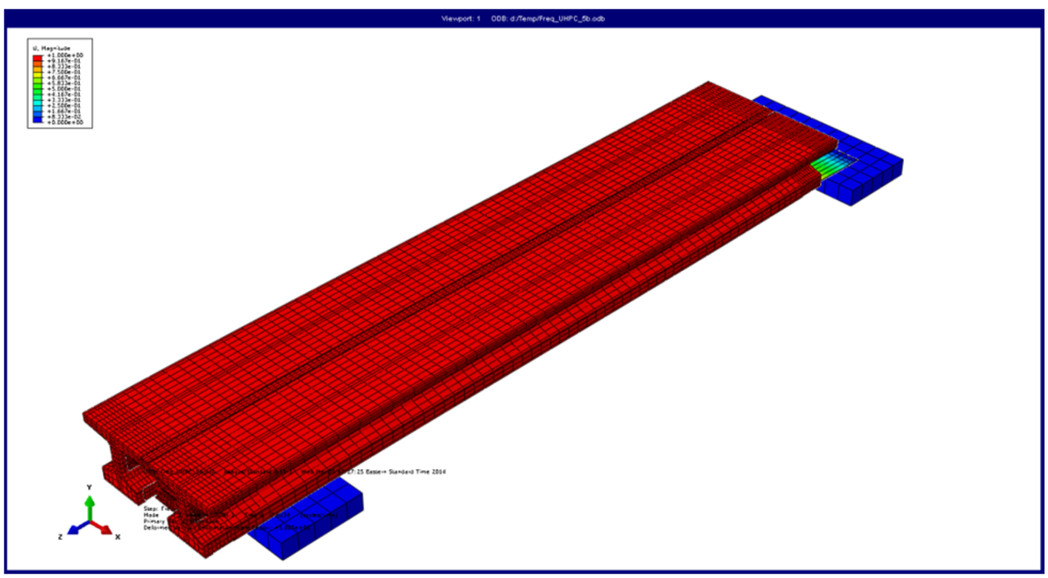

Figure 4-3 Longitudinal mode (frequency 7.62 Hz)

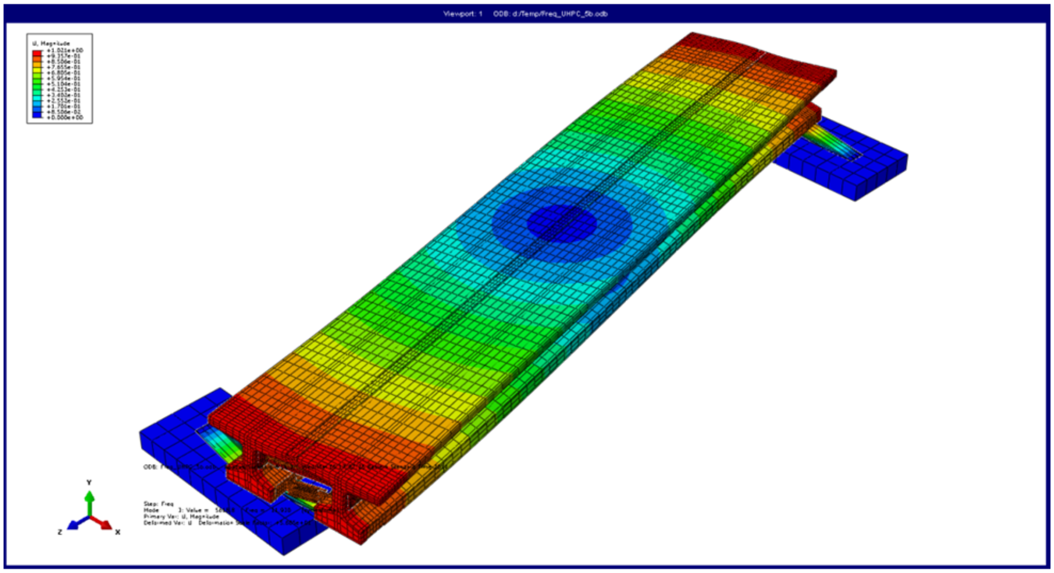

Figure 4-4 Rotational mode (frequency 11.91 Hz)

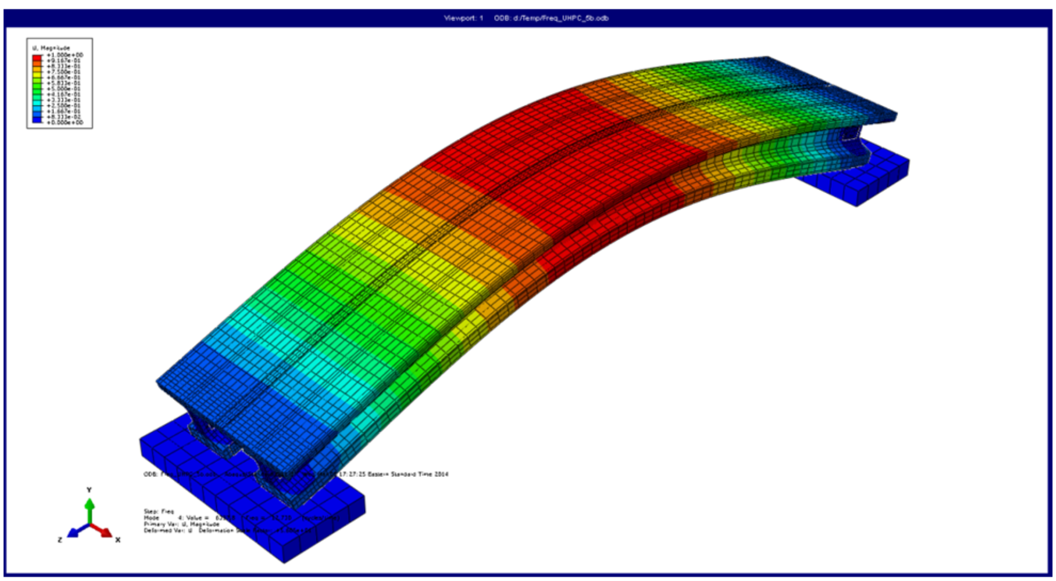

Figure 4-5 Vertical mode (frequency 12.73 Hz)

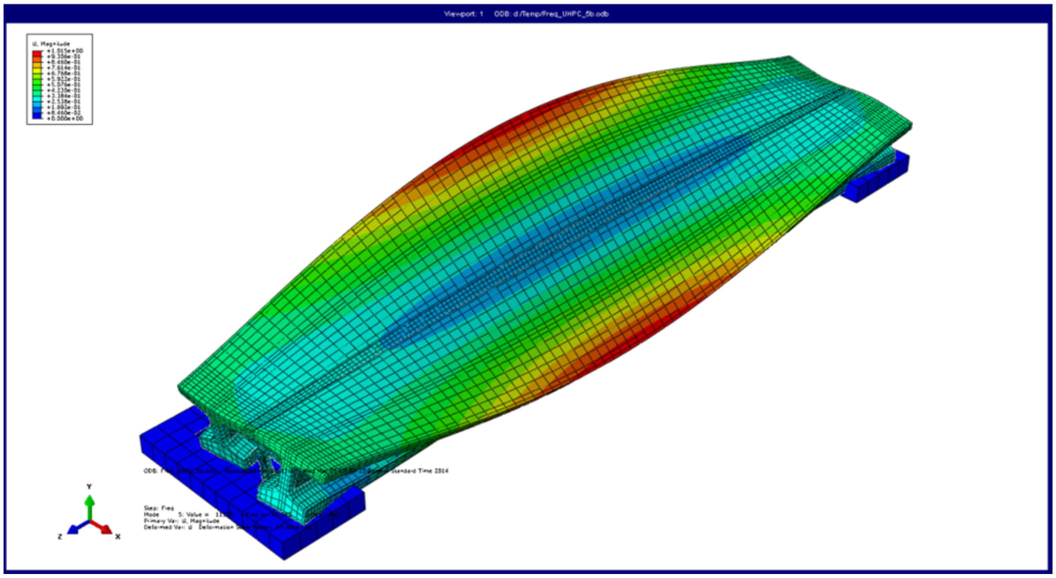

Figure 4-6 Combined vertical and transverse bending mode (frequency 16.95 Hz)

Table 4-2 presents both the experimental and numerical analysis values and Figure 4-7 through Figure 4-11 show the modes of the respective frequencies for the specimen in phase 2. The obtained parameters provide references for the design of the girder specimen.

Table 4-2 Natural frequencies of the specimen in phase 2

Modal Orders	Mode Shapes	FEM Model Frequencies (Hz)
1	Transverse translation	6.42
2	Longitudinal translation	7.02
3	Vertical bending	10.85
4	Rotation around vertical axis	11.91
5	Combined vertical and transverse bending	14.06

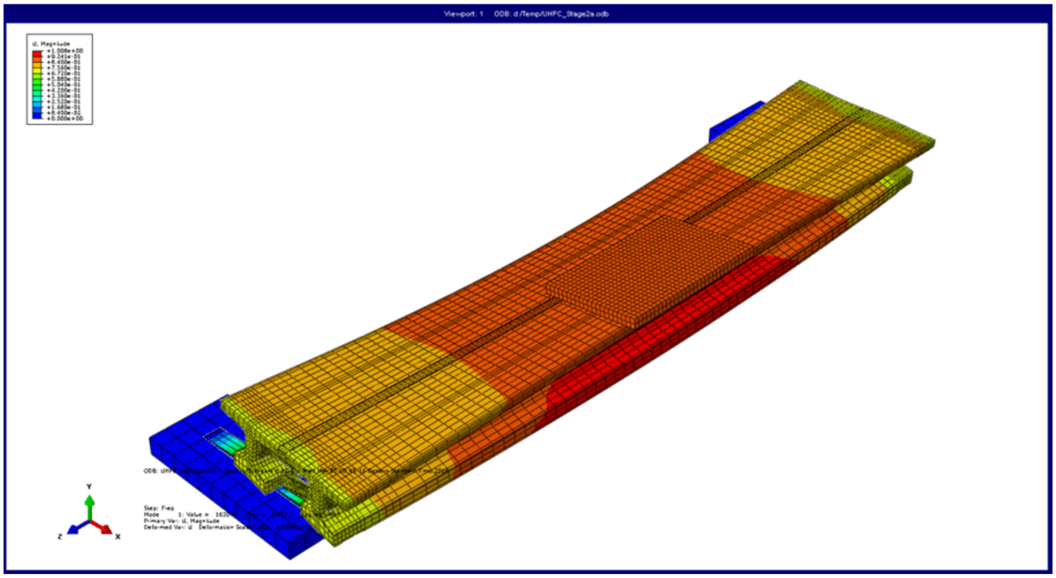

Figure 4-7 Transverse mode (frequency 6.42 Hz)

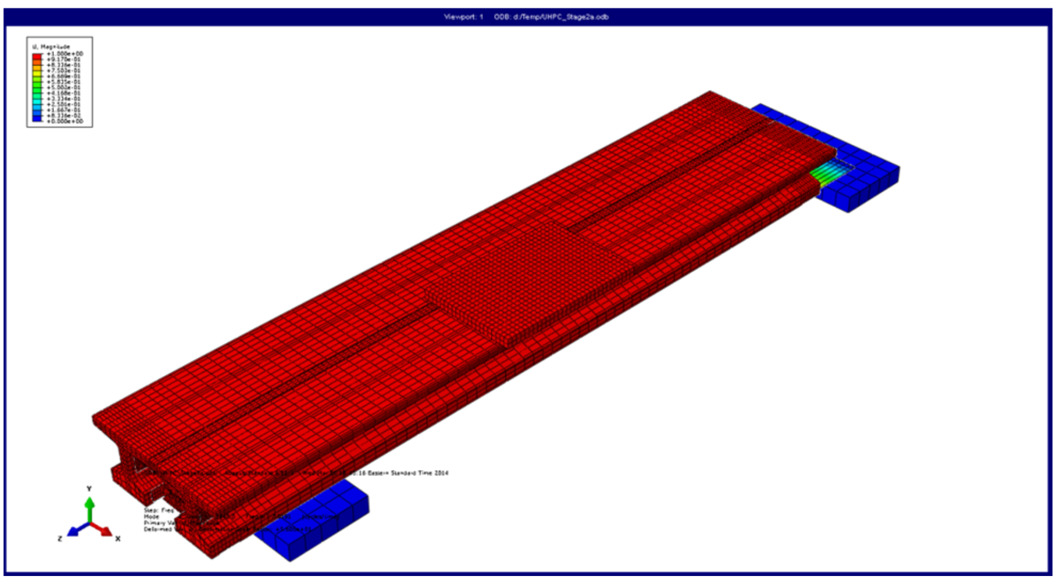

Figure 4-8 Longitudinal mode (frequency 7.02 Hz)

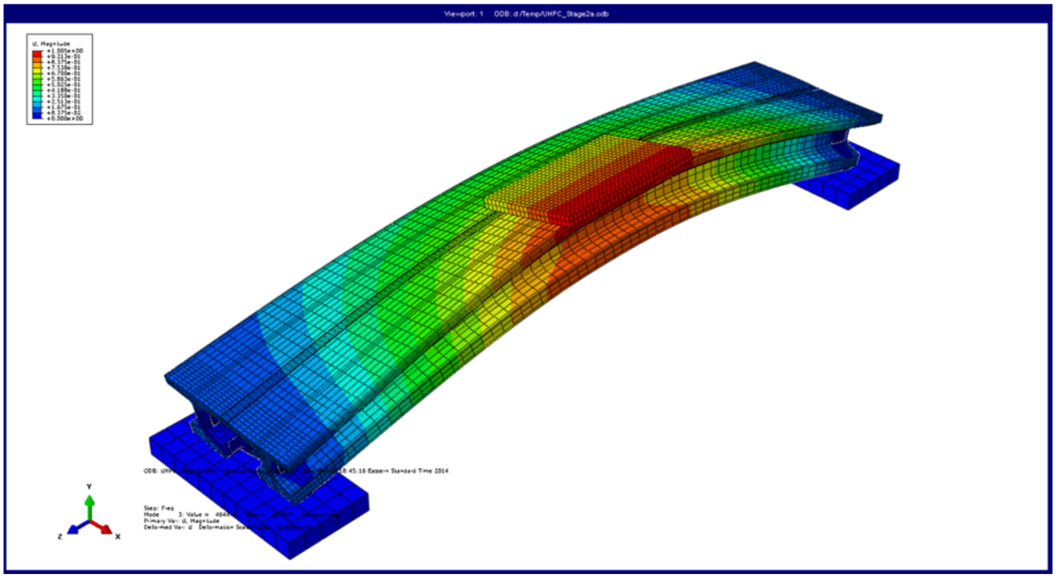

Figure 4-9 Vertical mode (frequency 10.85 Hz)

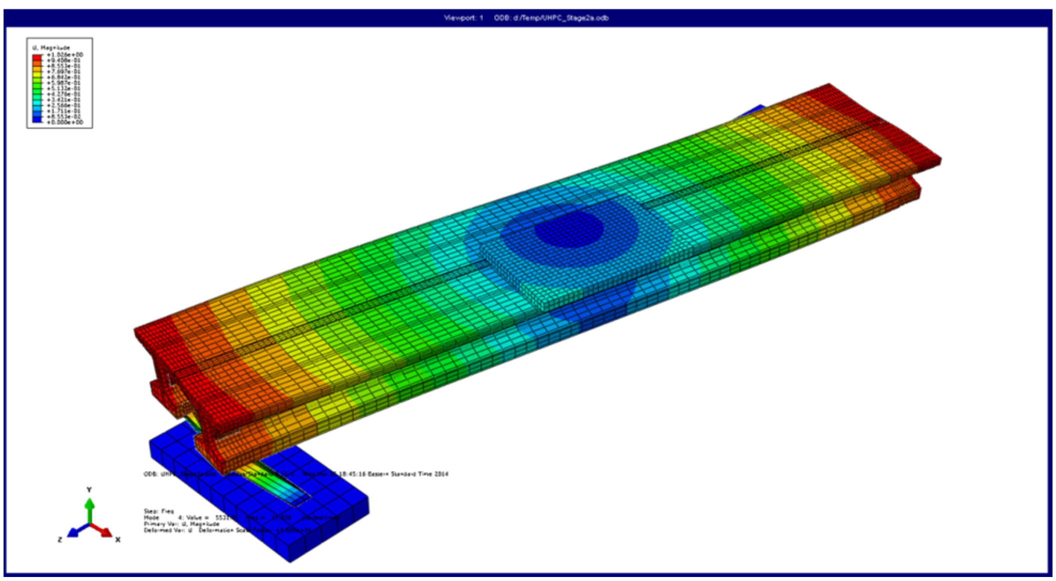

Figure 4-10 Rotational mode (frequency 11.82 Hz)

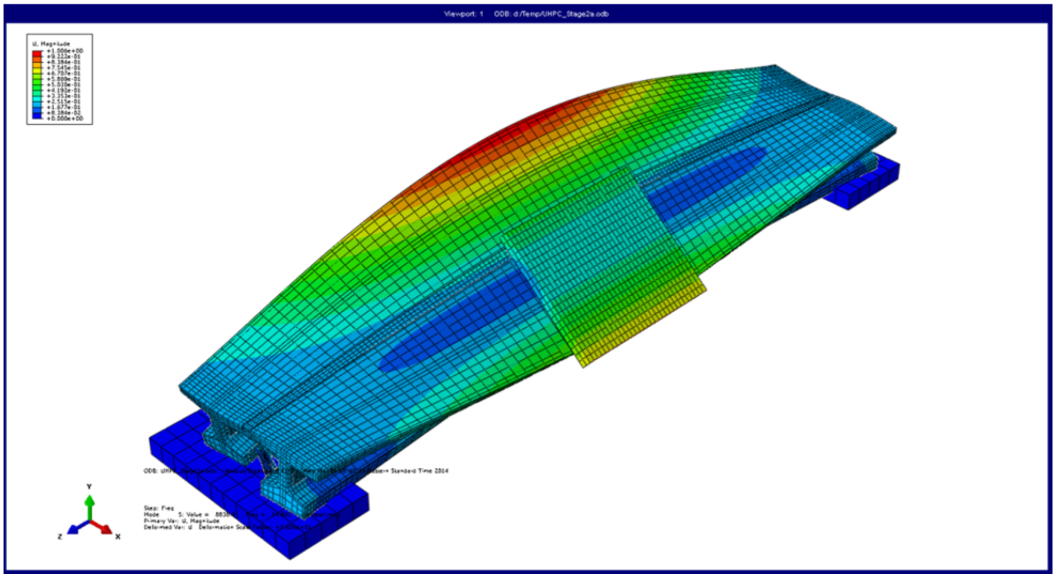

Figure 4-11 Combined vertical and transverse bending mode (frequency 14.06 Hz)

SECTION 5
SHAKE TABLE TESTING AND OBERSEVATIONS

5.1 Instrumentation

Before the shake table tests were conducted, 39 accelerometers, 19 linear variable differential transformers (LVDT) and 11 strain gages were installed on different locations of the specimen. The objective of the arrangements was focused on the seismic performance of the UHPC connection. A detailed list of all the instrumentation is given in Table 5-1. The arranged setup of accelerometers, LVDTs and strain gauges are shown in Figure 5-1,

Figure 5-2 and Figure 5-3, respectively.

Table 5-1 List of channel and sensors

No.	Channel Tag	Sensor Type	Position & Function	No. in Fig.
1	aext1x	Accelerometer (Capacity up to: 5g)	Shake Table 1, Longitudinal (E-W) Acceleration	1
2	aext1y	Accelerometer (Capacity up to: 5g)	Shake Table 1, Transverse (N-S) Acceleration	2
3	aext1z	Accelerometer (Capacity up to: 5g)	Shake Table 1, Vertical (U-D) Acceleration	3
4	aext2x	Accelerometer (Capacity up to: 5g)	Shake Table 2, Longitudinal (E-W) Acceleration	4
5	aext2y	Accelerometer (Capacity up to: 5g)	Shake Table 2, Transverse (N-S) Acceleration	5
6	aext2z	Accelerometer (Capacity up to: 5g)	Shake Table 2, Vertical (U-D) Acceleration	6
7	ABPWEW	Accelerometer (Capacity up to: 5g)	Midpoint of the Base Plate on the West Side, Longitudinal (E-W) Acceleration	7
8	ABPWNS	Accelerometer (Capacity up to: 5g)	Midpoint of the Base Plate on the West Side, Transverse (N-S) Acceleration	8
9	ABPWUD	Accelerometer (Capacity up to: 5g)	Midpoint of the Base Plate on the West Side, Vertical (U-D) Acceleration	9
10	ASPCNWEW	Accelerometer (Capacity up to: 5g)	North-West Corner of the Specimen, Longitudinal (E-W) Acceleration	10
11	ASPCNWNS	Accelerometer (Capacity up to: 5g)	North-West Corner of the Specimen, Transverse (N-S) Acceleration	11

No.	Channel Tag	Sensor Type	Position & Function	No. in Fig.
12	ASPCNWUD	Accelerometer (Capacity up to: 5g)	North-West Corner of the Specimen, Vertical (U-D) Acceleration	12
13	ASPCSWEW	Accelerometer (Capacity up to: 5g)	South-West Corner of the Specimen, Longitudinal (E-W) Acceleration	13
14	ASPCSWNS	Accelerometer (Capacity up to: 5g)	South-West Corner of the Specimen, Transverse (N-S) Acceleration	14
15	ASPCSWUD	Accelerometer (Capacity up to: 5g)	South-West Corner of the Specimen, Vertical (U-D) Acceleration	15
16	AOQSCEW	Accelerometer (Capacity up to: 5g)	One-Quarter Span of the Specimen on the Center, Longitudinal (E-W) Acceleration	16
17	AOQSCNS	Accelerometer (Capacity up to: 5g)	One-Quarter Span of the Specimen on the Center, Transverse (N-S) Acceleration	17
18	AOQSCUD	Accelerometer (Capacity up to: 5g)	One-Quarter Span of the Specimen on the Center, Vertical (U-D) Acceleration	18
19	ASPCMCEW	Accelerometer (Capacity up to: 5g)	Midpoint of the Specimen on the Center, Longitudinal (E-W) Acceleration	19
20	ASPCMCNS	Accelerometer (Capacity up to: 5g)	Midpoint of the Specimen on the Center, Transverse (N-S) Acceleration	20
21	ASPCMCUD	Accelerometer (Capacity up to: 5g)	Midpoint of the Specimen on the Center, Vertical (U-D) Acceleration	21
22	ASPCMNEW	Accelerometer (Capacity up to: 5g)	Midpoint of the Specimen on the North Side, Longitudinal (E-W) Acceleration	22
23	ASPCMNNS	Accelerometer (Capacity up to: 5g)	Midpoint of the Specimen on the North Side, Transverse (N-S) Acceleration	23
24	ASPCMNUD	Accelerometer (Capacity up to: 5g)	Midpoint of the Specimen on the North Side, Vertical (U-D) Acceleration	24
25	ASPCMSEW	Accelerometer (Capacity up to: 5g)	Midpoint of the Specimen on the South Side, Longitudinal (E-W) Acceleration	25
26	ASPCMSNS	Accelerometer (Capacity up to: 5g)	Midpoint of the Specimen on the South Side, Transverse (N-S) Acceleration	26
27	ASPCMSUD	Accelerometer (Capacity up to: 5g)	Midpoint of the Specimen on the South Side, Vertical (U-D) Acceleration	27

No.	Channel Tag	Sensor Type	Position & Function	No. in Fig.
28	ATQSCEW	Accelerometer (Capacity up to: 5g)	Three-Quarter Span of the Specimen on the Center, Longitudinal (E-W) Acceleration	28
29	ATQSCNS	Accelerometer (Capacity up to: 5g)	Three-Quarter Span of the Specimen on the Center, Transverse (N-S) Acceleration	29
30	ATQSCUD	Accelerometer (Capacity up to: 5g)	Three-Quarter Span of the Specimen on the Center, Vertical (U-D) Acceleration	30
31	ASPCNEEW	Accelerometer (Capacity up to: 5g)	North-East Corner of the Specimen, Longitudinal (E-W) Acceleration	31
32	ASPCNENS	Accelerometer (Capacity up to: 5g)	North-East Corner of the Specimen, Transverse (N-S) Acceleration	32
33	ASPCNEUD	Accelerometer (Capacity up to: 5g)	North-East Corner of the Specimen, Vertical (U-D) Acceleration	33
34	ASPCSEEW	Accelerometer (Capacity up to: 5g)	South-East Corner of the Specimen, Longitudinal (E-W) Acceleration	34
35	ASPCSENS	Accelerometer (Capacity up to: 5g)	South-East Corner of the Specimen, Transverse (N-S) Acceleration	35
36	ASPCSEUD	Accelerometer (Capacity up to: 5g)	South-East Corner of the Specimen, Vertical (U-D) Acceleration	36
37	ABPEEW	Accelerometer (Capacity up to: 5g)	Midpoint of the Base Plate on the East Side, Longitudinal (E-W) Acceleration	37
38	ABPENS	Accelerometer (Capacity up to: 5g)	Midpoint of the Base Plate on the East Side, Transverse (N-S) Acceleration	38
39	ABPEUD	Accelerometer (Capacity up to: 5g)	Midpoint of the Base Plate on the East Side, Vertical (U-D) Acceleration	39
40	DEXTNWEW	Displacement sensor (Capacity up to: +/- 10")	North-West Corner of the Extension Frame, Longitudinal (E-W) Displacement	1
41	DEXTNWNS	Displacement sensor (Capacity up to: +/- 10")	North-West Corner of the Extension Frame, Transverse (N-S) Displacement	2
42	DEXTNWUD	Displacement sensor (Capacity up to: +/- 10")	North-West Corner of the Extension Frame, Vertical (U-D) Displacement	3

No.	Channel Tag	Sensor Type	Position & Function	No. in Fig.
43	DSPCNWEW	Displacement sensor (Capacity up to: +/- 10"	North-West Corner of the Specimen, Longitudinal (E-W) Displacement	4
44	DSPCNWNS	Displacement sensor (Capacity up to: +/- 10"	North-West Corner of the Specimen, Transverse (N-S) Displacement	5
45	DSPCNWUD	Displacement sensor (Capacity up to: +/- 10"	North-West Corner of the Specimen, Vertical (U-D) Displacement	6
46	DSPCMSEW	Displacement sensor (Capacity up to: +/- 10"	Midpoint of the Specimen on the South Side, Longitudinal (E-W) Displacement	7
47	DSPCMSNS	Displacement sensor (Capacity up to: +/- 10"	Midpoint of the Specimen on the South Side, Transverse (N-S) Displacement	8
48	DSPCMSUD	Displacement sensor (Capacity up to: +/- 10"	Midpoint of the Specimen on the South Side, Vertical (U-D) Displacement	9
49	DSPCNEEW	Displacement sensor (Capacity up to: +/- 10"	North-East Corner of the Specimen, Longitudinal (E-W) Displacement	10
50	DSPCNENS	Displacement sensor (Capacity up to: +/- 10"	North-East Corner of the Specimen, Transverse (N-S) Displacement	11
51	DSPCNEUD	Displacement sensor (Capacity up to: +/- 10"	North-East Corner of the Specimen, Vertical (U-D) Displacement	12
52	DEXTNEEW	Displacement sensor (Capacity up to: +/- 10"	North-East Corner of the Extension Frame, Longitudinal (E-W) Displacement	13
53	DEXTNENS	Displacement sensor (Capacity up to: +/- 10"	North-East Corner of the Extension Frame, Transverse (N-S) Displacement	14
54	DEXTNEUD	Displacement sensor (Capacity up to: +/- 10"	North-East Corner of the Extension Frame, Vertical (U-D) Displacement	15

No.	Channel Tag	Sensor Type	Position & Function	No. in Fig.
55	DSPCRWEW	Displacement sensor (Capacity up to: +/- 10"	West Side of the Specimen, Relative Longitudinal (E-W) Displacement between Two Girder Decks	16
56	DSPCRWNS	Displacement sensor (Capacity up to: +/- 10"	West Side of the Specimen, Relative Transverse (N-S) Displacement between Two Girder Decks	17
57	DSPCRMEW	Displacement sensor (Capacity up to: +/- 10"	Mid-point of the Specimen, Relative Longitudinal (E-W) Displacement between Two Girder Decks	18
58	DSPCRMNS	Displacement sensor (Capacity up to: +/- 10"	Mid-point of the Specimen, Relative Transverse (N-S) Displacement between Two Girder Decks	19
59	SGDW	Strain gage 120 ohm	West Side of the Specimen, Strain of the Rebar in Girder 2	1
60	SUHW	Strain gage 120 ohm	West Side of the Specimen, Strain of the Rebar in UHPC Connection	2
61	SGDOQ	Strain gage 120 ohm	One-Quarter Span of the Specimen, Strain of the Rebar in Girder 2	3
62	SUHOQ	Strain gage 120 ohm	One-Quarter Span of the Specimen, Strain of the Rebar in UHPC Connection	4
63	SUHM1	Strain gage 120 ohm	Mid-span of the Specimen, Strain of the Rebar in UHPC Connection, Point1	5
64	SGDM1	Strain gage 120 ohm	Mid-span of the Specimen, Strain of the Rebar in Girder 2, Point1	6
65	SUHM2	Strain gage 120 ohm	Mid-span of the Specimen, Strain of the Rebar in UHPC Connection, Point2	7
66	SGDM2	Strain gage 120 ohm	Mid-span of the Specimen, Strain of the Rebar in Girder 1, Point2	8
67	SGDM3	Strain gage 120 ohm	Mid-span of the Specimen, Strain of the Rebar in Girder 2, Point3	9
68	SGDTQ	Strain gage 120 ohm	Three-Quarter Span of the Specimen, Strain of the Rebar in Girder 2	10
69	SUHTQ	Strain gage 120 ohm	Three-Quarter Span of the Specimen, Strain of the Rebar in UHPC Connection	11

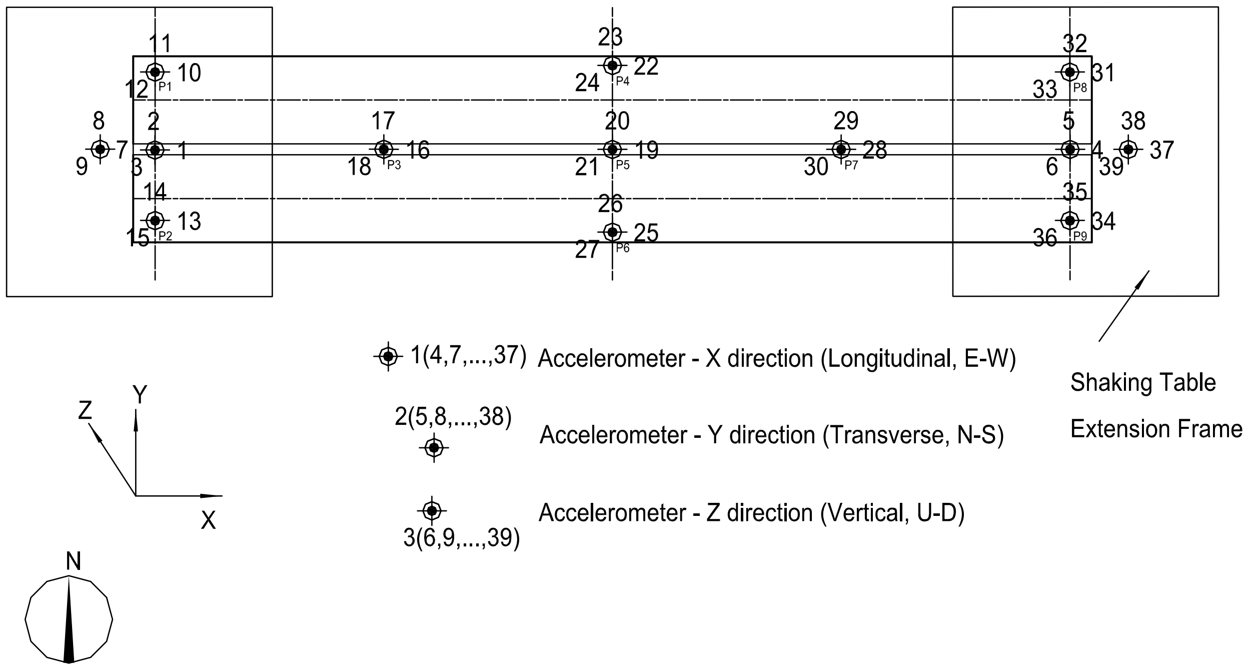

Figure 5-1 Setup of accelerometers

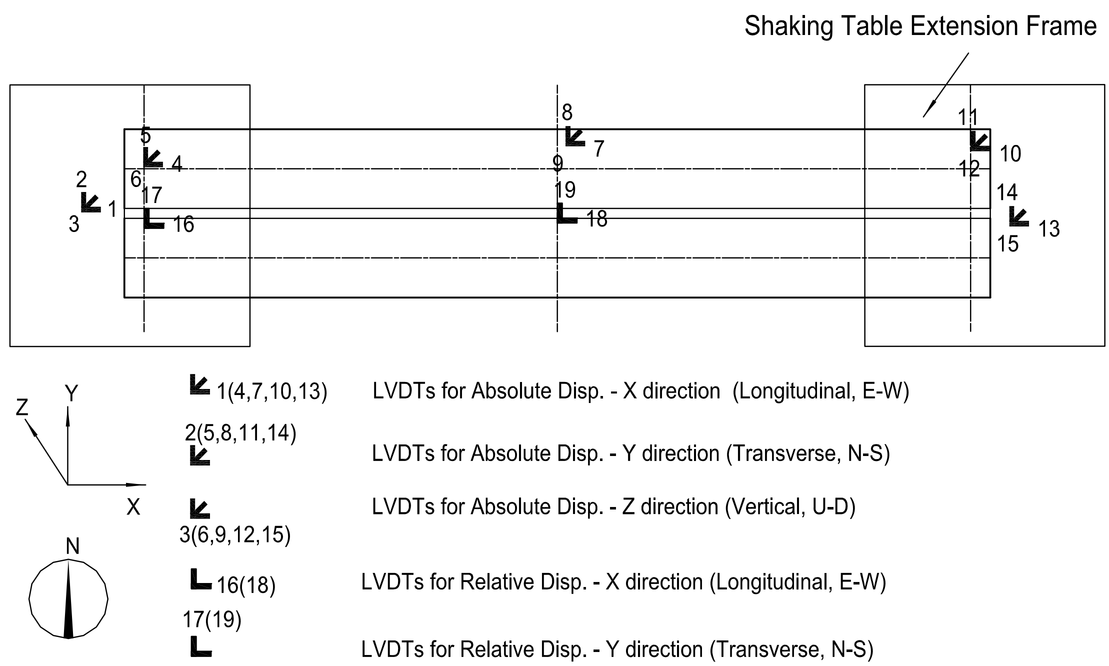

Figure 5-2 Setup of LVDTs

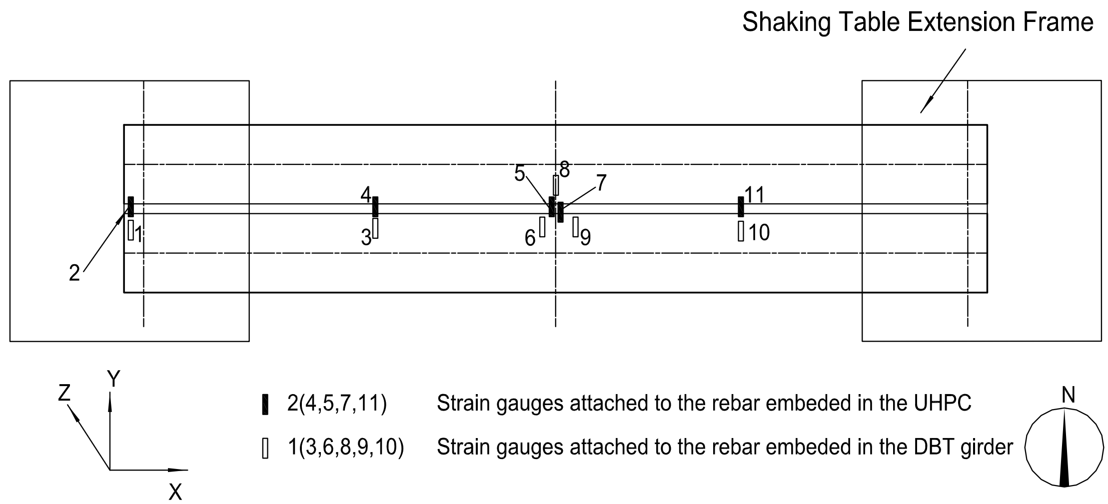

Figure 5-3 Setup of strain gauges

It is noteworthy that the relative displacements in both the longitudinal and transverse directions of the connection were measured in the mid span and the west side of the girder, as shown in Figure 5-4.

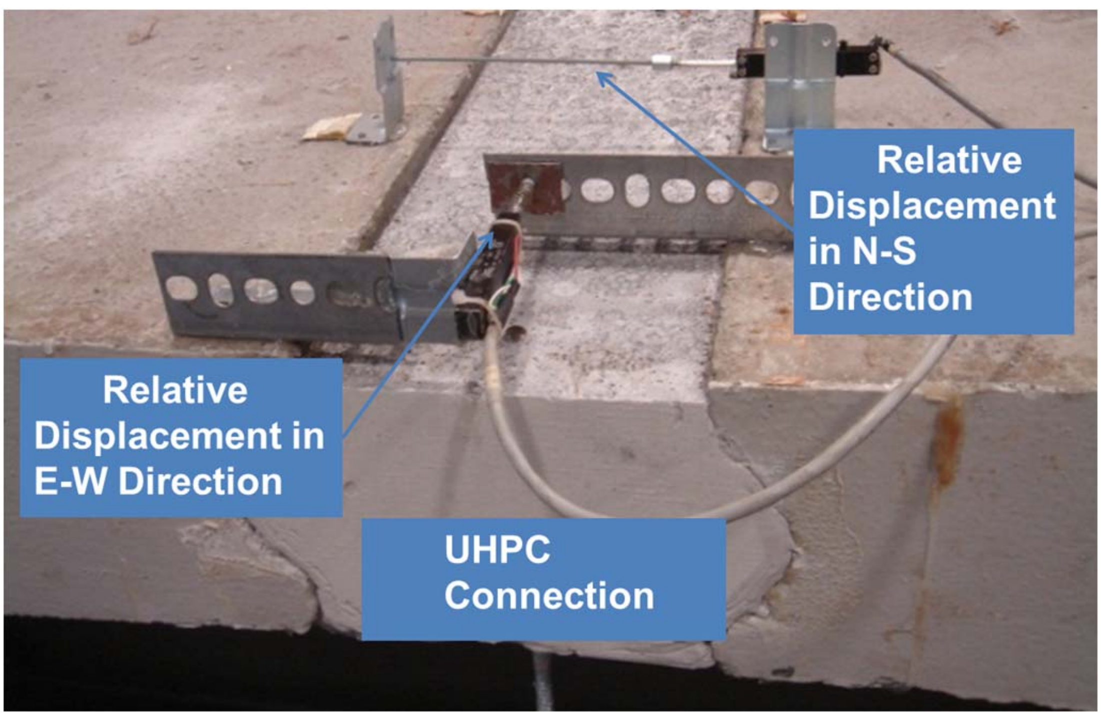

Figure 5-4 Setup of LVDTs measuring relative displacements

5.2 Selection of Ground Motion Records

Two ground motion (GM) ensembles were considered in this study; a Far-field GM set, including five GM records that were selected from the FEMA P695 Far-field GM ensemble (FEMA P695, 2009), and a Near-fault GM set, consisting of six GM records selected from the FEMA P695 Near-fault GM ensemble (FEMA P695, 2009). The FEMA P695 GM ensembles contain GMs that were recorded during strong earthquakes from all over the world and are representative of the seismicity in the Western United States. The GMs used in this test were selected based on the methodology developed by Sideris (2012). All the selected GMs are listed in Table 5-2.

Table 5-2 Experimental near-field ground motion set

No.	ID in FEMA 695	Magnitude	Year	Name	Pulse (defined by FEMA 695)
Far 1	4	7.1	1999	Hector Mine	No
Far 2	5	6.5	1979	Imperial Valley	No
Far 3	7	6.9	1995	Kobe, Japan	No
Far 4	12	7.3	1992	Landers	No
Far 5	19	7.6	1999	Chi-Chi, Taiwan	No
Near 1	1	6.5	1979	Imperial Valley	Yes
Near 2	7	7	1992	Cape Mendocino	Yes
Near 3	9	6.7	1994	Northridge	Yes
Near 4	15	6.8	1976	Gazli, USSR	No
Near 5	21	6.9	1989	Loma Prieta	No
Near 6	25	7.5	1999	Kocaeli, Turkey	No

Since this test is considered a full-size girder test, none of the GM ensembles were scaled in the time domain. The time-history of these GMs are shown in Appendix B. Also, the GM data were not processed in the frequency domain, except when slight processing of some components was needed to meet shake table limitations and avoid possible damage (to the shake table) due to the large displacement.

To investigate the seismic performance of the UHPC connected girders under different seismic levels, all the ground motions were linearly scaled to match several seismic hazard levels of interest, including an elastic limit (EL), a design earthquake (DE) having a probability of exceedance of 10% in 50 years (10%/50 years) given by the AASHTO LRFD Bridge Design Specification (2010), the maximum considered earthquake (MCE) defined as 3/2 of the DE hazard as recommended by ASCE/SEI 7-05 (2006), two times of DE (DE2) and the maximum possible acceleration (MAX).

Based on the previous research by Sideris (2012), the response spectrum of all components of the selected ground motions are shown in Figure 5-5.

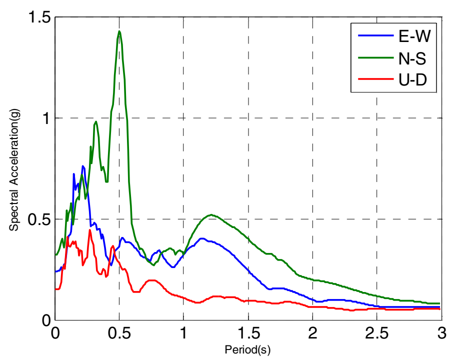

(a) Far 1

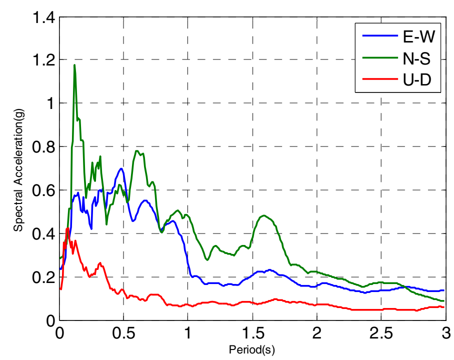

(b) Far 2

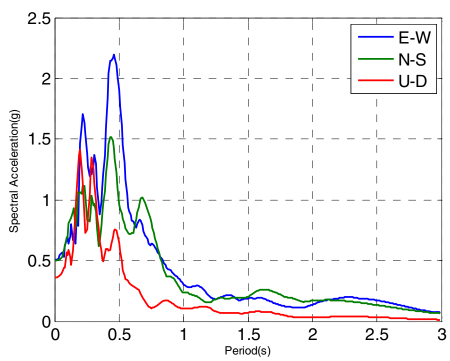

(c) Far 3

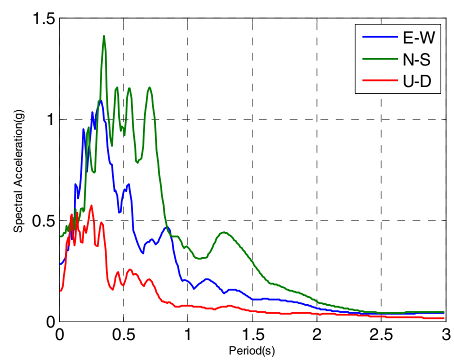

(d) Far 4

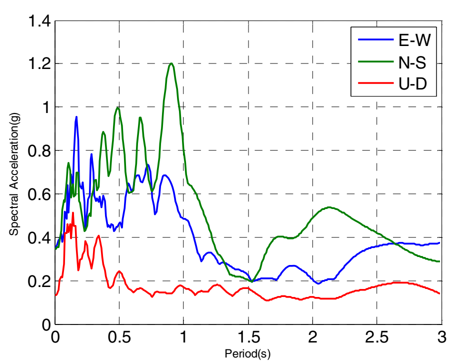

(e) Far 5

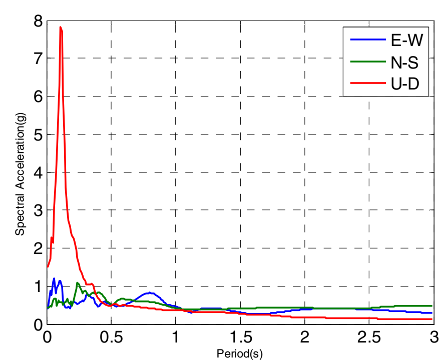

(f) Near 1

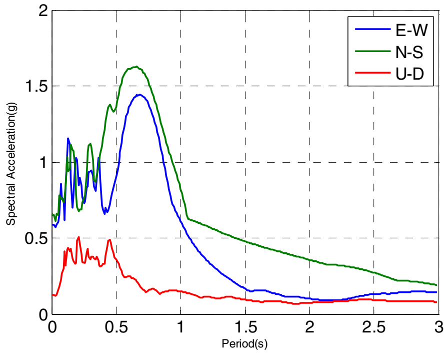

(g) Near 2

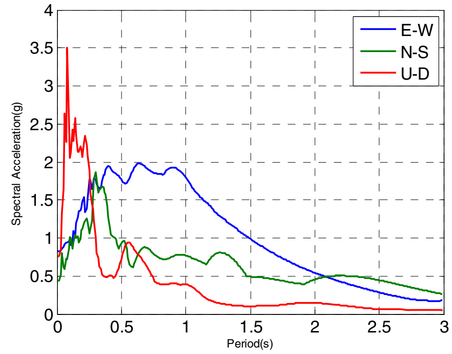

(h) Near 3

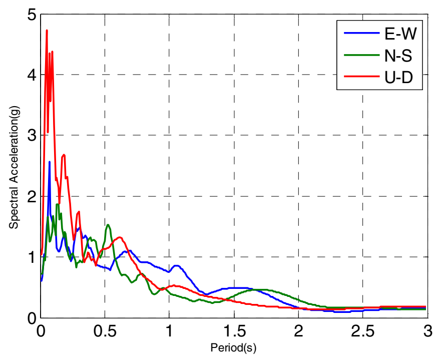

(i) Near 4

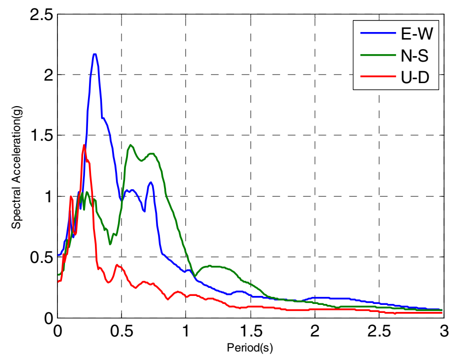

(j) Near 5

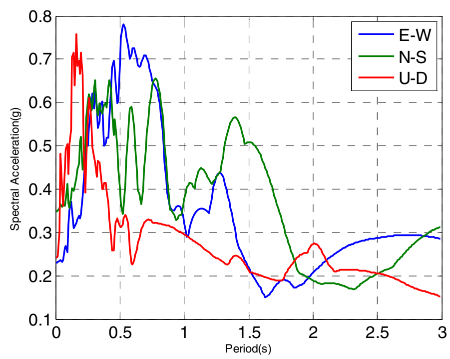

(k) Near 6

Figure 5-5 Response spectrum of selected GMs

5.3 Test Phases

Multiple seismic tests were conducted on the test specimen with three test phases, as shown in Table 5-3. The first phase was the two DBT girders with two sets of diaphragms at both ends, the second phase was the two girders loaded with two steel plates for simulating the live load, and the third phase was the two girders loaded with two steel plates but without any diaphragms. Low amplitude white noise tests were conducted between seismic levels and test phases to determine the changes of dynamic characteristics (natural frequencies, damping ratio etc.) of the test specimen and to identify the occurrence of damage during the increasing levels of ground motion excitations. Visual inspections were also conducted after each test phase.

Table 5-3 Summary of test phases

Test Phase	Test specimen configuration
1	Two girders connected by UHPC with diaphragms at both ends
2	Test Phase 1 specimen with two stacked steel plates (to simulate live load)
3	Test Phase 2 specimen without diaphragms

In phase two, to evaluate the worst scenario of UHPC connection in practical engineering, two steel plates were stacked on one of the girders to generate unbalanced live loads, as depicted in Figure 5-6.

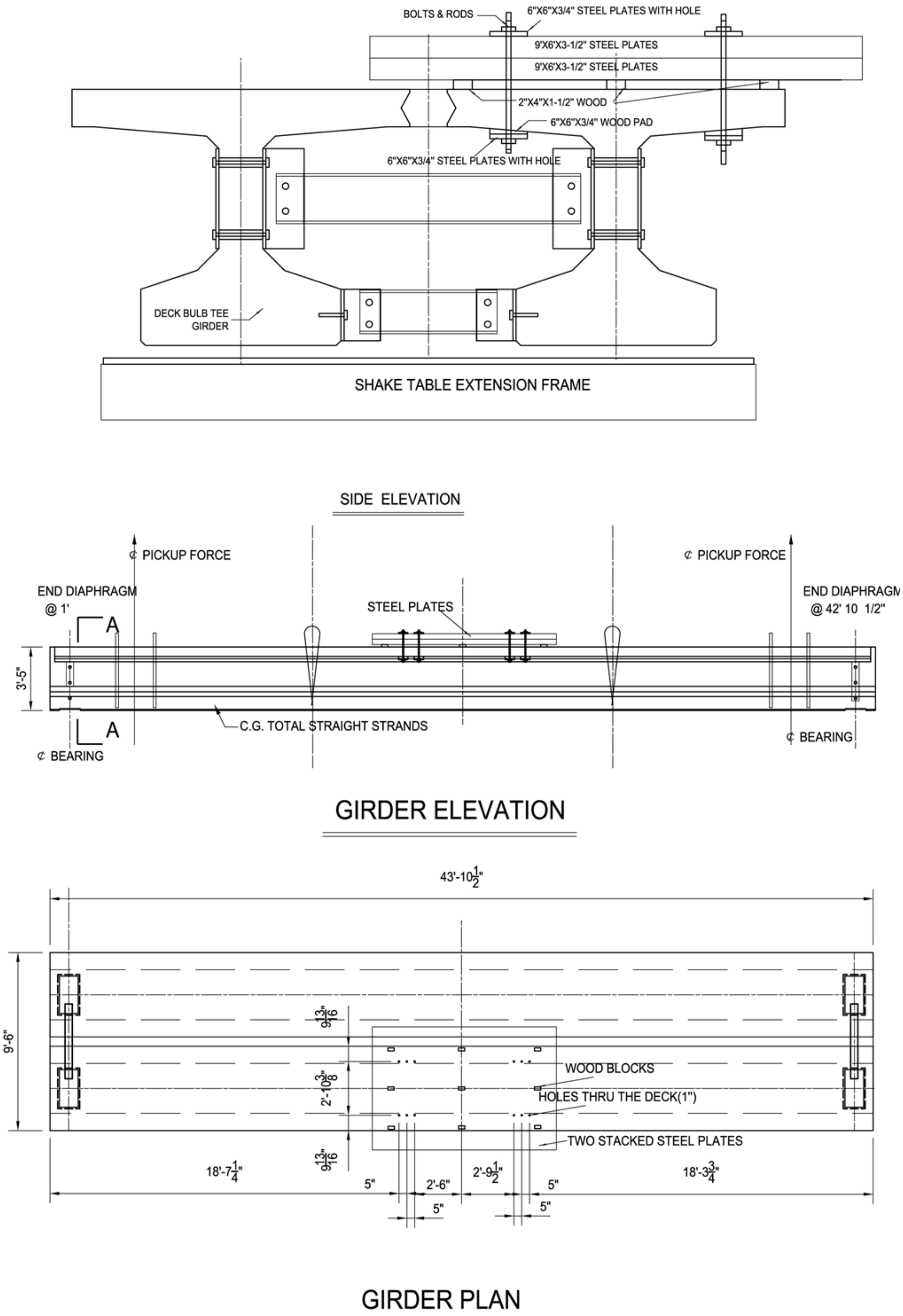

Figure 5-6 Test setup for phase 2 shake table test (with live load)

5.4 Test Protocol

Using the GM sets of Table 5-2, several shake table tests were conducted in the three test phases. All these combinations resulted in nearly 132 shake table tests, while 40 tests for the purpose of system identification (low amplitude white noise tests) were conducted between the seismic tests to monitor the progress of possible damage in the experimental specimen. A detailed list of shake table testing protocols is shown in Table 5-4. Note that the excitations of all GMs were amplified by 20% in phase 2 to test the specimen in the worst scenario. In test phase 3, the GM sets were excited on the shake tables only in their maximum accelerations.

Table 5-4 Test protocol

Test No.	Test Label	Excitation	PGA (highest DOF)	Target level (all DOFs)	Note
			g	%	
1	INIWN10	White Noise - H&V	0.1	N/A	System Identification (Initial)
2	Near5EL	Near5 - H&V	0.090	14	Elastic Range
3	Near3EL	Near3 - H&V	0.090	14	Elastic Range
4	Far5EL	Far5 - H&V	0.090	14	Elastic Range
5	Far4EL	Far4 - H&V	0.090	14	Elastic Range
6	Near4EL	Near4 - H&V	0.090	14	Elastic Range
7	Far1EL	Far1 - H&V	0.090	14	Elastic Range
8	Far3EL	Far3 - H&V	0.090	14	Elastic Range
9	Near6EL	Near6 - H&V	0.090	14	Elastic Range
10	Near1EL	Near1 - H&V	0.090	14	Elastic Range
11	Near2EL	Near2 - H&V	0.090	14	Elastic Range
12	Far2EL	Far2 - H&V	0.090	14	Elastic Range
13	WNEL10EW	White noise - long.	0.1	N/A	System identification
14	WNEL10NSR	White noise - lat	0.1	N/A	System identification
15	WNEL10UD	White noise - vert	0.1	N/A	System identification
15r	Near5DE	Near5 - H&V	0.180	28	Elastic Range
16	Near3DE	Near3 - H&V	0.180	28	Elastic Range
17	Far5DE	Far5 - H&V	0.180	28	Elastic Range
18	Far4DE	Far4 - H&V	0.180	28	Elastic Range
19	Near4DE	Near4 - H&V	0.180	28	Elastic Range
20	Far1DE	Far1 - H&V	0.180	28	Elastic Range
21	Far3DE	Far3 - H&V	0.180	28	Elastic Range
22	Near6DE	Near6 - H&V	0.180	28	Elastic Range
23	Near1DE	Near1 - H&V	0.180	28	Elastic Range
24	Near2DE	Near2 - H&V	0.180	28	Elastic Range
25	Far2DE	Far2 - H&V	0.180	28	Elastic Range
26	WNDE10EW	White noise - long.	0.1	N/A	System identification

Test No.	Test Label	Excitation	PGA (highest DOF)	Target level (all DOFs)	Note
			g	%	
27	WNDE10NS	White noise - lat	0.1	N/A	System identification
28	WNDE10UD	White noise - vert	0.1	N/A	System identification
29	Near5MCE	Near5 - H&V	0.270	42	Elastic Range
30	Near3MCE	Near3 - H&V	0.270	42	Elastic Range
31	Far5MCE	Far5 - H&V	0.270	42	Elastic Range
32	Far4MCE	Far4 - H&V	0.270	42	Elastic Range
33	Near4MCE	Near4 - H&V	0.270	42	Elastic Range
34	Far1MCE	Far1 - H&V	0.270	42	Elastic Range
35	Far3MCE	Far3 - H&V	0.270	42	Elastic Range
36	Near6MCE	Near6 - H&V	0.270	42	Elastic Range
37	Near1MCE	Near1 - H&V	0.270	42	Elastic Range
38	Near2MCE	Near2 - H&V	0.270	42	Elastic Range
39	Far2MCE	Far2 - H&V	0.270	42	Elastic Range
40	WNMCE10EW	White noise - long.	0.1	N/A	System identification
41	WNMCE10NS	White noise - lat	0.1	N/A	System identification
42	WNMCE10UD	White noise - vert	0.1	N/A	System identification
43	Near5DEX2	Near5 - H&V	0.432	67	Elastic Range
44	Near3DEX2	Near3 - H&V	0.432	67	Elastic Range
45	Far5DEX2	Far5 - H&V	0.432	67	Elastic Range
46	Far4DEX2	Far4 - H&V	0.432	67	Elastic Range
47	Near4DEX2	Near4 - H&V	0.432	67	Elastic Range
48	Far1DEX2	Far1 - H&V	0.432	67	Elastic Range
49	Far3DEX2	Far3 - H&V	0.432	67	Elastic Range
50	Near6DEX2	Near6 - H&V	0.432	67	Elastic Range
51	Near1DEX2	Near1 - H&V	0.432	67	Elastic Range
52	Near2DEX2	Near2 - H&V	0.432	67	Elastic Range
53	Far2DEX2	Far2 - H&V	0.432	67	Elastic Range
54	WN2DE10EW	White noise - long.	0.1	N/A	System identification
55	WN2DE10NS	White noise - lat	0.1	N/A	System identification
56	WN2DE10UD	White noise - vert	0.1	N/A	System identification
57	Near5MAX	Near5 - H&V	0.648	100	Elastic Range
58	Near3MAX	Near3 - H&V	0.648	100	Elastic Range
59	Far5MAX	Far5 - H&V	0.648	100	Elastic Range
60	Far4MAX	Far4 - H&V	0.648	100	Elastic Range
61	Near4MAX	Near4 - H&V	0.648	100	Elastic Range
62	Far1MAX	Far1 - H&V	0.648	100	Elastic Range
63	Far3MAX	Far3 - H&V	0.648	100	Elastic Range
64	Near6MAX	Near6 - H&V	0.648	100	Elastic Range
65	Near1MAX	Near1 - H&V	0.648	100	Elastic Range

Test No.	Test Label	Excitation	PGA (highest DOF)	Target level (all DOFs)	Note
			g	%	
66	Near2MAX	Near2 - H&V	0.648	100	Elastic Range
67	Far2MAX	Far2 - H&V	0.648	100	Elastic Range
68	WNMAX10EW	White noise - long.	0.1	N/A	System identification
69	WNMAX10NS	White noise - lat	0.1	N/A	System identification
70	WNMAX10UD	White noise - vert	0.1	N/A	System identification
71	WNINI10EWP2	White noise - long.	0.1	N/A	System identification
72	WNINI10NSP2	White noise - lat	0.1	N/A	System identification
73	WNINI10UDP2	White noise - vert	0.1	N/A	System identification
74	Near5ELP2	Near5 - H&V	0.090	14	Elastic Range
75	Near3ELP2	Near3 - H&V	0.090	14	Elastic Range
76	Far5ELP2	Far5 - H&V	0.090	14	Elastic Range
77	Far4ELP2	Far4 - H&V	0.090	14	Elastic Range
78	Near4ELP2	Near4 - H&V	0.090	14	Elastic Range
79	Far1ELP2	Far1 - H&V	0.090	14	Elastic Range
80	Far3ELP2	Far3 - H&V	0.090	14	Elastic Range
81	Near6ELP2	Near6 - H&V	0.090	14	Elastic Range
82	Near1ELP2	Near1 - H&V	0.090	14	Elastic Range
83	Near2ELP2	Near2 - H&V	0.090	14	Elastic Range
84	Far2ELP2	Far2 - H&V	0.090	14	Elastic Range
85	WNEL10EWP2	White noise - long.	0.1	N/A	System identification
86	WNEL10NSP2	White noise - lat	0.1	N/A	System identification
87	WNEL10UDP2	White noise - vert	0.1	N/A	System identification
88	Near5DEP2P2	Near5 - H&V	0.180	28	Elastic Range
89	Near3DEP2	Near3 - H&V	0.180	28	Elastic Range
90	Far5DEP2	Far5 - H&V	0.180	28	Elastic Range
91	Far4DEP2	Far4 - H&V	0.180	28	Elastic Range
92	Near4DEP2	Near4 - H&V	0.180	28	Elastic Range
93	Far1DEP2	Far1 - H&V	0.180	28	Elastic Range
94	Far3DEP2	Far3 - H&V	0.180	28	Elastic Range
95	Near6DEP2	Near6 - H&V	0.180	28	Elastic Range
96	Near1DEP2	Near1 - H&V	0.180	28	Elastic Range
97	Near2DEP2	Near2 - H&V	0.180	28	Elastic Range
98	Far2DEP2	Far2 - H&V	0.180	28	Elastic Range
99	WNDEP210EWP2	White noise - long.	0.1	N/A	System identification
100	WNDEP210NSP2	White noise - lat	0.1	N/A	System identification
101	WNDEP210UDP2	White noise - vert	0.1	N/A	System identification
102	Near5MCEP2	Near5 - H&V	0.270	42	Elastic Range
103	Near3MCEP2	Near3 - H&V	0.270	42	Elastic Range

Test No.	Test Label	Excitation	PGA (highest DOF)	Target level (all DOFs)	Note
			g	%	
104	Far5MCEP2	Far5 - H&V	0.270	42	Elastic Range
105	Far4MCEP2	Far4 - H&V	0.270	42	Elastic Range
106	Near4MCEP2	Near4 - H&V	0.270	42	Elastic Range
107	Far1MCEP2	Far1 - H&V	0.270	42	Elastic Range
108	Far3MCEP2	Far3 - H&V	0.270	42	Elastic Range
109	Near6MCEP2	Near6 - H&V	0.270	42	Elastic Range
110	Near1MCEP2	Near1 - H&V	0.270	42	Elastic Range
111	Near2MCEP2	Near2 - H&V	0.270	42	Elastic Range
112	Far2MCEP2	Far2 - H&V	0.270	42	Elastic Range
113	WNMCE10EWP2	White noise - long.	0.1	N/A	System identification
114	WNMCE10NSP2	White noise - lat	0.1	N/A	System identification
115	WNMCE10UDP2	White noise - vert	0.1	N/A	System identification
116	Near5DEX2P2	Near5 - H&V	0.432	67	Elastic Range
117	Near3DEX2P2	Near3 - H&V	0.432	67	Elastic Range
118	Far5DEX2P2	Far5 - H&V	0.432	67	Elastic Range
119	Far4DEX2P2	Far4 - H&V	0.432	67	Elastic Range
120	Near4DEX2P2	Near4 - H&V	0.432	67	Elastic Range
121	Far1DEX2P2	Far1 - H&V	0.432	67	Elastic Range
122	Far3DEX2P2	Far3 - H&V	0.432	67	Elastic Range
123	Near6DEX2P2	Near6 - H&V	0.432	67	Elastic Range
124	Near1DEX2P2	Near1 - H&V	0.432	67	Elastic Range
125	Near2DEX2P2	Near2 - H&V	0.432	67	Elastic Range
126	Far2DEX2P2	Far2 - H&V	0.432	67	Elastic Range
127	WN2DE10EWP2	White noise - long.	0.1	N/A	System identification
128	WN2DE10NSP2	White noise - lat	0.1	N/A	System identification
129	WN2DE10UDP2	White noise - vert	0.1	N/A	System identification
130	Near5MAXP2	Near5 - H&V	0.648	100	Elastic Range
131	Near3MAXP2	Near3 - H&V	0.648	100	Elastic Range
132	Far5MAXP2	Far5 - H&V	0.648	100	Elastic Range
133	Far4MAXP2	Far4 - H&V	0.648	100	Elastic Range
134	Near4MAXP2	Near4 - H&V	0.648	100	Elastic Range
135	Far1MAXP2	Far1 - H&V	0.648	100	Elastic Range
136	Far3MAXP2	Far3 - H&V	0.648	100	Elastic Range
137	Near6MAXP2	Near6 - H&V	0.648	100	Elastic Range
138	Near1MAXP2	Near1 - H&V	0.648	100	Elastic Range
139	Near2MAXP2	Near2 - H&V	0.648	100	Elastic Range
140	Far2MAXP2	Far2 - H&V	0.648	100	Elastic Range
141	WNMAX10EWP2	White noise - long.	0.1	N/A	System identification
142	WNMAX10NSP2	White noise - lat	0.1	N/A	System identification

Test No.	Test Label	Excitation	PGA (highest DOF)	Target level (all DOFs)	Note
			g	%	
143	WNMAX10UDP2	White noise - vert	0.1	N/A	System identification
144	Near5X120P2	Near5 - H&V	0.778	100	Elastic Range
145	Near3X120P2	Near3 - H&V	0.778	100	Elastic Range
146	Far5X120P2	Far5 - H&V	0.778	100	Elastic Range
147	Far4X120P2	Far4 - H&V	0.778	100	Elastic Range
148	Near4X120P2	Near4 - H&V	0.778	100	Elastic Range
149	Far1X120P2	Far1 - H&V	0.778	100	Elastic Range
150	Far3X120P2	Far3 - H&V	0.778	100	Elastic Range
151	Near6X120P2	Near6 - H&V	0.778	100	Elastic Range
152	Near1X120P2	Near1 - H&V	0.778	100	Elastic Range
153	Near2X120P2	Near2 - H&V	0.778	100	Elastic Range
154	Far2X120P2	Far2 - H&V	0.778	100	Elastic Range
155	WN10X120EWP3	White noise - long.	0.1	N/A	System identification
156	WN10X120NSP3	White noise - lat	0.1	N/A	System identification
157	WN10X120UDP3	White noise - vert	0.1	N/A	System identification
158	Near6X115P2	Near6 - H&V	0.778	100	Elastic Range
159	Near5MAXP3	Near5 - H&V	0.648	100	Elastic Range
153r	Near3MAXP3	Near3 - H&V	0.648	100	Elastic Range
160	Far5MAXP3	Far5 - H&V	0.648	100	Elastic Range
161	Far4MAXP3	Far4 - H&V	0.648	100	Elastic Range
162	Near4MAXP3	Near4 - H&V	0.648	100	Elastic Range
163	Far1MAXP3	Far1 - H&V	0.648	100	Elastic Range
164	Far3MAXP3	Far3 - H&V	0.648	100	Elastic Range
165	Near6MAXP3	Near6 - H&V	0.648	100	Elastic Range
166	Near1MAXP3	Near1 - H&V	0.648	100	Elastic Range
167	Near2MAXP3	Near2 - H&V	0.648	100	Elastic Range
168	Far2MAXP3	Far2 - H&V	0.648	100	Elastic Range
169	WNMAX10EWP3	White noise - long.	0.1	N/A	System identification
170	WNMAX10NSP3	White noise - lat	0.1	N/A	System identification
171	WNMAX10UDP3	White noise - vert	0.1	N/A	System identification

5.5 Response of the Girder

The acceleration histories recorded at the mid-span and at the foundation based on data obtained during this test are presented in Figure 5-7. According to this figure, significant amplification (3.92 times) of the imposed motion was recorded at the mid-span of the deck, which may be attributed to resonance as considerable portions of the energy of the imposed motion were distributed in a frequency range that contains the fundamental (vertical) frequency of the superstructure, as shown in Figure 5-8. The maximum acceleration recorded was 6.1 g.

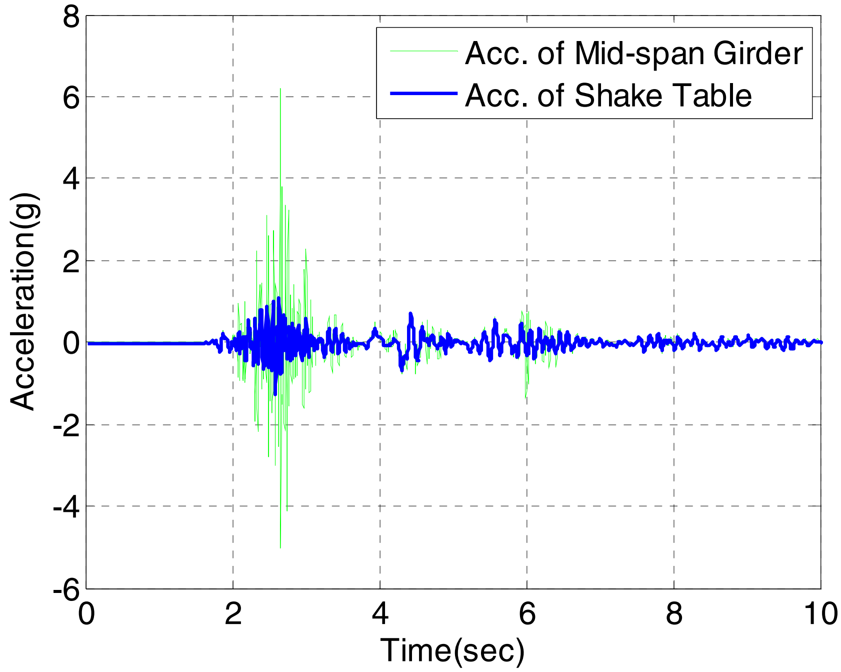

Figure 5-7 Maximum acceleration response of shake table and girder, phase 1

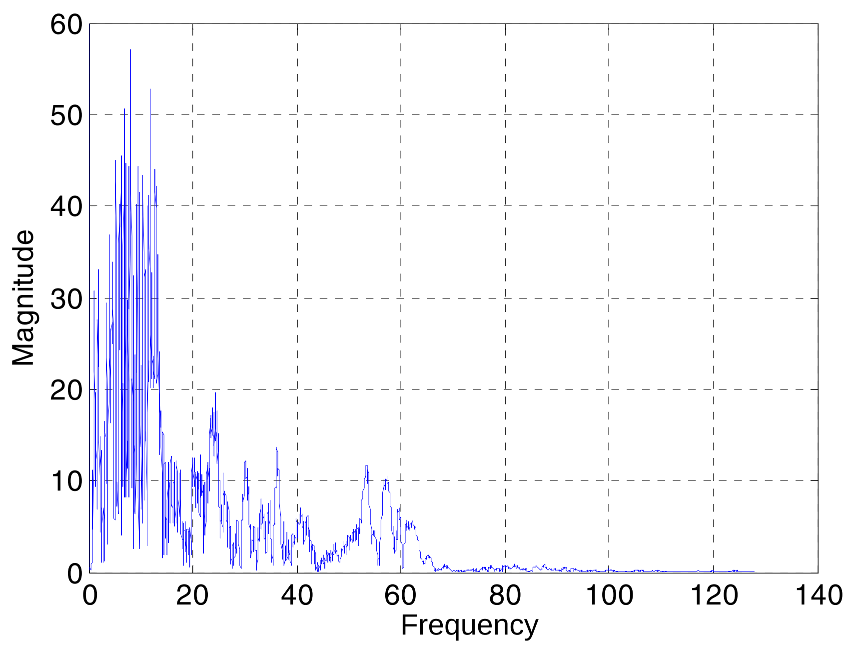

Figure 5-8 Frequency component of shake table input, phase 1

5.6 Observed Minor Concrete Cracks in the Test Specimen

Throughout the entire test program, no obvious damage was found in the girder specimen. The only damage observed included some hairline cracking on the bottom side of the UHPC connection at mid-span. These cracks were observed prior to the start of the seismic loading. The width of that crack was less than 0.007 in. (0.18 mm), as shown in Figure 5-9. These cracks were likely the result of the restrained shrinkage of the field-cast UHPC.

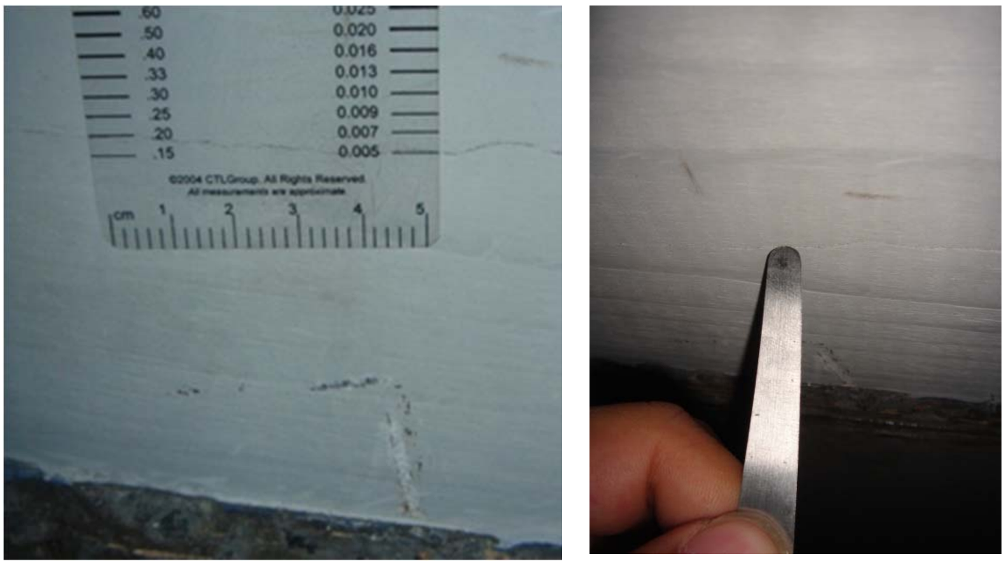

Figure 5-9 Minor cracks underneath the connection

SECTION 6
RESULTS AND ANALYSIS OF THE SHAKE TABLE TESTS

6.1 System Identification based on Test Results (Low Amplitude White Noise)

System identification is the process of establishing models for an unknown system based on a group of input–outputs. This method has been widely used in different fields of engineering (Puscasu and Codres 2011). In the area of structural system identification, this method can be implemented to identify structural dynamic parameters such as frequencies, mode shapes, and damping ratios, etc. (Sirca and Adeli 2012). System identification is an effective methodology to identify possible structural damage by monitoring the change of these dynamic parameters (Saiidi et al 2013A, Song et al 2008) .

Several system identification tests were conducted to monitor the change in the global dynamic characteristics of the bridge specimen. Hence, the progress of possible damage imposed due to consecutive seismic testing can be identified. The specimen was excited with a low amplitude white-noise acceleration input having a uniform spectrum with 0.5 ~ 40 Hz frequency band and root mean square (RMS) amplitude of approximately 0.10 g. Note that for all configurations, the lateral restrainers (girder keepers) were not in contact with the deck during these identification tests.

In this study, the input signal was the data from the accelerometers installed at the bottom of the steel extension frame. The steel frame was installed on each shake table to expand the supporting area, which can be considered a rigid body. In this case, the steel frame could transfer the signal from the bottom to the top without loss of the signal characteristics. Therefore, the signals from the accelerometers installed on two steel base plates were selected as the inputs. The output signals were from the accelerometers installed on the top of the girder deck levels, as shown in Figure 6-1.

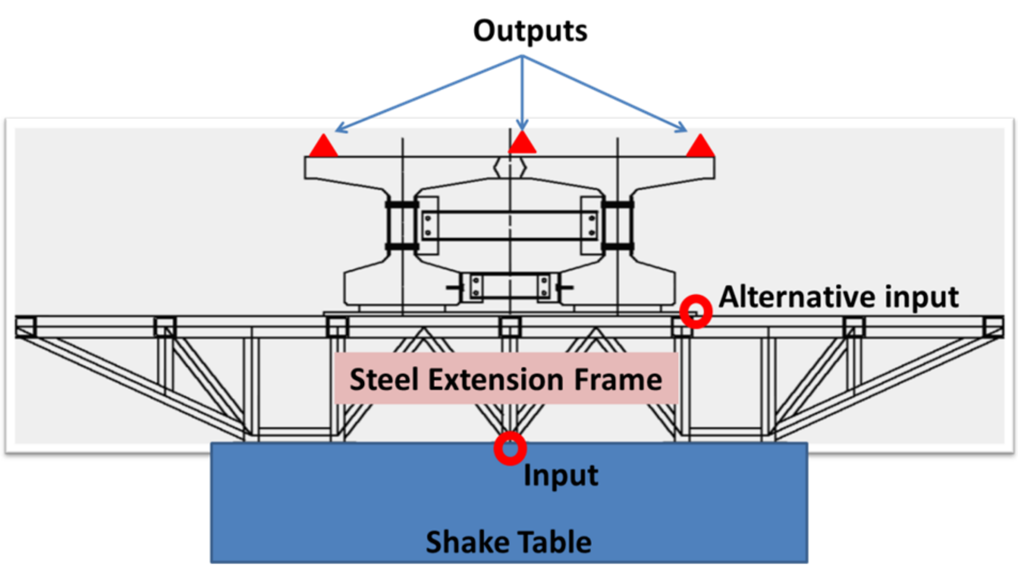

Figure 6-1 Locations of input and output signals

The natural periods and mode shapes were determined through frequency response function estimations of the acceleration response of the structure and those of the base plate. All the response results are given in Appendix C. Twenty-seven accelerometers located at nine points (P1~P9 shown in Figure 3-10) at the top of the girders (at bridge deck level) and six accelerometers located on the twin shake tables were used to generate the results for each white-noise test.

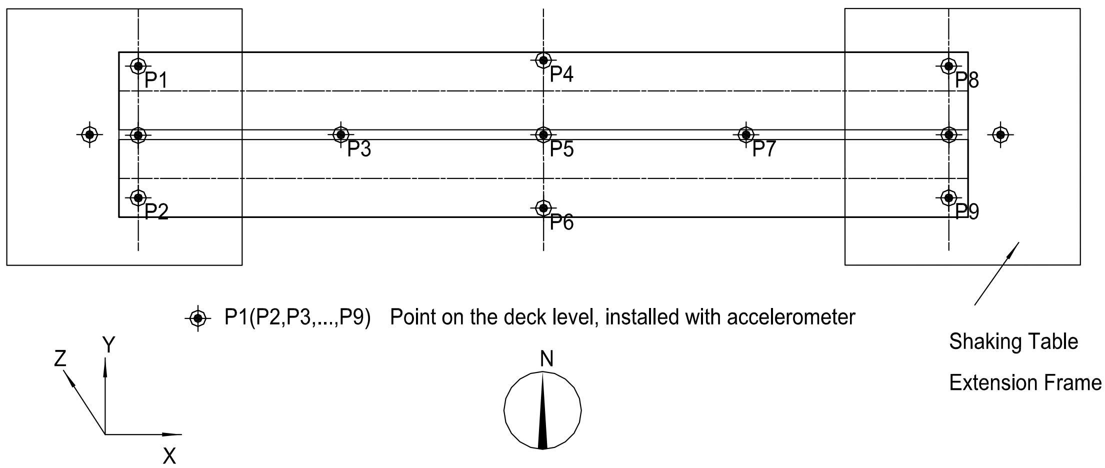

Figure 6-2 Monitoring points on the deck level

6.1.1 System identification theory

Based on Bracci et al (1992), modal identifications can be conducted from frequency domain analysis procedures. Eq. (6.1) shows the general equation of motion for a multi-degree of freedom system which is excited by a horizontal ground motion, $\ddot{x}_g(t)$.

$$\mathbf{M}\ddot{\mathbf{x}}(t)+\mathbf{C}\dot{\mathbf{x}}(t)+\mathbf{K}\mathbf{x}(t)=\mathbf{MJ}\ddot{x}_g(t) \tag{6.1}$$

where **M** is the mass matrix of the system,

C is the viscous damping matrix of the system,

K is the stiffness matrix of the system,

J is the influence matrix which contains the resultant displacement vectors of the mass to a static application of a unit ground displacement,

$\mathbf{x}(t)$ is the displacement vector time history,

$\dot{\mathbf{x}}(t)$ is the velocity vector time history,

$\ddot{\mathbf{x}}(t)$ is the acceleration vector time history, and

$\ddot{x}_g(t)$ is the ground acceleration time history.

The displacement vector, $\mathbf{x}(t)$, can be expressed as:

$$\mathbf{x}(t) = \mathbf{\Phi}\mathbf{z}(t) \tag{6.2}$$

where $\mathbf{\Phi}$ is the modal shape matrix, and

$\mathbf{z}(t)$ is the modal displacement vector.

Substituting Eq.(6.2) and the time derivatives into Eq. (6.1), Eq. (6.1) can be rewritten as

$$\mathbf{M\Phi\ddot{z}}(t) + \mathbf{C\Phi\dot{z}}(t) + \mathbf{K\Phi z}(t) = \mathbf{M\Phi J}\ddot{x}_{\mathrm{g}}(t) \tag{6.3}$$

Multiplying Eq. (6.3) by the transpose of the k^{th} mode shape factor, $\varphi_{\mathrm{k}}^{\mathrm{T}}$, and using the orthogonal properties of mode shape, the resulting uncoupled equation for the k^{th} mode is

$$M_{\mathrm{k}}^{*}\ddot{z}_{\mathrm{k}}(t) + C_{\mathrm{k}}^{*}\dot{z}_{\mathrm{k}}(t) + K_{\mathrm{k}}^{*}z_{\mathrm{k}}(t) = -\varphi_{\mathrm{k}}^{\mathrm{T}}M_{\mathrm{k}}^{*}\mathrm{J}\ddot{x}_{g}(t) \tag{6.4}$$

where $M_{\mathrm{k}}^{*} = \varphi_{\mathrm{k}}^{\mathrm{T}}\mathbf{M}\varphi_{\mathrm{k}}$, is the kth modal mass,

$C_{\mathrm{k}}^{*} = \varphi_{\mathrm{k}}^{\mathrm{T}}\mathbf{C}\varphi_{\mathrm{k}}$, is the kth modal viscous damping, and

$K_{\mathrm{k}}^{*} = \varphi_{\mathrm{k}}^{\mathrm{T}}\mathbf{K}\varphi_{\mathrm{k}}$. is the kth modal stiffness.

Assuming the mode shapes are normalized by setting the mass matrix $M_{\mathrm{k}}^{*} = 1$, and by applying the Fourier Transform into both sides of Eq. (6.4), the resulting equation of motion for k^{th} mode in the frequency domain can be written as

$$-\omega^{2}Z_{\mathrm{k}}(\omega) + 2i\omega\xi_{\mathrm{k}}\omega_{\mathrm{k}}Z_{\mathrm{k}}(\omega) + \omega_{\mathrm{k}}^{2}Z_{\mathrm{k}}(\omega) = -\Gamma_{\mathrm{k}}\ddot{X}_{\mathrm{g}}(\omega) \tag{6.5}$$

where ω is the angular frequency (rad/sec),

ξ_{k} is the damping ratio for k^{th} mode,

ω_{k} is the k^{th} angular natural frequency (rad/sec), and

$\Gamma_{\mathrm{k}} = \mathbf{\Phi}_{\mathrm{k}}^{\mathrm{T}}\mathbf{MJ}$ is the k^{th} modal participation factor.

Solving $Z_{\mathrm{k}}(\omega)$ from Eq. (6.5), in the frequency domain, that is,

$$Z_{\mathrm{k}}(\omega) = \frac{\Gamma_{\mathrm{k}} \cdot \ddot{X}_{\mathrm{g}}(\omega)}{\omega_{\mathrm{k}}^{2} - \omega^{2} + 2i\omega\xi_{\mathrm{k}}\omega_{\mathrm{k}}} \tag{6.6}$$

The absolute acceleration at the top of structure, $\ddot{\mathbf{a}}(t)$ is

$$\ddot{\mathbf{a}}(t) = \ddot{\mathbf{x}}(t) + \mathbf{J}\ddot{x}_{\mathrm{g}}(t) \tag{6.7}$$

Converting Eq. (6.7) to frequency domain,

$$\ddot{\mathbf{A}}(\omega) = \mathbf{J}\ddot{X}_{\mathrm{g}}(\omega) - \omega^{2}\Phi\mathbf{Z}(\omega) \tag{6.8}$$

Multiplying by $\Phi_{\mathrm{k}}^{\mathrm{T}}\mathbf{M}$,

$$\Phi_k^T \mathbf{M}\ddot{\mathbf{A}}(\omega) = \Phi_k^T \mathbf{MJ}\ddot{X}_g(\omega) \text{-} \omega^2 \mathbf{Z}(\omega) \tag{6.9}$$

Based on Song et al (2008), the absolute k^{th} modal acceleration, $\zeta_k(\omega)$ can be expressed as

$$\zeta_k(\omega) = \Phi_k^T \mathbf{M}\ddot{\mathbf{A}}(\omega) = \Gamma_k \ddot{X}_g(\omega) \text{-} \omega^2 Z_k(\omega) \tag{6.10}$$

Eq.(6.5) can be rewritten as

$$\zeta_k(\omega) + 2i\omega\xi_k\omega_k Z_k(\omega) + \omega_k^2 Z_k(\omega) = 0 \tag{6.11}$$

Solving $\zeta_k(\omega)$ from Eq.(6.11) and substituting Eq. (6.6), the k^{th} modal acceleration can be expressed as

$$\zeta_k(\omega) = \frac{\Gamma_k\left(2i\omega\xi_k\omega_k + \omega_k^2\right)}{\omega_k^2\omega^2 + 2i\omega\xi_k\omega_k}\ddot{X}_g(\omega) \tag{6.12}$$

According to the superposition of the modes, the j^{th} absolute acceleration, $A_j(\omega)$, can be written as

$$A_j(\omega) = \sum_{k=1}^{n}\left[\Phi_{jk}\zeta_k(\omega)\right] \tag{6.13}$$

Substituting Eq. (6.12) into Eq. (6.13),

$$A_j(\omega) = \sum_{k=1}^{n}\left[\phi_{j,k}\cdot A_k(\omega)\right] = \sum_{k=1}^{n}\left[\frac{\Gamma_k\left(2i\omega\xi_k\omega_k + \omega_k^2\right)}{\omega_k^2\cdot\omega^2 + 2i\omega\xi_k\omega_k}\phi_{j,k}\right]\cdot\ddot{X}_g(\omega) \tag{6.14}$$

where n is the mode number, and

$\phi_{j,k}$ is the k^{th} mass normalized mode shape for the j^{th} degree of freedom.

Therefore, the frequency response function (FRF) for the j^{th} degree of freedom, $\mathbf{H}_j(\omega)$, is defined as

$$\mathbf{H}_j(\omega) = \frac{A_j(\omega)}{\ddot{X}_g(\omega)} = \sum_{k=1}^{n}\frac{\Gamma_k\cdot\left(2i\omega\xi_k\omega_k + \omega_k^2\right)}{\omega_k^2\cdot\omega^2 + 2i\omega\xi_k\omega_k}\phi_{jk} = \sum_{k=1}^{n}\mathbf{H}_k(\omega)\cdot\phi_{jk} \tag{6.15}$$

The peak of j^{th} function at the k^{th} can be represented by

$$\left|\mathbf{H}_j(\omega_k)\right| = \frac{\Gamma_k\sqrt{1+4\xi_k^2}}{2\xi_k}\Phi_{jk} \tag{6.16}$$

The phase angle is defined as

$$\theta_j(\omega_k) = \tan^{-1}\left\{\frac{\text{Imaginary}\left[H_j(\omega_k)\right]}{\text{real}\left[H_j(\omega_k)\right]}\right\} \tag{6.17}$$

where $\theta_{\mathrm{j}}(\omega_{\mathrm{k}})$ is the phase angle for the j^{th} degree of freedom at ω_{k},

ω_{k} is the k^{th} angular natural frequency,

$\text{Imaginary}\left[H_{\mathrm{j}}(\omega_{\mathrm{k}})\right]$ is the imaginary part of the FRF, and

$\text{real}\left[H_{\mathrm{j}}(\omega_{\mathrm{k}})\right]$ is the real part of the FRF.

The ratio of the absolute value of k^{th} mode shape at i^{th} degree of freedom, $\left|\phi_{\mathrm{i,k}}\right|$, and j^{th} degree of freedom, $\left|\phi_{\mathrm{j,k}}\right|$, can be approximately determined by the ratio of the corresponding transfer function amplitude as shown in Eq. (6.18)

$$\frac{\left|\phi_{\mathrm{j,k}}\right|}{\left|\phi_{\mathrm{i,k}}\right|} \approx \frac{\left|H_{\mathrm{j}}(\omega_{\mathrm{k}})\right|}{\left|H_{\mathrm{i}}(\omega_{\mathrm{k}})\right|} \tag{6.18}$$

The equivalent damping ratio can be determined by half-power (bandwidth) method and calculated by Eq. (6.19).

$$\xi_{\mathrm{k}} = \frac{f_2 - f_1}{f_2 + f_1} = \frac{f_2 - f_1}{f_{\mathrm{k}}} \tag{6.19}$$

in which f_1 and f_2 are the frequencies when $\rho_{\mathrm{f}1}, \rho_{\mathrm{f}2} = \frac{\rho_{\mathrm{fk}}}{\sqrt{2}}$, and f_{k} is the k^{th} natural frequency.

6.1.2 System identification of test phase 1

To provide some insight into the dynamic characteristics of the bridge specimen, the initial modal properties (before execution of all shake table testing) in the three major directions are provided in Table 6-1 for the phase 1 specimen (no steel plate on the deck).

Table 6-1 Initial properties of test specimen in phase 1

Mode	Natural Frequency (Hz)	Damping ratio	Mode shape
1	6.30	9.5%	Horizontal deck translation (North-South direction)
2	7.38	6.2%	Horizontal deck translation (East-West direction)
3	12.53	3.2%	Vertical deck bending (Vertical direction)

The frequency response function (FRF) magnitudes and phases for three directions of the specimen are shown in Figure 6-3 and Figure 6-4. It can be seen that in the Y-direction (N-S direction), only one mode shape can be identified. All nine monitoring points were moving in the same direction with the same magnitude, which indicates the mode (translation in N-S direction) was affected by the rubber bearing. This phenomenon was caused by the large stiffness of the girder in the Y-direction. Note that the frequency range around 13 Hz may be affected by the third mode (vertical bending of Z-direction).

For the X-direction (E-W direction), the magnitudes exhibited similar characteristics with those of X-direction. The second mode shape was also nine points translating towards the same direction.

For the Z-direction (U-D direction), it is obvious the frequency for the third mode was around 13 Hz. The four monitoring locations close to the shake table (P1, P2, P8, P9) exhibited a very low magnitude because they were close to the support. The locations in the mid-span (P4, P5, P6) exhibited the largest magnitude.

Sketches of the first three mode shapes in three directions are shown in Figure 6-5, Figure 6-6, and Figure 6-7.

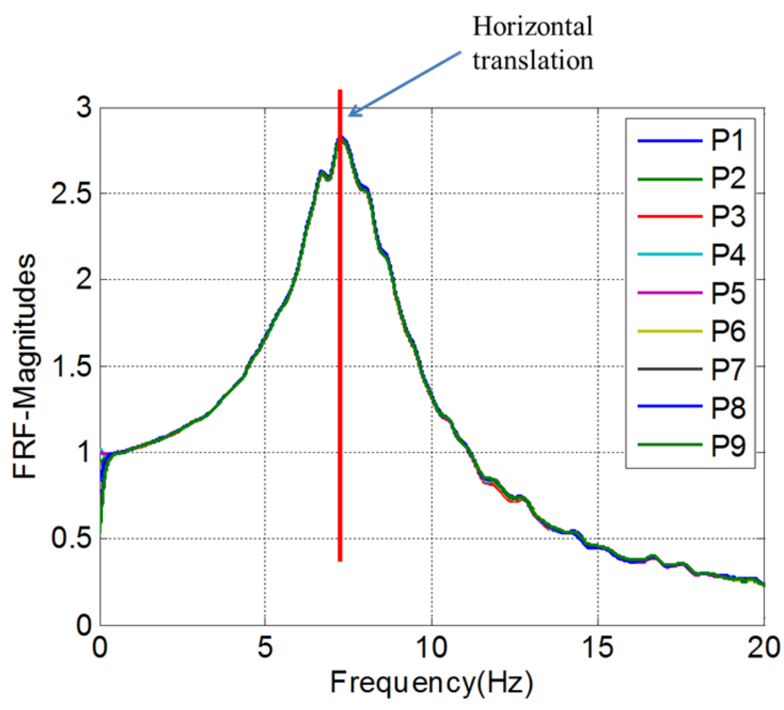

(a) E-W direction

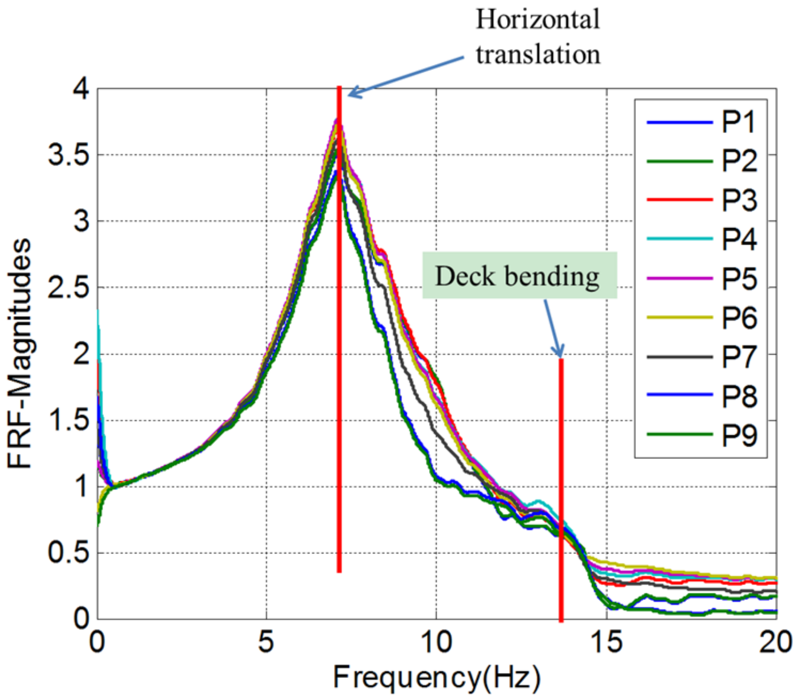

(b) N-S direction

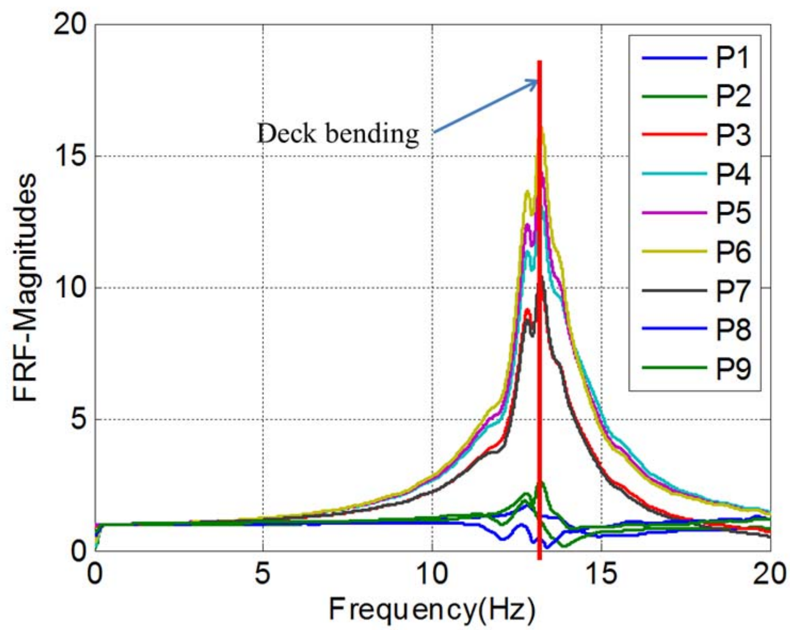

(c) U-D direction

Figure 6-3 Magnitude results of initial properties of test phase 1

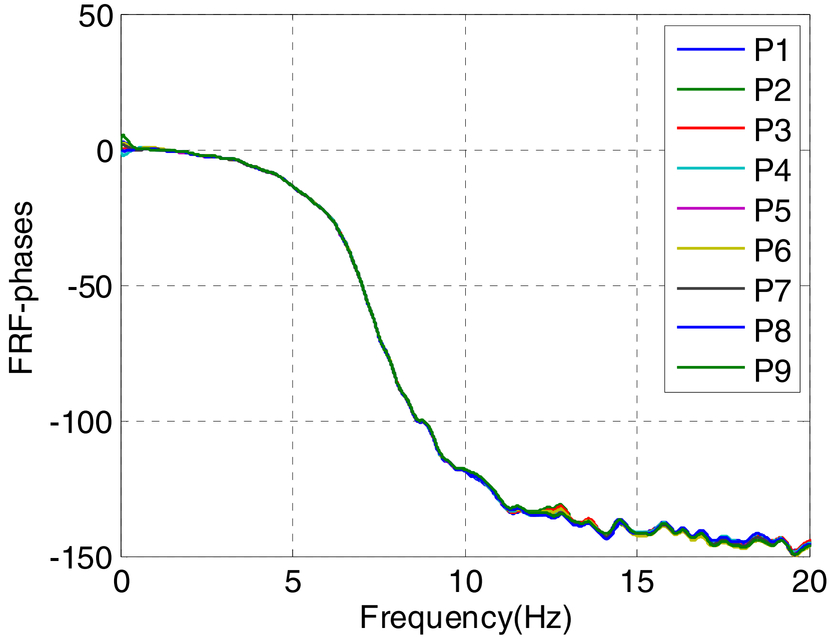

(a) E-W direction

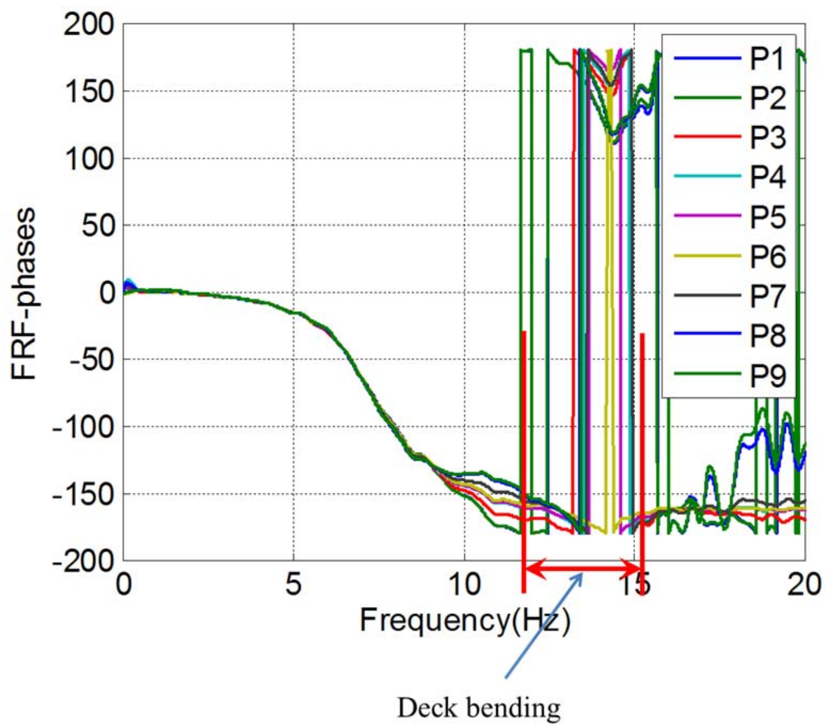

(b) N-S direction

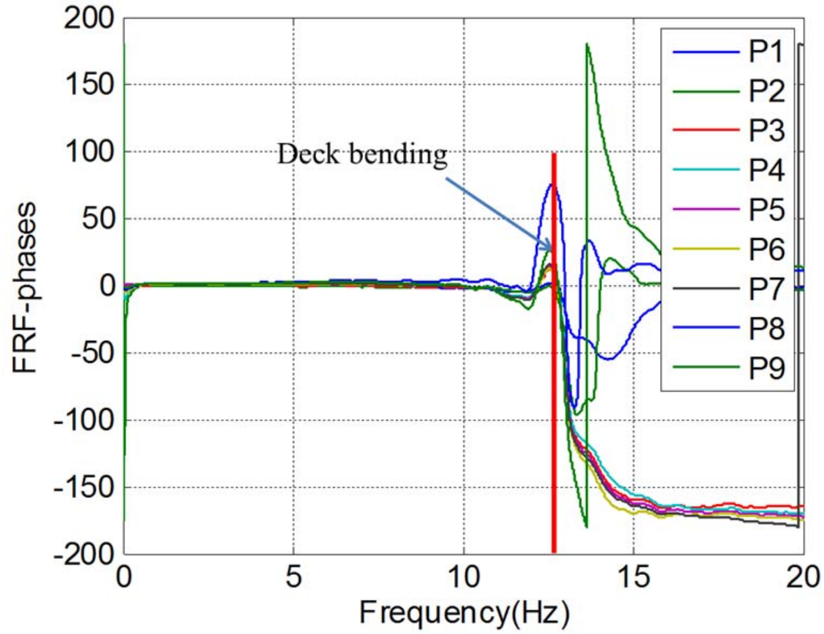

(c) U-D direction

Figure 6-4 Phase results of initial properties of test phase 1

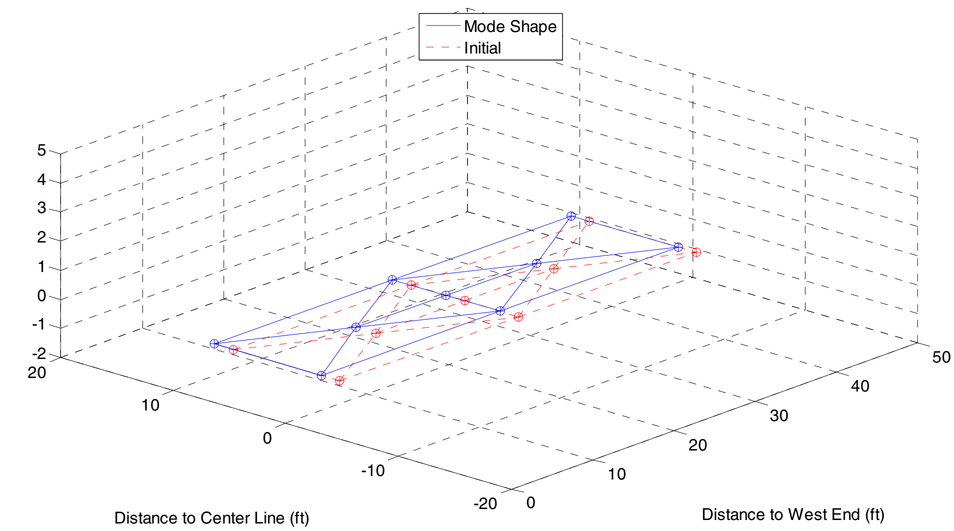

(a) 3-D view

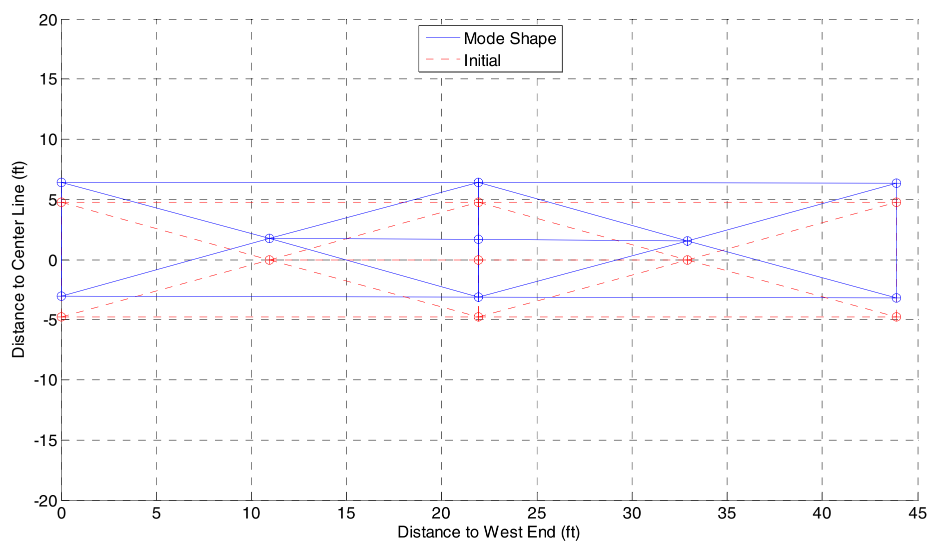

(b) Plan view

Figure 6-5 First mode in N-S direction

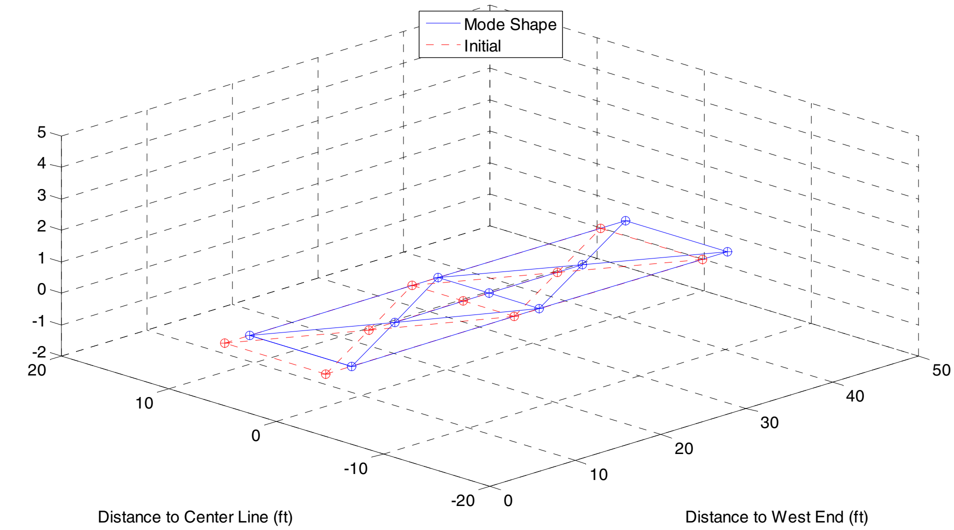

(a) 3-D view

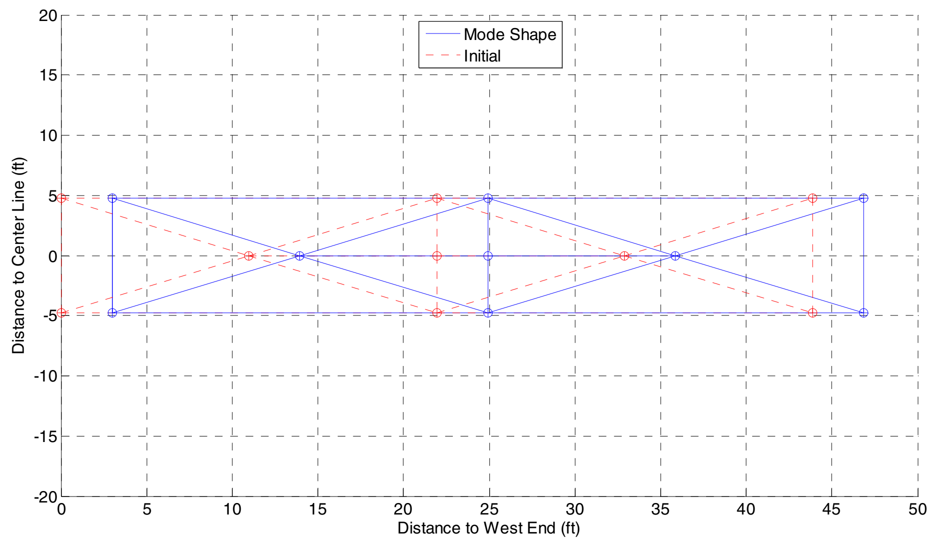

(b) Plan view

Figure 6-6 Second mode in E-W direction

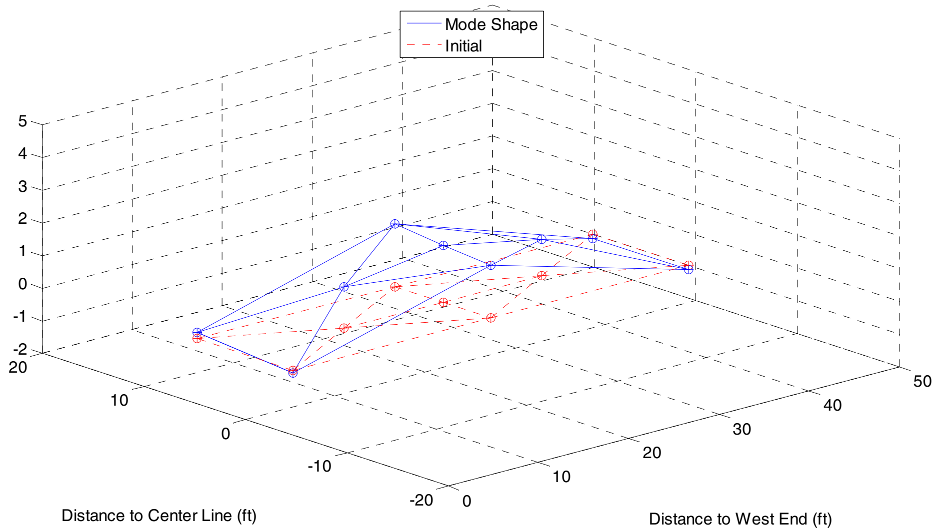

(a) 3-D view

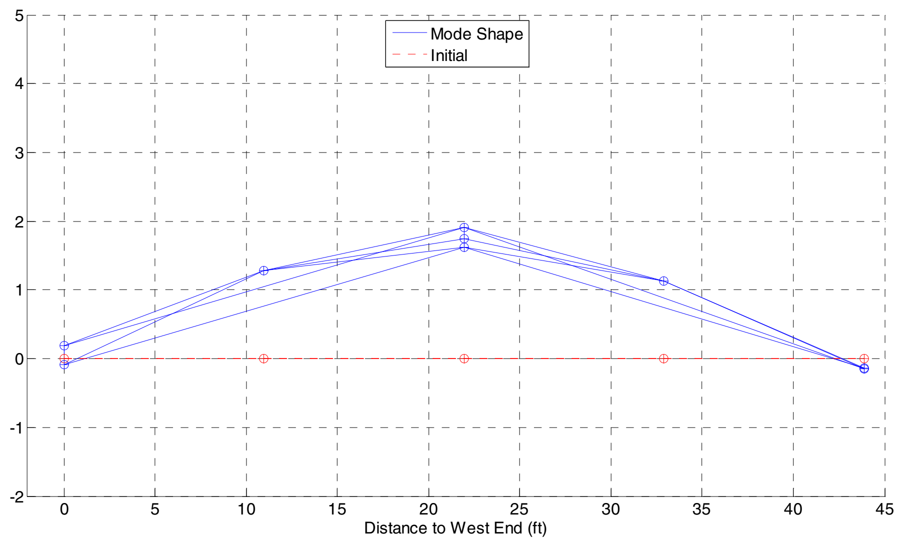

(b) E-W elevation view

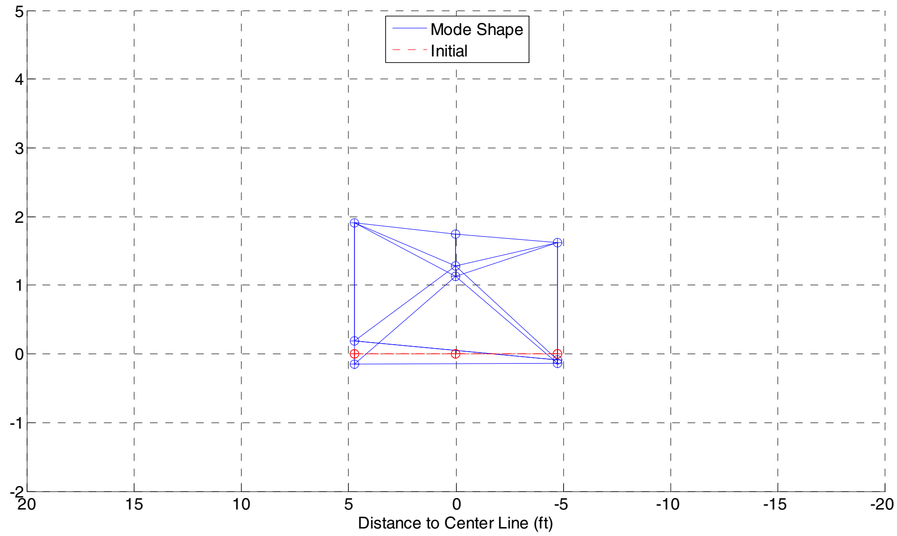

(c) N-S elevation view

Figure 6-7 Third mode in U-D direction

Table 6-2, Table 6-3, and Figure 6-8 illustrate the changes in the dynamic properties of the test specimen in three directions through the various levels of seismic tests that have been conducted. The changes of frequencies in three directions before and after the tests were small, Changes in the E-W and N-S direction were within 15%, whereas those in the U-D direction were within 3%. The changes in E-W and N-S direction were relatively large because of the dynamic property changes of the bearing pads. It is noteworthy that under the maximum excitation, the girder may move apart from the bearing pads, and then be lifted and placed in the initial position. The lifting procedure may change the girder behavior since the boundary condition of the original structure changes. The changes in U-D direction reflect the changes of dynamic properties of the girder specimen. In addition, the damping ratios in all three directions hardly increased in the test procedure. Therefore, it can be concluded that the global dynamic properties of the girder specimen changed slightly and the specimen stayed in elastic range after the seismic tests.

Table 6-2 Frequency of the first three modes in phase 1

Seismic level	Direction		
	E-W	**N-S**	**U-D**
Ini	7.38	6.30	12.53
EL	7.58	6.97	12.77
DE	7.65	6.25	12.83
MCE	7.32	6.12	12.78
2DE	7.11	5.95	12.81
Max	6.70	5.54	12.69

Table 6-3 Damping ratio of the first three modes in phase 1

Seismic level	Direction		
	E-W	**N-S**	**U-D**
Ini	9.3%	7.0%	2.1%
EL	9.5%	6.2%	3.1%
DE	9.8%	6.9%	1.6%
MCE	9.9%	7.0%	2.0%
2DE	10.0%	7.1%	2.5%
Max	9.3%	7.1%	2.1%

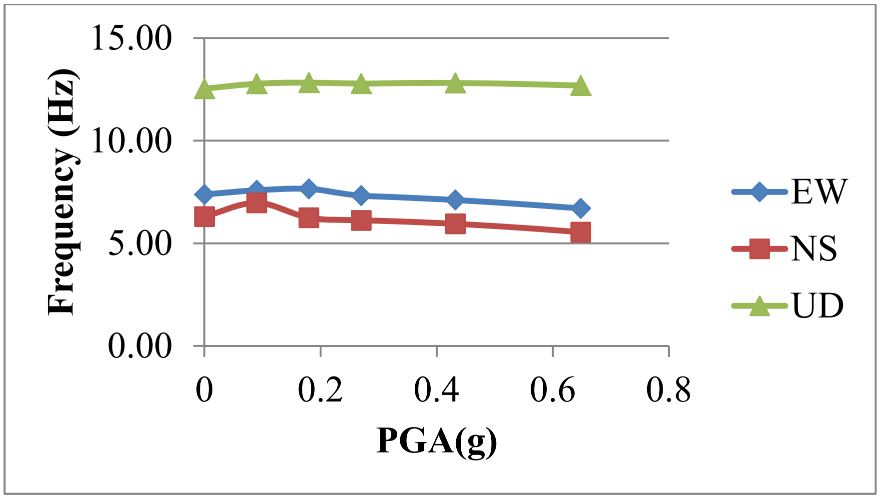

(a) Frequency

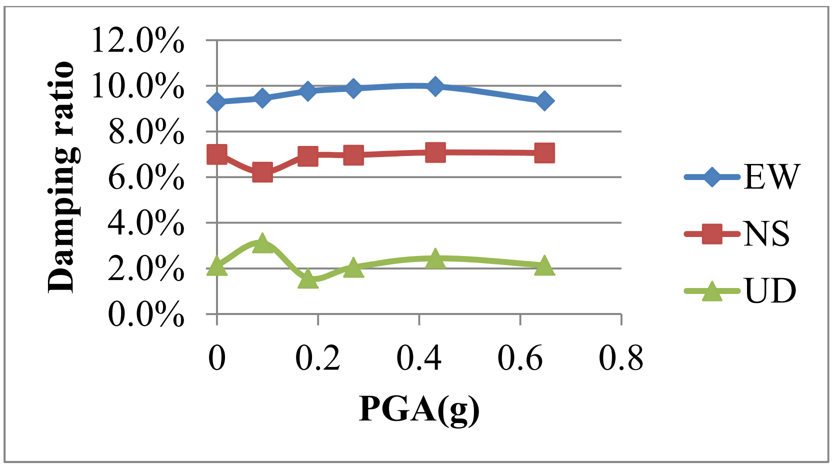

(b) Damping ratio

Figure 6-8 Change in the dynamic properties of the specimen in phase 1

6.1.3 System identification of test phase 2

After the two steel plates were installed on girder 2, the natural frequency, damping ratio and mode shape (before execution of all shake table testing) in the three major directions were measured and analyzed, as shown in Table 6-4. Similar mode shapes were observed as well as a considerable decrease in frequency compared to the unloaded specimen.

Table 6-4 Initial properties of the test specimen in phase 2

Mode	Natural Frequency (Hz)	Damping ratio	Mode shape
1	5.20	9.3%	Horizontal deck translation and bending (North-South direction)
2	6.21	7.7%	Horizontal deck translation (East-West direction)
3	10.46	2.4%	Vertical deck bending (Vertical direction)

The FRF magnitudes and phases for three directions of the specimen are shown in Figure 6-9 and Figure 6-10. For the Y-direction (N-S direction), a similar decrease in the frequency exhibited in the first mode, i.e., the first frequency decreased from 6.30 Hz in phase 1 to 5.20 Hz in phase 2. The magnitudes exhibited similar characteristics with phase 1. Several peaks in magnitude occurred in the higher frequency range (20~40 Hz). These peaks might have been caused by the vibration of the steel plates, so the focus of the study is placed on the first frequency again.

Compared to the results of phase 1, there is still only one mode that can be identified in the X-direction (E-W direction). However, the frequency shifted to the lower value, i.e., from 7.38 Hz in phase 1 to 6.21 Hz in phase 2. The decrease is because the installation of the steel plates induced an additional mass. Based on fundamental structural dynamics, an increased mass leads to a decrease in frequency. All nine monitoring points were still moving towards the same direction with the same magnitude, which indicates the second mode was affected by the rubber bearing.

For the Z-direction (U-D direction), it is obvious that the frequency in the third mode decreased from 12.53 Hz to 10.46 Hz. It is interesting to observe that the second peak occurred around the frequency of 12 Hz. This phenomenon can be explained as the effect of second deck bending mode. Compared to the first deck bending mode, the peak magnitude of the monitoring point on the deck edge of girder 1 (P4, North side in the mid span, see Figure 6-2) was significantly larger than other points. It indicates that the deck was bending unevenly due to the existence of the steel plate. This behavior can be further verified in a later section that describes preliminary finite element analysis (FEA).

Sketches of the first four mode shapes in three directions are shown in Figures 6-11, 6-12, 6-13, and 6-14.

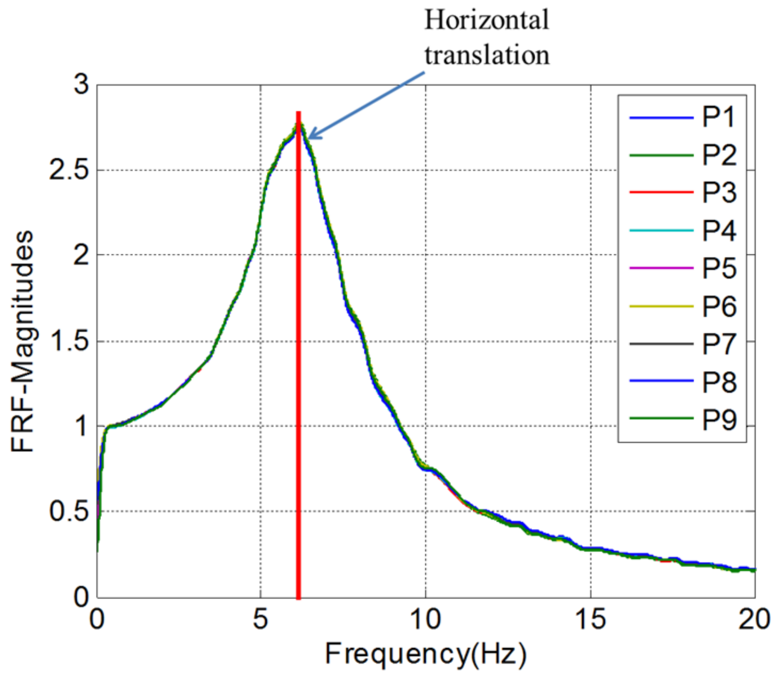

(a) E-W direction

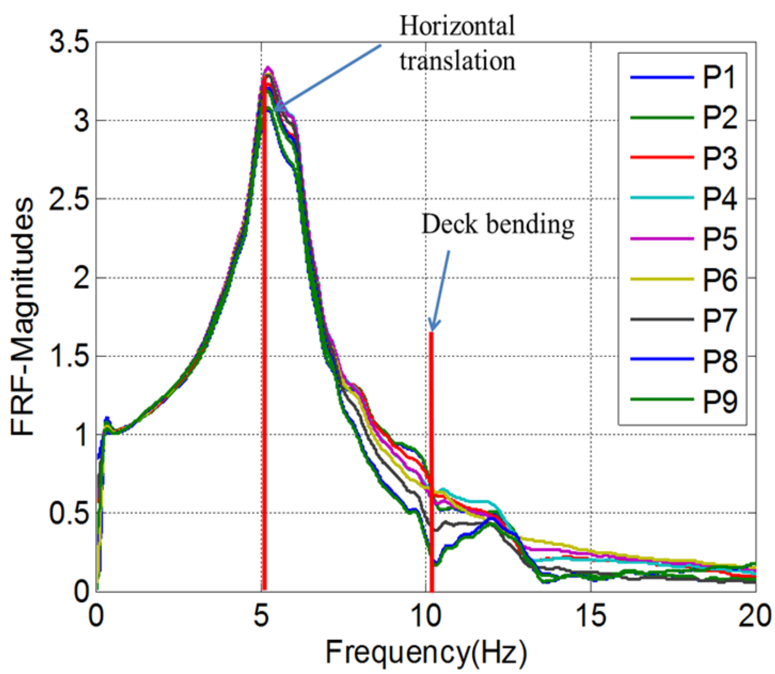

(b) N-S direction

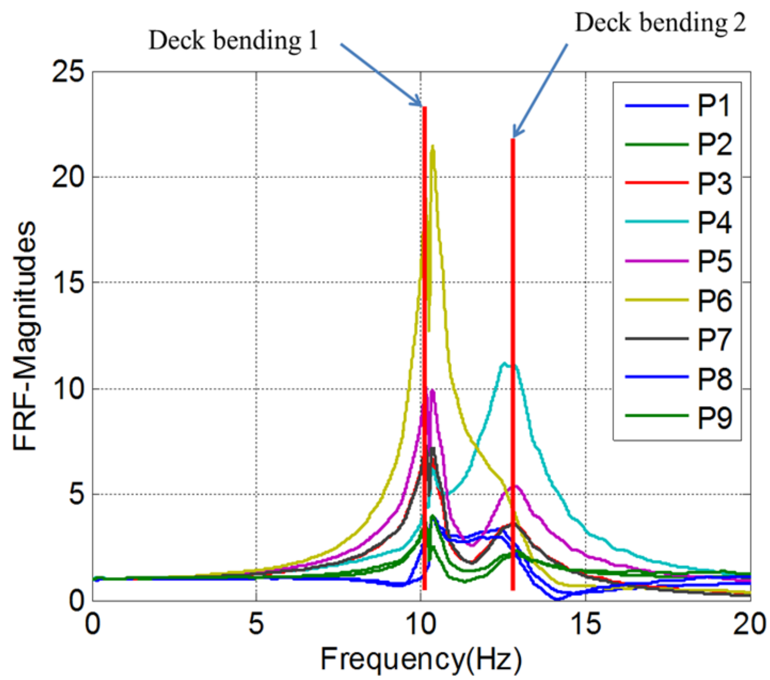

(c) U-D direction

Figure 6-9 Magnitude results of initial properties of test phase 2

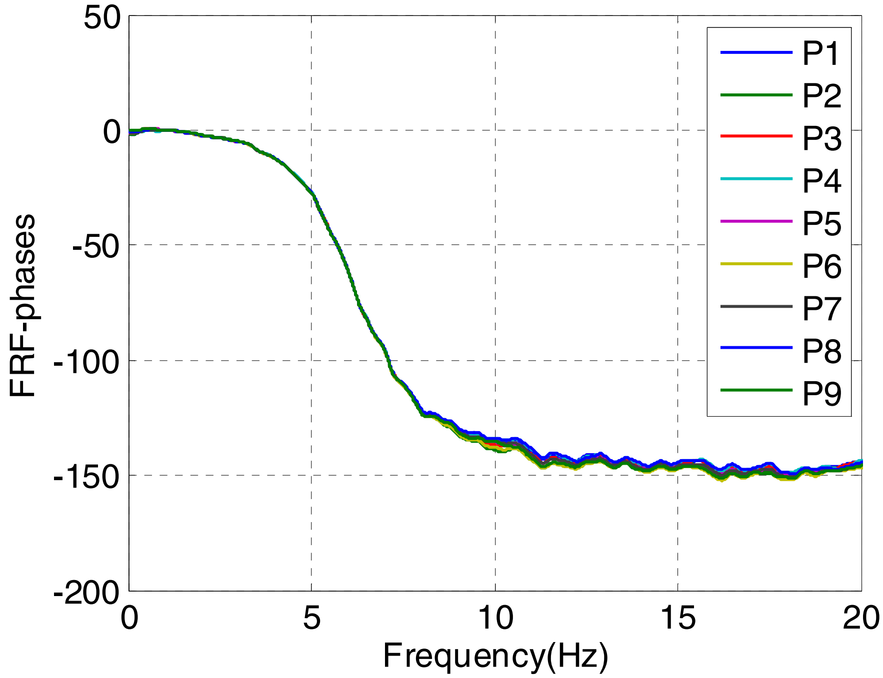

(a) E-W direction

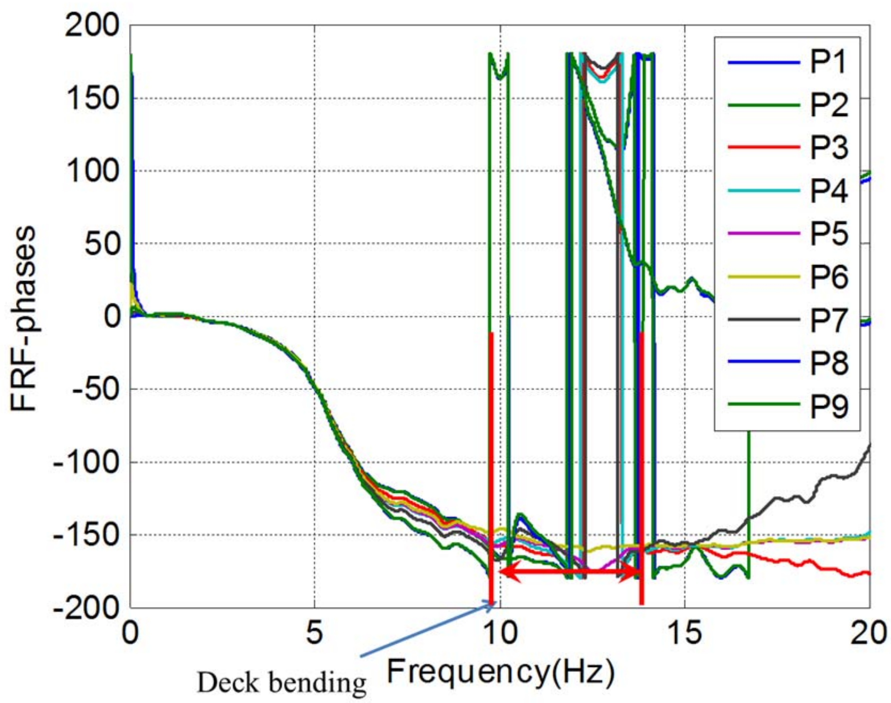

(b) N-S direction

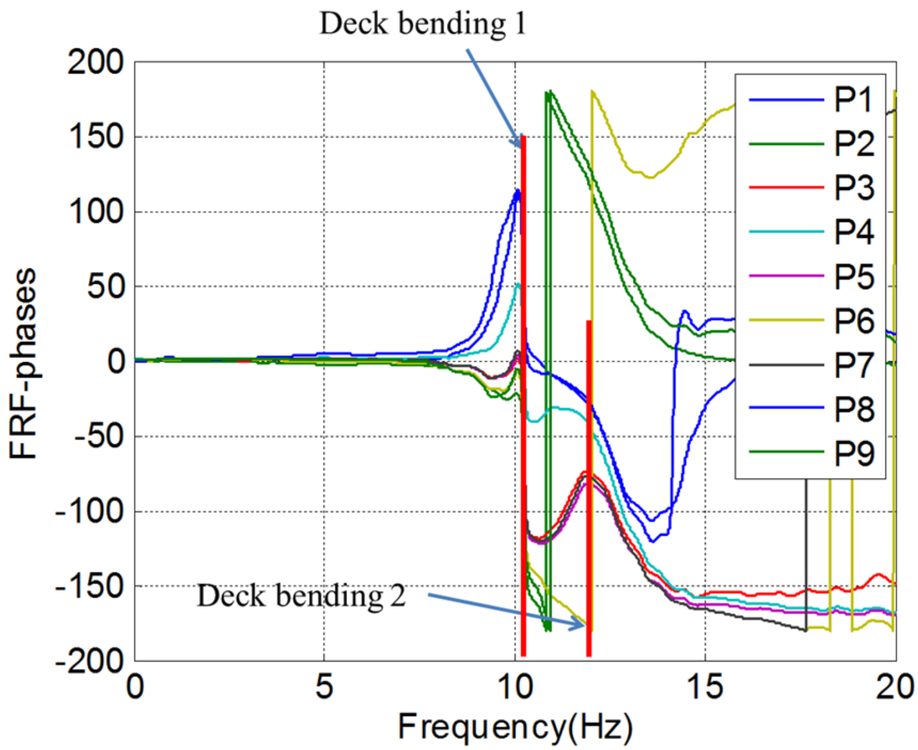

(c) U-D direction

Figure 6-10 Phase results of initial properties of test phase 2

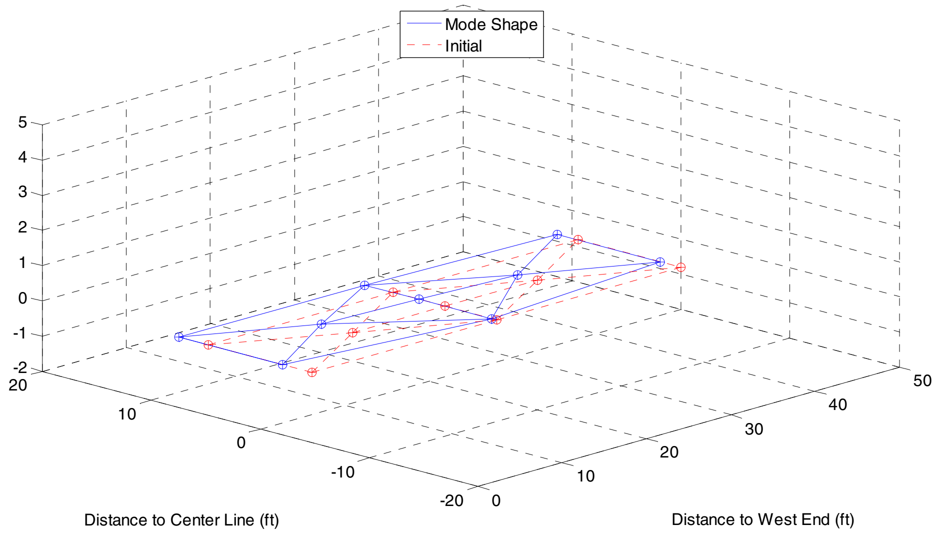

(a) 3-D view

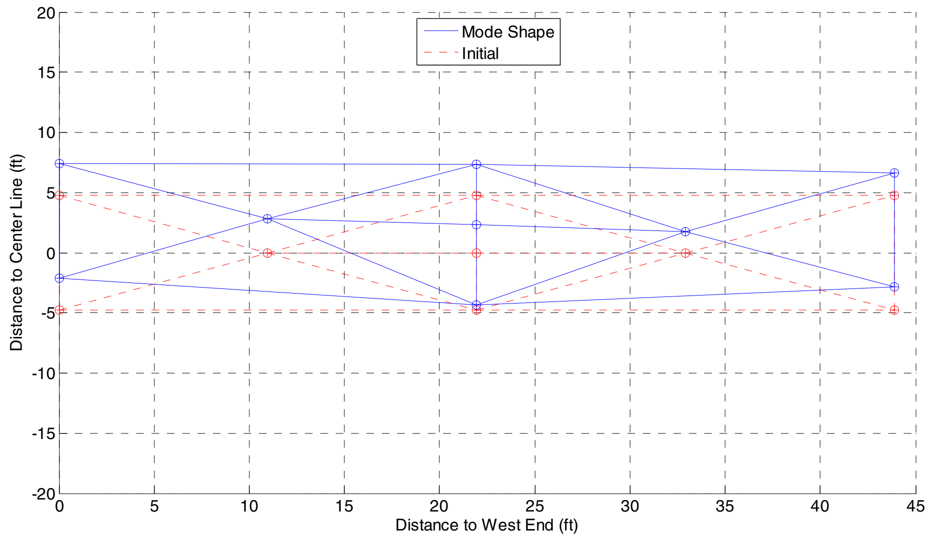

(b) Plan view

Figure 6-11 First mode in N-S direction for phase 2

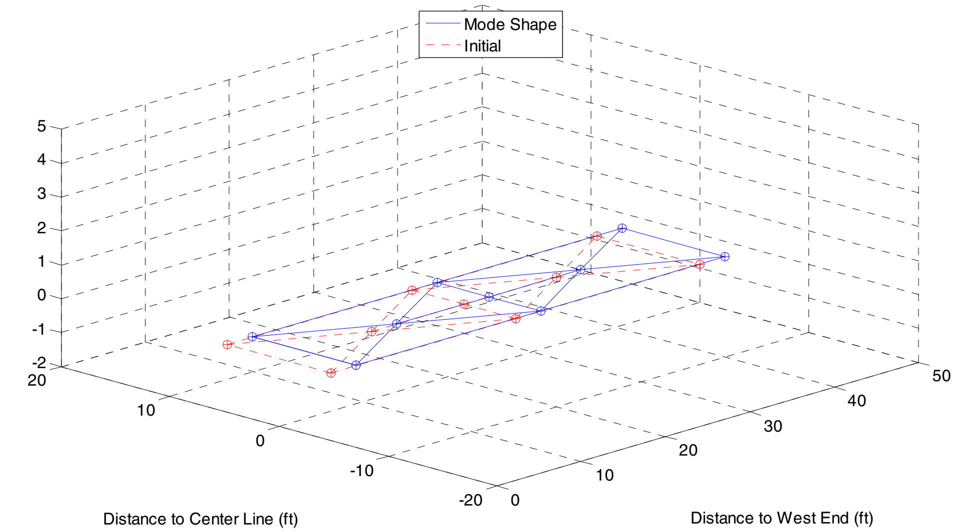

(a) 3-D view

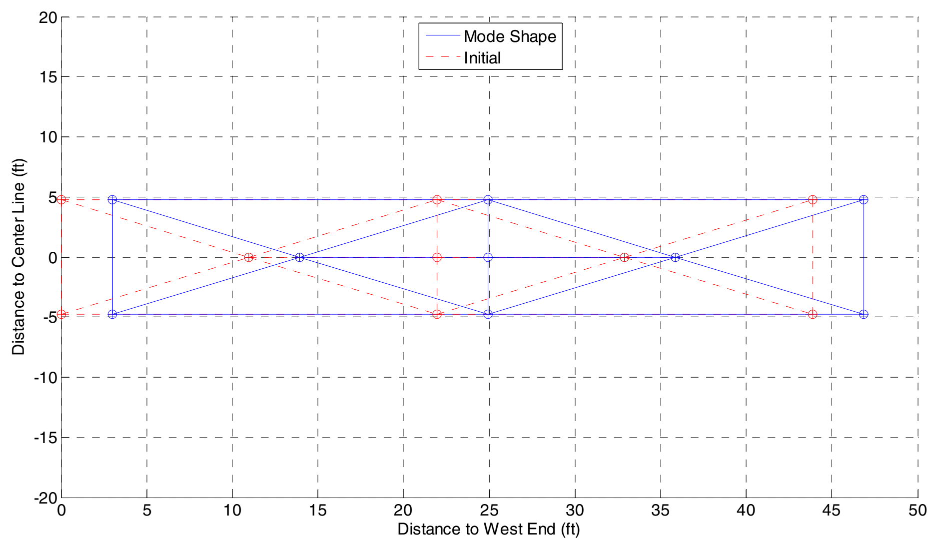

(b) Plan view

Figure 6-12 Second mode in E-W direction for phase 2

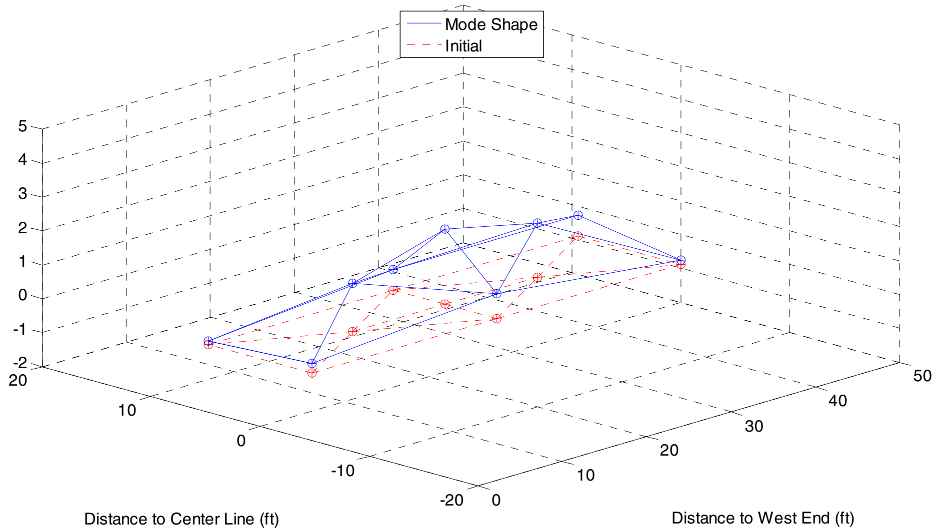

(a) 3-D view

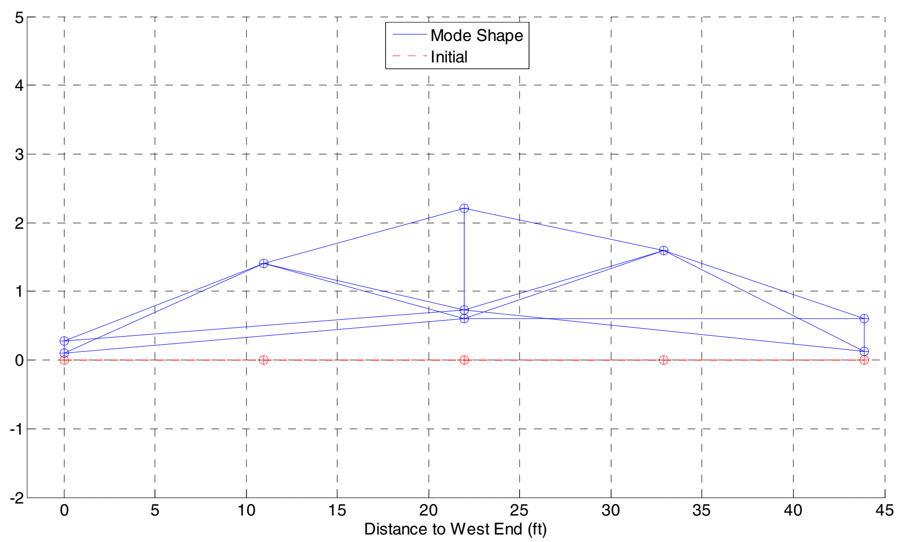

(b) E-W elevation view

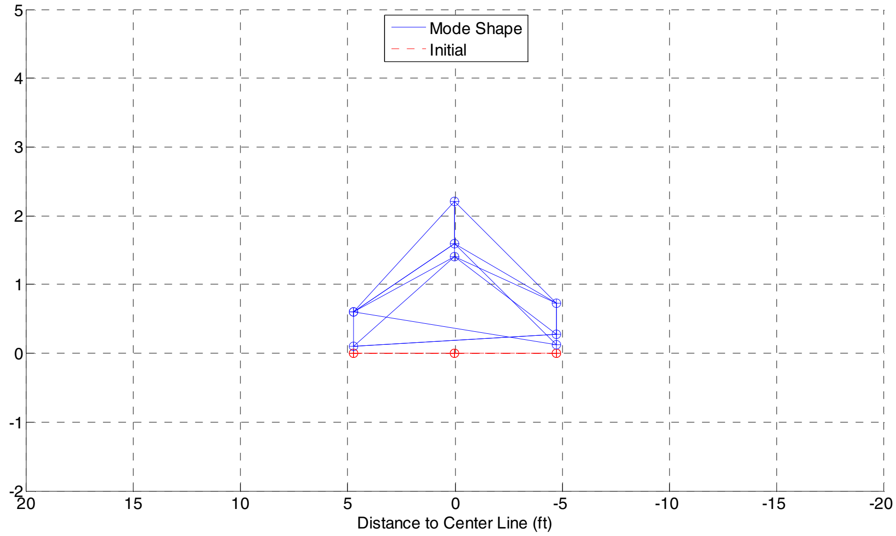

(c) N-S elevation view

Figure 6-13 Third mode in U-D direction for phase 2

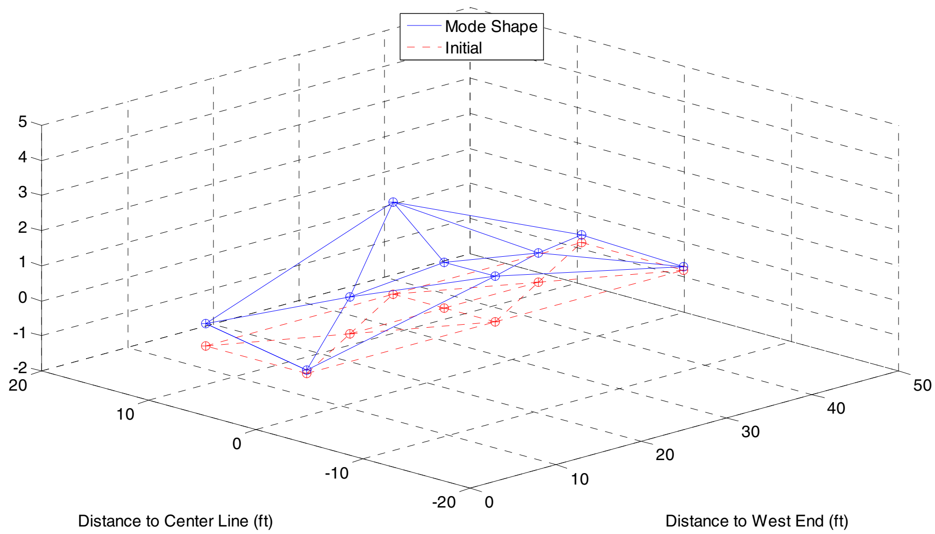

(a) 3-D view

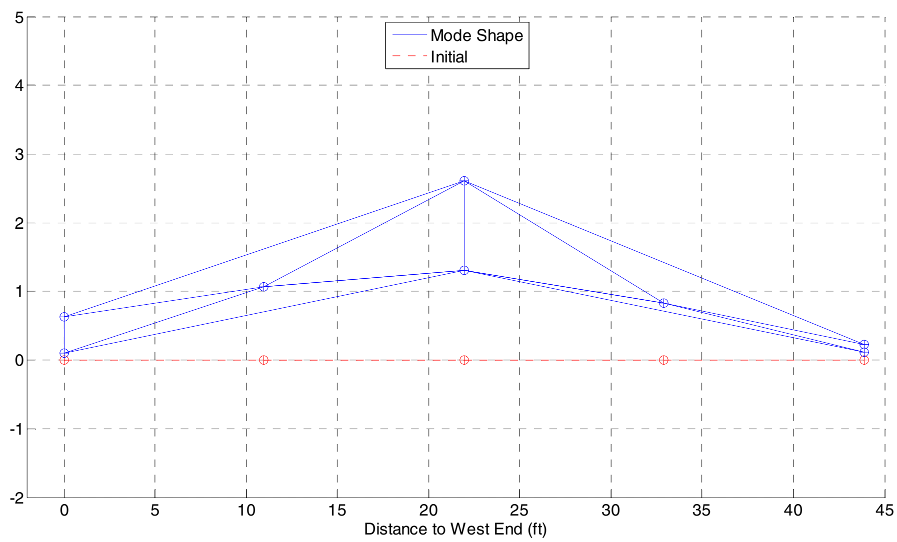

(b) E-W elevation view

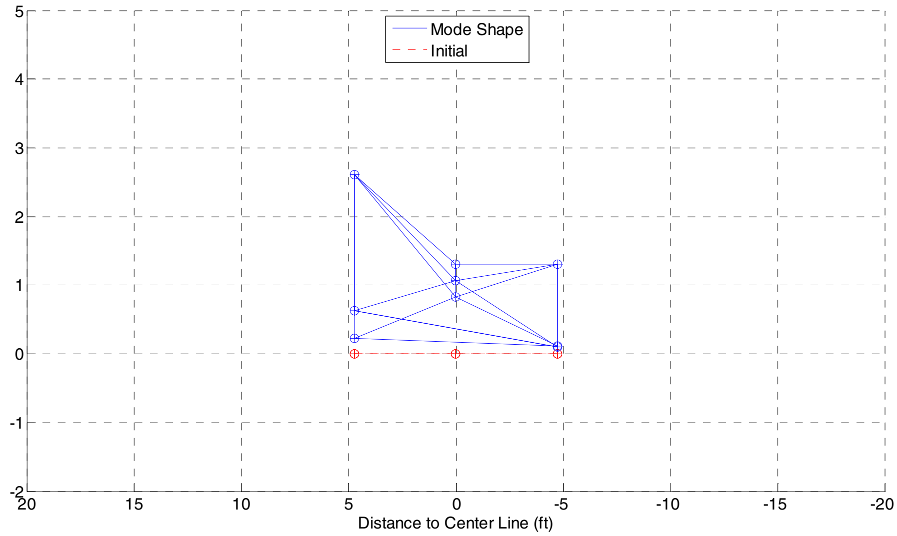

(c) N-S elevation view

Figure 6-14 Fourth mode in U-D direction for phase 2

Table 6-5, Table 6-6 and Figure 6-15 illustrate the change in dynamic properties of the test specimen in three directions through the various levels of seismic tests in phase 2. It can be seen that the observations found in phase 1 applied to the changes of frequencies and damping ratio in three directions. The changes in U-D direction, which reflect the changes in dynamic properties of the girder specimen, stayed within a very small range of 4% for both the first and second modes. It is concluded that the global dynamic properties of the girder specimen changed slightly and the specimen stayed in elastic range after all the seismic tests in phase 2.

Table 6-5 Frequency of the first four modes in phase 2

Seismic levels	Direction			
	E-W	N-S	U-D #1	U-D #2
INI	6.21	5.20	10.46	12.13
EL	6.34	5.23	10.62	12.19
DE	6.30	4.94	10.70	12.20
MCE	6.07	4.25	11.14	12.20
2DE	6.02	4.43	10.70	12.18
Max	5.73	4.50	10.77	12.32
Max*1.2	5.44	3.90	10.24	12.12

Table 6-6 Damping ratio of the first four modes in phase 2

Seismic levels	Direction			
	E-W	N-S	U-D #1	U-D #2
INI	9.3%	7.7%	2.8%	6.0%
EL	9.3%	7.6%	4.5%	3.9%
DE	9.2%	8.4%	4.5%	3.7%
MCE	9.6%	7.5%	5.1%	3.7%
2DE	9.4%	8.0%	4.4%	3.8%
Max	9.4%	7.8%	5.2%	4.3%
Max*1.2	9.1%	8.5%	3.5%	5.3%

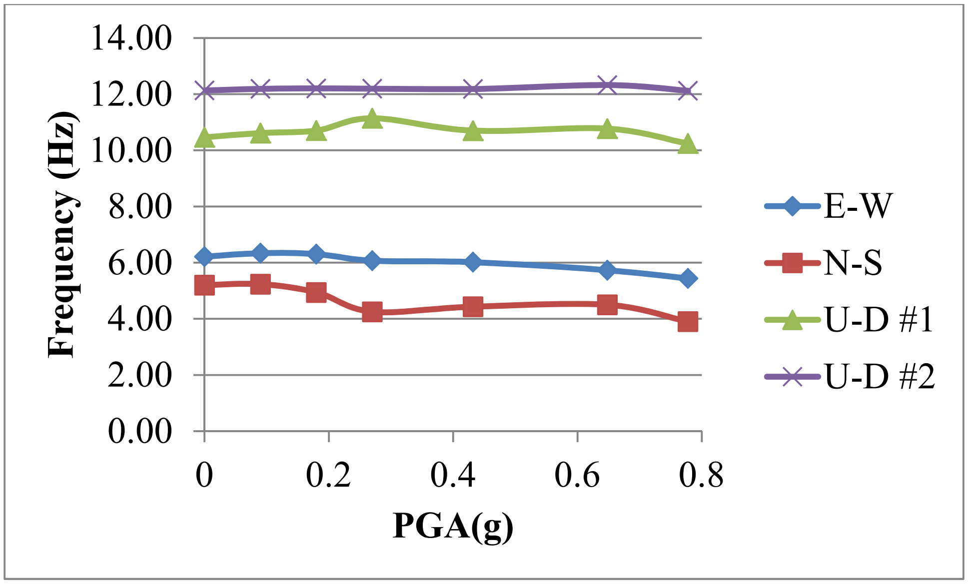

(a) Frequency

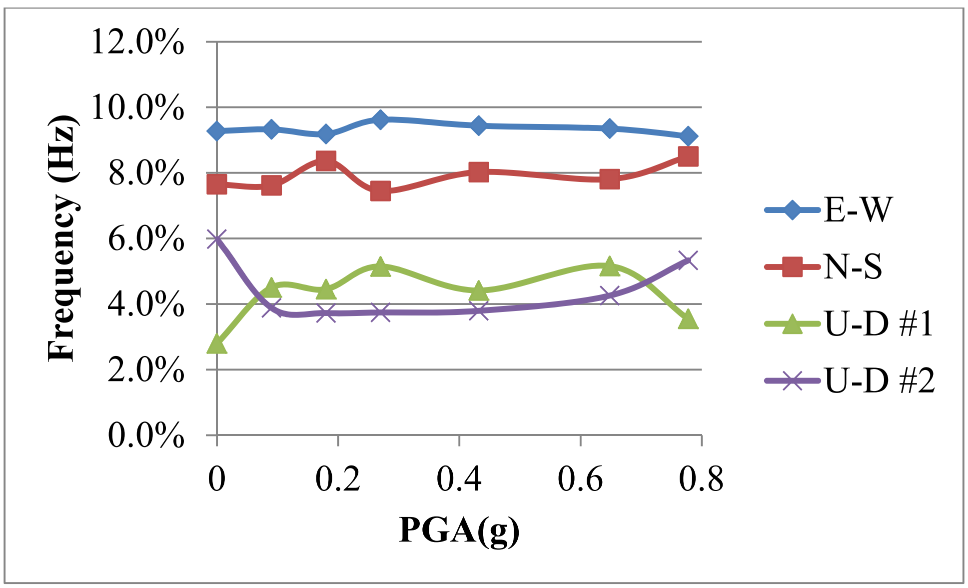

(b) Damping ratio

Figure 6-15 Change in the dynamic properties of the specimen in phase 2

6.1.4 System identification of test phase 3

The results for system identification tests in phase 3 are briefly given in Table 6-7 and Figure 6-16. The test phenomena are generally the same as those in phase 2. Detailed descriptions are not repeated herein.

Table 6-7 Dynamic properties of test specimen in phase 3

Mode	Direction	Natural Frequency (Hz)	Damping ratio	Mode shape
1	E-W	2.71	9.2%	Horizontal deck translation (North-South direction)
2	N-S	5.62	8.2%	Horizontal deck translation (East-West direction)
3	U-D #1	10.23	2.8%	Vertical deck bending (Vertical direction)
4	U-D #2	12.14	3.6%	Combined vertical and transverse deck bending (Vertical and transverse direction)

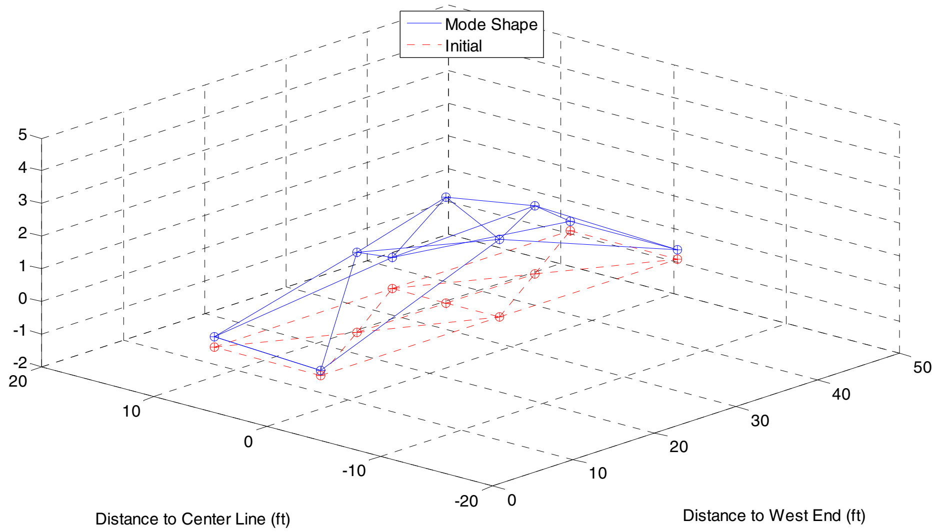

(a) First mode

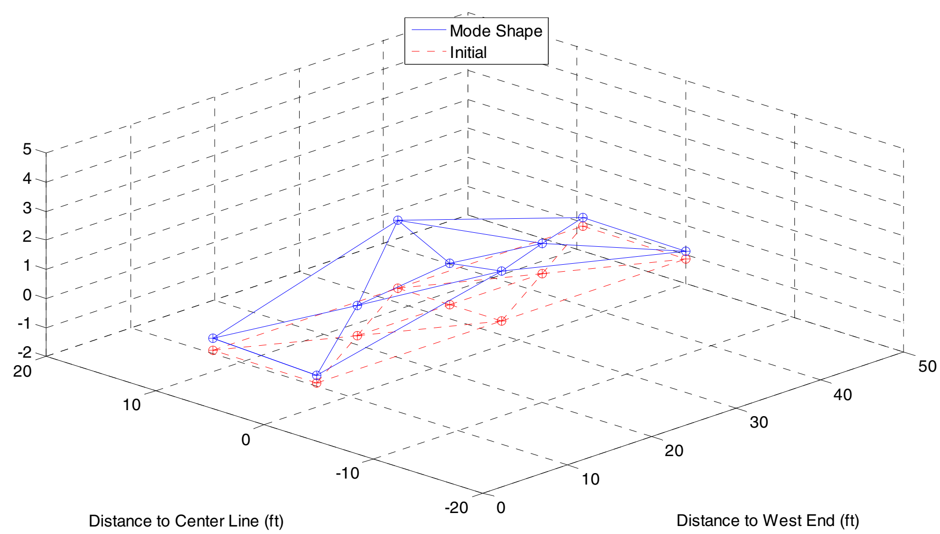

(b) Second mode

Figure 6-16 Mode shapes in U-D direction for phase 3

6.2 Seismic Test Results

6.2.1 Response of the strain of the UHPC connection

The maximum strains recorded during each seismic test, which were measured by 11 strain gauges installed on the rebar embedded in the UHPC connection and precast girders, are given in Appendix D.

6.2.1.1 Phase 1

The maximum strains recorded among all 11 strain gauges for each test in phase 1 are summarized in Table 6-8 and Table 6-9. It can be seen that the maximum strain occurred when Near 3 GMs were applied. For several seismic excitations, the maximum strain in the precast girder exceeded 1400 microstrain. This indicates that some local regions of the precast girder deck may have been subjected to limited damage. The maximum strain in the UHPC connection was 43 microstrain. According to Russell and Graybeal (2013), the first tensile cracking strength of UHPC is approximately 1.3 ksi for steam-cured specimens and approximately 0.9 ksi without any heat treatment. According to Graybeal and Baby (2013), the elastic regime for tensile strain ranged from 34 to 129 microstrain. The tensile cracking strength of the UHPC deployed in this test was not tested, but could be estimated as approximately 1.03 ksi by the equation provided in Russell and Graybeal (2013), as shown in Eq. (6.20). The tensile strain was estimated as 145 microstrain by combining Eq. (6.21) and Eq. (6.22), which is provided in Russell and Graybeal (2013). Thus, in this phase, it can be concluded that the UHPC stayed well within the elastic range.

$$f_{ct} = 6.7\sqrt{f_c'} \tag{6.20}$$

where f_{ct} and f_c' are the tensile strength and compressive strength of UHPC, respectively.

$$\varepsilon_{ct} = \frac{f_{ct}}{E_c} \tag{6.21}$$

$$E_c = 46200\sqrt{f_c'} \tag{6.22}$$

where ε_{ct} and E_c are the tensile strain and modulus of elasticity for UHPC, respectively.

Table 6-8 Maximum strains of the precast girder in phase 1

GM set	Seismic Level				
	Elastic	DE	MCE	DEx2	Max
Far 1	3	5	9	16	24
Far 2	4	7	11	17	28
Far 3	4	6	9	17	25
Far 4	4	4	10	18	23
Far 5	3	5	9	19	22
Near 1	6	6	11	19	958
Near 2	3	5	9	15	26
Near 3	6	9	14	307	1420
Near 4	4	6	12	20	695
Near 5	4	4	8	18	21
Near 6	5	6	9	18	26

Table 6-9 Maximum strains of the UHPC connection in phase 1

GM set	Seismic Level				
	Elastic	**DE**	**MCE**	**DEx2**	**Max**
Far 1	2	3	5	8	15
Far 2	4	4	7	11	19
Far 3	3	4	5	8	15
Far 4	2	3	6	9	15
Far 5	2	3	5	8	13
Near 1	4	5	9	16	28
Near 2	3	3	4	8	15
Near 3	5	9	13	19	43
Near 4	3	6	10	16	25
Near 5	3	2	4	8	14
Near 6	3	4	6	11	18

Figure 6-17 illustrates the strain time-histories at the mid-span of the UHPC connection under Near 3 GMs with the maximum level of amplitude in test phase 1, i.e. peak ground acceleration (PGA) equal to 0.65 g. The results show that the maximum strain for the deck of a girder and the UHPC are 1420 and 43 microstrain, respectively. Figure 6-18 illustrates the strain distribution along the girder's longitudinal direction. There was only one strain gauge that exhibited extra-large strain value. The maximum value from other strain gauges, including those strain gauges located at the mid-span, was 61 microstrain. Thus, the extra-large strain indicates that damage may occur in the mid-span but definitely within a very limited range. Based on the estimated elastic modulus of UHPC, the maximum tensile stress in the mid-span is 280 psi.

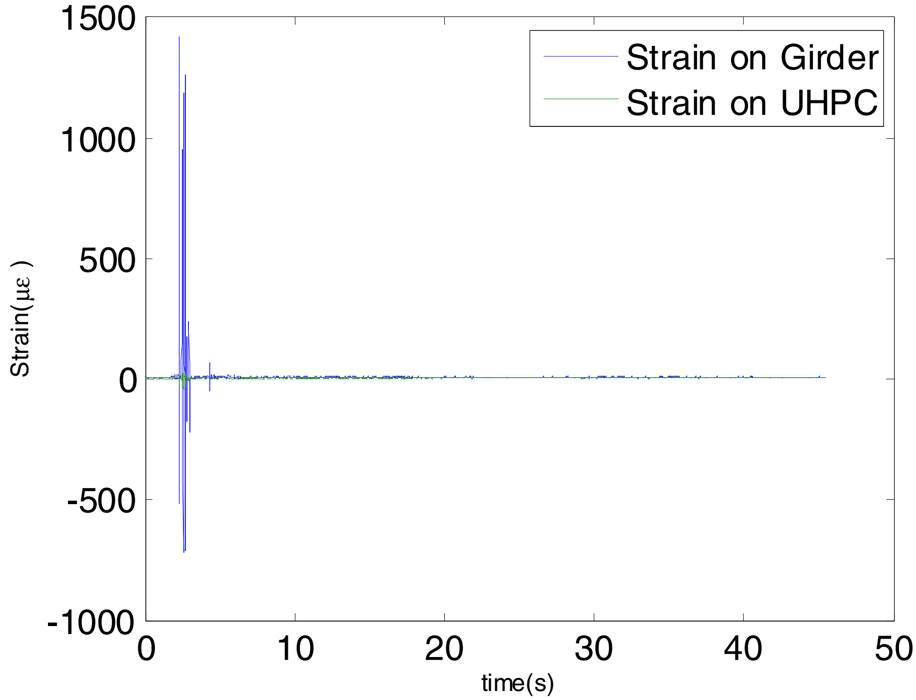

Figure 6-17 Phase 1, Near 3 Max, Strain time-history comparison on the girder and UHPC

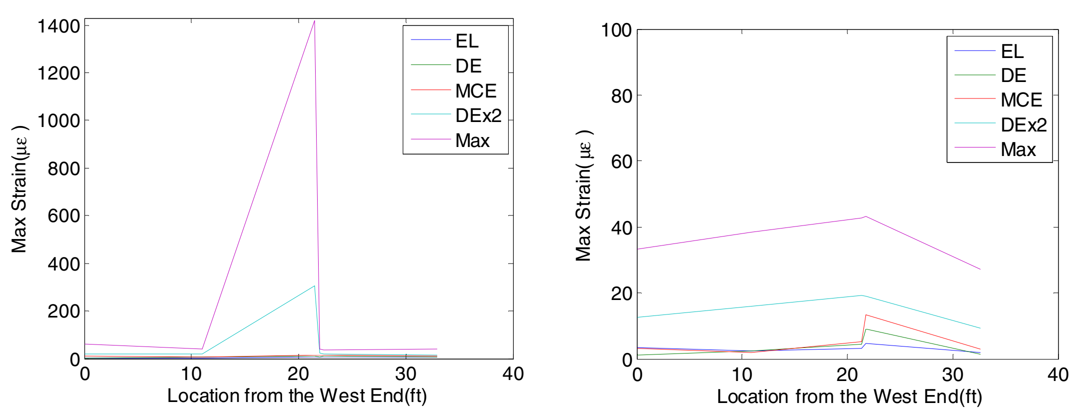

(a) Deck-bulb-Tee girder (b) the UHPC Connection

Figure 6-18 Maximum strain response along the girder under Near 3, PGA = 0.65 g in Phase 1

6.2.1.2 Phase 2

The maximum strains recorded among all 11 strain gauges for each test in phase 2 are summarized in Table 6-10 and Table 6-11. The maximum strain occurred when Near 1 GMs were applied. The maximum strain in the precast girder and the UHPC was 1700 microstrain and 121 microstrain. Since the UHPC strain was still lower than 145 microstrain, the UHPC stayed well within the elastic range. For phase 2, it is noteworthy that the strain at the west end of the girder was larger than in the quarter-locations. The difference can be attributed to the superimposed tension strain in the end of girder caused by the plate.

Table 6-10 Maximum strains of the precast girder in phase 2

GM set	Seismic Level					
	Elastic	**DE**	**MCE**	**DEx2**	**Max**	**Max*1.2**
Far 1	51	50	53	63	112	164
Far 2	49	49	51	60	106	138
Far 3	50	50	53	69	132	196
Far 4	50	49	53	66	121	155
Far 5	50	48	53	66	124	155
Near 1	50	49	53	741	1356	1721
Near 2	50	49	52	63	122	168
Near 3	50	47	53	62	254	715
Near 4	50	48	53	178	296	715
Near 5	50	47	54	65	128	336
Near 6	50	49	50	60	101	130

Table 6-11 Maximum strains of the UHPC connection in phase 2

GM set	Seismic Level					
	Elastic	**DE**	**MCE**	**DEx2**	**Max**	**Max*1.2**
Far 1	30	35	34	32	32	27
Far 2	30	35	34	33	31	27
Far 3	30	36	34	32	31	27
Far 4	30	36	35	33	33	25
Far 5	30	35	34	31	32	25
Near 1	31	37	39	56	112	121
Near 2	30	35	33	32	30	26
Near 3	31	37	37	43	48	57
Near 4	31	38	38	42	51	57
Near 5	30	36	35	34	36	35
Near 6	30	35	34	33	31	29

Figure 6-19 illustrates the strain time-histories at the mid-span of the UHPC connection under Near 1 GMs with the 120% maximum level of amplitude in test phase 1, i.e. peak ground acceleration (PGA) equal to 0.77 g. and illustrates the strain distribution along the girder longitudinal direction. Similar conclusions can be drawn from the strain distribution.

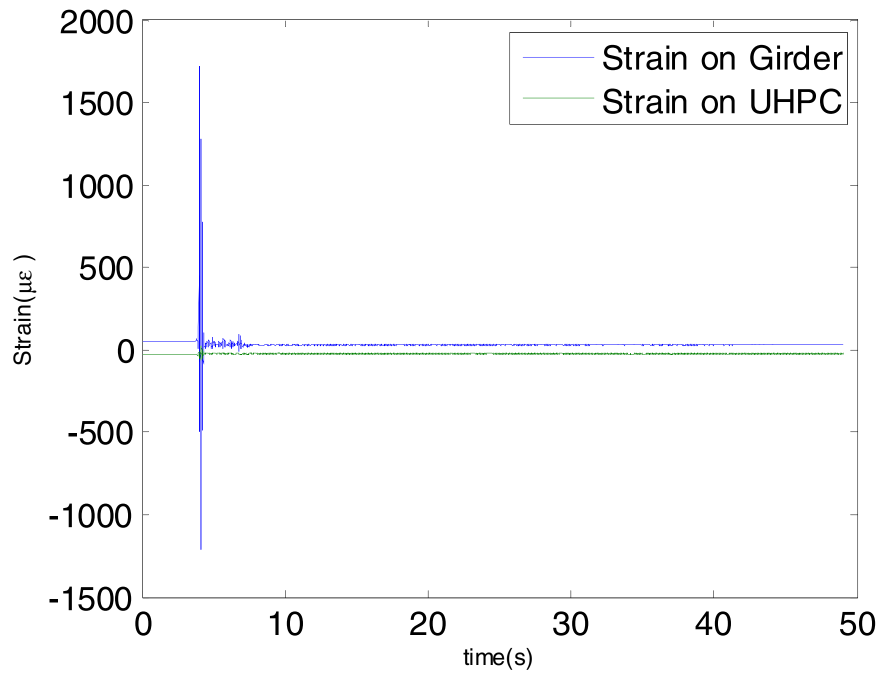

Figure 6-19 Phase 2, Near 1 Max, Strain time-history comparison on the girder and UHPC

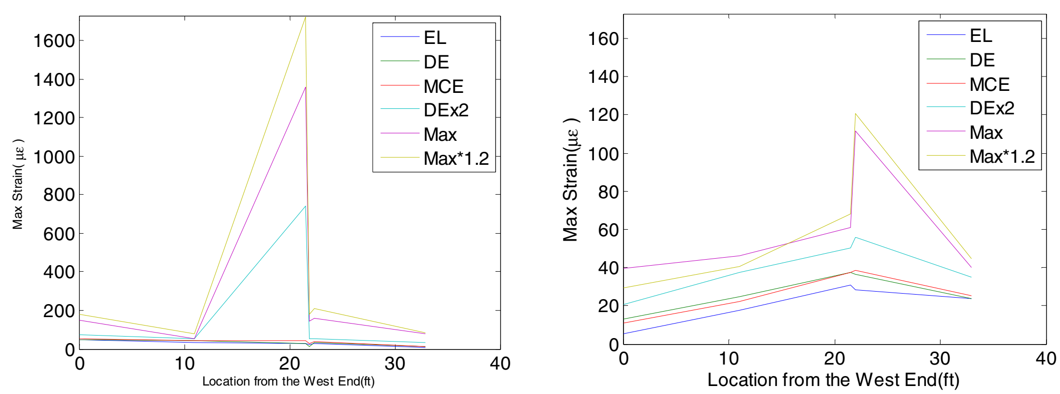

(a) Deck-bulb-Tee girder (b) the UHPC Connection

Figure 6-20 Maximum strain response along the girder under Near 3, PGA = 0.77 g in Phase 2

6.2.1.3 Phase 3

The maximum strains recorded among all 11 strain gauges for each test in phase 3 are summarized in Table 6-12. The maximum strain for each case did not exceed those of phase 2.

Table 6-12 Maximum strains of the precast girder and UHPC connection in phase 3

GM set	Max-Girder	Max-UHPC
Far 1	173	36
Far 2	165	29
Far 3	204	44
Far 4	177	67
Far 5	126	33
Near 1	1437	90
Near 2	167	28
Near 3	199	51
Near 4	420	52
Near 5	180	42
Near 6	143	28

6.2.2 Response of the relative displacement of the UHPC connection

6.2.2.1 Phase 1

The maximum relative displacements recorded among the LVDTs in the longitudinal and transverse directions for each test in phase 1 are summarized in Table 6-12 and 6-13. Similarly, it can be seen that the maximum relative displacement in the longitudinal direction was 0.00098 in, which also occurred when Near 3 GMs were applied. The maximum relative displacement in the transverse direction was 0.00074 in, which occurred when Far 5 GMs were applied. By converting the relative displacement into the average strain in the connection, the maximum value is 123 and 93 microstrain, respectively. The transverse maximum strain did not exceed 145 microstrain, which complies with the conclusion drawn in Section 6.2.1.

Table 6-13 Maximum relative longitudinal displacements of the precast girder in phase 1 (Unit: 10^{-3}in)

GM set	Seismic Level				
	Elastic	DE	MCE	DEx2	Max
Far 1	0.24	0.27	0.25	0.29	0.43
Far 2	0.25	0.25	0.22	0.28	0.29
Far 3	0.23	0.24	0.26	0.33	0.40
Far 4	0.22	0.25	0.23	0.23	0.28
Far 5	0.27	0.27	0.26	0.26	0.53
Near 1	0.25	0.25	0.29	0.25	0.47
Near 2	0.24	0.26	0.26	0.23	0.36
Near 3	0.27	0.26	0.48	0.98	0.87
Near 4	0.21	0.25	0.27	0.23	0.37
Near 5	0.28	0.26	0.25	0.60	0.35
Near 6	0.19	0.26	0.27	0.29	0.29

Table 6-14 Maximum relative transverse displacements of the UHPC connection in phase 1(Unit: 10^{-3}in)

GM set	Seismic Level				
	Elastic	DE	MCE	DEx2	Max
Far 1	0.30	0.23	0.26	0.41	0.63
Far 2	0.28	0.27	0.28	0.27	0.39
Far 3	0.26	0.25	0.27	0.26	0.31
Far 4	0.25	0.24	0.26	0.26	0.42
Far 5	0.26	0.25	0.26	0.34	0.74
Near 1	0.26	0.24	0.27	0.32	0.54
Near 2	0.26	0.25	0.22	0.38	0.49
Near 3	0.24	0.23	0.27	0.60	0.64
Near 4	0.25	0.22	0.26	0.44	0.73
Near 5	0.30	0.28	0.28	0.47	0.54
Near 6	0.24	0.26	0.23	0.27	0.37

Figure 6-21 illustrates the transverse relative displacement time-histories at the west end and mid-span of the UHPC connection under Far 5 GMs with the maximum level of amplitude in test phase 1, i.e. peak ground acceleration (PGA) equal to 0.65 g. The figure does not clearly show the displacement response because the response was very small, and thus submerged by the environmental noises. Figure 6-22 illustrates the relative displacement increases with the increase of PGA, but the maximum value stayed within a very small range, i.e., below 0.001 in.

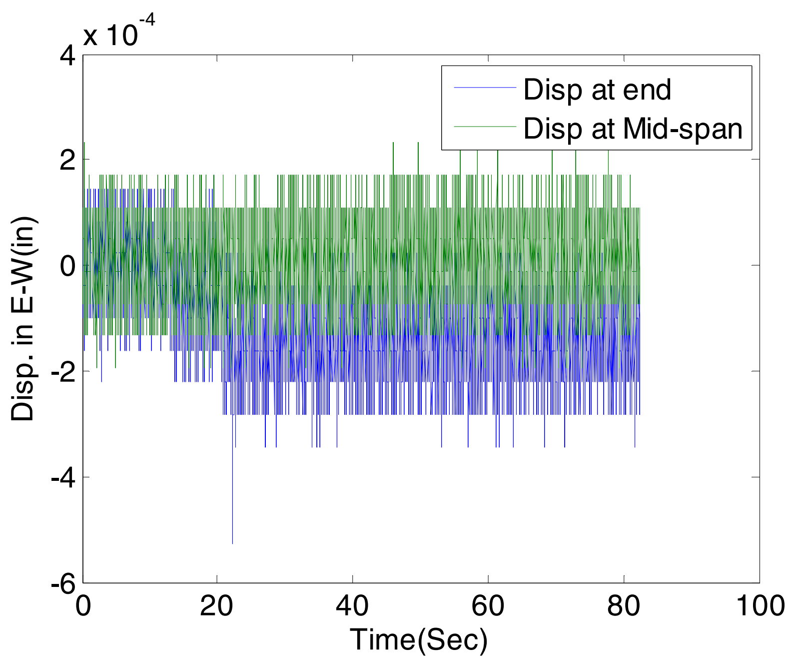

Figure 6-21 Phase 1, Far 5 Max, Relative displacement time-history on the girder end and midspan

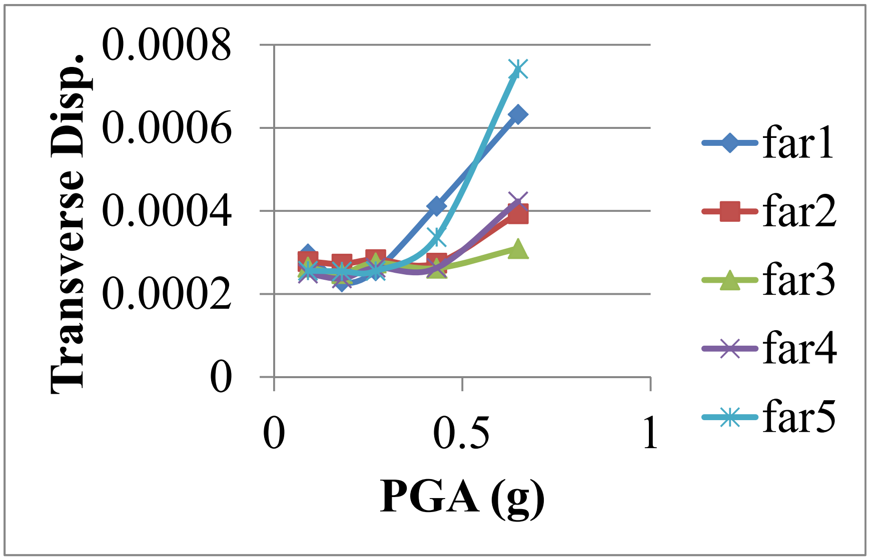

(a) Far field

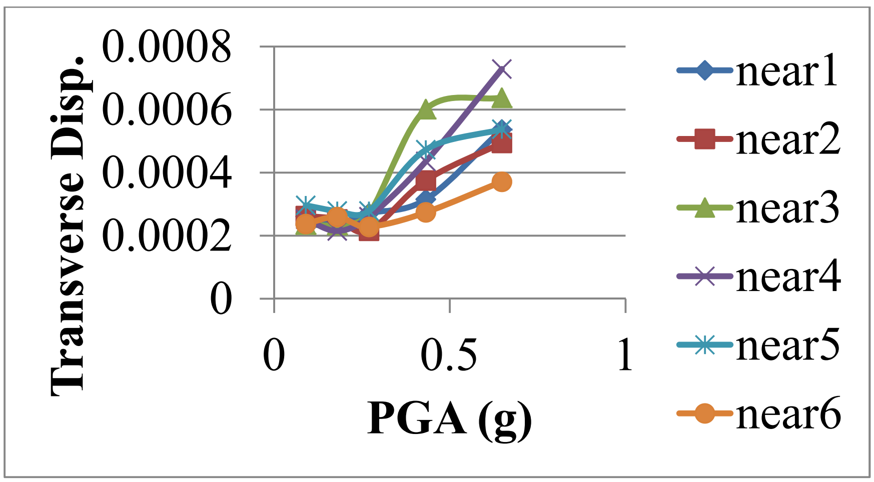

(b) Near fault

Figure 6-22 Maximum relative displacement response in Phase 1

6.2.2.2 Phase 2

The maximum relative displacements recorded among the LVDTs in longitudinal and transverse directions for each test in phase 2 are summarized in Table 6-15 and Table 6-16. The maximum relative displacement in the longitudinal direction was 0.0024 in and occurred when Near 1 GMs were applied, whereas the maximum relative displacement in the transverse direction was 0.00396 in and also occurred when Near 1 GMs were applied. The maximum relative displacement in Phase 2 was 5.3 times that of Phase 1. These results can be explained in two ways: 1) the steel plate imposed an excessive unbalanced stress on the connection, and 2) the Near 1 GMs exhibited strong excitation in the vertical direction, especially after the steel plate was applied.

Table 6-15 Maximum relative longitudinal displacements of the precast girder in phase 2 (Unit: 10^{-3}in)

GM set	Seismic Level					
	Elastic	DE	MCE	DEx2	Max	Max*1.2
Far 1	0.24	0.26	0.25	0.34	0.43	0.63
Far 2	0.23	0.28	0.25	0.29	0.35	0.41
Far 3	0.25	0.23	0.27	0.33	0.70	0.48
Far 4	0.22	0.22	0.27	0.35	0.62	0.47
Far 5	0.25	0.27	0.26	0.31	0.92	0.82
Near 1	0.24	0.24	0.27	0.74	1.80	2.40
Near 2	0.26	0.23	0.23	0.34	0.44	0.57
Near 3	0.24	0.41	0.28	0.53	0.64	0.79
Near 4	0.24	0.22	0.29	0.47	0.68	0.79
Near 5	0.25	0.27	0.29	0.36	0.64	0.59
Near 6	0.22	0.29	0.22	0.30	0.28	0.36

Table 6-16 Maximum relative transverse displacements of the UHPC connection in phase 2 (Unit: 10^{-3}in)

GM set	Seismic Level					
	Elastic	DE	MCE	DEx2	Max	Max*1.2
Far 1	0.23	0.24	0.33	1.08	2.21	2.56
Far 2	0.23	0.24	0.29	0.51	0.80	1.09
Far 3	0.23	0.26	0.26	0.55	1.55	2.83
Far 4	0.23	0.20	0.24	0.62	1.15	2.27
Far 5	0.23	0.24	0.25	1.03	2.81	2.52
Near 1	0.23	0.23	1.02	2.57	3.83	3.96
Near 2	0.22	0.23	0.25	1.08	2.11	3.14
Near 3	0.23	0.27	0.26	1.67	2.82	3.76
Near 4	0.22	0.22	2.15	2.06	3.36	3.76
Near 5	0.29	0.24	0.58	1.22	2.70	3.37
Near 6	0.23	0.26	0.25	0.58	0.78	1.34

Figure 6-23 illustrates the transverse relative displacement time-histories at the end and mid-span of the UHPC connection under Near 1 GMs with the maximum level of amplitude in test phase 2, i.e. peak ground acceleration (PGA) equal to 0.78 g. The residual of relative displacement was relatively small; thus, the UHPC connection exhibited a strong bond behavior between these two girders. Figure 6.24 illustrates the relative displacement increases with the increase of PGA. The maximum strain was below 0.004 in.

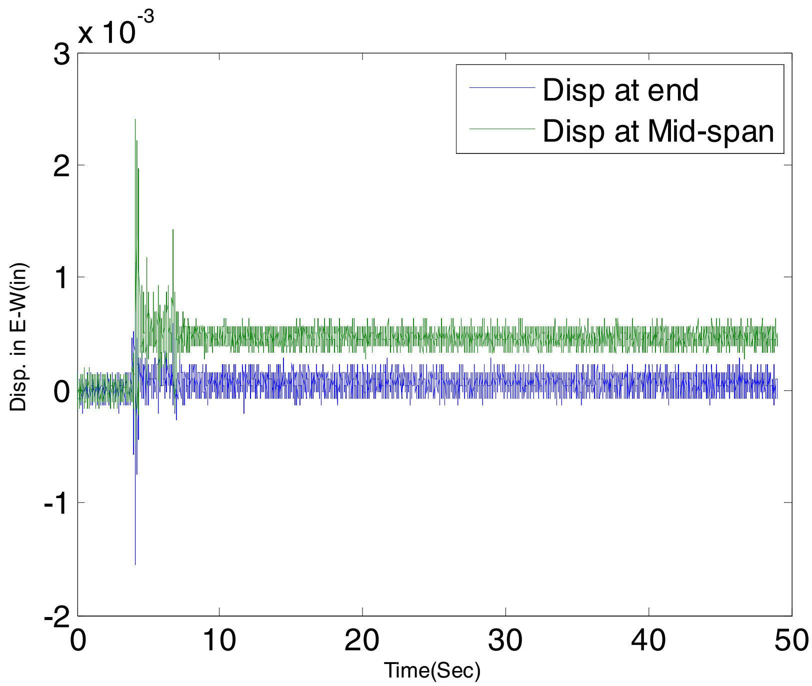

Figure 6-23 Phase 2, Near 1 Max*1.2, Relative displacement time-history on the girder end and midspan

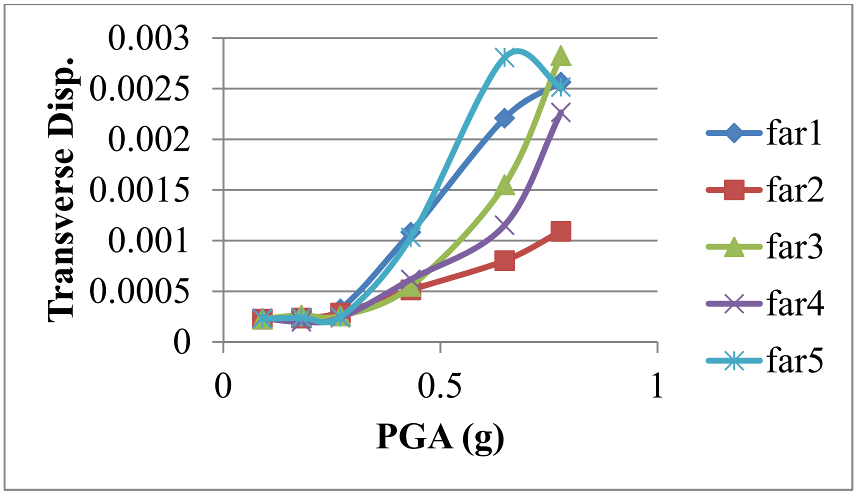

(a) Far field

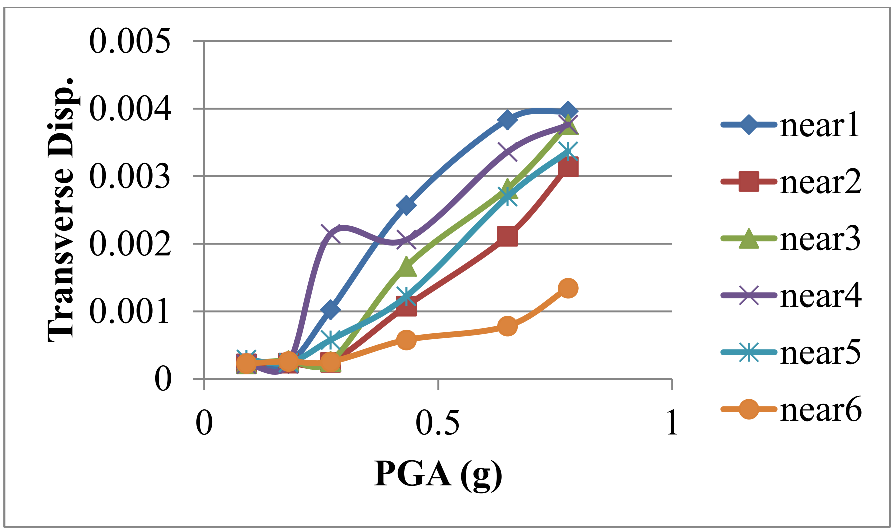

(b) Near fault

Figure 6-24 Maximum relative displacement response in Phase 2

6.2.2.3 Phase 3

The maximum relative displacements recorded among the LVDTs in longitudinal and transverse directions for each test in phase 3 are summarized in Table 6-17. Without the constraint of diaphragms, the relative displacement increased dramatically. For the longitudinal direction, the relative displacement increased up to 2 times that of Phase 2.

Figure 6-25 shows the transverse relative displacement time-histories at the end and mid-span of the UHPC connection under Near 3 GMs with the maximum level of amplitude in test phase 3. Apparently, the residual displacement of the end was larger than that in phase 2 due to the removal of steel diaphragms. Although the specimen still provided sufficient performance under all seismic testing, it is recommended to install the diaphragms at a certain distance in the practical use of precast girders in high seismic regions to increase the integrity of the superstructure and prohibit excessively large deformation.

Table 6-17 Maximum relative longitudinal displacements of the UHPC connection in phase 3 (Unit: 10^{-3}in)

GM set	Max - Longitudinal	Max - Transverse
Far 1	0.61	8.80
Far 2	0.32	3.83
Far 3	1.19	5.09
Far 4	9.80	8.14
Far 5	0.65	3.72
Near 1	2.00	6.55
Near 2	0.64	5.63
Near 3	2.51	8.26
Near 4	1.51	6.04
Near 5	1.11	6.56
Near 6	16.32	5.14

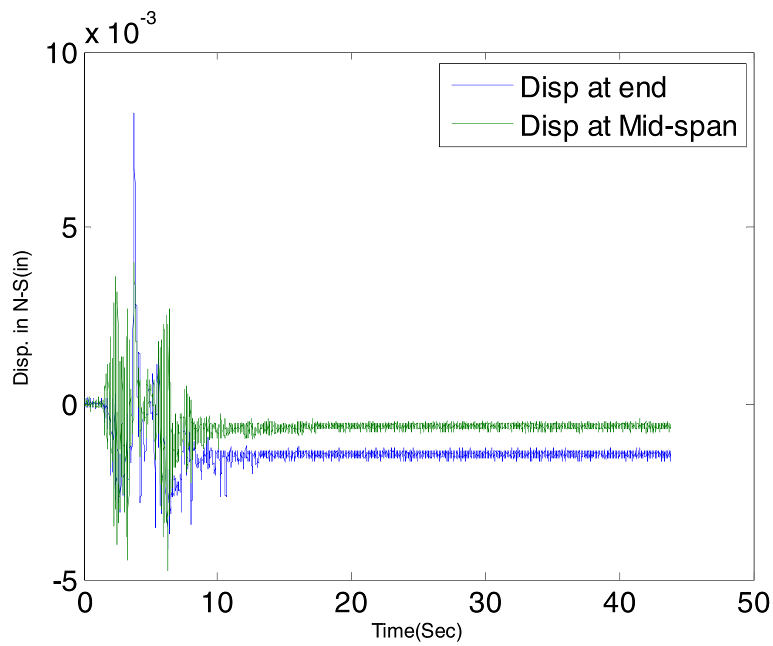

Figure 6-25 Phase 3, Near 3 Max, relative displacement time-history on the girder end and midspan

6.3 Seismic Analysis using FEM Model

The comparisons on the frequency result of shake table test and FEM analysis are listed in Table 6-18 and Table 6-19.

Table 6-18 Natural frequencies of the specimen in phase 1

Modal Shapes	Experimental Frequencies (Hz)	FEM Model Frequencies (Hz)	Differences of Test/FEA
Transverse translation	6.30	6.97	10.6%
Longitudinal translation	7.38	7.62	3.1%
Rotation around vertical axis	N/A	11.91	N/A
Vertical bending	12.53	12.73	1.6%
Combined vertical and transverse bending	N/A	16.95	N/A

Table 6-19 Natural frequencies of the specimen in phase 2

Modal Shapes	Experimental Frequencies (Hz)	FEM Model Frequencies (Hz)	Differences of Test/FEA
Transverse translation	5.20	6.42	19.0%
Longitudinal translation	6.21	7.02	11.5%
Vertical bending	10.46	10.85	3.6%
Rotation around vertical axis	N/A	11.91	N/A
Combined vertical and transverse bending	N/A	14.06	N/A

For the numerical analysis, one set of near field ground motions, the Near 3 ground motion, was selected. The analysis was run on the server of the University at Buffalo's Center for Computational Research (CCR). The CCR consists of 128 CPUs and thus provides extremely high calculation power. However, the maximum time-cap of 72 hours was necessary for analysis in CCR. Due to this time-cap limit, the server was unable to run the analyses for the full ground motion record. Approximately 8 seconds of analysis could be completed within this time for the selected ground motion. Therefore, a simplified model is needed to conduct in-depth seismic analysis.

Since it is unrealistic to use the refined 3-D model to predict the seismic behavior of the UHPC connected girder, a simplified model is established by SAP 2000. The model is shown in Figure 6-26.

A brief description of the simplified SAP2000 model is presented below:

Elements: The concrete girder and UHPC connection were modeled with shell elements. The diaphragms and prestressed tendons were modeled by frame elements. The elastomeric bearings were modeled by link elements.

Materials: The bridge deck was modeled with concrete material. The structural steel shapes were modeled by A60 steel material. All materials were considered in their elastic range.

Contact: It is assumed that the contacts between UHPC connection and girders, the girders and the bearings, the bearings and the shake tables are fixed. The shake tables are fixed to the ground in the model.

The comparison of the acceleration response of experimental and numerical results for Far 1 ground motion is shown in Figure 6-27. The acceleration responses of test and FEA results show good agreement with each other.

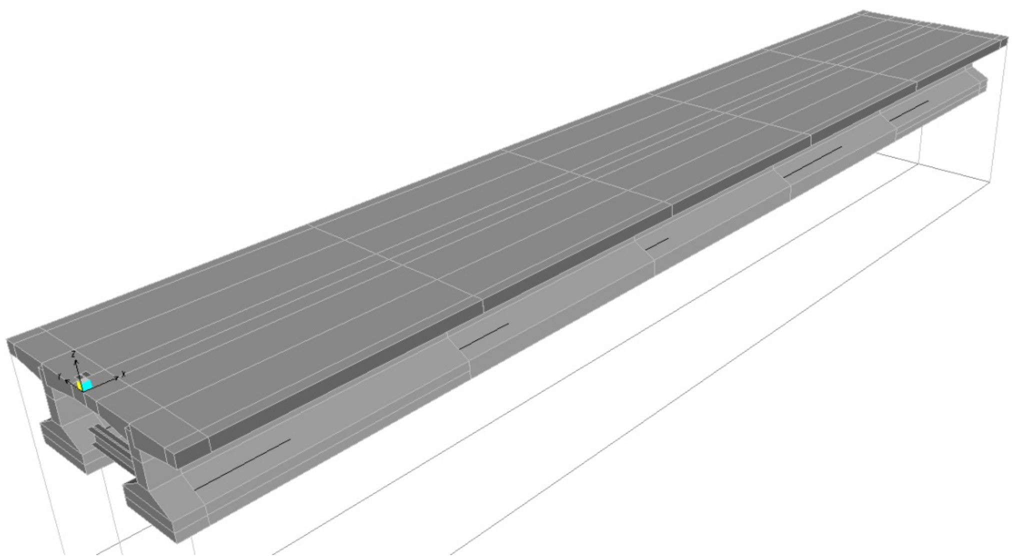

Figure 6-26 A simplified 3-D model built by SAP 2000

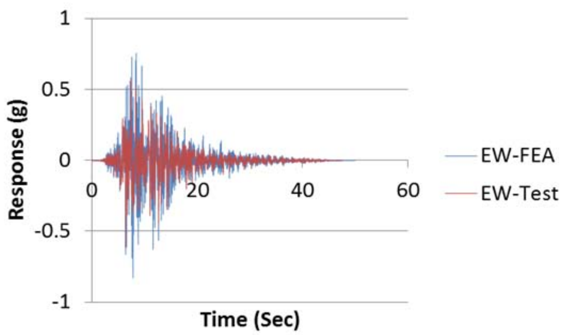

(a) Far 1 at maximum level, E-W direction

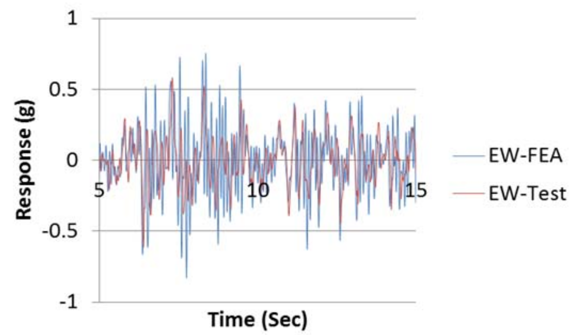

(b) Far 1 at maximum level, E-W direction, 5-15 sec

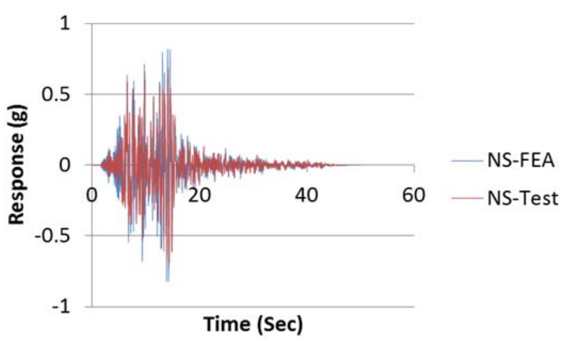

(c) Far 1 at maximum level, N-S direction

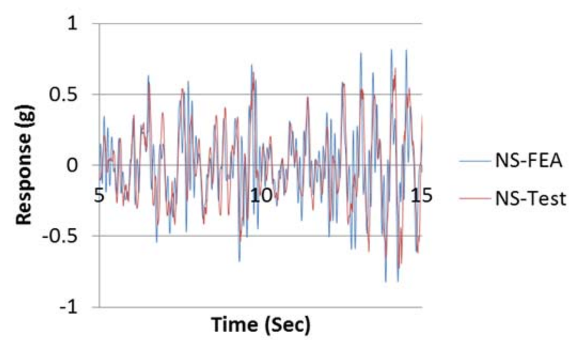

(d) Far 1 at maximum level, N-S direction, 5-15 sec

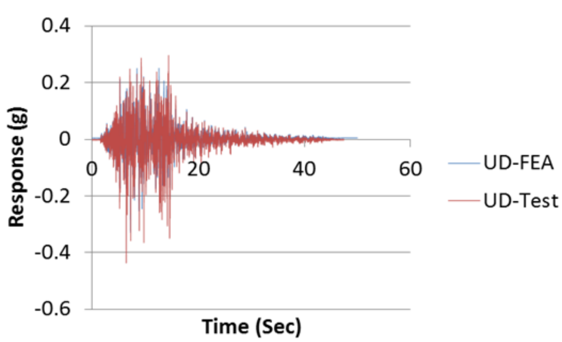

(e) Far 1 at maximum level, U-D direction

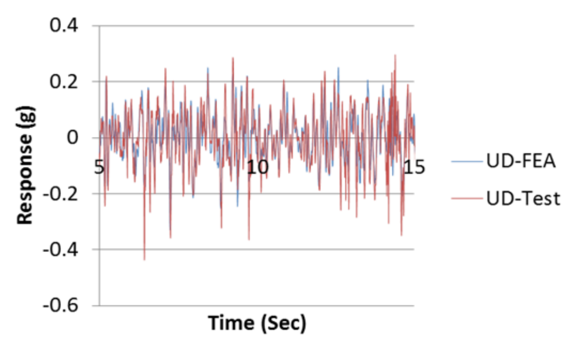

(f) Far 1 at maximum level, U-D direction, 5-15 sec

Figure 6-27 Comparison of acceleration response in test and numerical models

The comparisons of the maximum acceleration responses at the P1 and P5 (see Figure 5-1) of experimental and numerical results for all the ground motions are shown in Figure 6-28. It can be seen that the numerical model can accurately predict the responses in two horizontal directions (E-W and N-S). The responses in the vertical direction (U-D) in the test are significantly higher than those from the numerical model in some cases; this is mainly because the model does not take the detachment of bearings into account. The differences at P5 (at mid-span) are smaller than those at P1 (at girder end) because the detachment effect has a larger influence on the girder end.

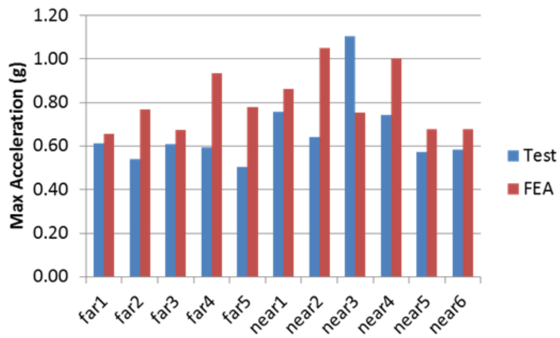

(a) E-W direction, P1, Phase 1

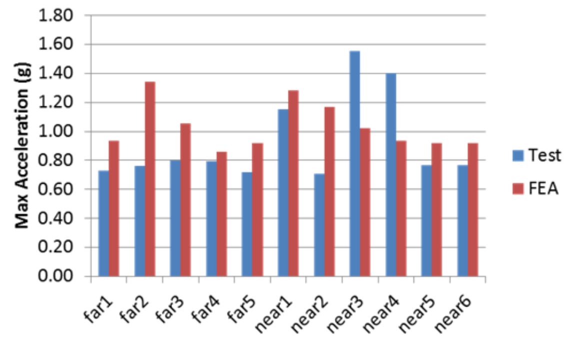

(b) N-S direction, P1, Phase 1

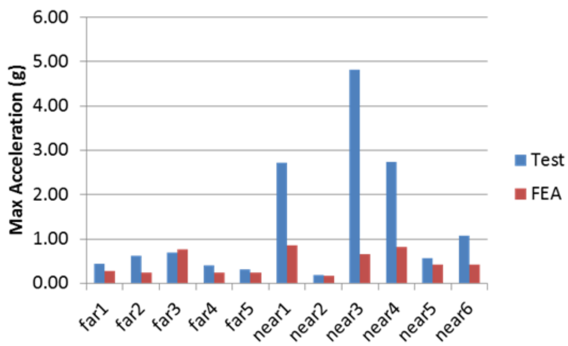

(c) U-D direction, P1, Phase 1

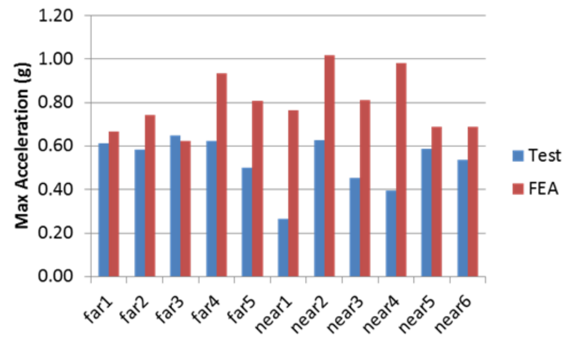

(d) E-W direction, P5, Phase 1

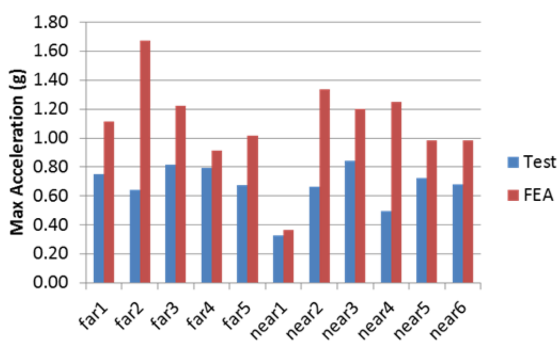

(e) N-S direction, P5, Phase 1

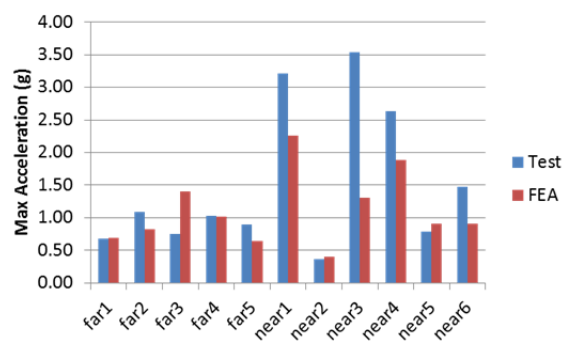

(f) U-D direction, P5, Phase 1

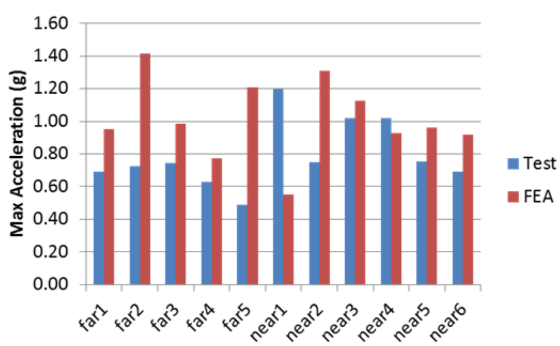

(g) E-W direction, P1, Phase 2

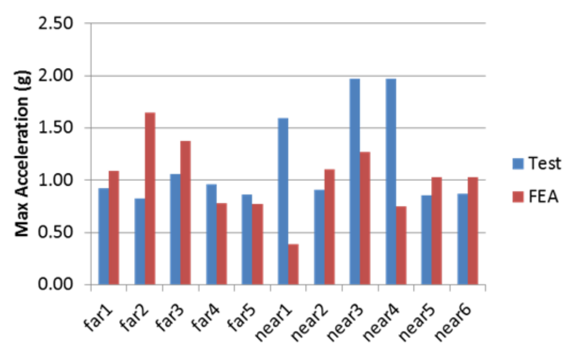

(h) N-S direction, P1, Phase 2

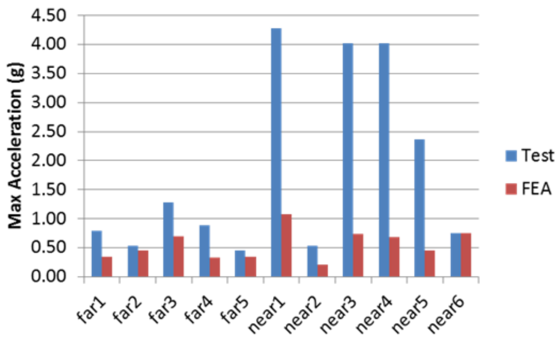

(i) U-D direction, P1, Phase 2

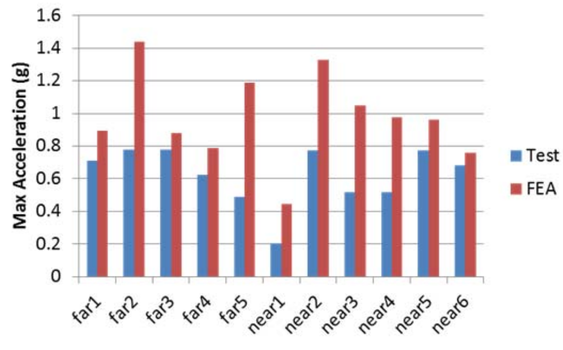

(j) E-W direction, P5, Phase 2

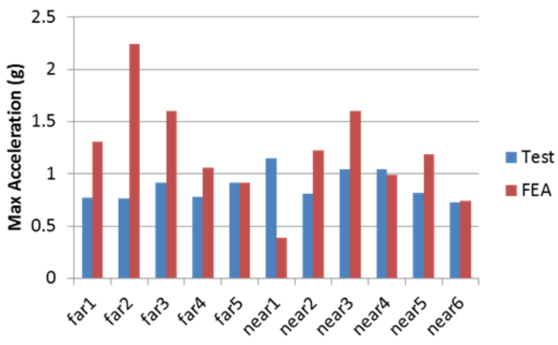

(k) N-S direction, P5, Phase 2

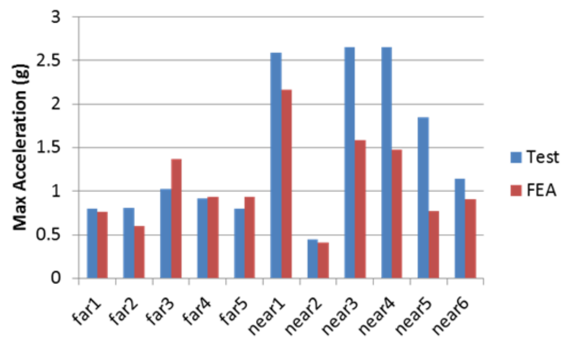

(l) U-D direction, P5, Phase 2

Figure 6-28 Comparison of maximum acceleration response in test and numerical models

SECTION 7
CONCLUSIONS

Several conclusions are drawn from the research tests:

1. The system identification test results show that the dynamic properties of the bridge structure exhibited slight change. The frequency change in the horizontal direction may be attributed to the change of bearing pads as well as to the boundary conditions. The structural dynamic behavior in the Z direction hardly changed.
2. The global response of two UHPC-connected prestressed girders show that under severe earthquakes with PGA up to 0.77 g (with the mid-span of specimen subjected up to 6.1 g in acceleration), and during a resonant response, which imposed very high moment demand at the superstructure, the bridge deck resilience of seismic excitation is verified since no severe damage was found.
3. The analysis of the maximum strain of the UHPC connection shows that the UHPC connection remained in the elastic range during all the seismic tests. The girder may have been subjected to some damage, but it was limited to a small region near the mid-span. This further proves that the strength and seismic performance of UHPC is stronger than that of common concrete.
4. Based on the analysis of maximum relative displacement results, the UHPC connection exhibited sufficient seismic performance under all tests. The relative displacement in the girders without diaphragms increased dramatically compared to the previous phases. It is recommended to install diaphragms at a certain distance in the practical use of precast girders in high seismic regions to increase the integrity of the superstructure and prohibit excessively large deformation.
5. Based on these experimental results, it can be concluded that the UHPC connections with short, straight rebar provide sufficient seismic resistance even under high-level seismic ground motions.
6. Future research objectives: The test specimen in this study approximates a bridge with a short to mid-span length. For a long-span bridge, the connection will be subjected to more severe and complicated stress conditions and will exhibit more complex dynamic responses. In addition, the tests in this project were conducted based on the assumption that the girders directly seat on abutments. The excitations will be modified and the girders may exhibit different conditions if they are supported by columns. Therefore, future research, including experimental and numerical study, could focus on the connection applicable to the long-span bridge and in different supporting conditions.

SECTION 8
REFERENCES

AASHTO (2010). *AASHTO LRFD Bridge Specifications*, American Association of State Highway and Transportation Officials, Washington, D.C.

Arias-Acosta, J.G. and Sanders, D.H. (2010). "Shake Table Testing of Bridge Columns under Combined Actions," *2010 Structures Congress*: Orlando, FL.

ASCE/SEI 7-05 (2006). *Minimum design loads for buildings and others Structures*. American Society of Civil Engineers (ASCE).

Bracci, J.M., Reinhorn, A.M. and Mander, J.B. (1992). *Seismic Resistance of Reinforced Concrete Frame Structures Designed Only for Gravity Loads: Part I - Design and Properties of a One-Third Scale Model Structure*. Technical Report NCEER-92-0027, Buffalo, NY.

Chen, Y.B., Feng, M.Q. and Soyoz, S. (2008), "Large-scale shake table test verification of bridge condition assessment methods," *Journal of Structural Engineering-ASCE*: 134(7), p. 1235-1245.

FEMA P695 (2009). *Quantification of Building Seismic Performance Factors*. Federal Emergency Management Agency.

Graybeal, B.A. and Baby, F. (2013). "Development of a Direct Tension Test Method for UHPFRC," *ACI Materials Journal*: 110(2).

Graybeal, B.A. (2006). *Material Property Characterization of Ultra-High Performance Concrete*. PUBLICATION NO. FHWA-HRT-06-103, Federal Highway Administration.

Graybeal, B.A., (2010). "Behavior of Field-Cast Ultra-High Performance Concrete Bridge Deck Connections Under Cyclic and Static Structural Loading," *Federal Highway Administration, National Technical Information Service Accession No. PB2011-101995*: Washington, D.C.

Graybeal, B.A., (2012). "Ultra-High Performance Concrete Composite Connections for Precast Concrete Bridge Decks," *Federal Highway Administration, National Technical Information Service Accession No. PB2012-107569*: Washington D.C.

Johnson, N., et al (2008). "Seismic testing of a two-span reinforced concrete bridge," *Journal of Bridge Engineering*: 13(2), p. 173-182.

Kajiwara, K., M. Sato, and M. Nakashima (2006). "Shaking table and activities at E-Defense," *Proceedings of the First European Conference on Earthquake Engineering and Seismology*: Geneva, Switzerland.

Kawashima, K., et al. (2012). "Seismic Performance of a Full-Size Polypropylene Fiber-Reinforced Cement Composite Bridge Column Based on E-Defense Shake Table Experiments," *Journal of Earthquake Engineering*: 16(4), p. 463-495.

Li, J. (2013). "Long-term Mission of Tongji Multi-functional Shaking Tables," in *30th Anniversary Celebration of Seismic Research for MTS*: Shanghai, China.

Nakashima, N., et al (2008). "Shake Table Experimental Project on the Seismic Performance of Bridges Using E-Defense," *The 14th World Conference on Earthquake Engineering*: Beijing.

Noguez, C.A.C. and Saiidi, M.S. (2012). “Shake-Table Studies of a Four-Span Bridge Model with Advanced Materials,” *Journal of Structural Engineering-ASCE*. 138(2), p. 182-191.

Ozcelik, O., et al (2008). “Experimental characterization, modeling and identification of the NEES-UCSD shake table mechanical system.” *Earthquake Engineering & Structural Dynamics*: 37(2), p. 243-264.

Ozer, E. and S. Soyoz, (2003). “Vibration-Based Damage Detection and Seismic Performance Assessment of Bridges,” *Earthquake Spectra* (In press).

Park, S.W., W.P. Yen, and I. Cooper, J. D. (2003). “A Comparative Study of U.S.-Japan Seismic Design of Highway Bridges: II. Shake-Table Model Tests,” *Earthquake Spectra*: 19(4), p. 933-958.

Puscasu, G. and Codres B. (2011). “Nonlinear system identification and control based on modular neural networks,” *International Journal of Neural Systems*: 21(4), pp. 319–334

Qu, W., Sun, W. and Zhou, Q. (2005). “Shaking Table Test Research on Insufficient-mass Model of Wanzhou Yangtze River Bridge,” J*ournal of Wuhan University of Technology*: 27(8), p. 45-48.

Reitherman, R.K.(2003). “Development of the Network for Earthquake Engineering Simulation,” *2003 Pacific Conference on Earthquake Engineering*: Christchurch, New Zealand.

Russell H.G., and Graybeal, B.A. (2013). *Ultra-High Performance Concrete: A State-of-the-Art Report for the Bridge Community*. Publication No. FHWA-HRT-13-060, Federal Highway Administration.

Saiidi, S.M., Vosooghi, A., Choi, H. and Somerville, P. (2013A). “Shake Table Studies and Analysis of A Two-span RC Bridge Model Subjected to A Fault Rupture,” *Journal of Bridge Engineering* (In press).

Saiidi, M.S., Vosooghi, A. and Nelson, R.B. (2013B). “Shake-Table Studies of a Four-Span Reinforced Concrete Bridge,” *Journal of Structural Engineering*: 139(8), p. 1352-1361.

Sakai, J. and S. Unjoh (2006). “Earthquake Simulation Test of Circular Reinforced Concrete Bridge Column under Multidirectional Seismic Excitation,” *Earthquake Engineering and Engineering Vibration*: 5(1), p. 103-110.

Sideris, P. (2012). “Seismic Analysis and Design of Precast Concrete Segmental Bridges,” Dissertation, Civil, Structural and Environmental Engineering, University at Buffalo, The State University of New York: Buffalo, NY.

Sirca, G.F. Jr., and Adeli, H. (2012). “System identification in structural engineering,” *Scientia Iranica*: 19(6), pp. 1355–1364.

Song, J.W., Chu, Y.L., Liang, Z., and Lee, G.C. (2008). *Modal Analysis of Generally Damped Linear Structures Subjected to Seismic Excitations*. Technical report MCEER-08-0005, Buffalo, NY.

Zaghi, A.E., M.S. Saiidi, and A. Mirmiran (2012). “Shake table response and analysis of a concrete-filled FRP tube bridge column,” *Composite Structures*: 94(5): p. 1564-1574.

APPENDIX A

SHOP DRAWINGS OF DECK BULB TEE GIRDERS

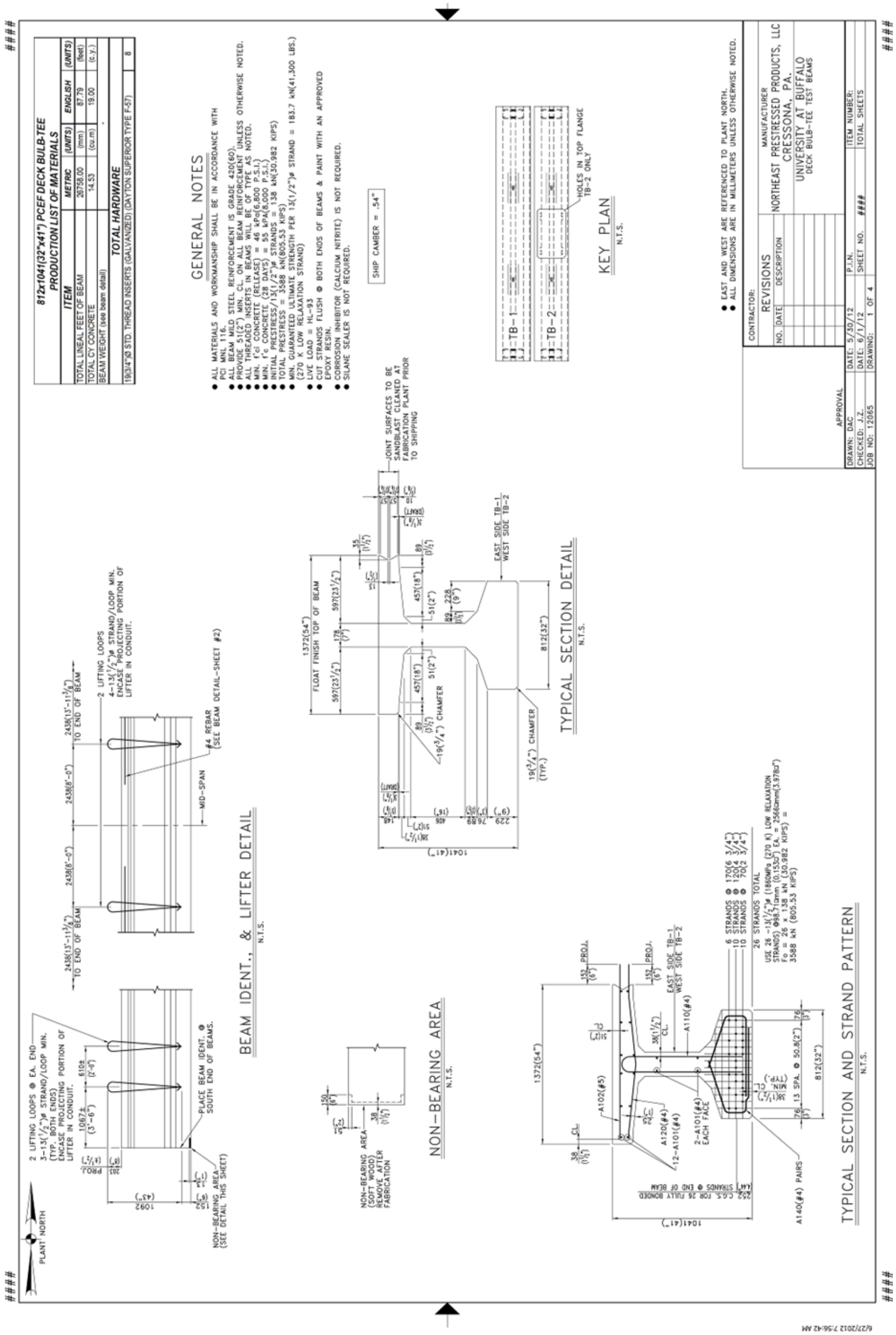

(a)

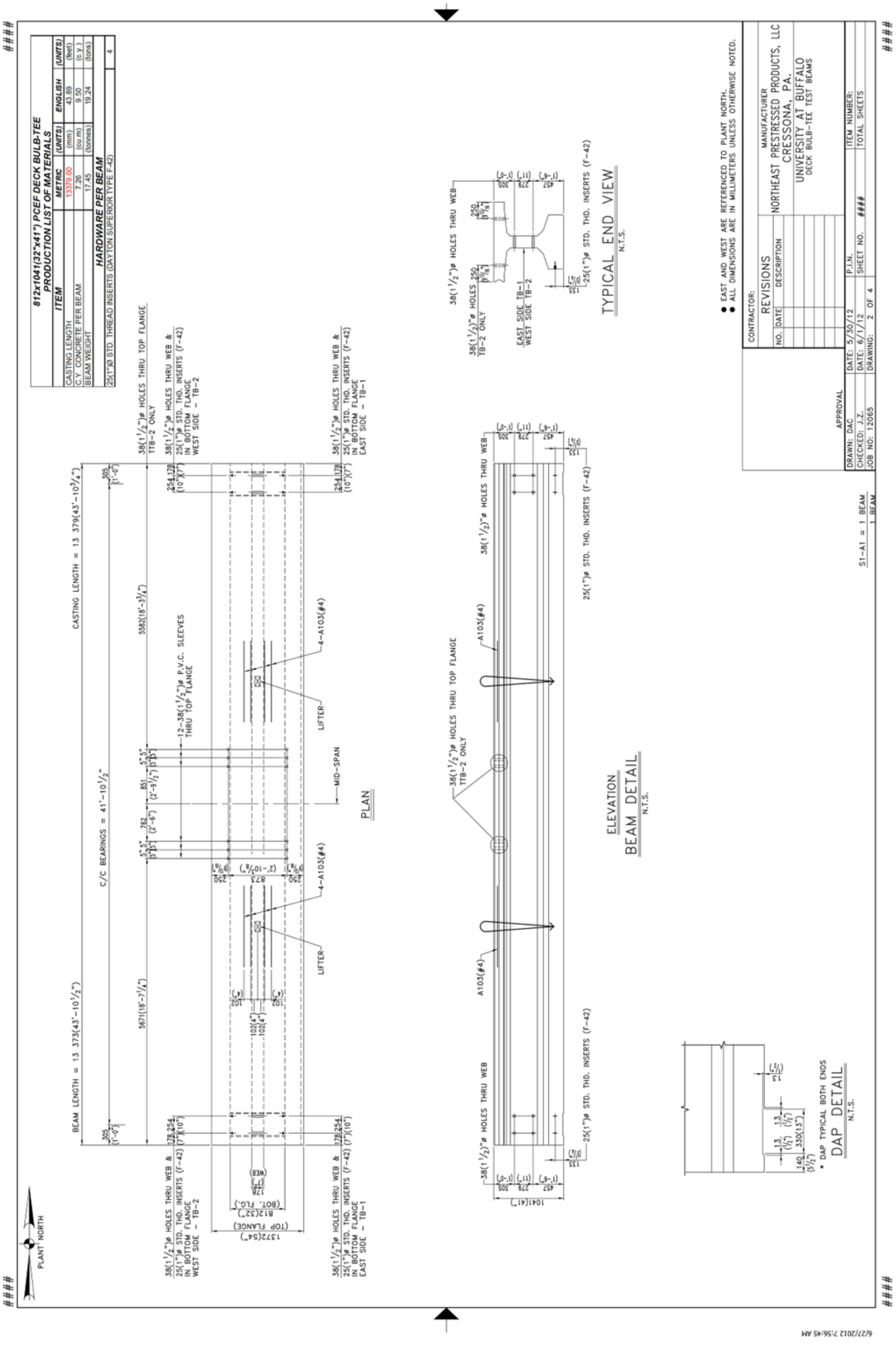

812x1041(32"x41") PCEF DECK BULB-TEE
PRODUCTION LIST OF MATERIALS
HARDWARE PER BEAM
PLAN
ELEVATION
BEAM DETAIL
N.T.S.
TYPICAL END VIEW
N.T.S.
DAP DETAIL
N.T.S.
MANUFACTURER
NORTHEAST PRESTRESSED PRODUCTS, LLC
CRESSONA, PA.
UNIVERSITY AT BUFFALO
DECK BULB-TEE TEST BEAMS
REVISIONS

(b)

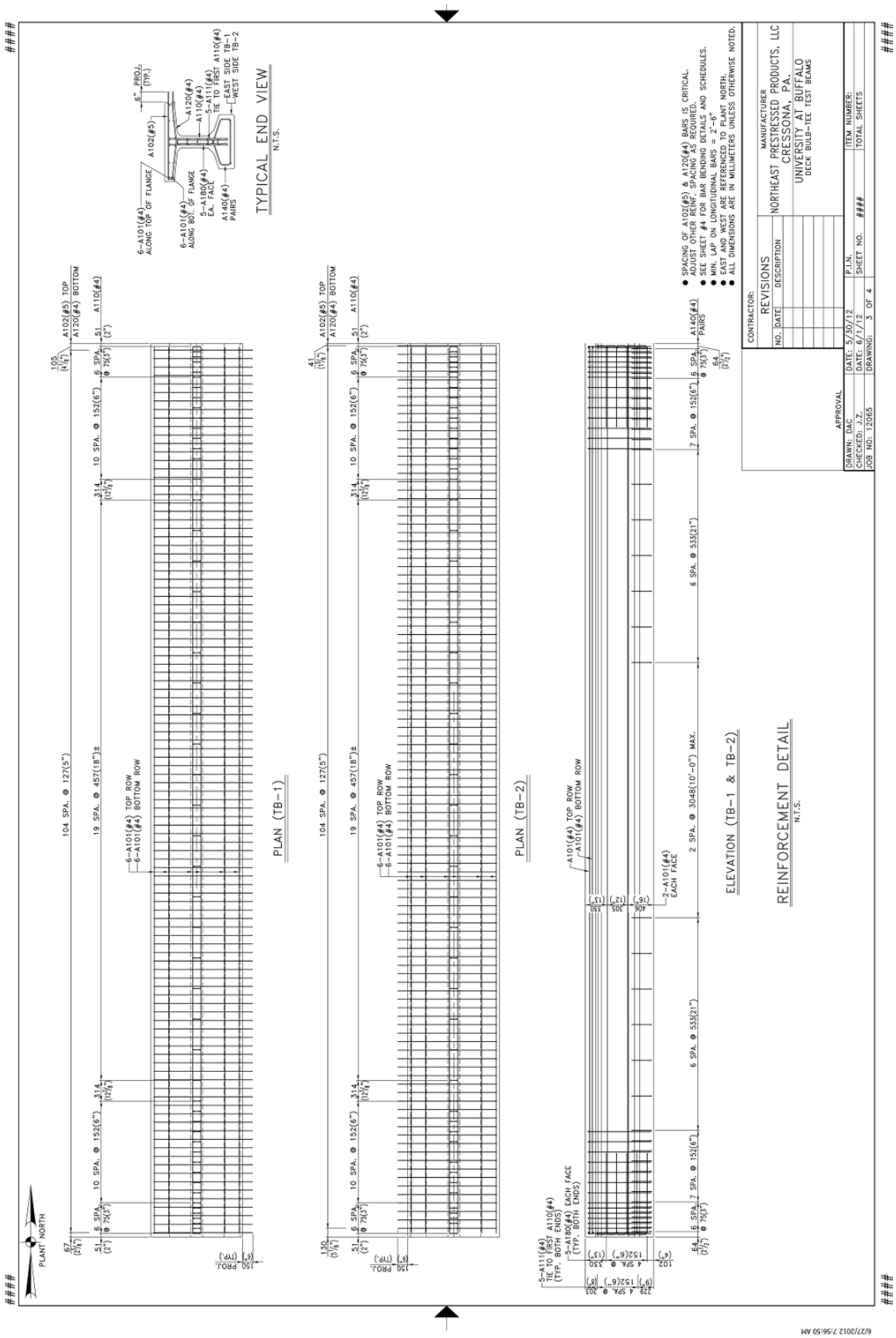

(c)

Figure A-1 Shop Drawings of Deck Bulb Tee Girders

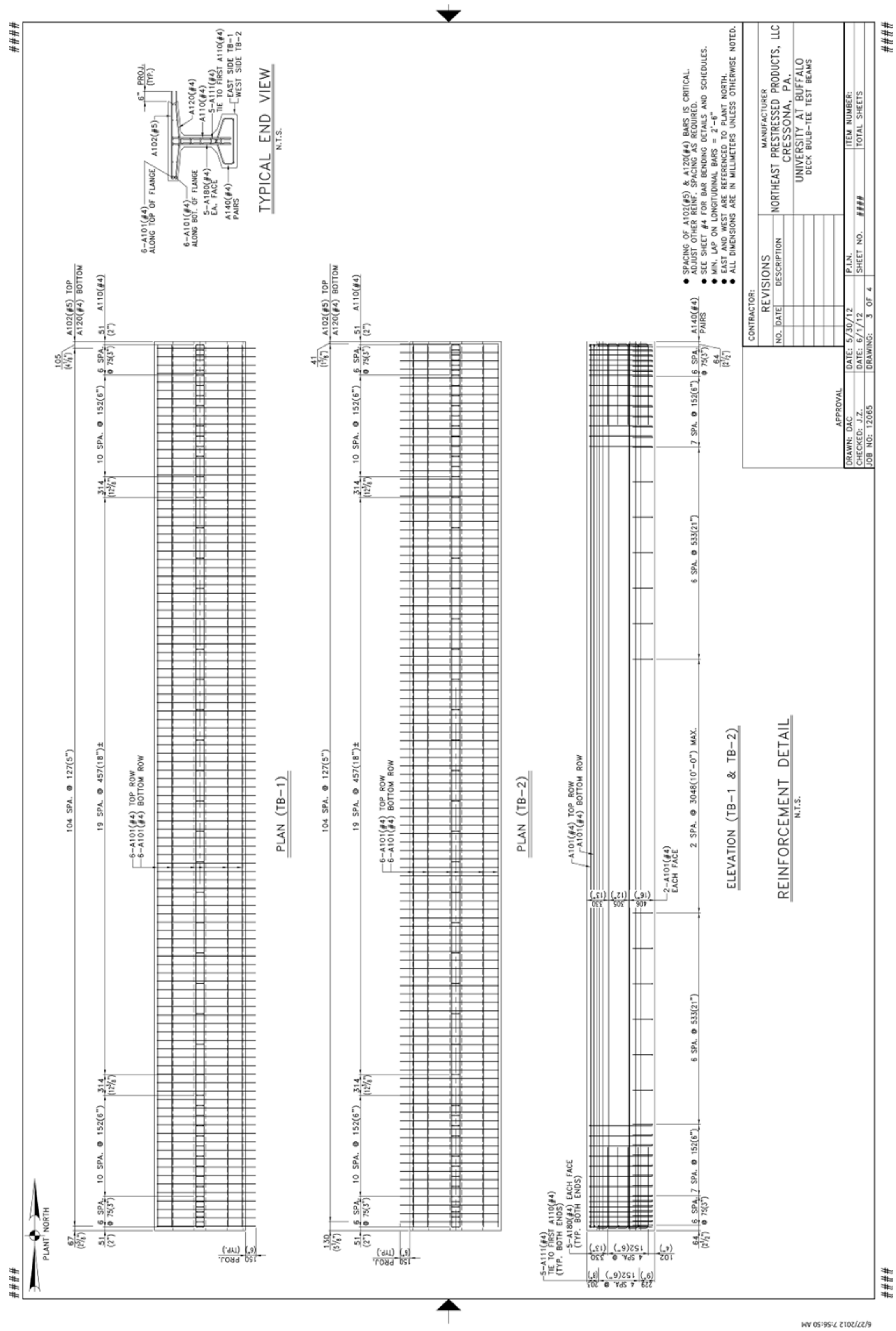

(c)

Figure A-1 Shop Drawings of Deck Bulb Tee Girders

APPENDIX B

TIME-HISTORY OF SELECTED GROUND MOTIONS

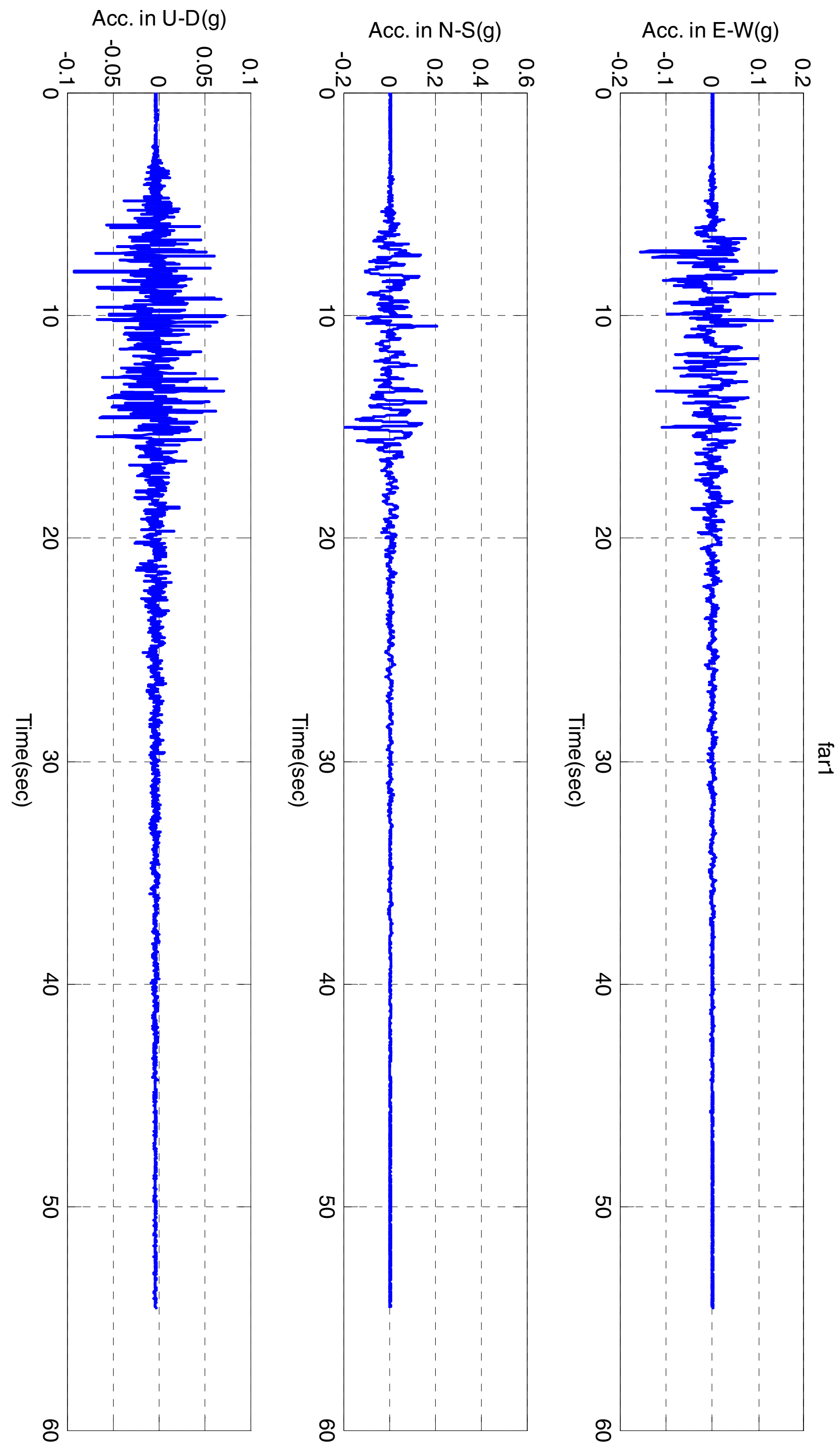

(a) Far 1

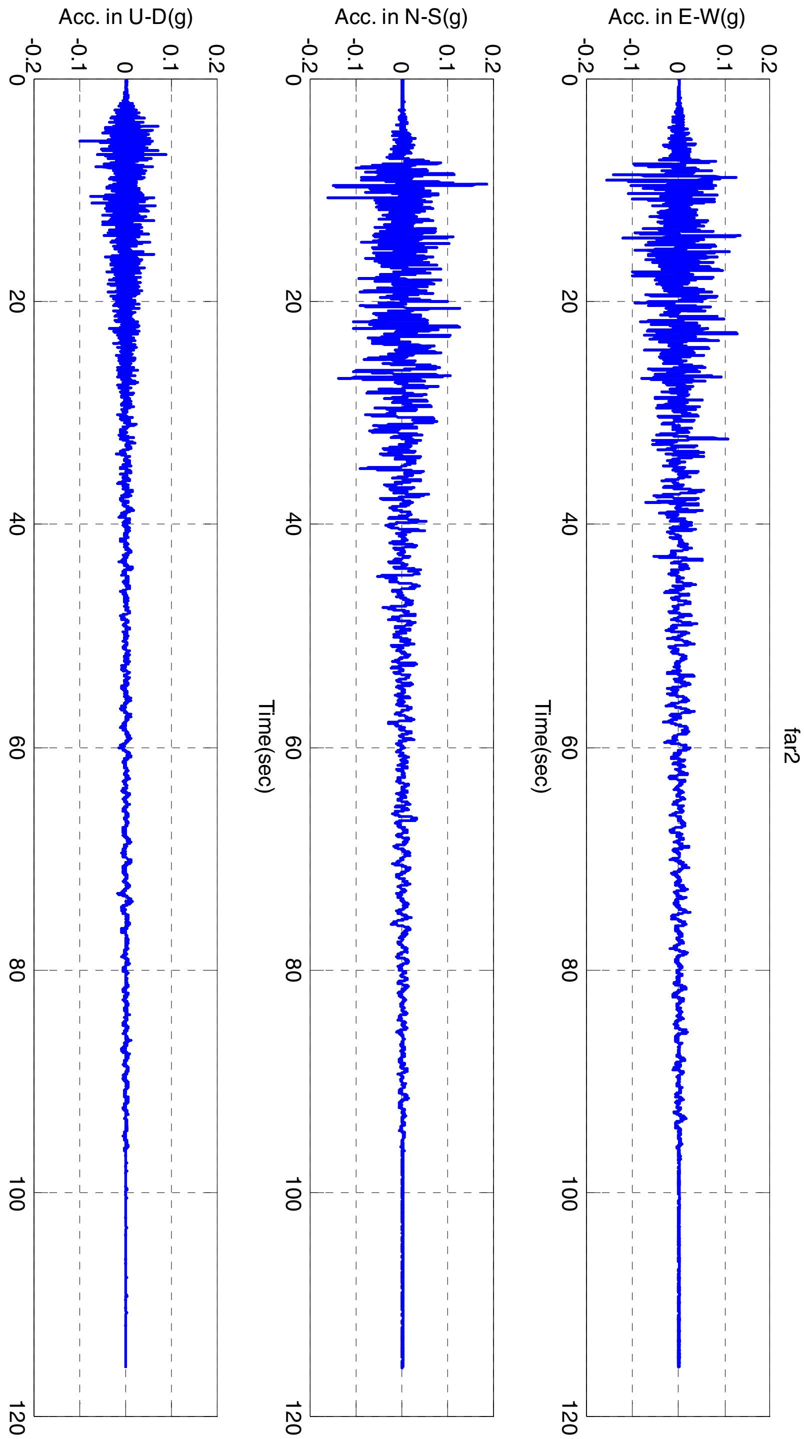
far2
Acc. in E-W(g)
Acc. in N-S(g)
Acc. in U-D(g)
Time(sec)
Time(sec)
Time(sec)
-0.2
-0.1
0
0.1
0.2
0
20
40
60
80
100
120

(b) Far 2

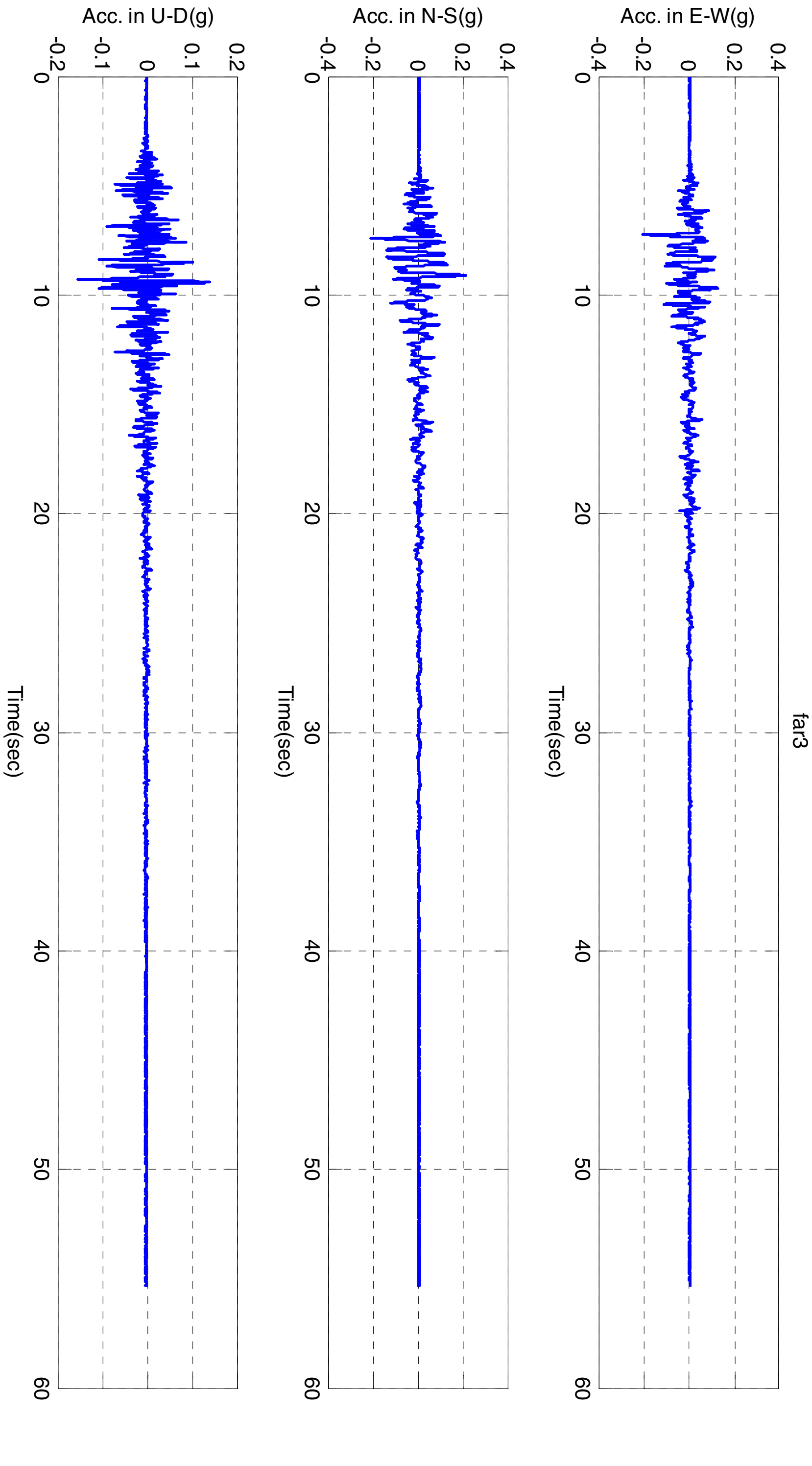

(c) Far 3

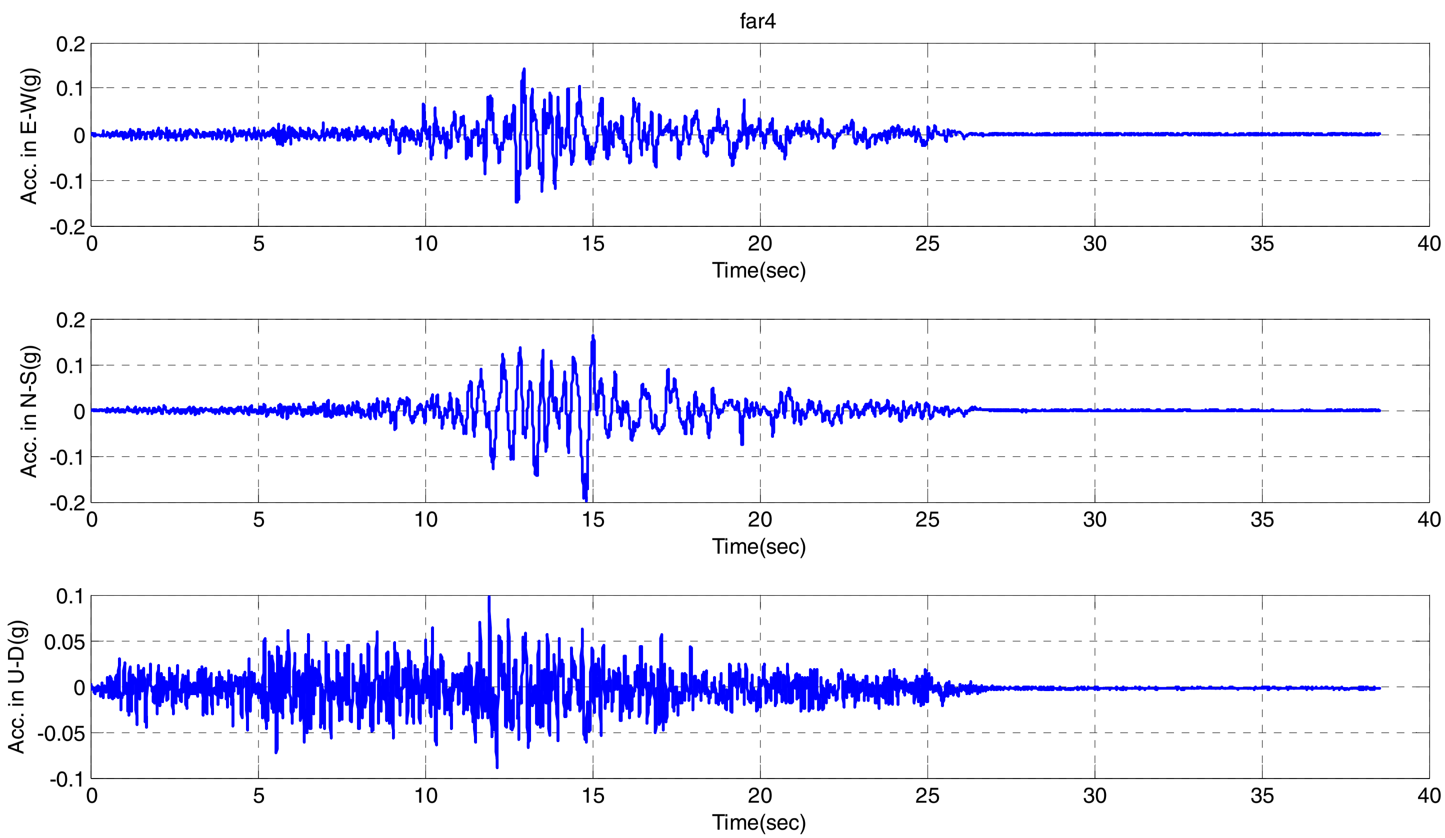

(d) Far 4

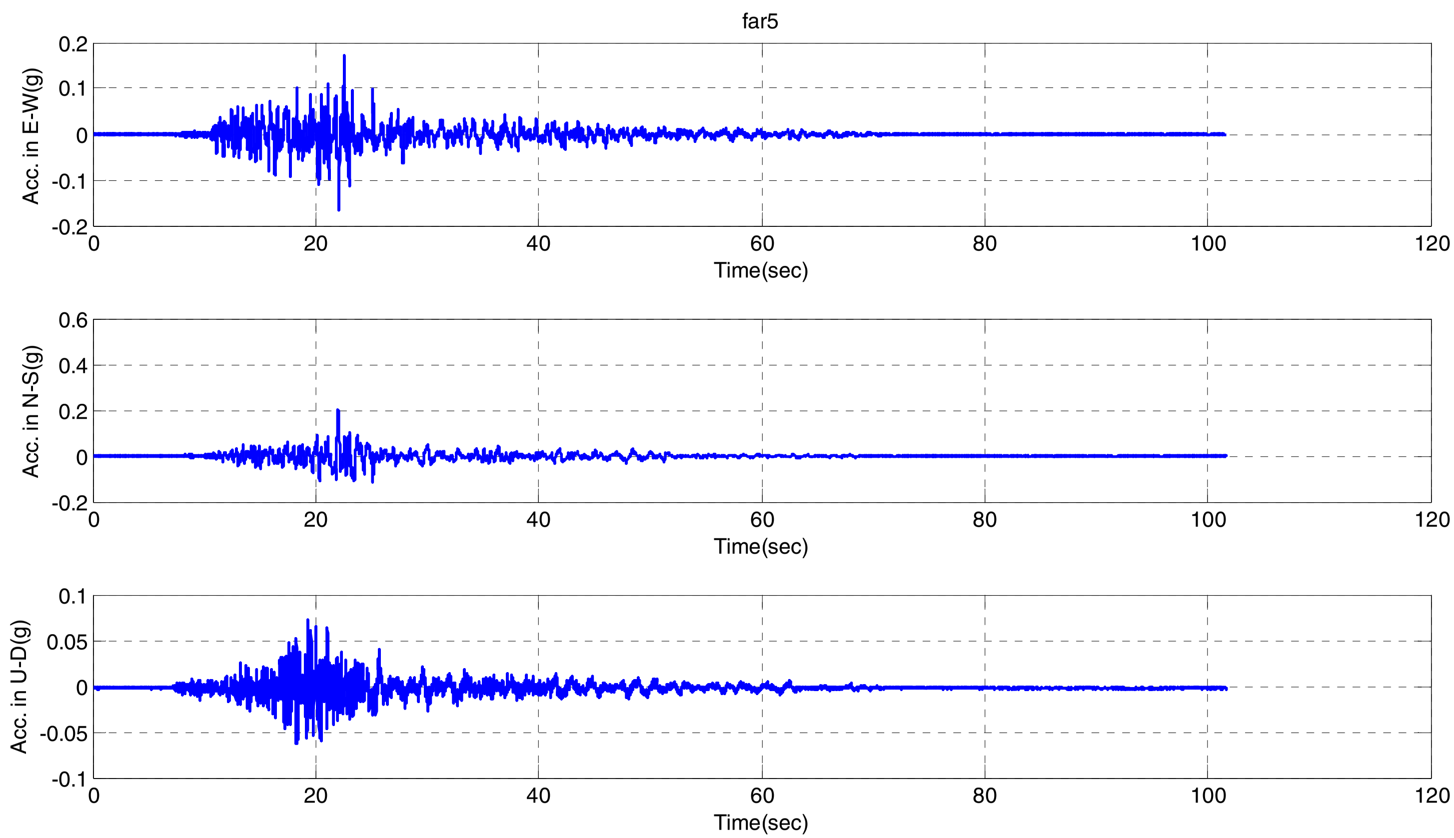
far5
Acc. in E-W(g)
0.2
0.1
0
-0.1
-0.2
Time(sec)
Acc. in N-S(g)
0.6
0.4
0.2
0
-0.2
Time(sec)
Acc. in U-D(g)
0.1
0.05
0
-0.05
-0.1
0
20
40
60
80
100
120
Time(sec)

(e) Far 5

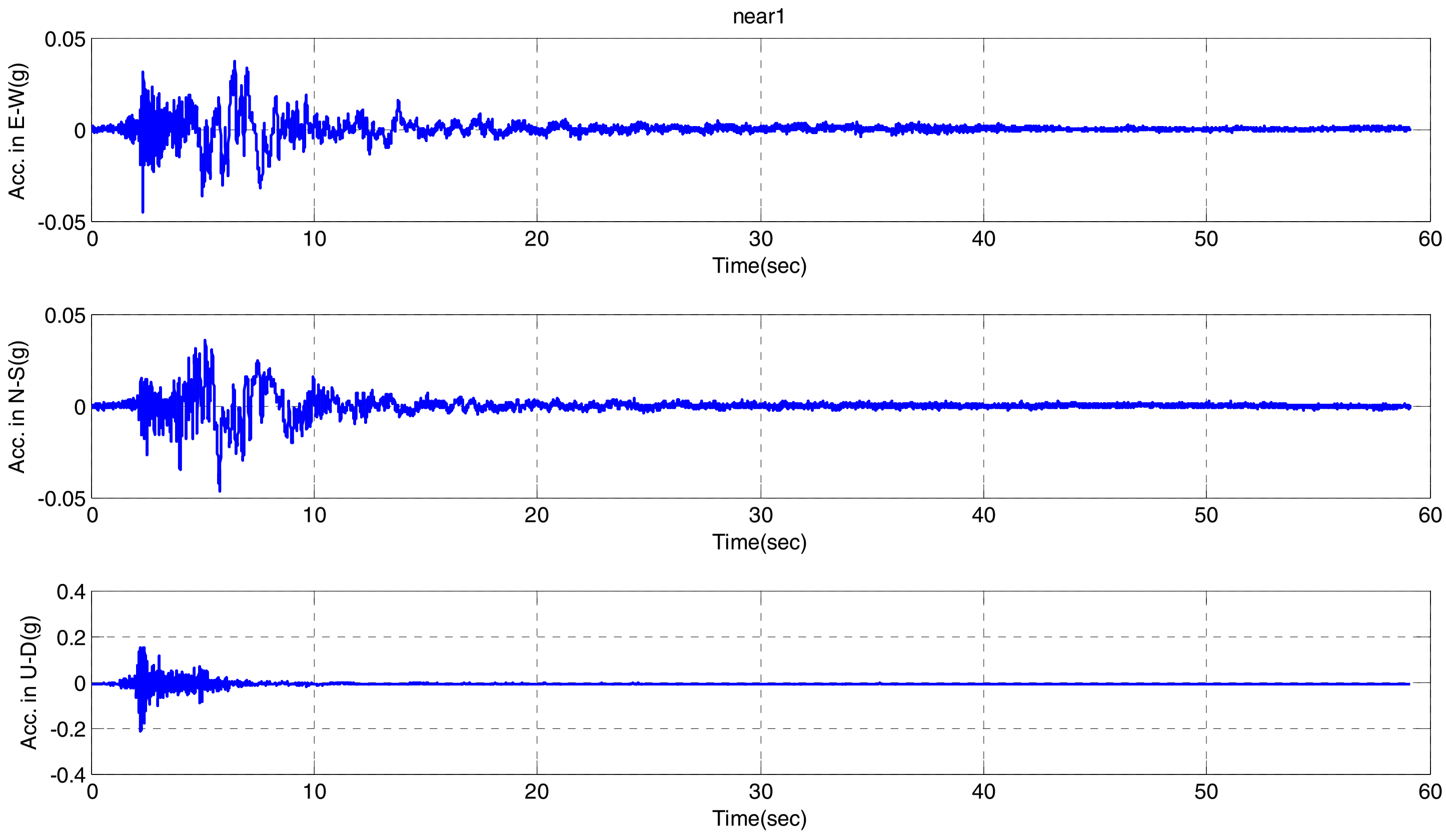
near1
Acc. in E-W(g)
0.05
0
-0.05
Time(sec)
Acc. in N-S(g)
Acc. in U-D(g)
0.4
0.2
-0.2
-0.4
0
10
20
30
40
50
60

(f) Near 1

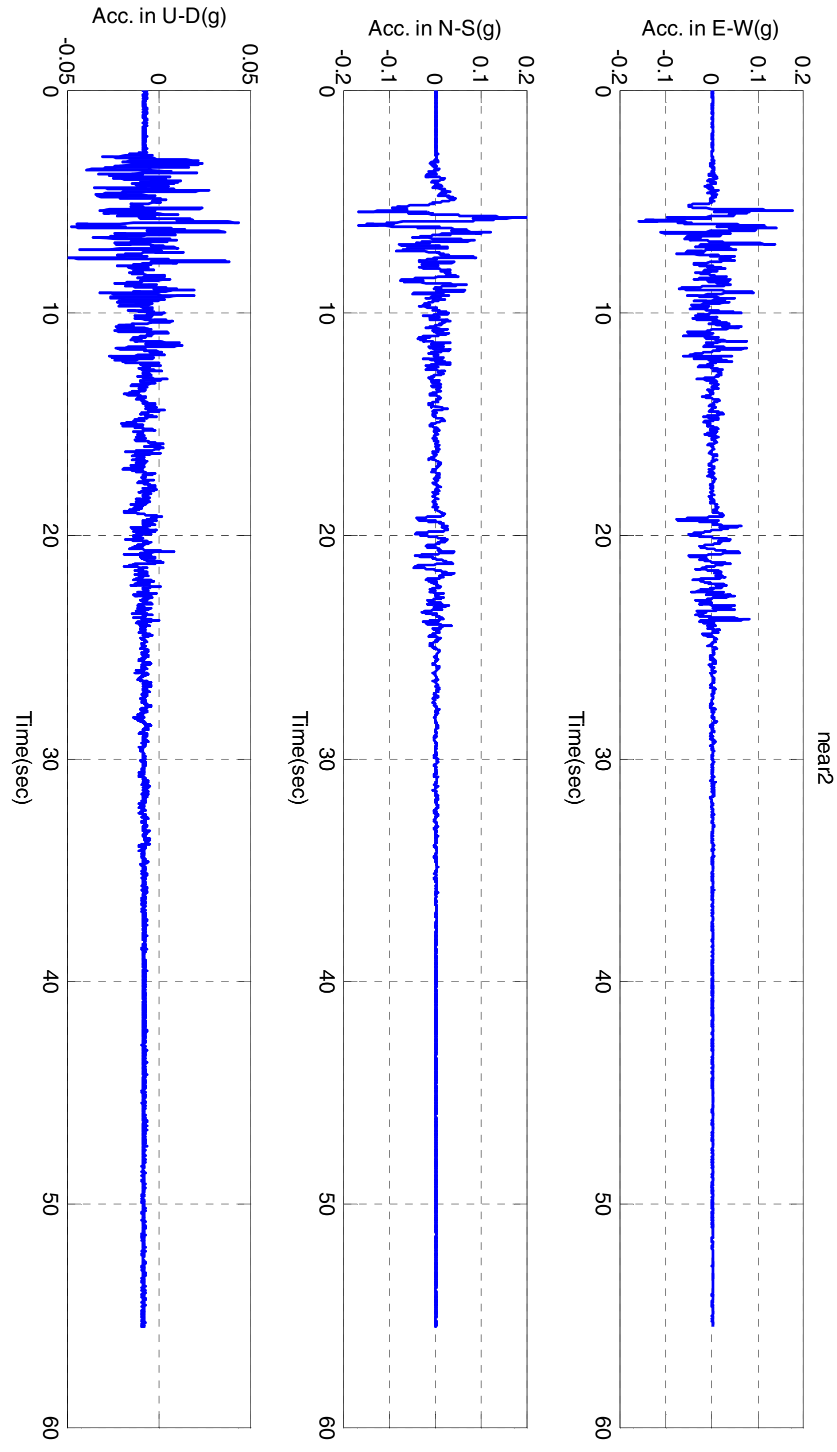
near2
Acc. in E-W(g)
Acc. in N-S(g)
Acc. in U-D(g)
Time(sec)
Time(sec)
Time(sec)

(g) Near 2

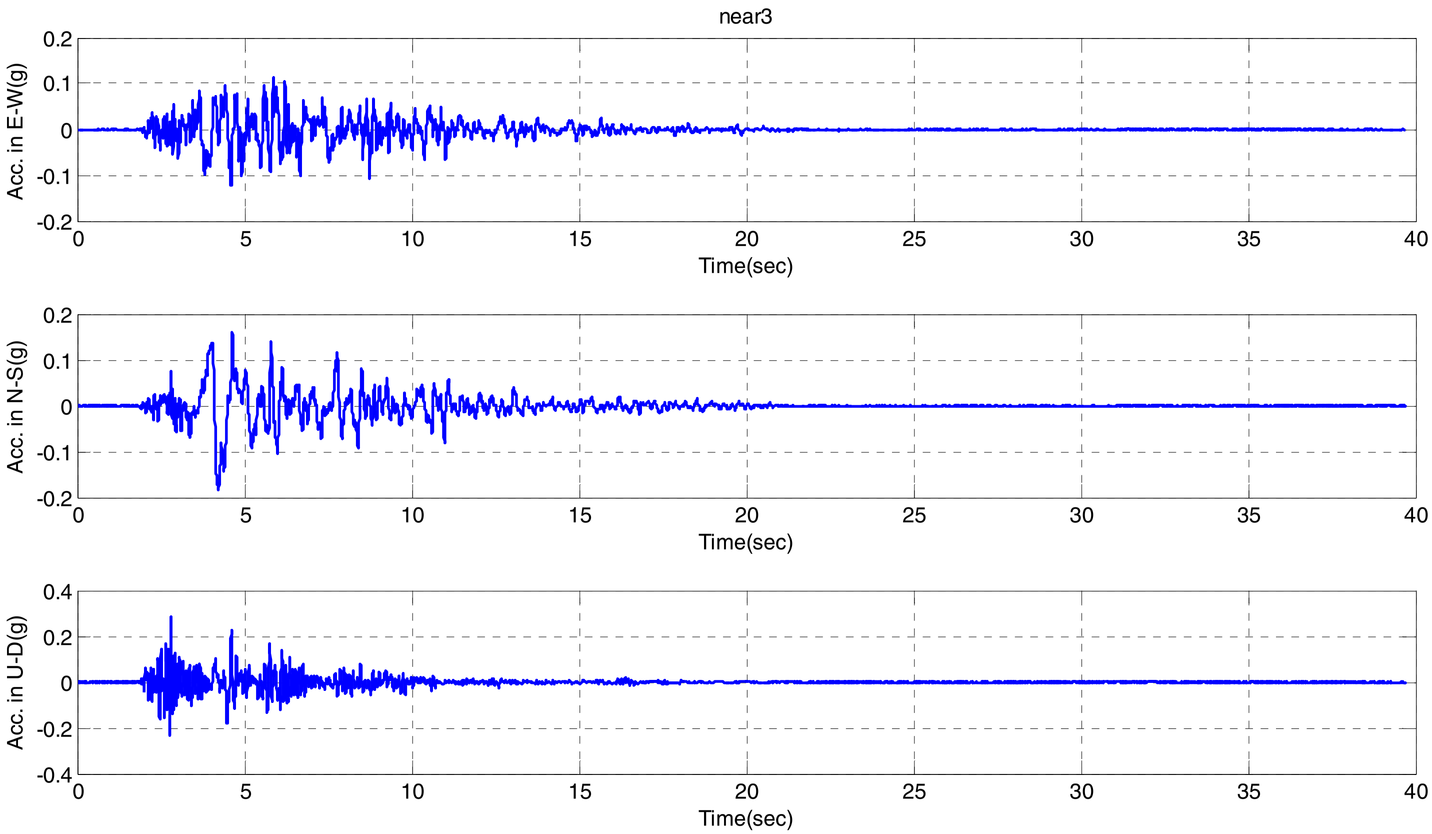
near3
Acc. in E-W(g)
Acc. in N-S(g)
Acc. in U-D(g)
Time(sec)
Time(sec)
Time(sec)

(h) Near 3

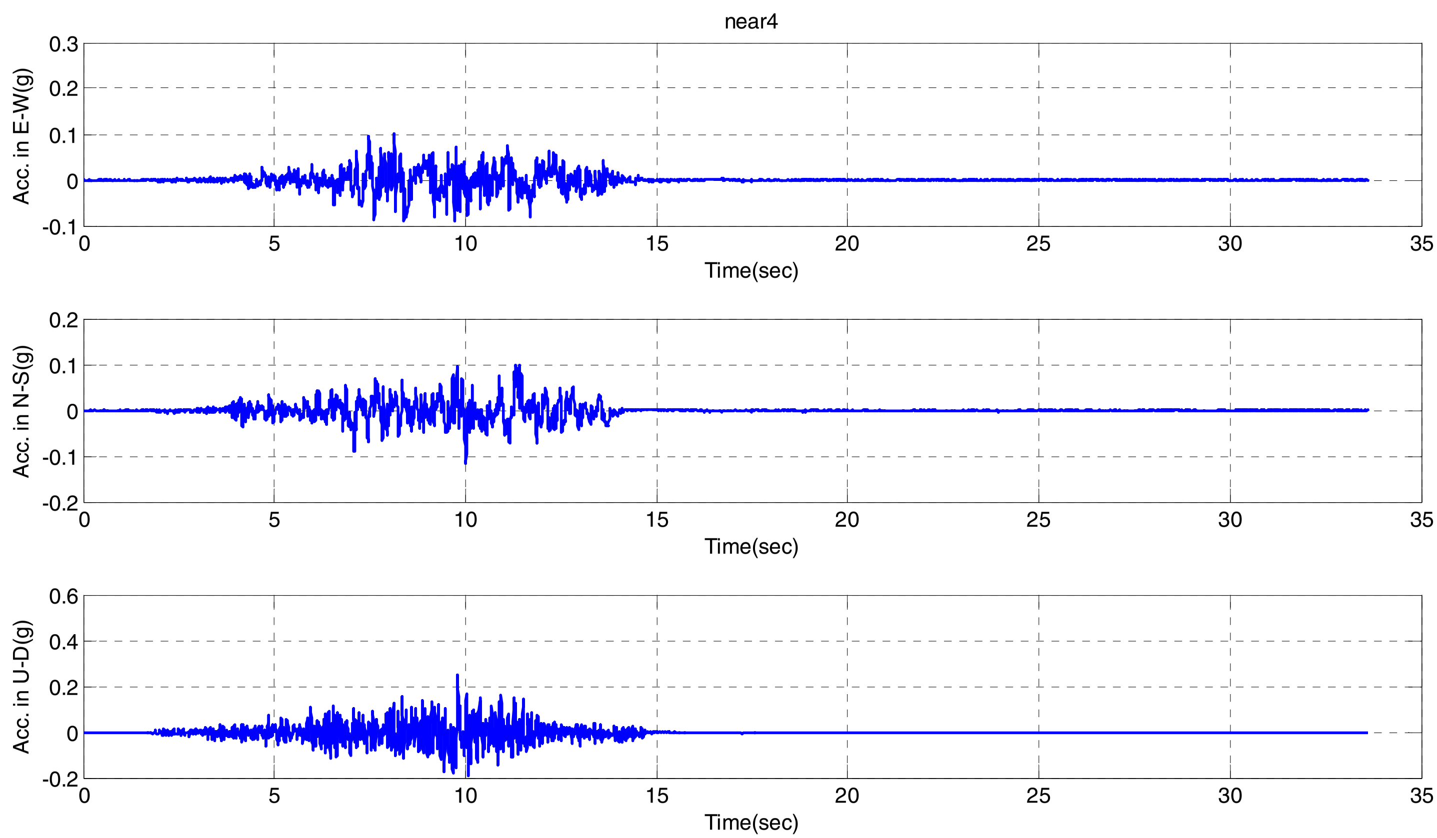
near4
Acc. in E-W(g)
0.3
0.2
0.1
0
-0.1
Acc. in N-S(g)
0.2
0.1
0
-0.1
-0.2
Acc. in U-D(g)
0.6
0.4
0.2
0
-0.2
0 5 10 15 20 25 30 35
Time(sec)

(i) Near 4

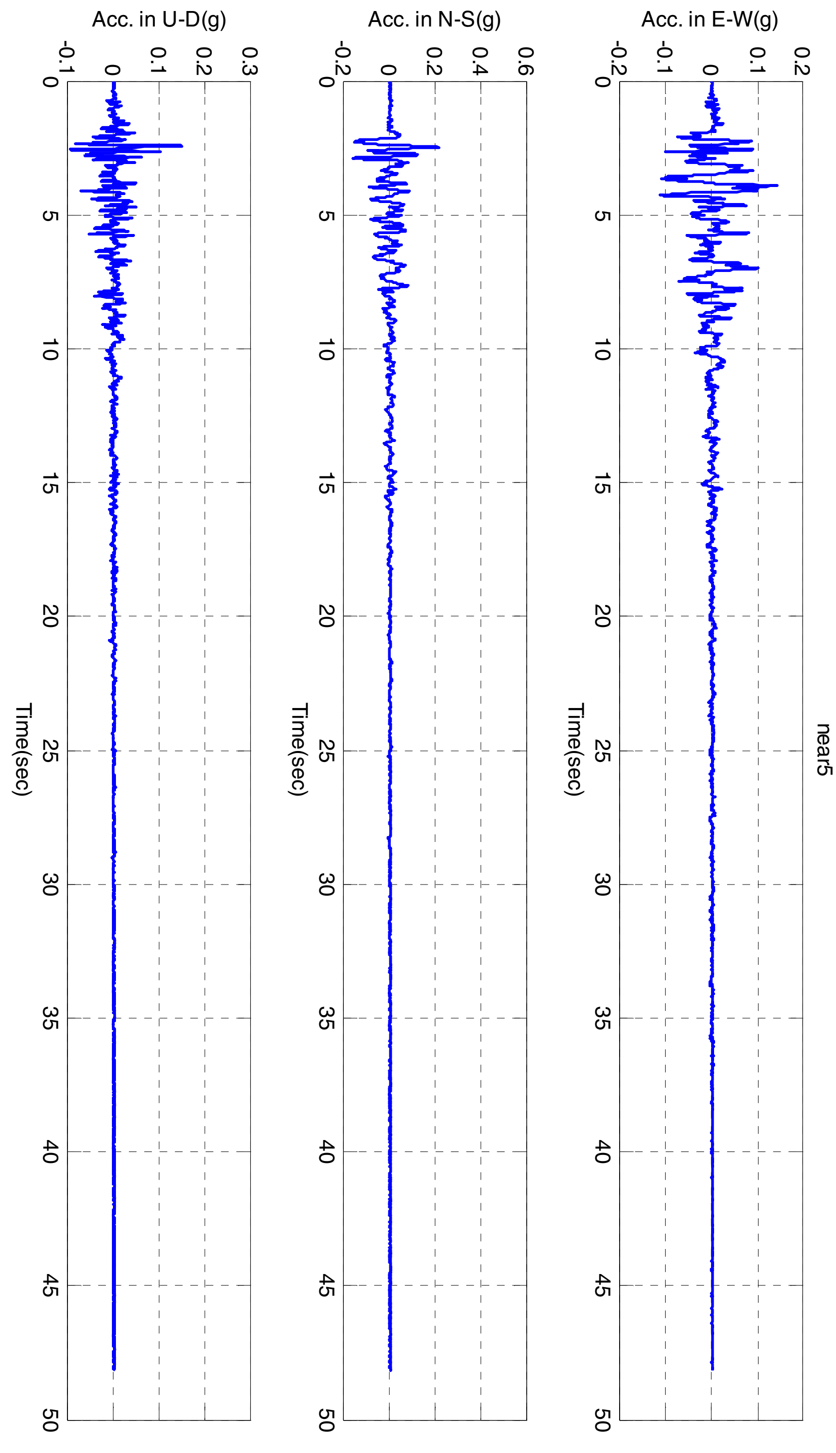
near5
Acc. in E-W(g)
Acc. in N-S(g)
Acc. in U-D(g)
Time(sec)
Time(sec)
Time(sec)

(j) Near 5

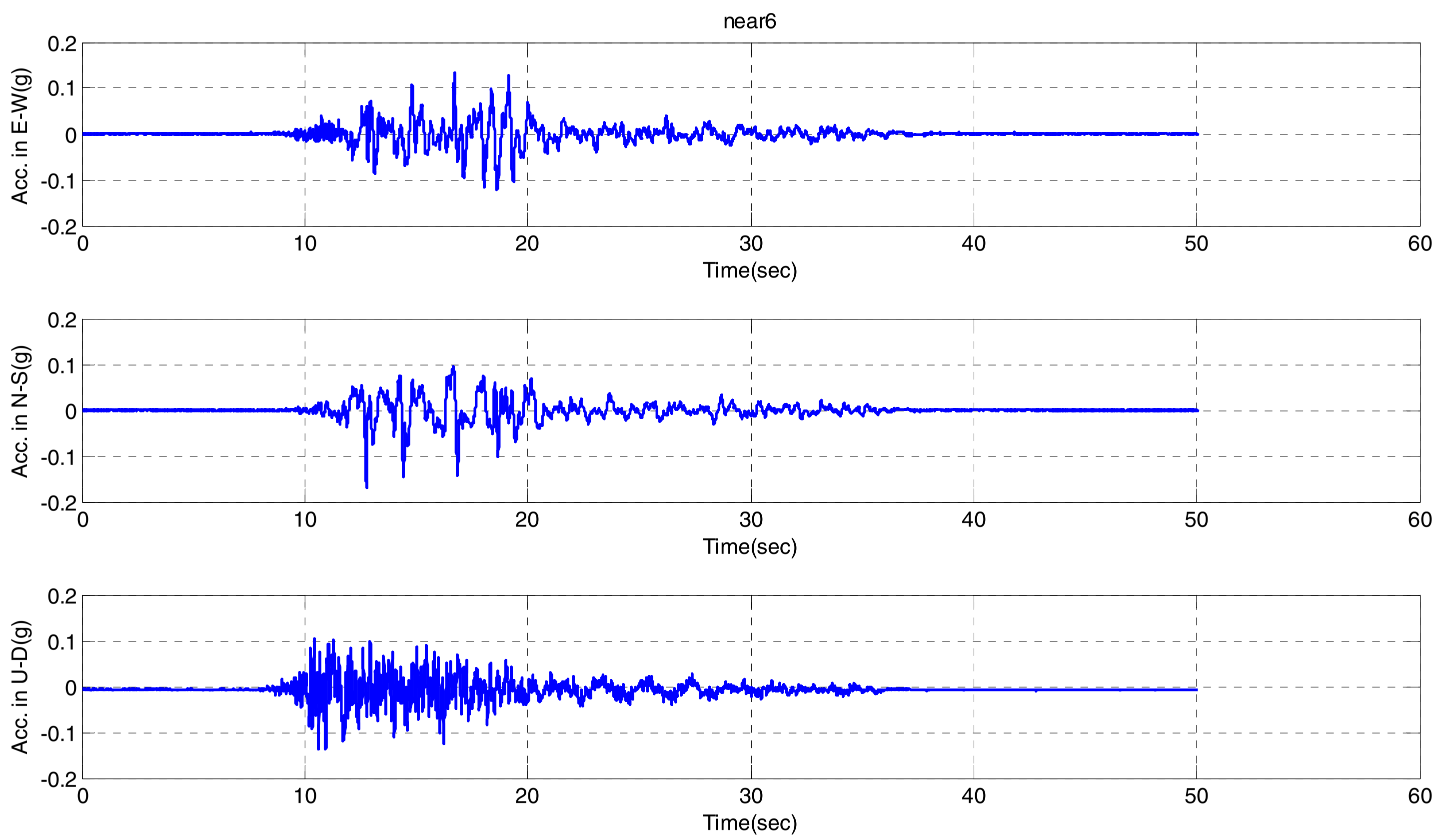

(k) Near 5

Figure B-1 Time history of all selected GMs

APPENDIX C

DYNAMIC PROPERTY IDENTIFICATION

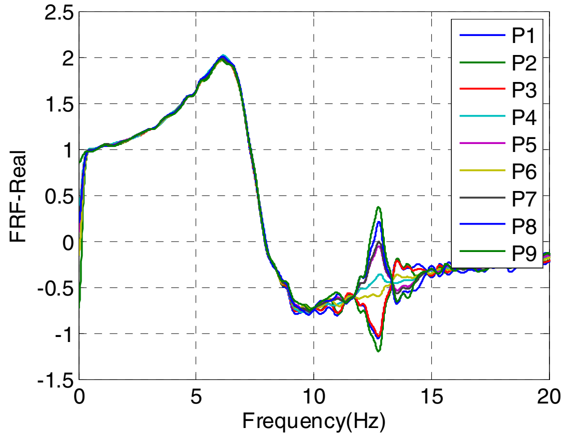

(a) Real components - Test results

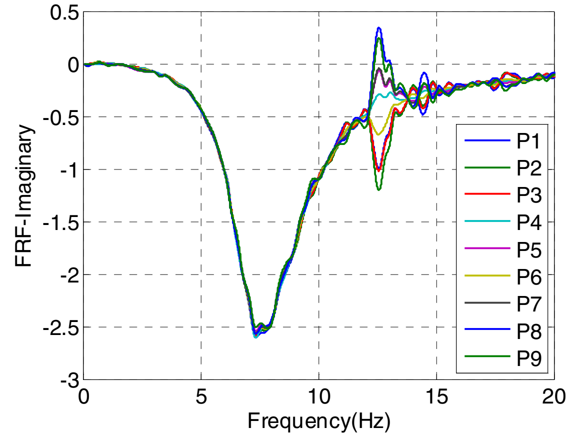

(b) Imaginary components - Test results

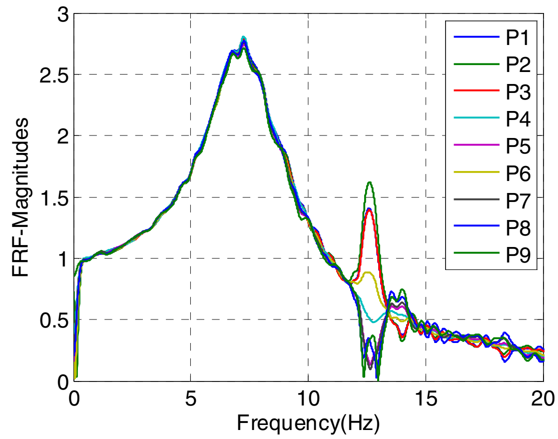

(c) Magnitudes - Test results

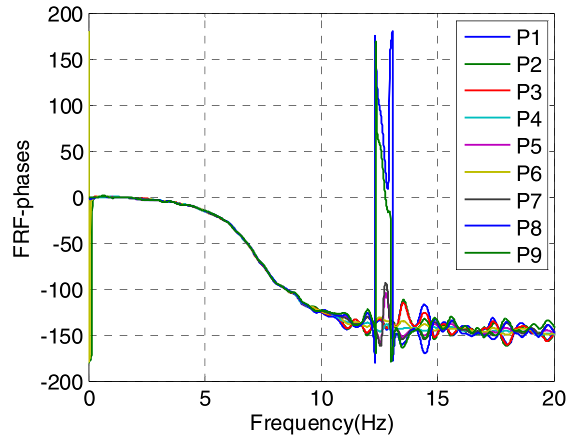

(d) Phases - Test results

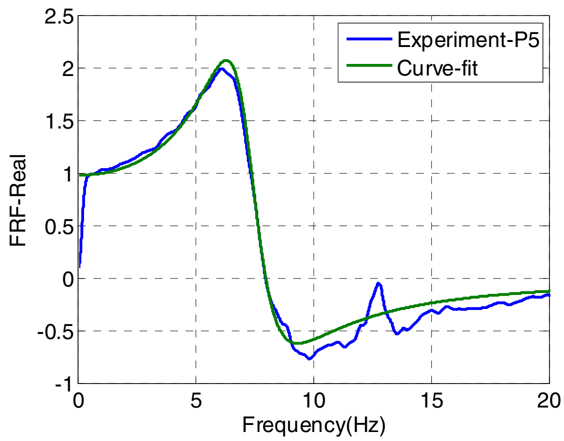

(e) Test result and Curve-fitting -Real

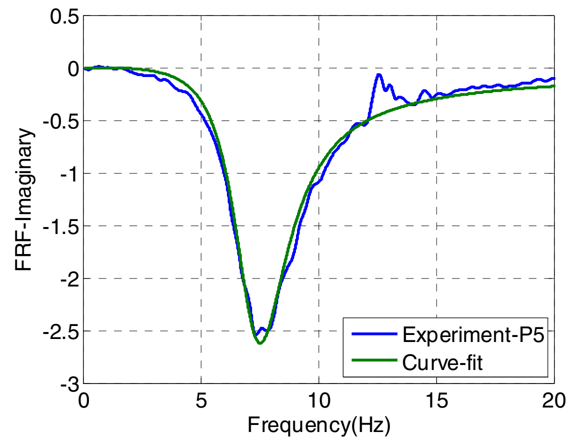

(f) Test result and Curve-fitting - Imaginary

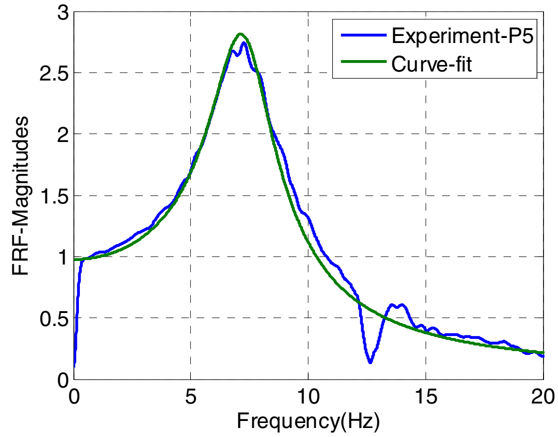

(g) Test result and Curve-fitting –Magn.

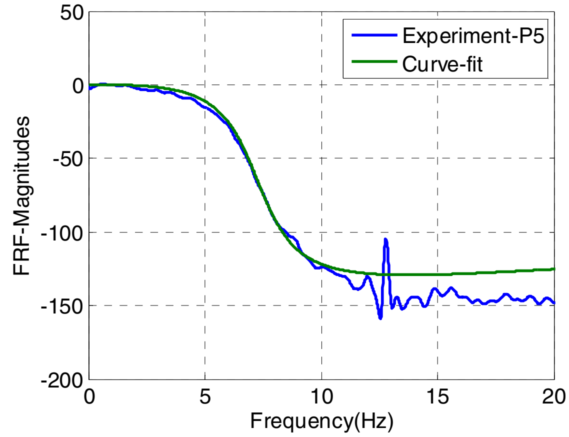

(h) Test result and Curve-fitting –Phases

Figure C-1 Phase 1, EW, Initial

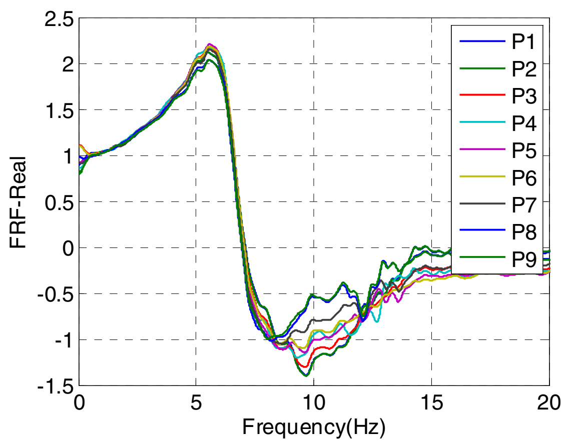

(a) Real components - Test results

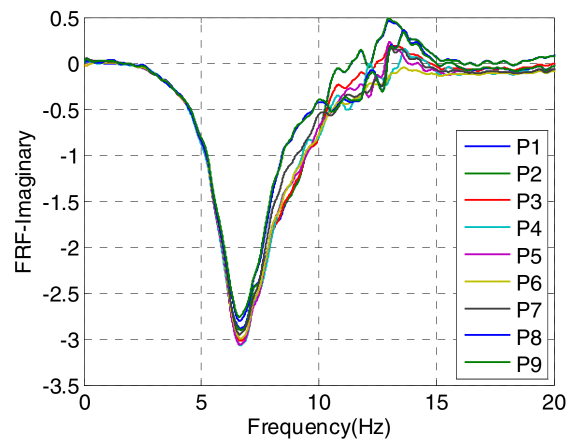

(b) Imaginary components - Test results

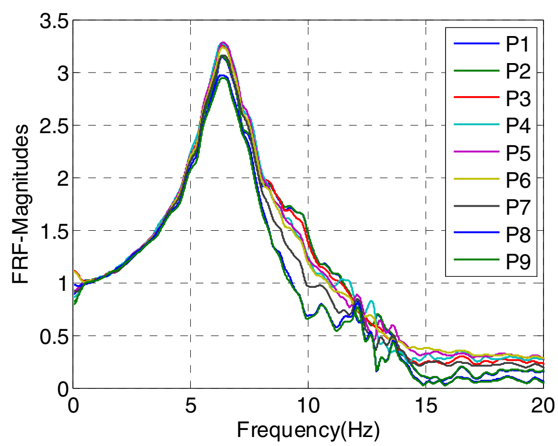

(c) Magnitudes - Test results

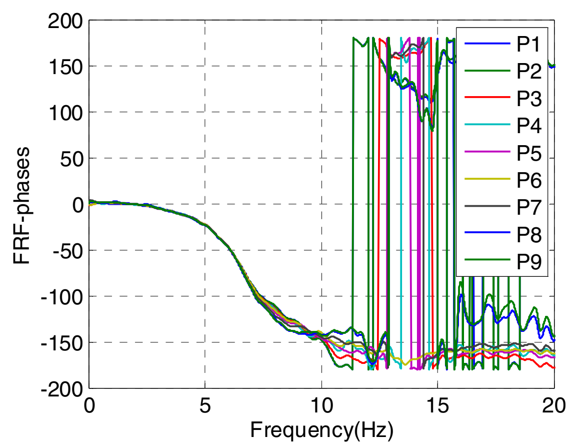

(d) Phases - Test results

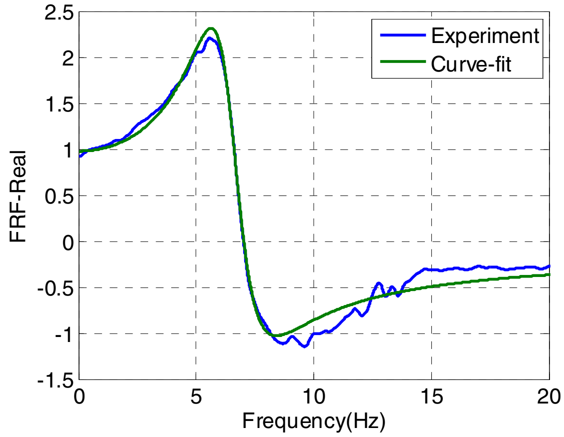

(e) Test result and Curve-fitting -Real

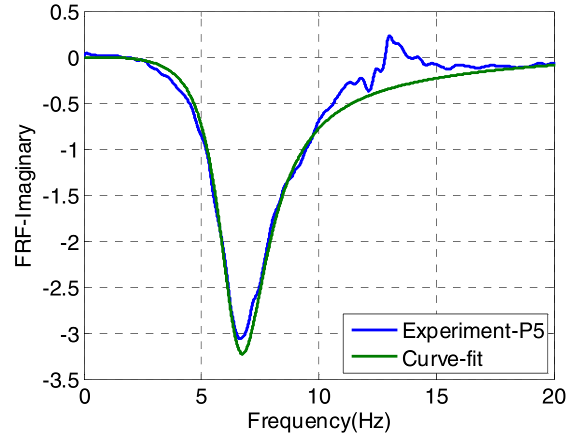

(f) Test result and Curve-fitting - Imaginary

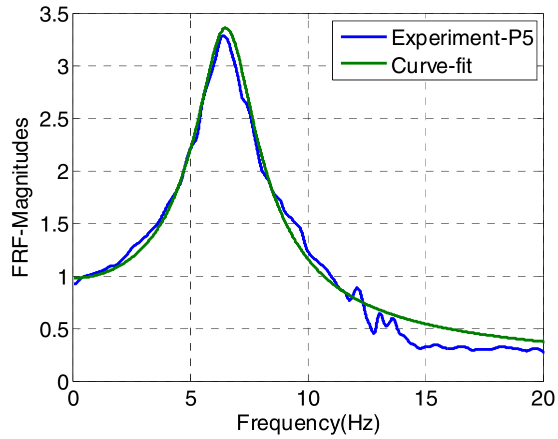

(g) Test result and Curve-fitting –Magn.

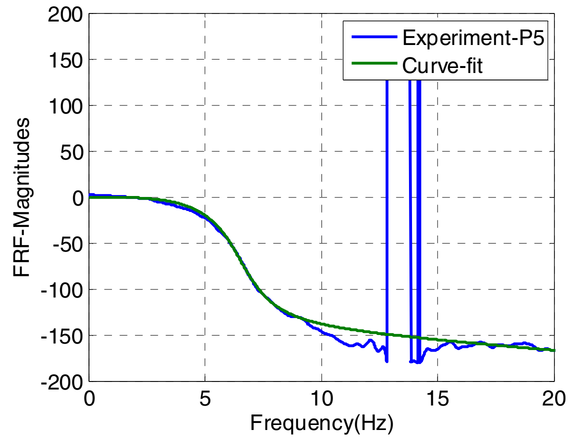

(h) Test result and Curve-fitting –Phases

Figure C-2 Phase 1, NS, Initial

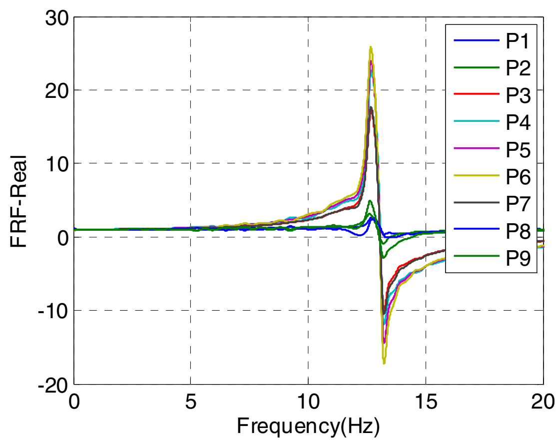

(a) Real components - Test results

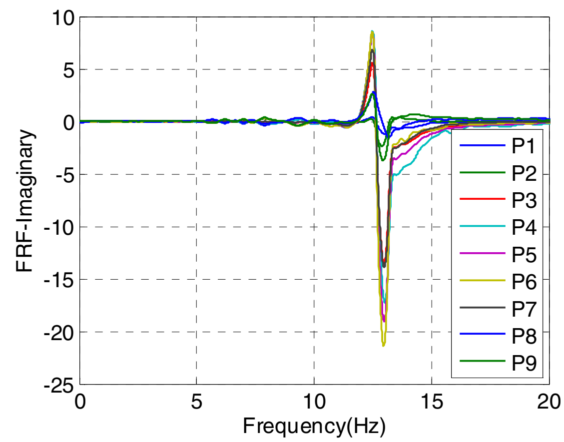

(b) Imaginary components - Test results

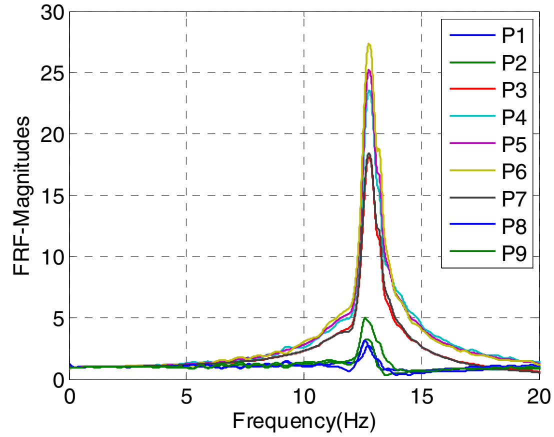

(c) Magnitudes - Test results

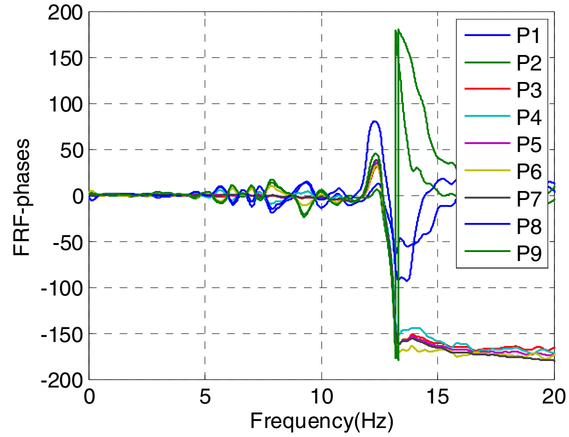

(d) Phases - Test results

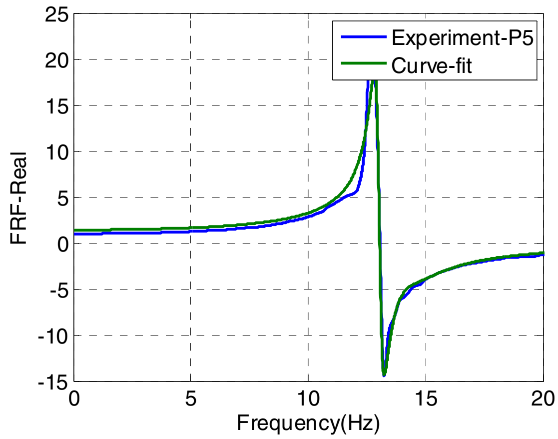

(e) Test result and Curve-fitting -Real

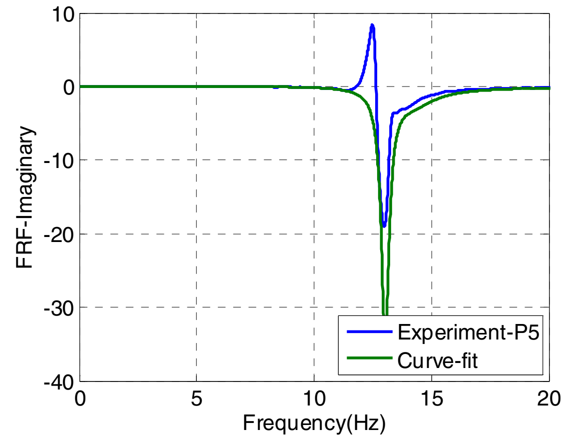

(f) Test result and Curve-fitting - Imaginary

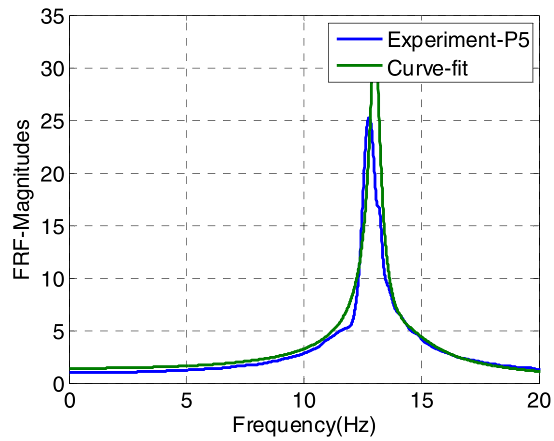

(g) Test result and Curve-fitting –Magn.

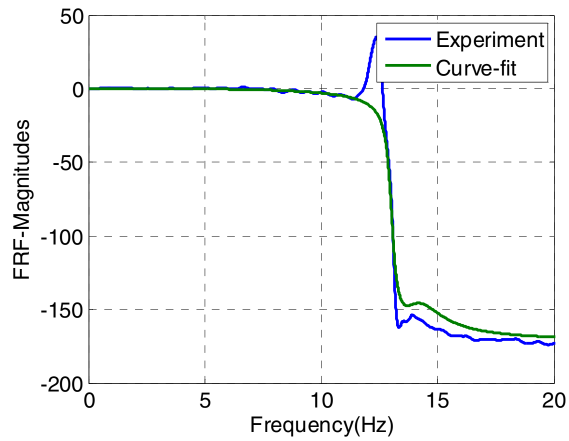

(h) Test result and Curve-fitting –Phases

Figure C-3 Phase 1, UD, Initial

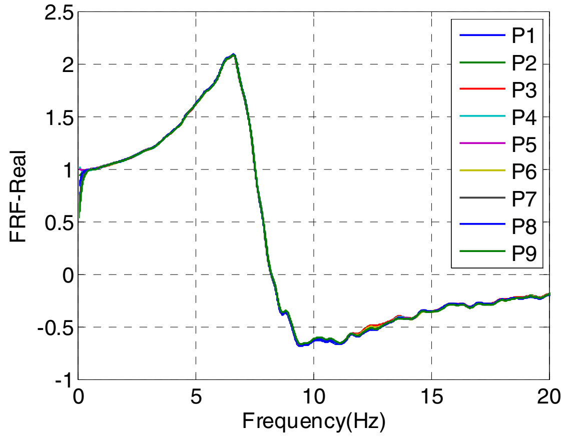

(a) Real components - Test results

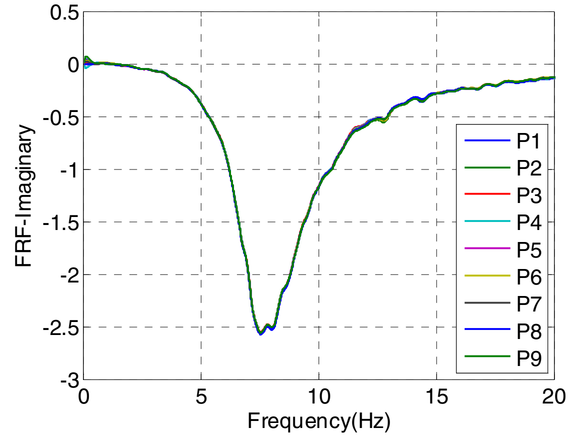

(b) Imaginary components - Test results

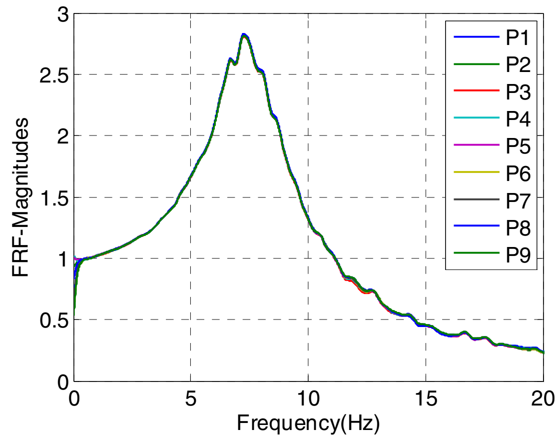

(c) Magnitudes - Test results

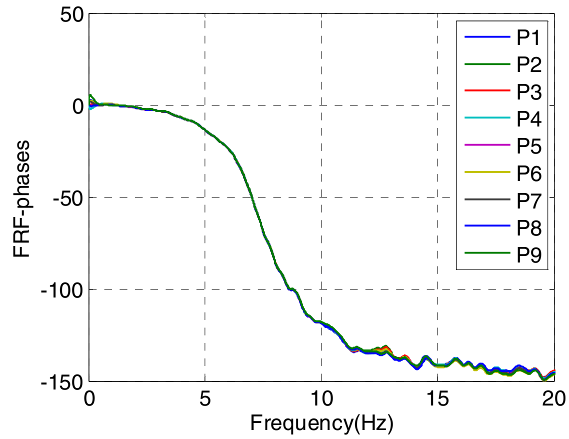

(d) Phases - Test results

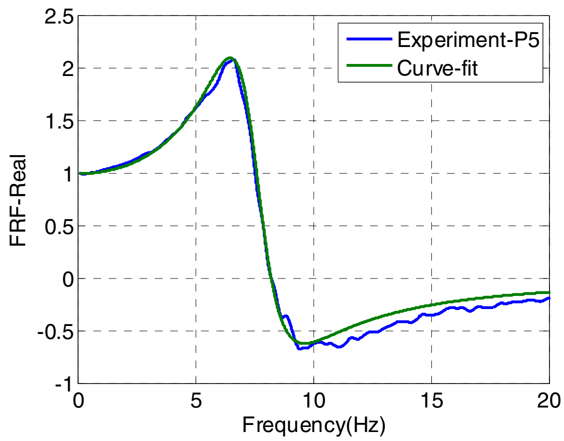

(e) Test result and Curve-fitting -Real

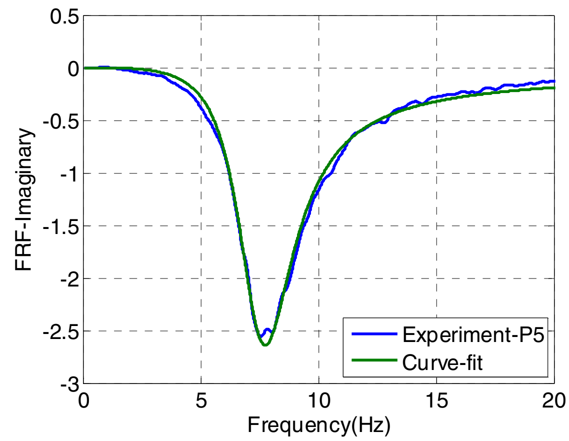

(f) Test result and Curve-fitting - Imaginary

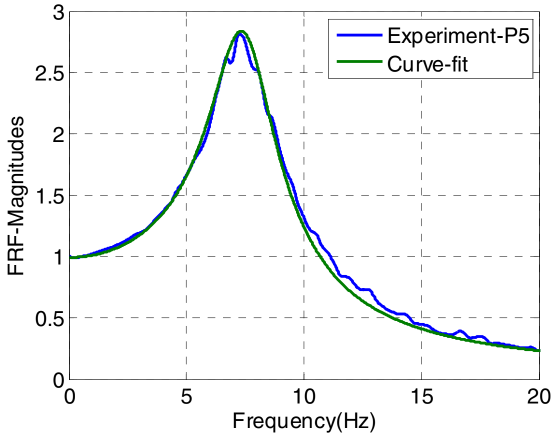

(g) Test result and Curve-fitting –Magn.

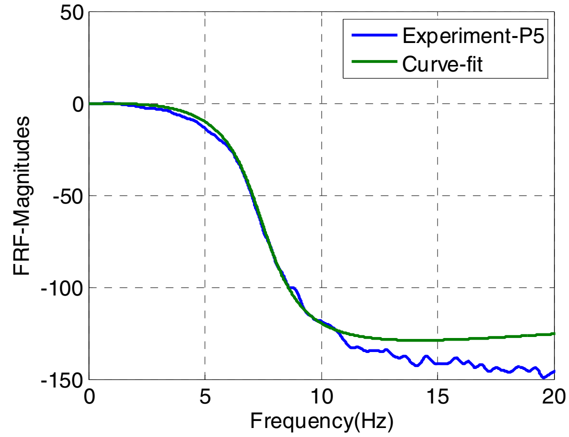

(h) Test result and Curve-fitting –Phases

Figure C-4 Phase 1, EW, After EL

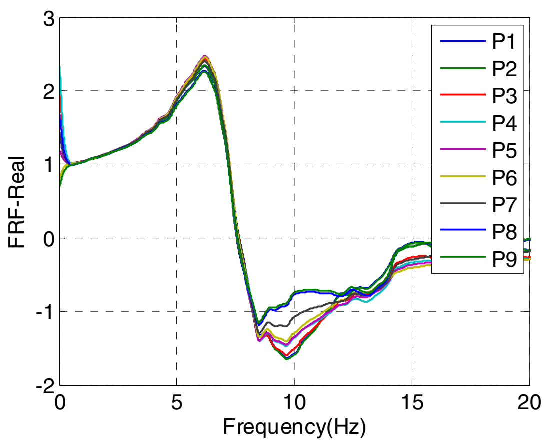

(a) Real components - Test results

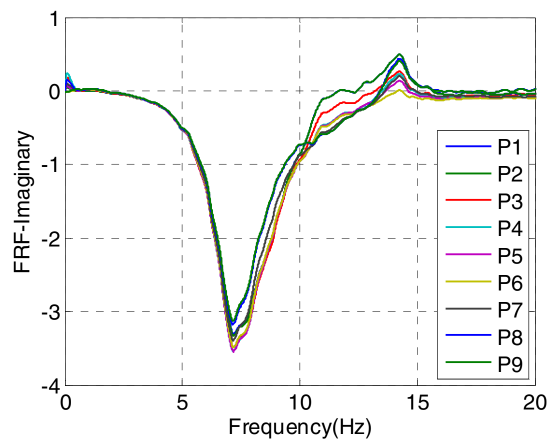

(b) Imaginary components - Test results

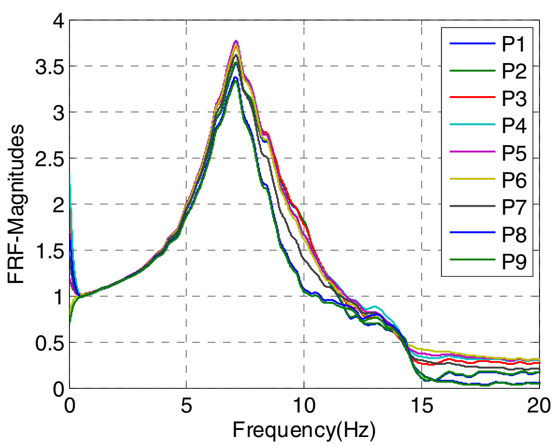

(c) Magnitudes - Test results

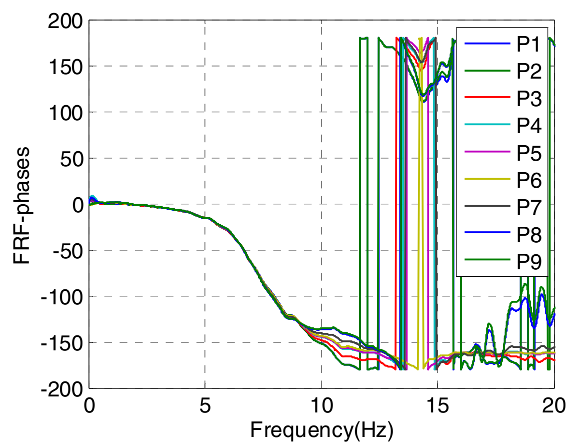

(d) Phases - Test results

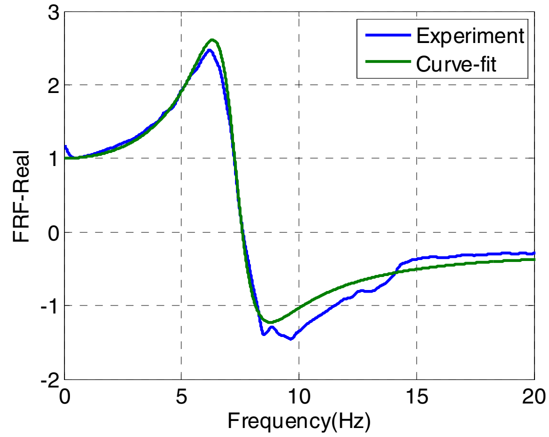

(e) Test result and Curve-fitting -Real

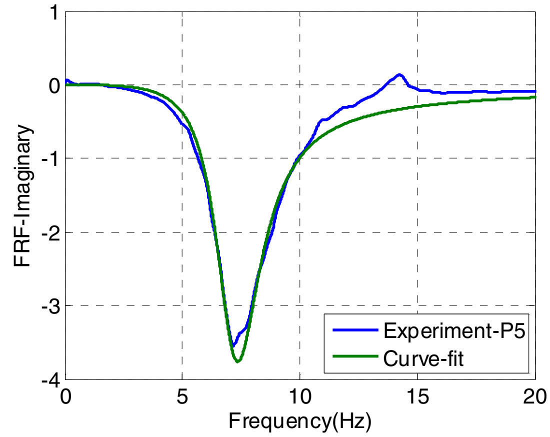

(f) Test result and Curve-fitting - Imaginary

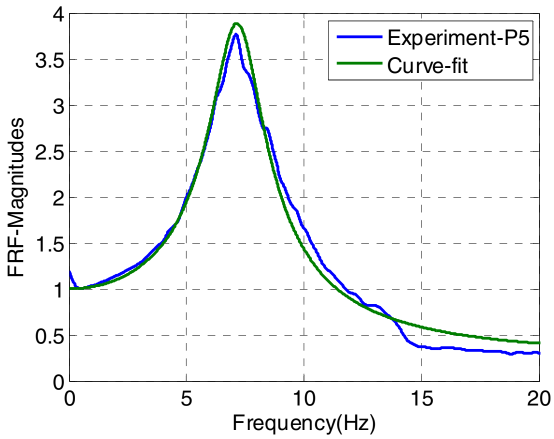

(g) Test result and Curve-fitting –Magn.

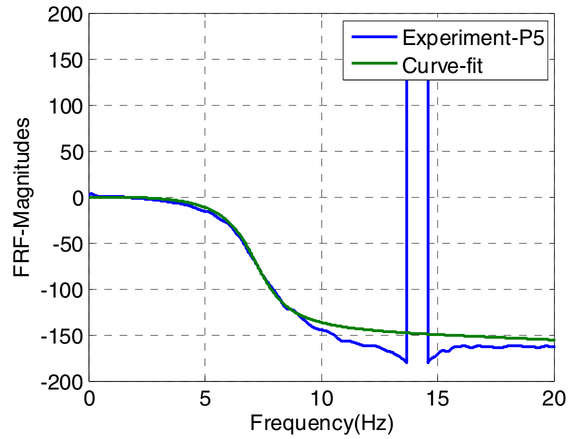

(h) Test result and Curve-fitting –Phases

Figure C-5 Phase 1, NS, After EL

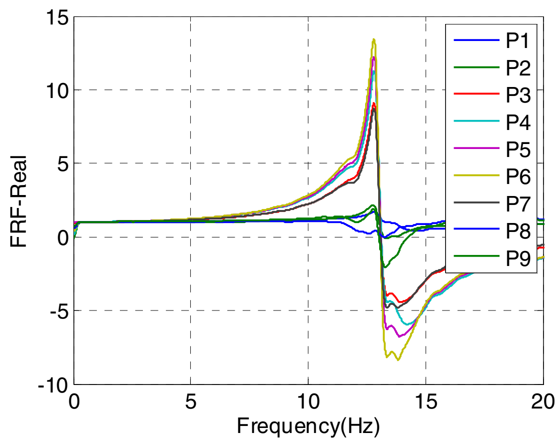

(a) Real components - Test results

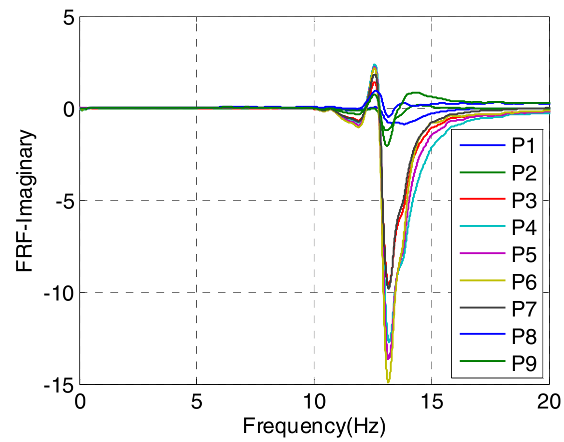

(b) Imaginary components - Test results

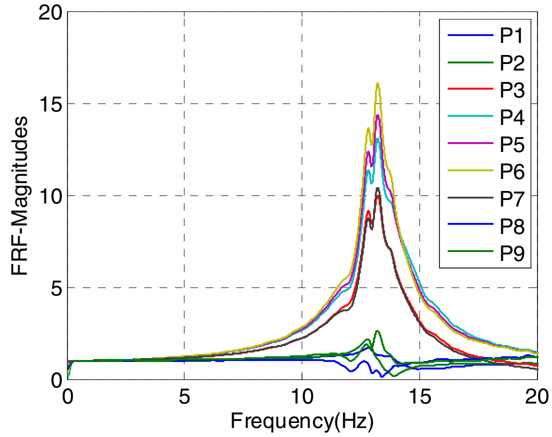

(c) Magnitudes - Test results

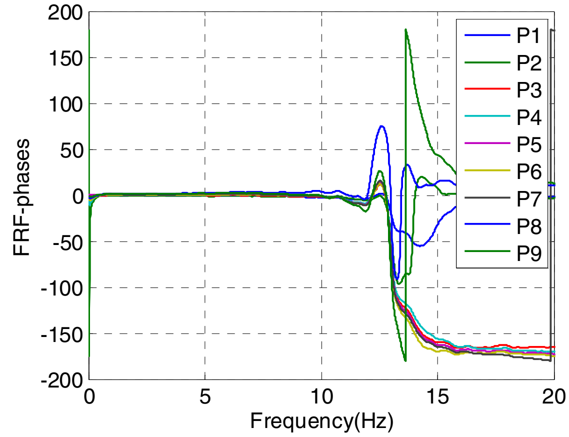

(d) Phases - Test results

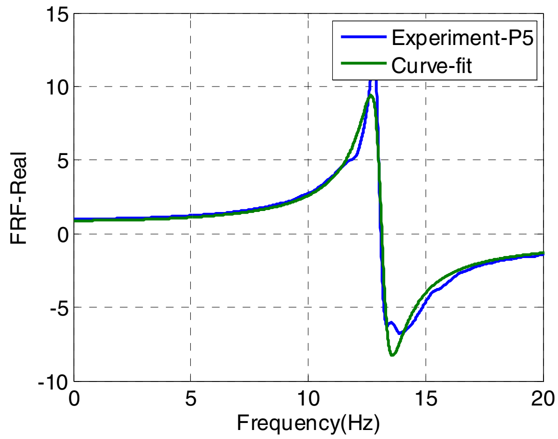

(e) Test result and Curve-fitting -Real

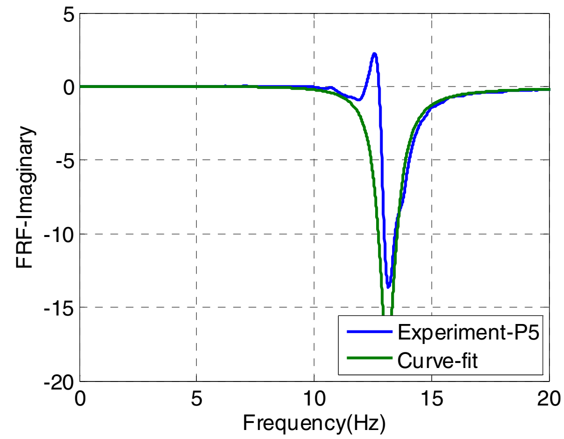

(f) Test result and Curve-fitting - Imaginary

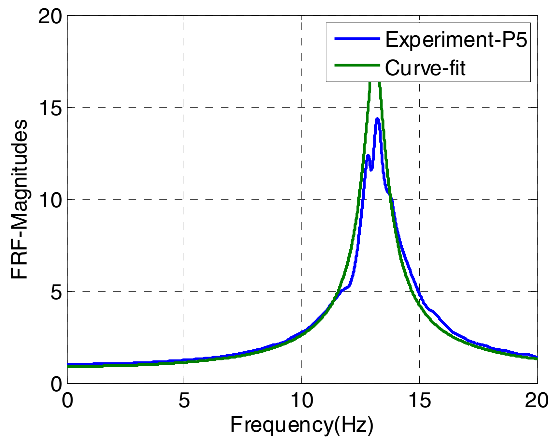

(g) Test result and Curve-fitting –Magn.

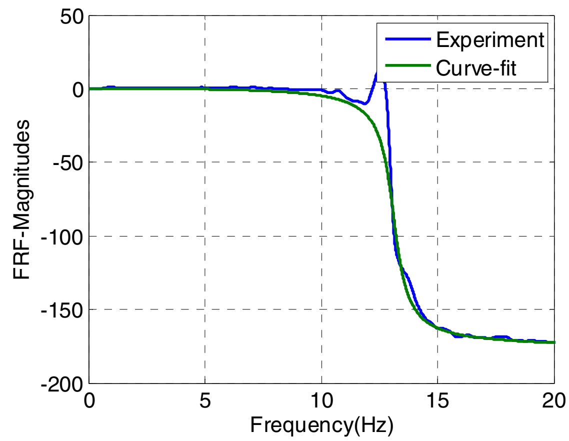

(h) Test result and Curve-fitting –Phases

Figure C-6 Phase 1, UD, After EL

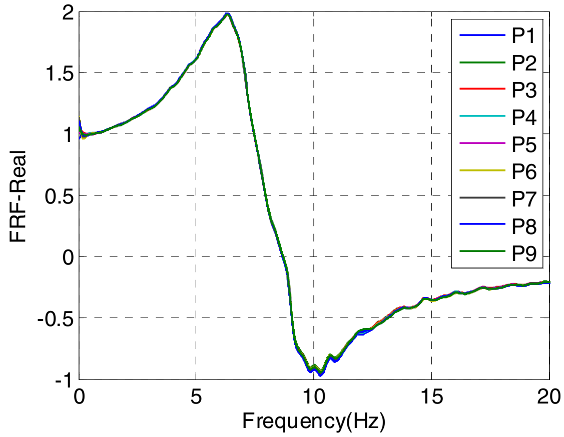

(a) Real components - Test results

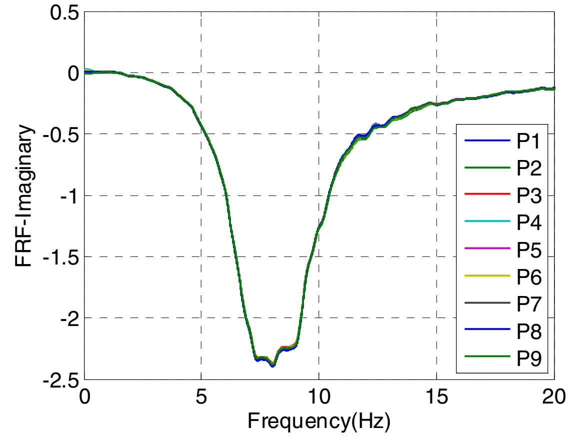

(b) Imaginary components - Test results

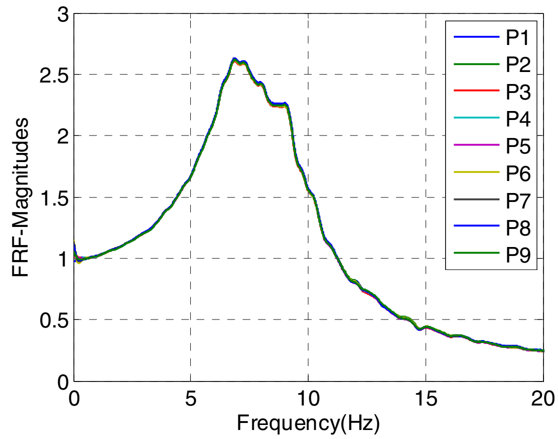

(c) Magnitudes - Test results

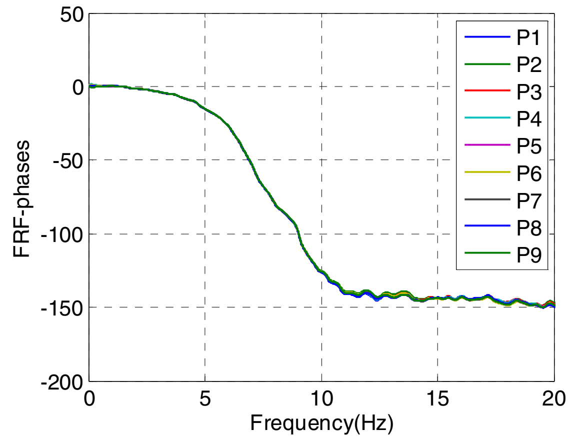

(d) Phases - Test results

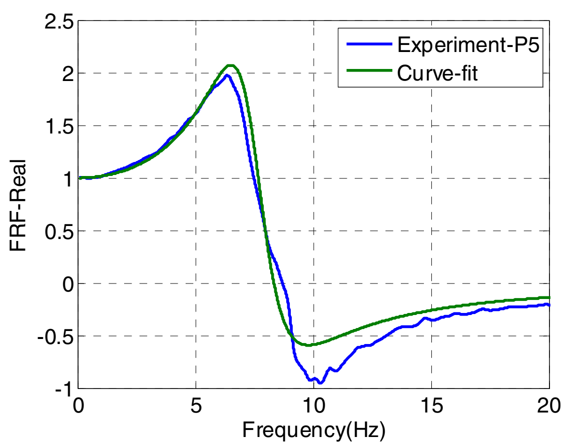

(e) Test result and Curve-fitting -Real

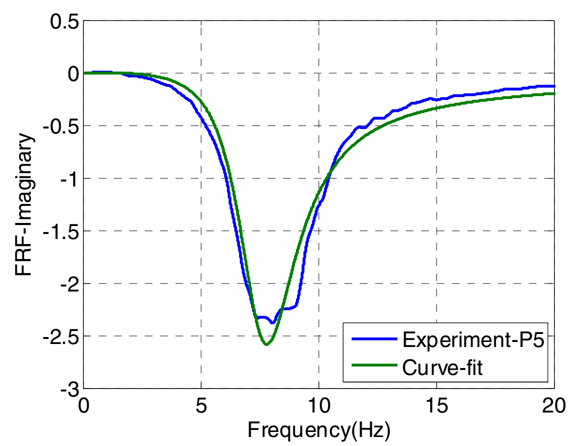

(f) Test result and Curve-fitting - Imaginary

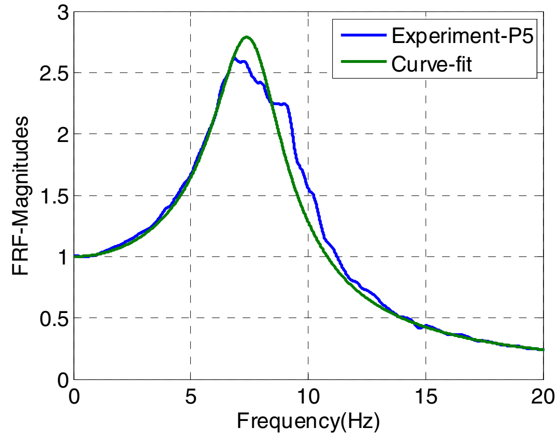

(g) Test result and Curve-fitting –Magn.

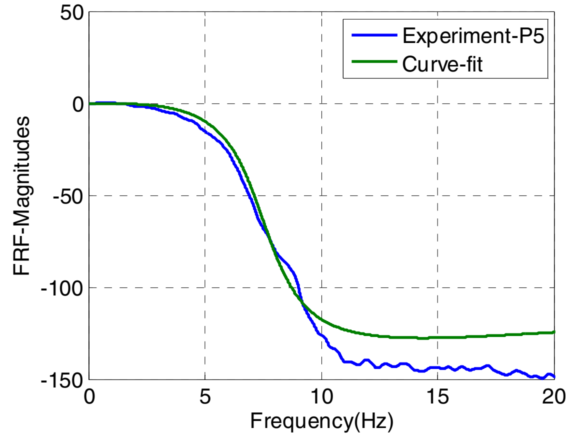

(h) Test result and Curve-fitting –Phases

Figure C-7 Phase 1, EW, After DE

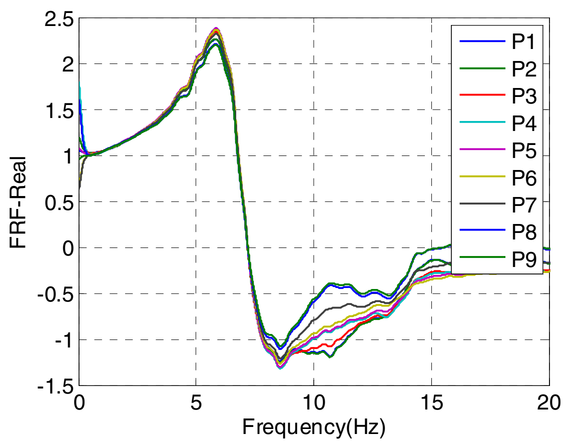

(a) Real components - Test results

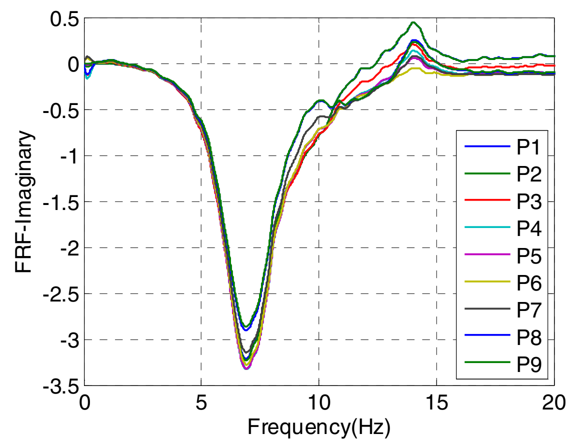

(b) Imaginary components - Test results

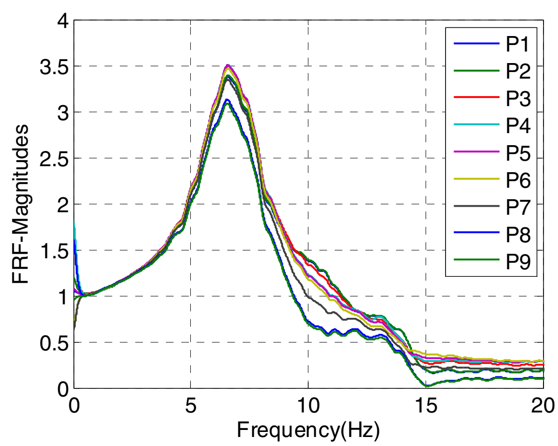

(c) Magnitudes - Test results

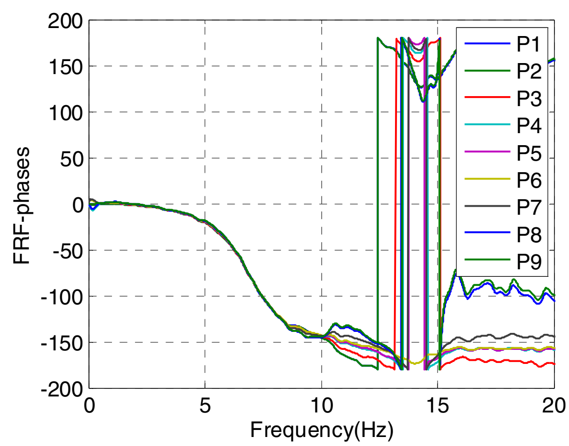

(d) Phases - Test results

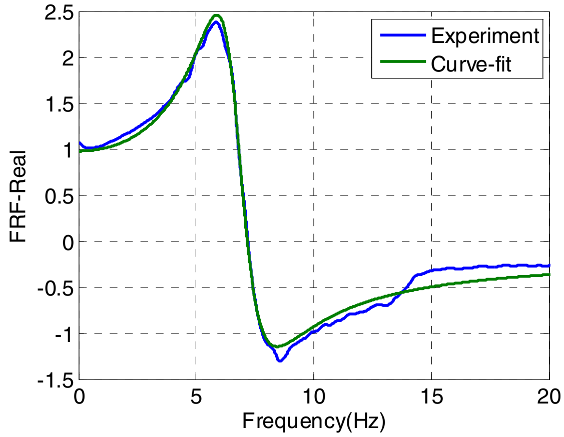

(e) Test result and Curve-fitting -Real

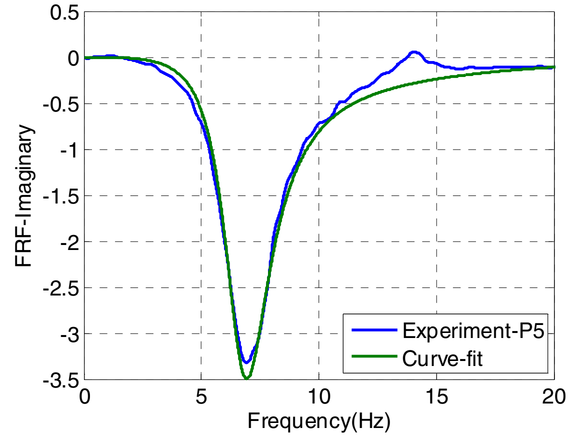

(f) Test result and Curve-fitting - Imaginary

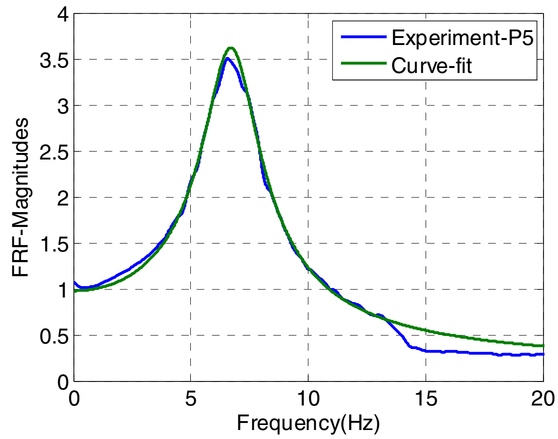

(g) Test result and Curve-fitting –Magn.

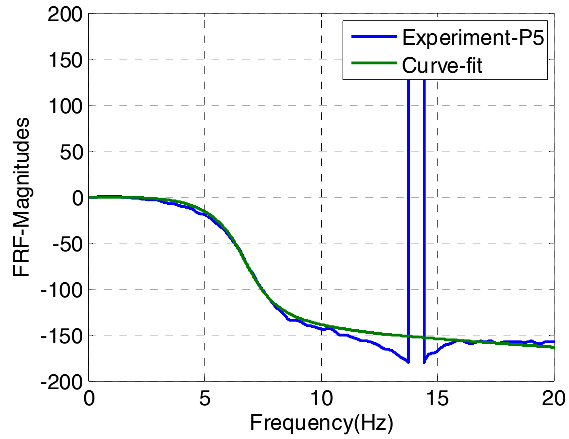

(h) Test result and Curve-fitting –Phases

Figure C-8 Phase 1, NS, After DE

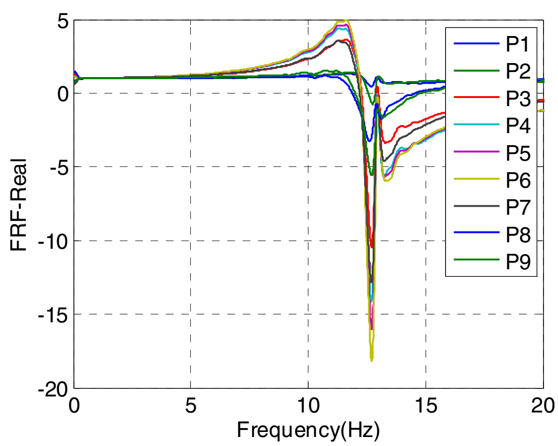

(a) Real components - Test results

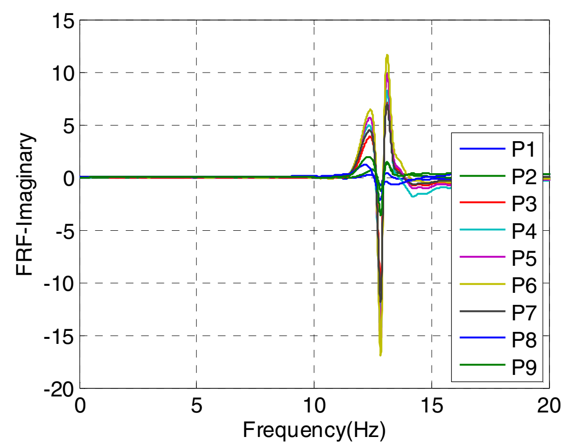

(b) Imaginary components - Test results

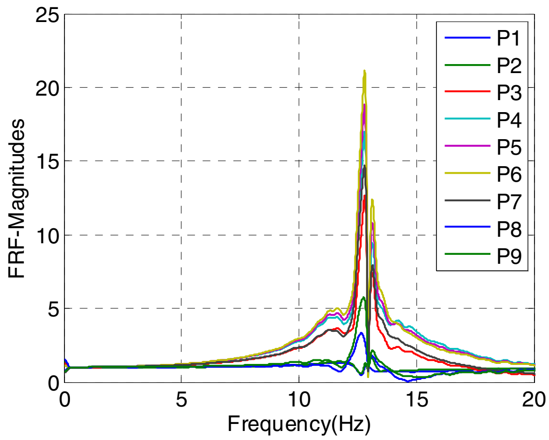

(c) Magnitudes - Test results

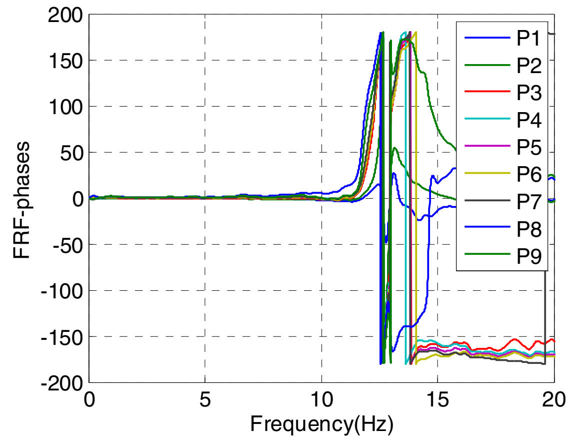

(d) Phases - Test results

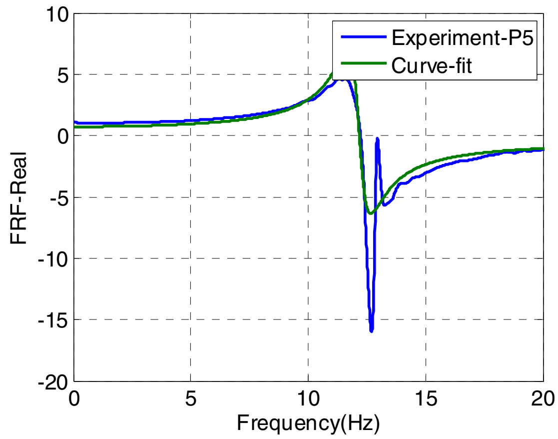

(e) Test result and Curve-fitting -Real

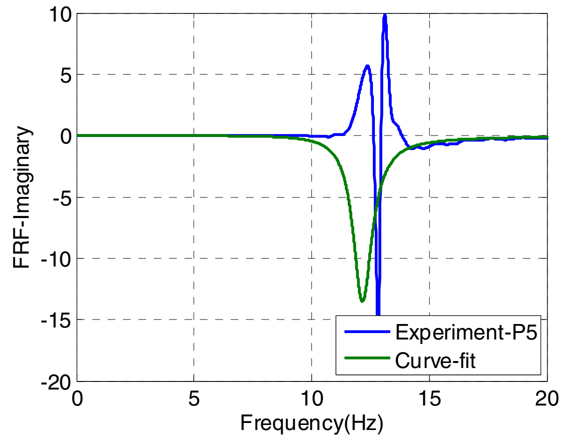

(f) Test result and Curve-fitting - Imaginary

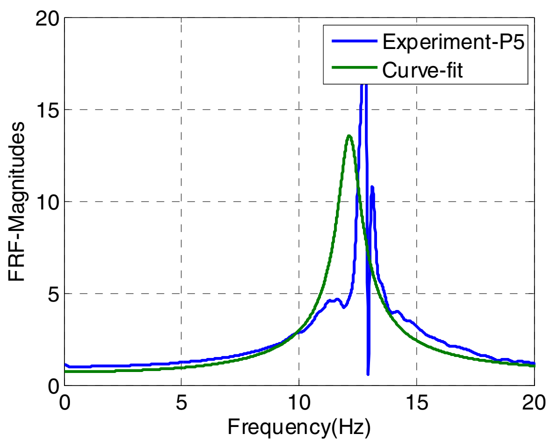

(g) Test result and Curve-fitting –Magn.

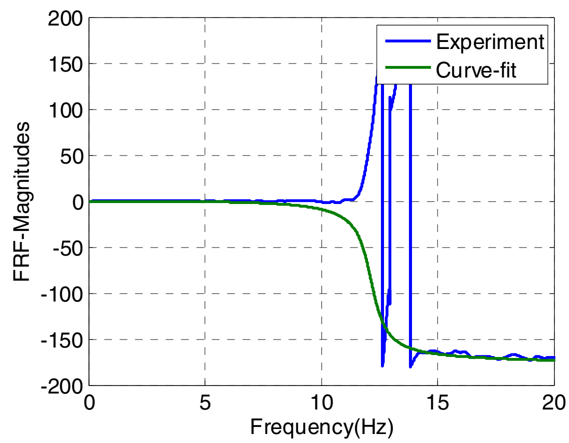

(h) Test result and Curve-fitting –Phases

Figure C-9 Phase 1, UD, After DE

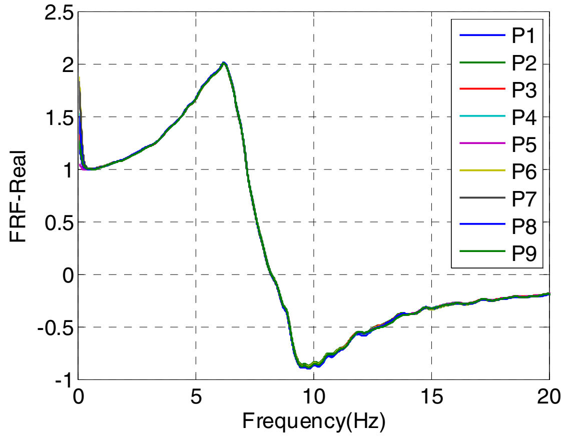

(a) Real components - Test results

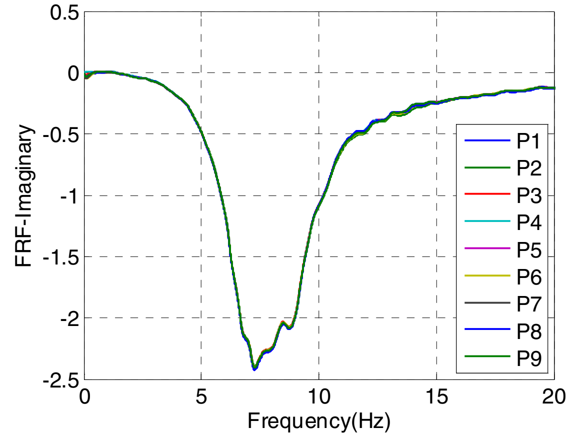

(b) Imaginary components - Test results

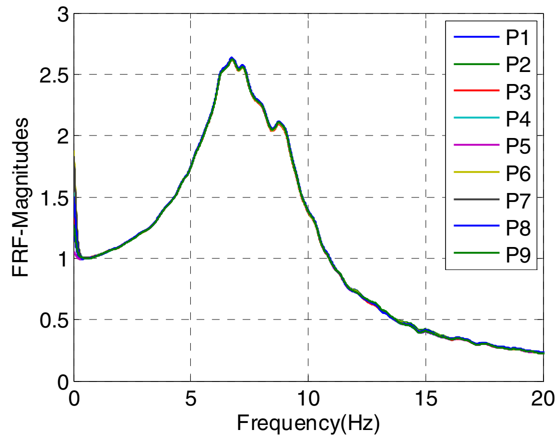

(c) Magnitudes - Test results

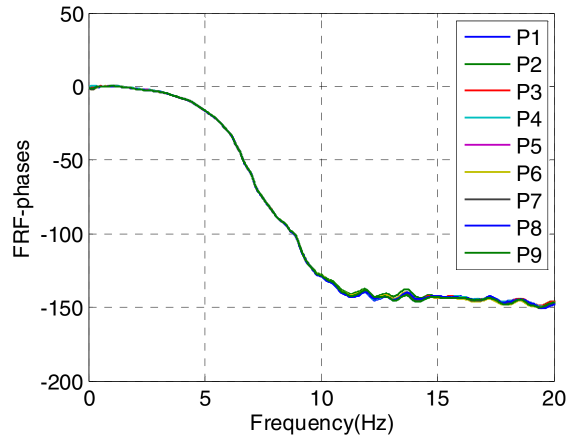

(d) Phases - Test results

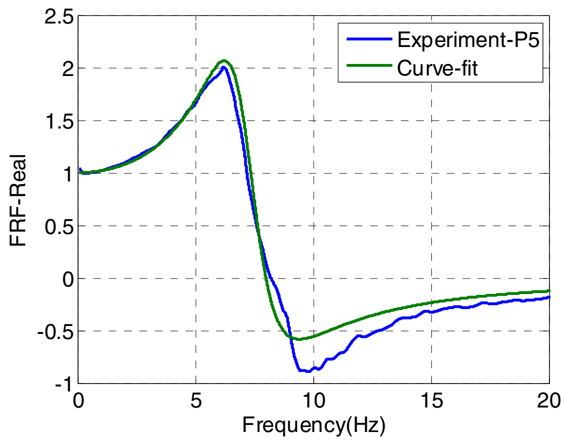

(e) Test result and Curve-fitting -Real

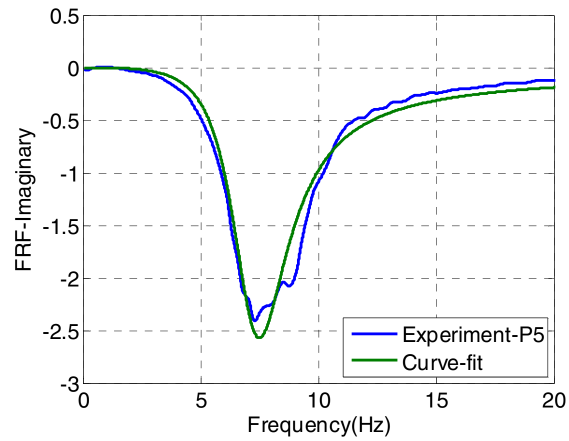

(f) Test result and Curve-fitting - Imaginary

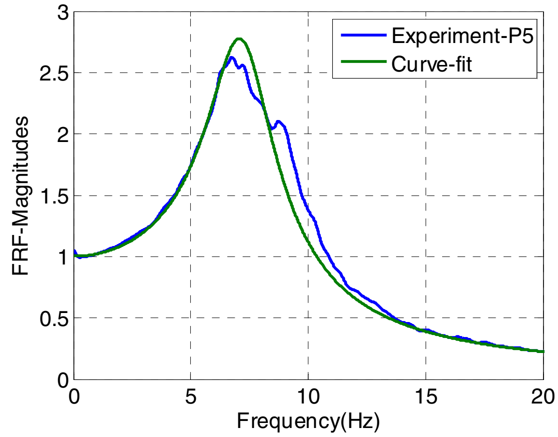

(g) Test result and Curve-fitting –Magn.

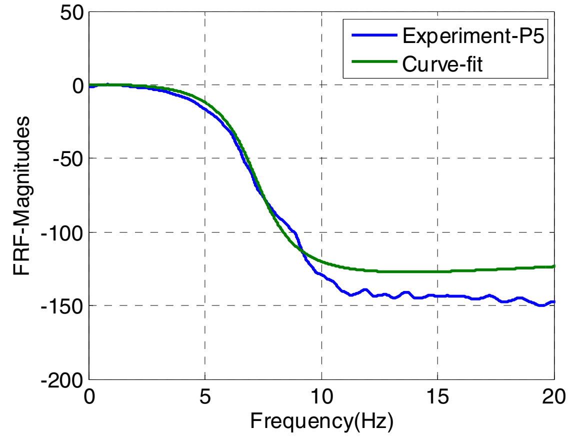

(h) Test result and Curve-fitting –Phases

Figure C-10 Phase 1, EW, After MCE

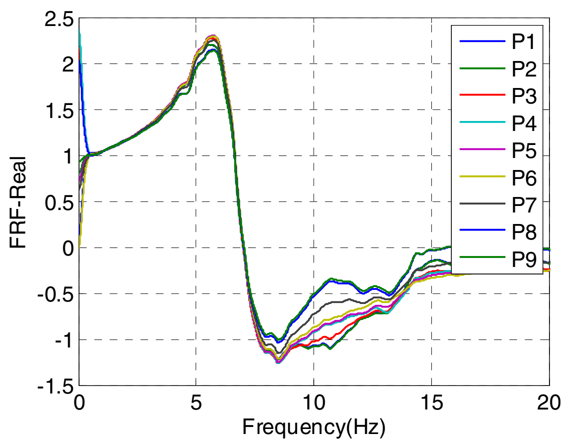

(a) Real components - Test results

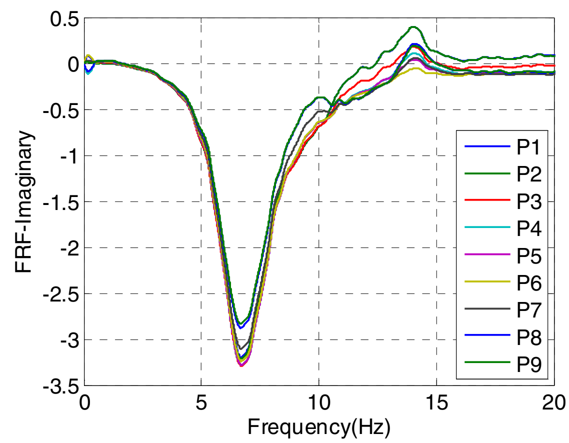

(b) Imaginary components - Test results

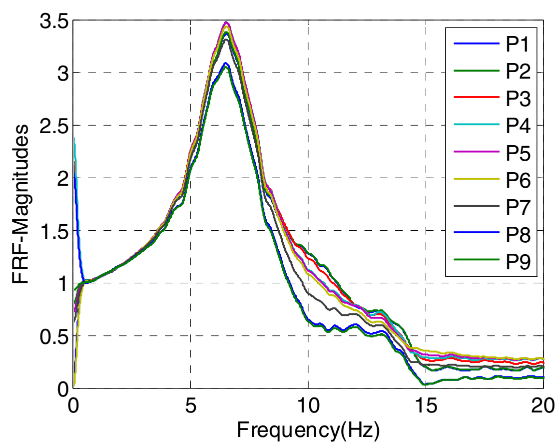

(c) Magnitudes - Test results

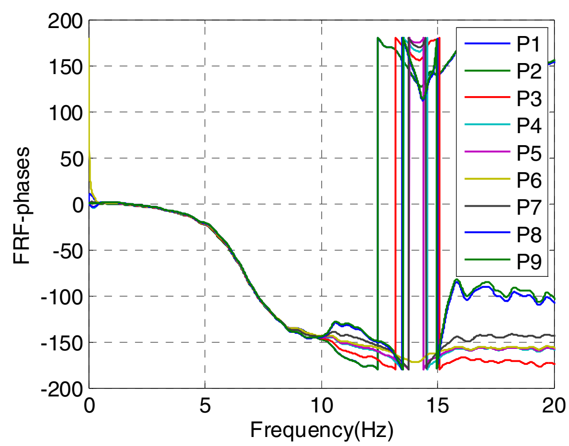

(d) Phases - Test results

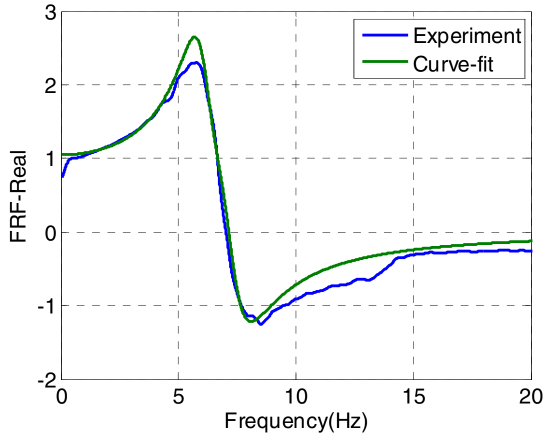

(e) Test result and Curve-fitting -Real

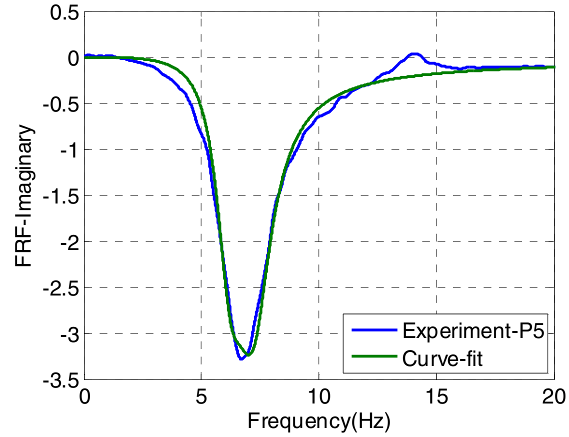

(f) Test result and Curve-fitting - Imaginary

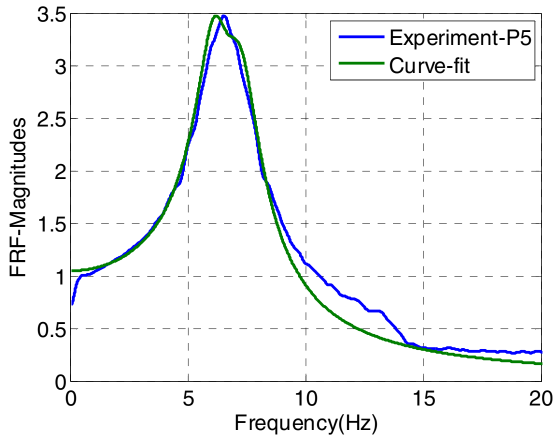

(g) Test result and Curve-fitting –Magn.

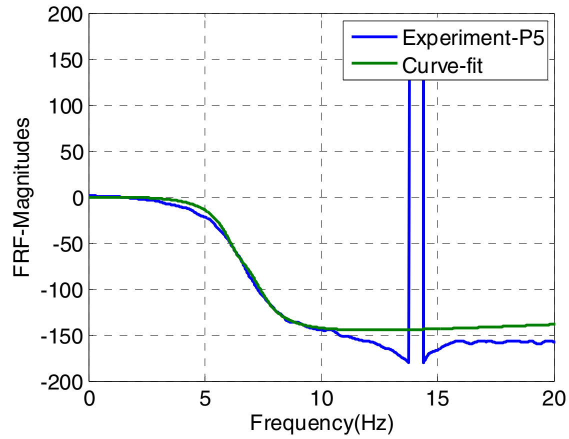

(h) Test result and Curve-fitting –Phases

Figure C-11 Phase 1, NS, After MCE

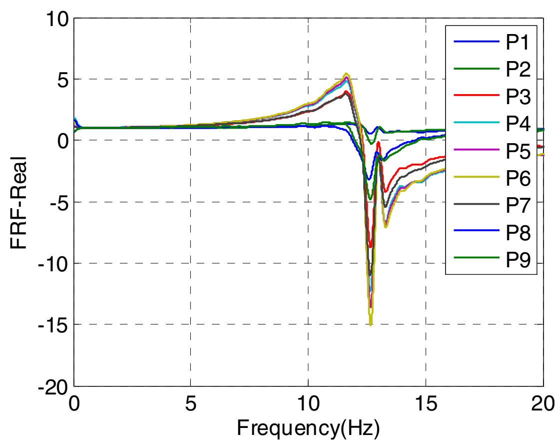

(a) Real components - Test results

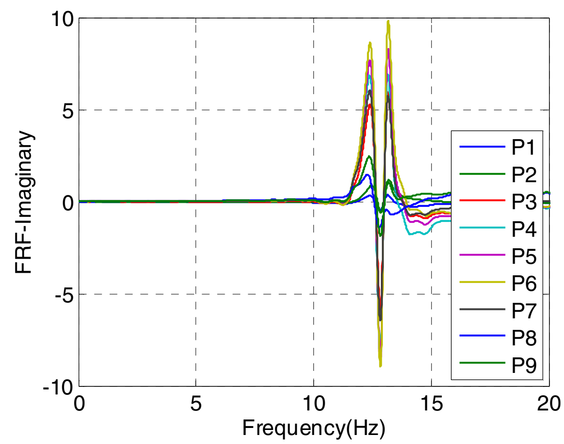

(b) Imaginary components - Test results

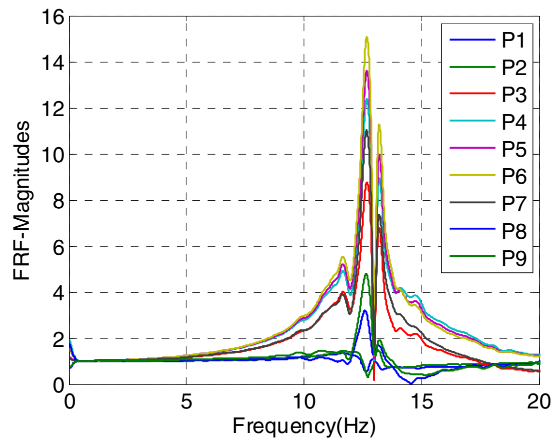

(c) Magnitudes - Test results

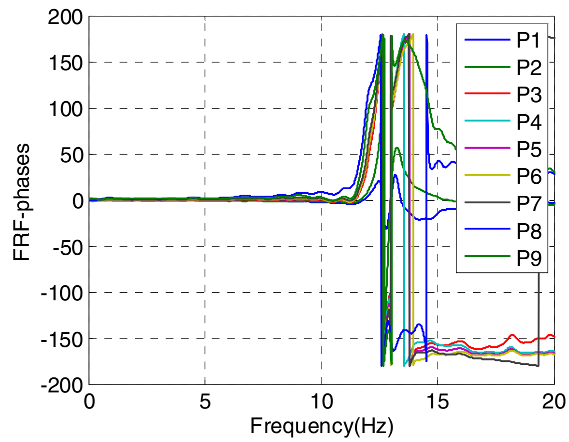

(d) Phases - Test results

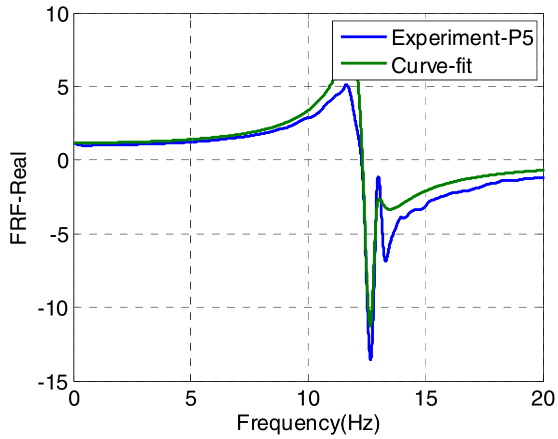

(e) Test result and Curve-fitting -Real

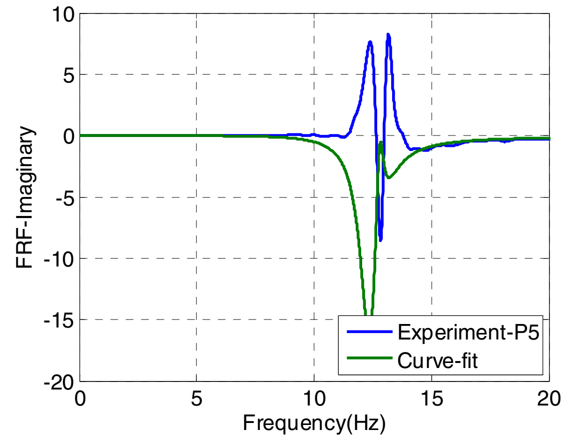

(f) Test result and Curve-fitting - Imaginary

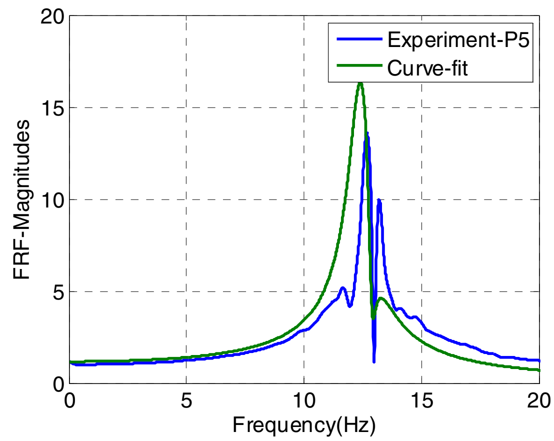

(g) Test result and Curve-fitting –Magn.

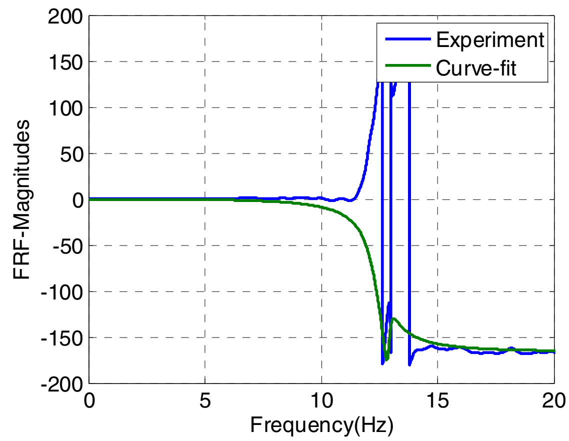

(h) Test result and Curve-fitting –Phases

Figure C-12 Phase 1, UD, After MCE

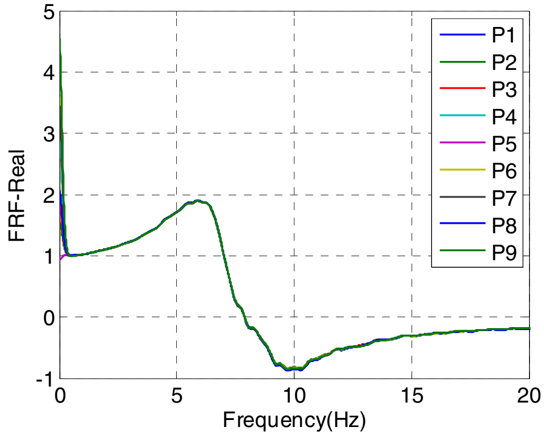

(a) Real components - Test results

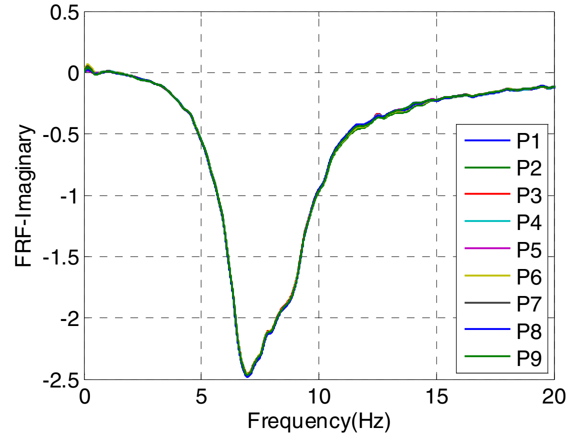

(b) Imaginary components - Test results

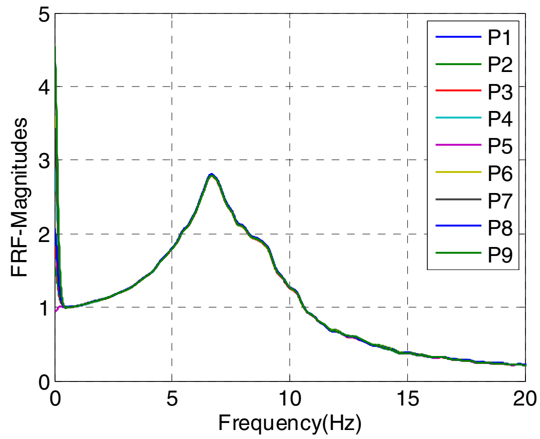

(c) Magnitudes - Test results

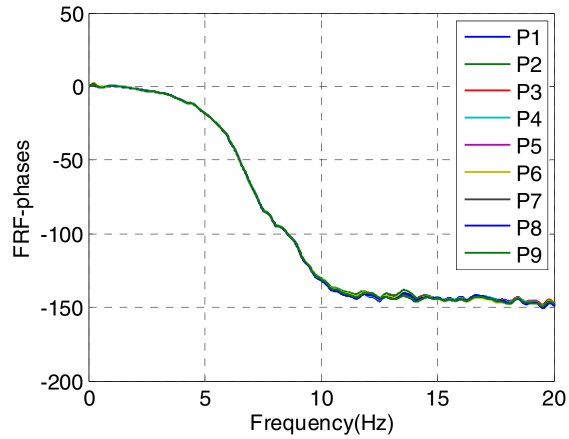

(d) Phases - Test results

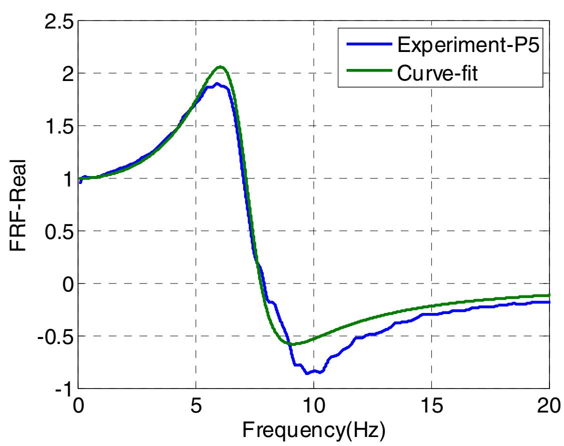

(e) Test result and Curve-fitting -Real

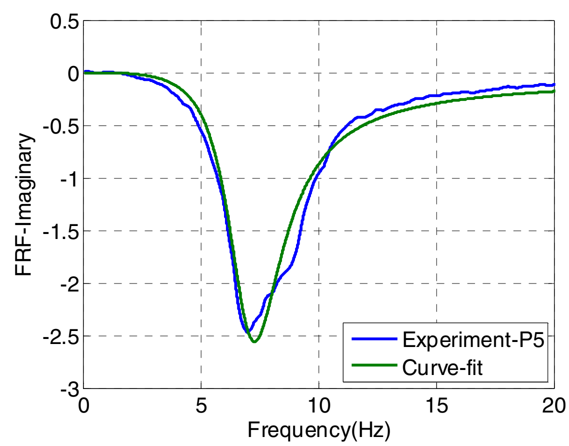

(f) Test result and Curve-fitting - Imaginary

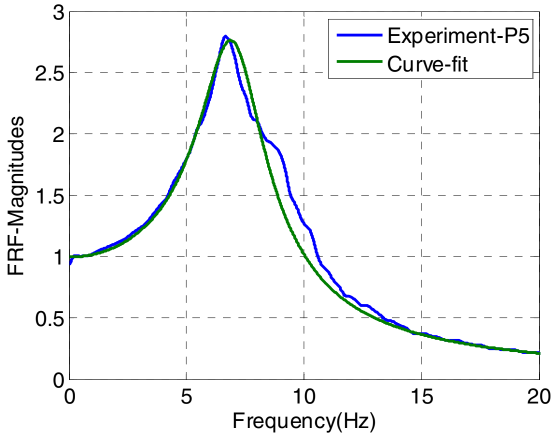

(g) Test result and Curve-fitting –Magn.

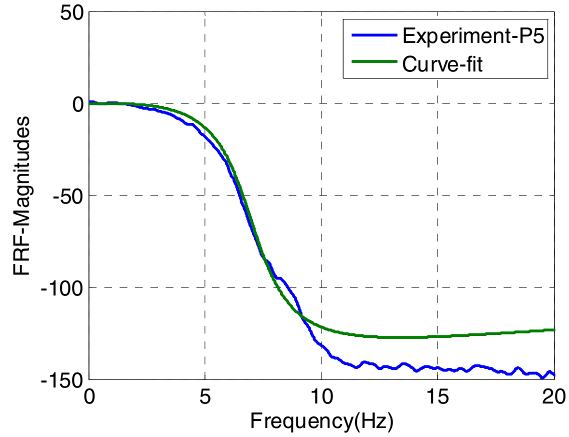

(h) Test result and Curve-fitting –Phases

Figure C-13 Phase 1, EW, After DE2

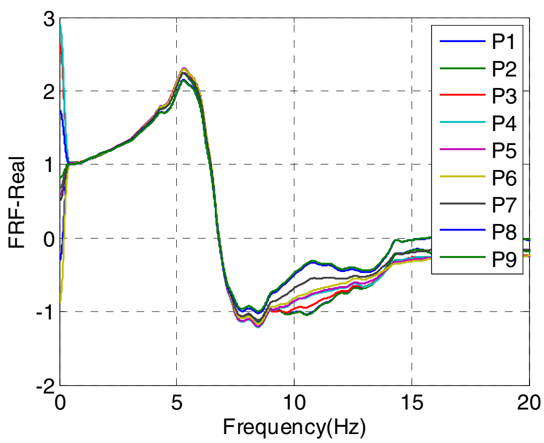

(a) Real components - Test results

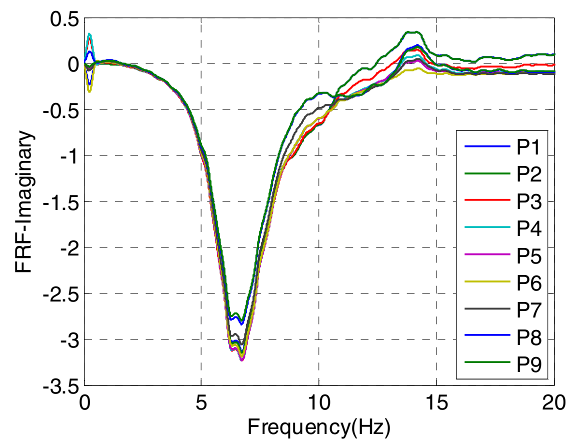

(b) Imaginary components - Test results

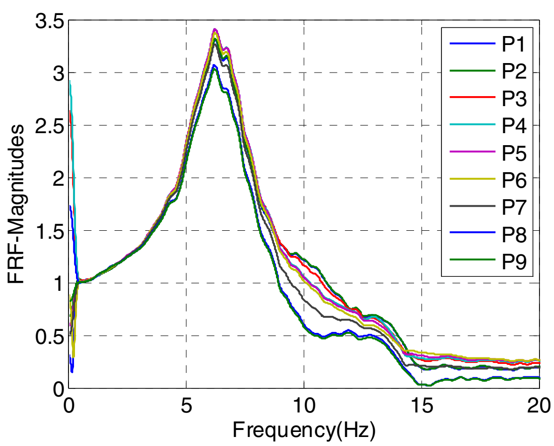

(c) Magnitudes - Test results

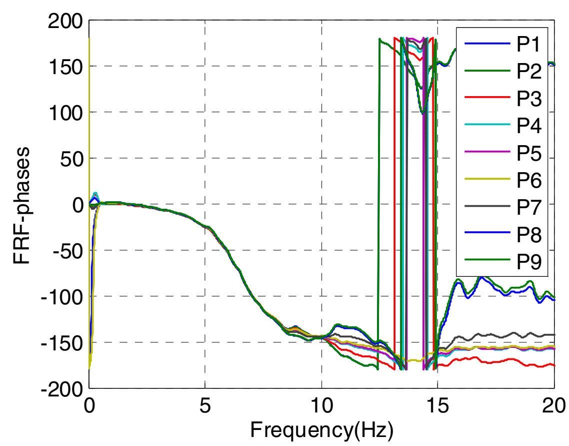

(d) Phases - Test results

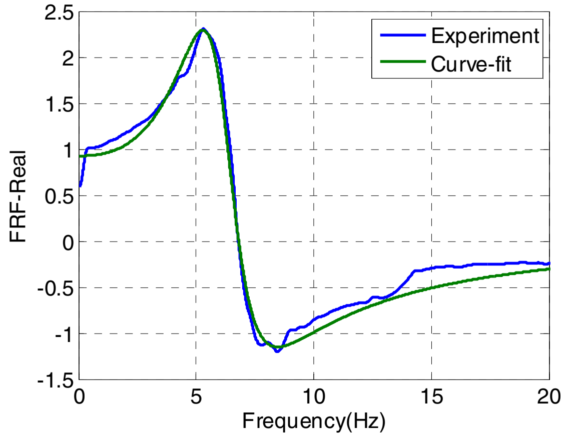

(e) Test result and Curve-fitting -Real

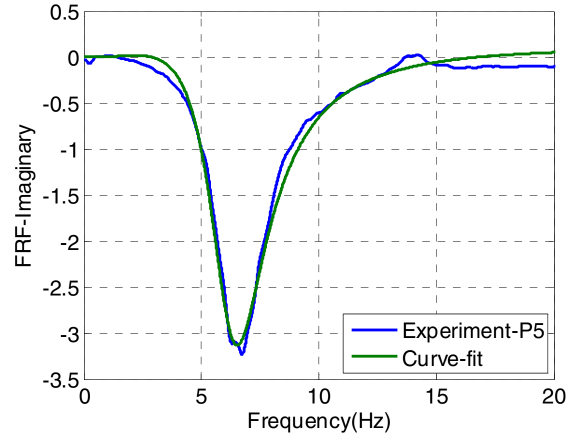

(f) Test result and Curve-fitting - Imaginary

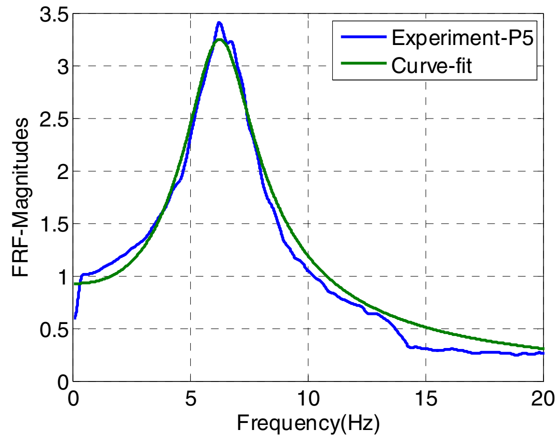

(g) Test result and Curve-fitting –Magn.

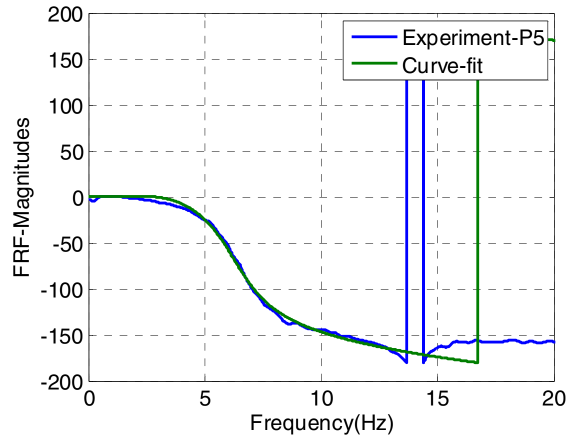

(h) Test result and Curve-fitting –Phases

Figure C-14 Phase 1, NS, After DE2

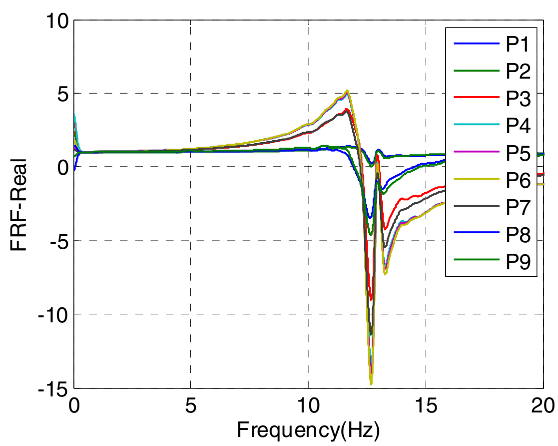

(a) Real components - Test results

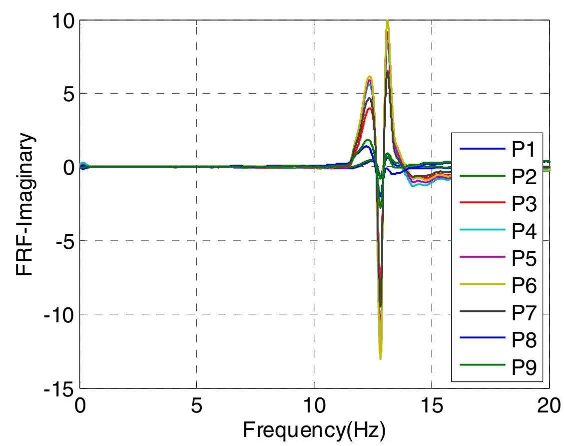

(b) Imaginary components - Test results

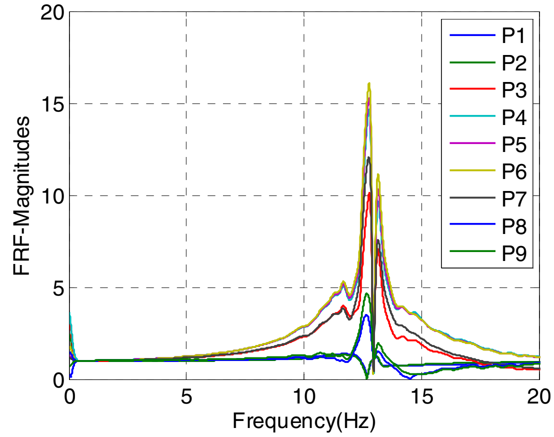

(c) Magnitudes - Test results

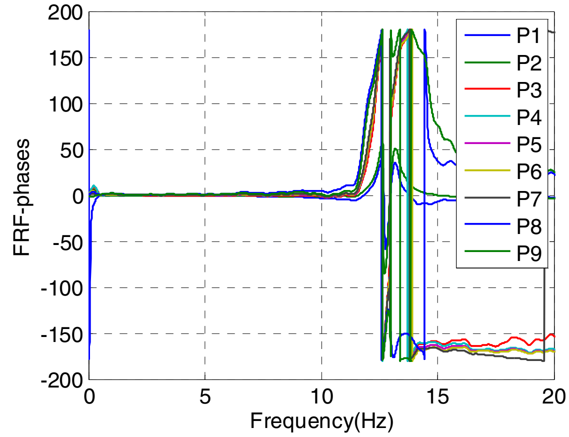

(d) Phases - Test results

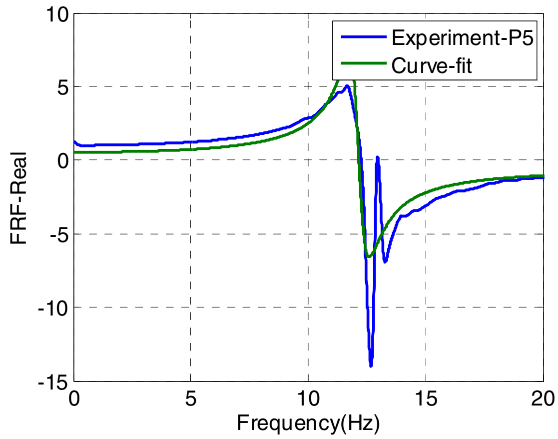

(e) Test result and Curve-fitting -Real

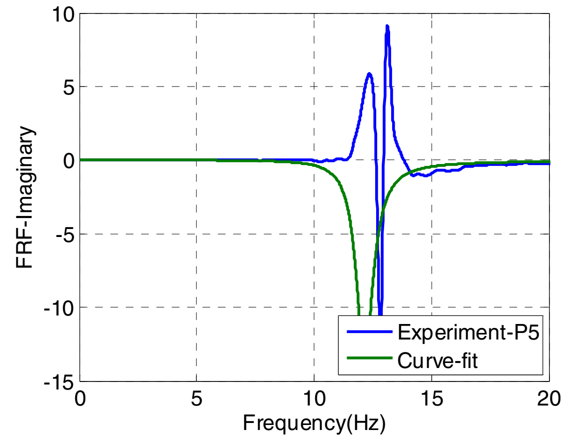

(f) Test result and Curve-fitting - Imaginary

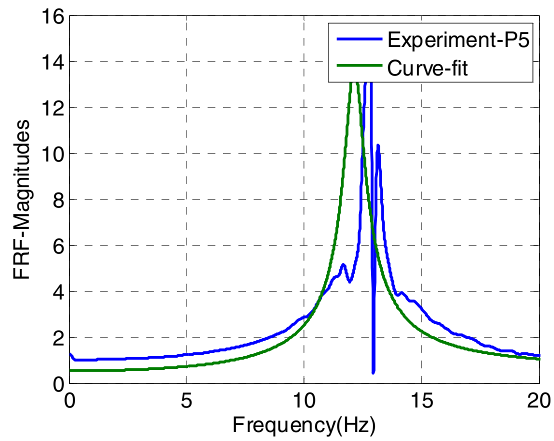

(g) Test result and Curve-fitting –Magn.

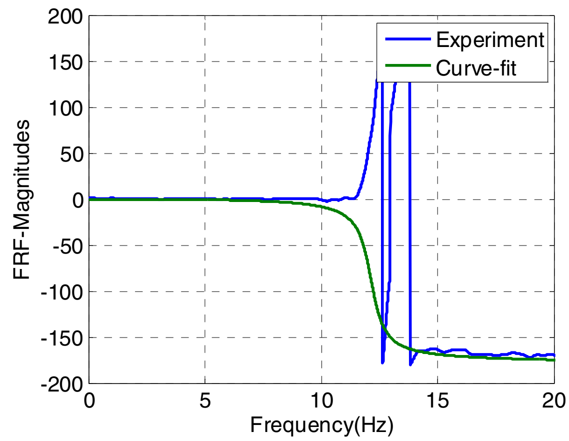

(h) Test result and Curve-fitting –Phases

Figure C-15 Phase 1, UD, After DE2

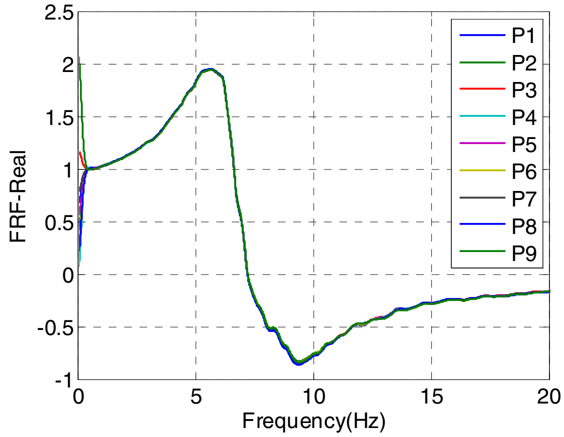

(a) Real components - Test results

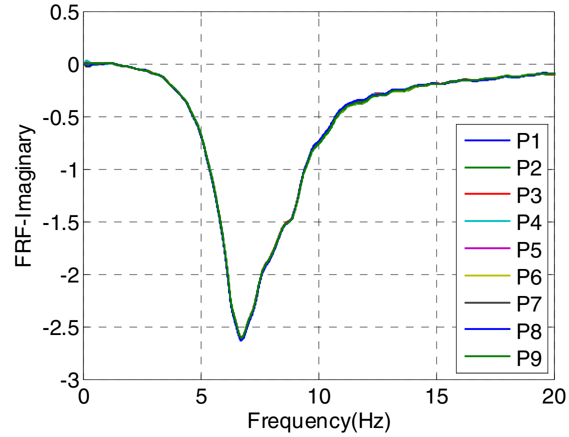

(b) Imaginary components - Test results

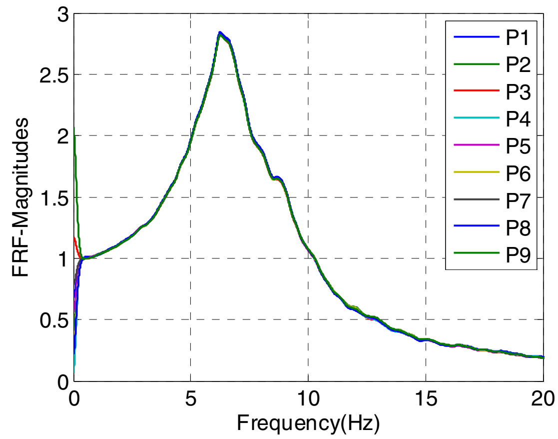

(c) Magnitudes - Test results

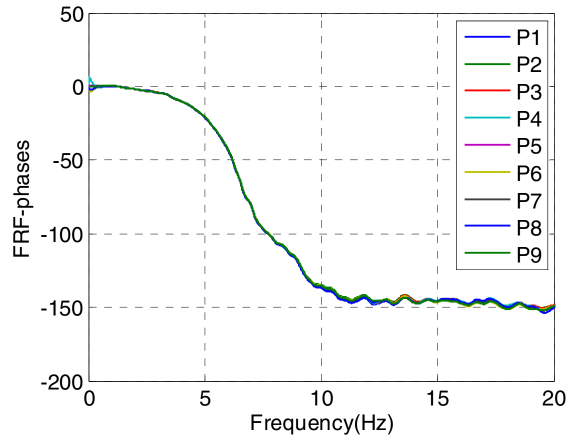

(d) Phases - Test results

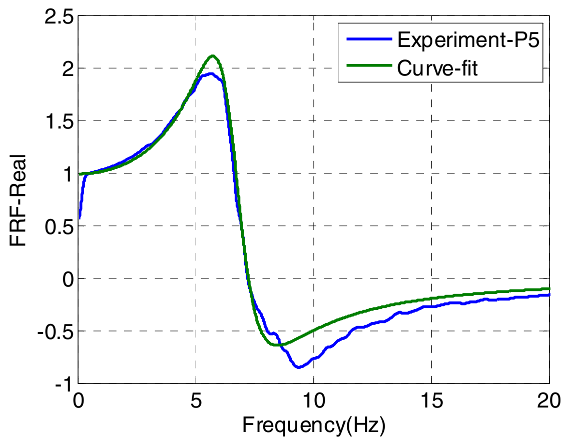

(e) Test result and Curve-fitting -Real

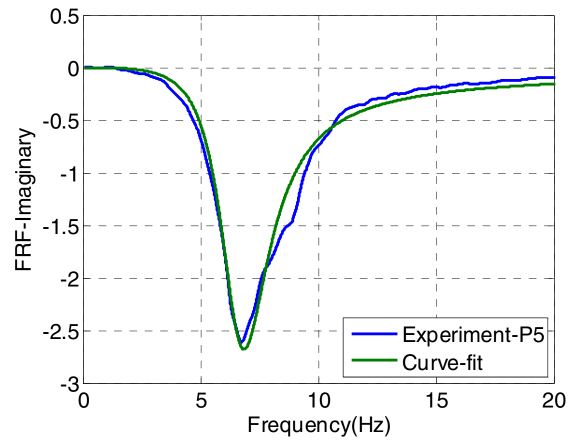

(f) Test result and Curve-fitting - Imaginary

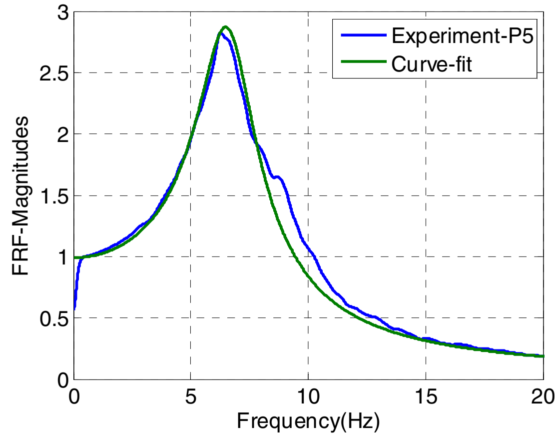

(g) Test result and Curve-fitting –Magn.

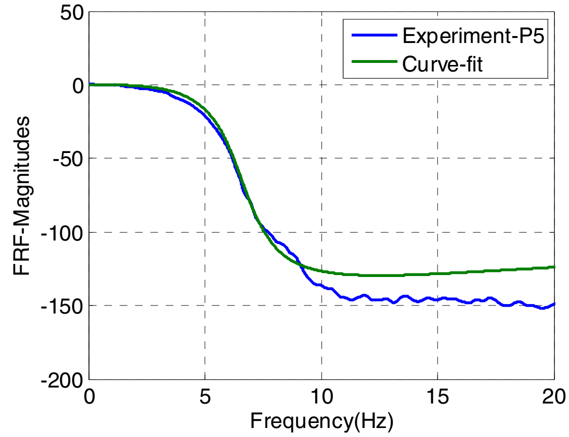

(h) Test result and Curve-fitting –Phases

Figure C-16 Phase 1, EW, After Max

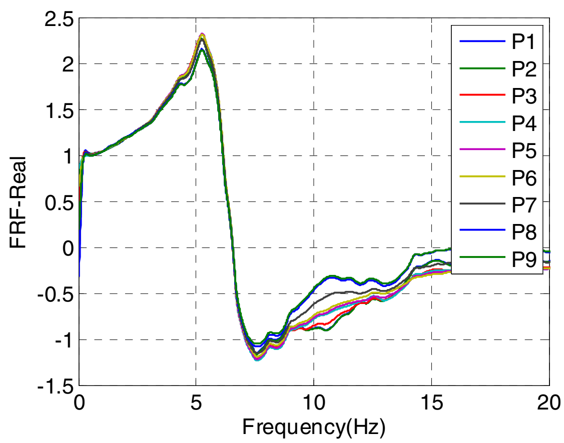

(a) Real components - Test results

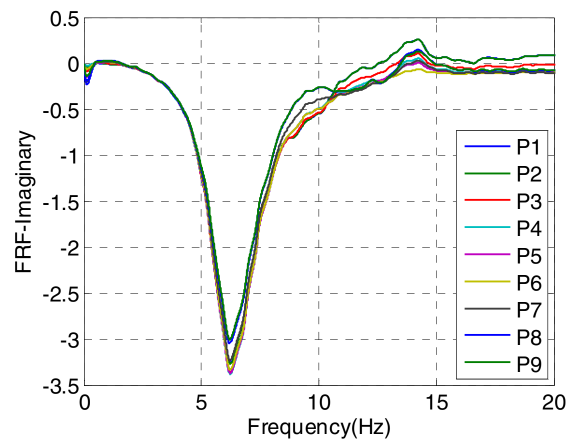

(b) Imaginary components - Test results

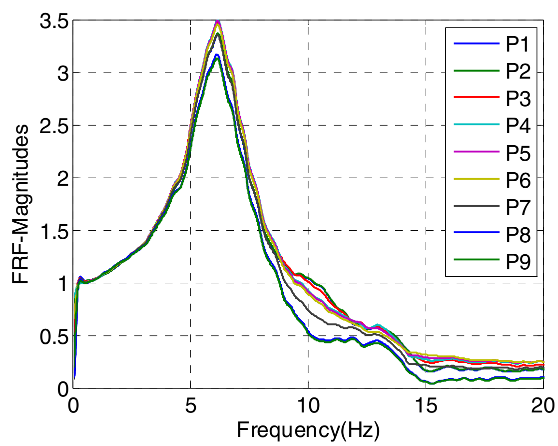

(c) Magnitudes - Test results

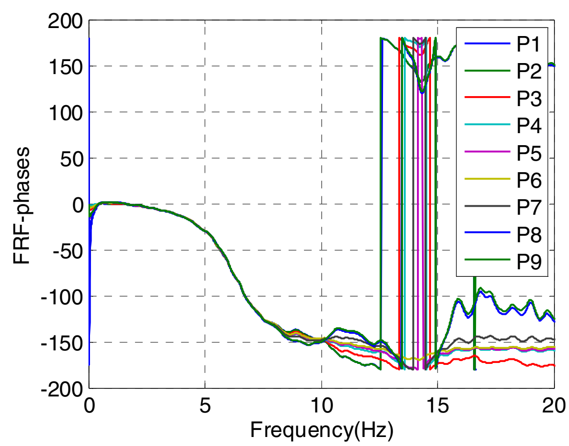

(d) Phases - Test results

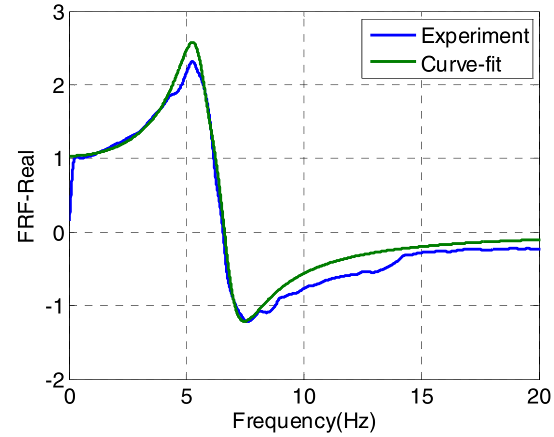

(e) Test result and Curve-fitting -Real

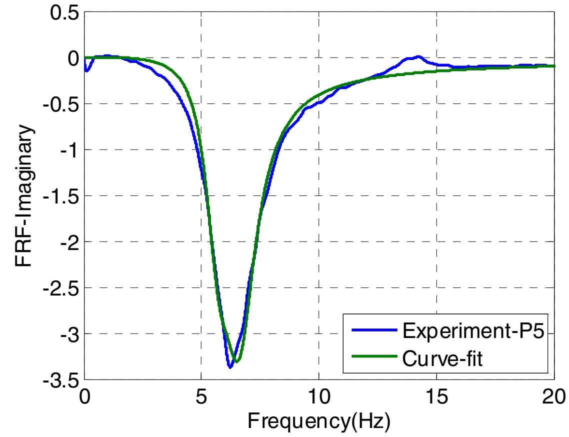

(f) Test result and Curve-fitting - Imaginary

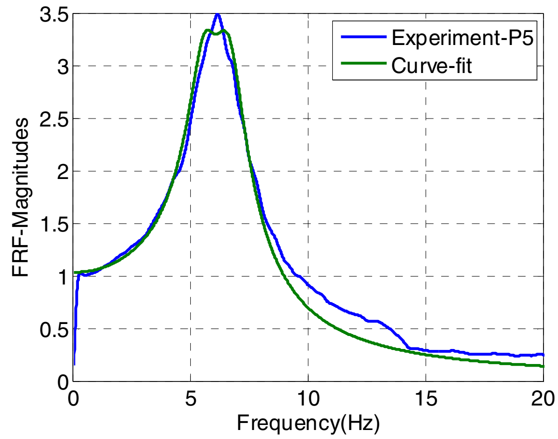

(g) Test result and Curve-fitting –Magn.

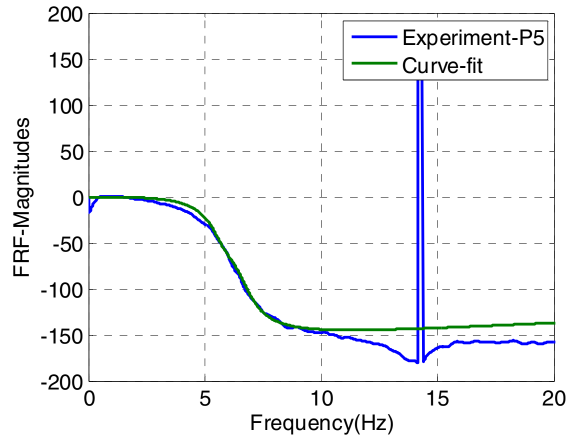

(h) Test result and Curve-fitting –Phases

Figure C-17 Phase 1, NS, After Max

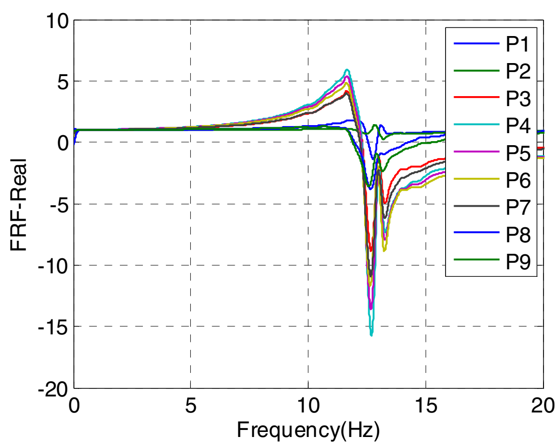

(a) Real components - Test results

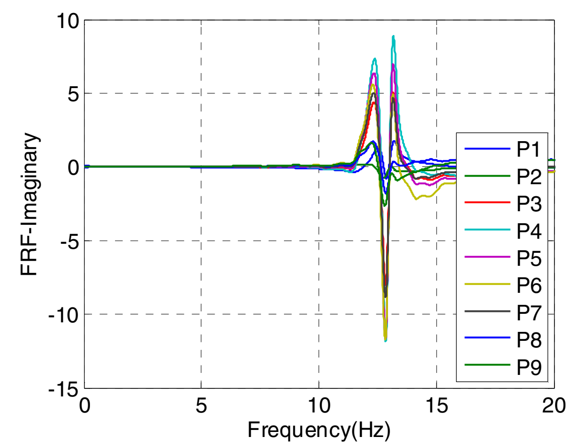

(b) Imaginary components - Test results

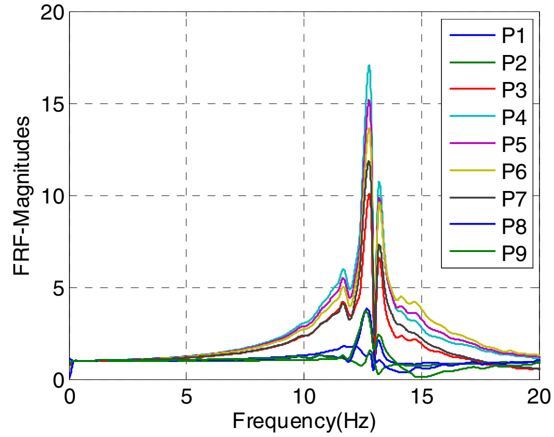

(c) Magnitudes - Test results

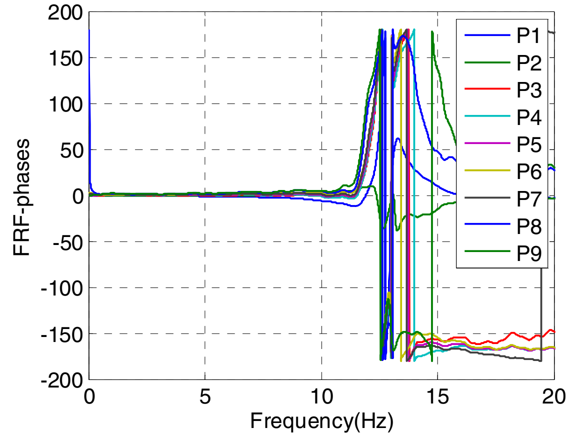

(d) Phases - Test results

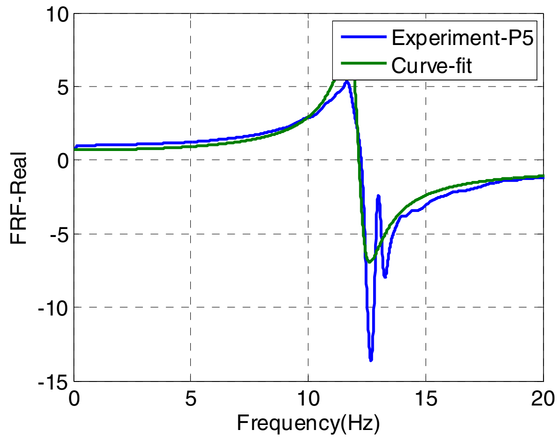

(e) Test result and Curve-fitting -Real

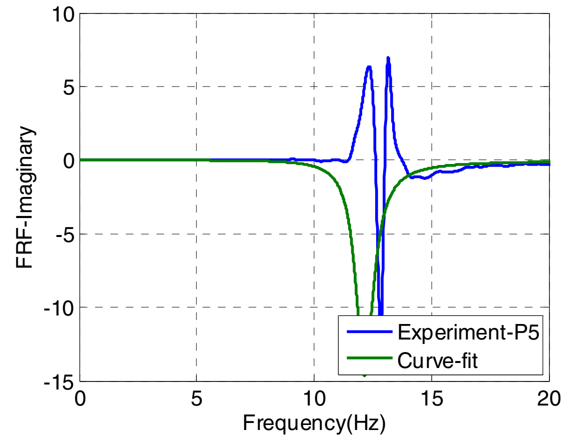

(f) Test result and Curve-fitting - Imaginary

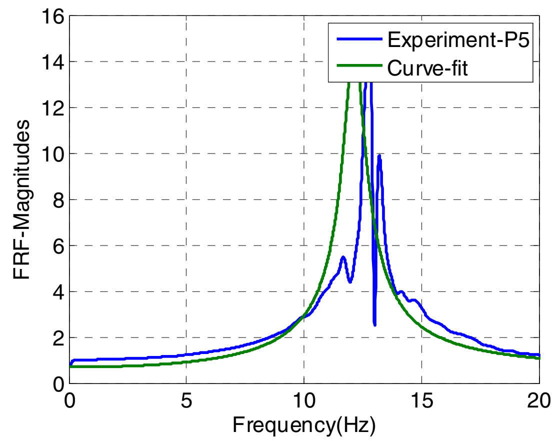

(g) Test result and Curve-fitting –Magn.

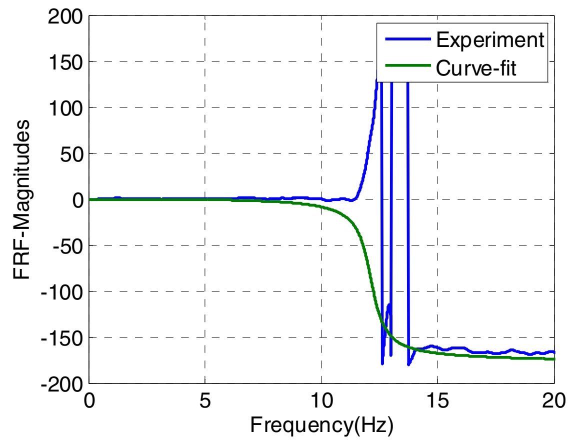

(h) Test result and Curve-fitting –Phases

Figure C-18 Phase 1, UD, After Max

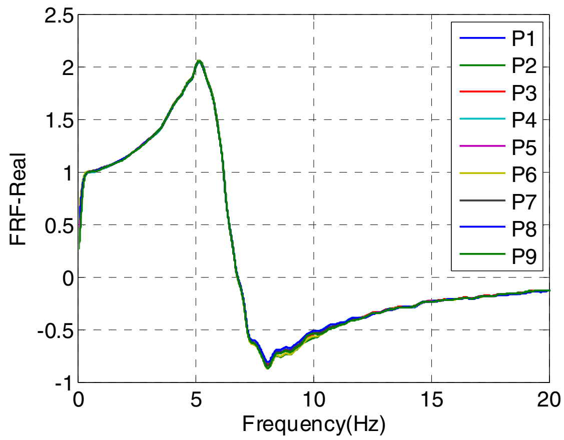

(a) Real components - Test results

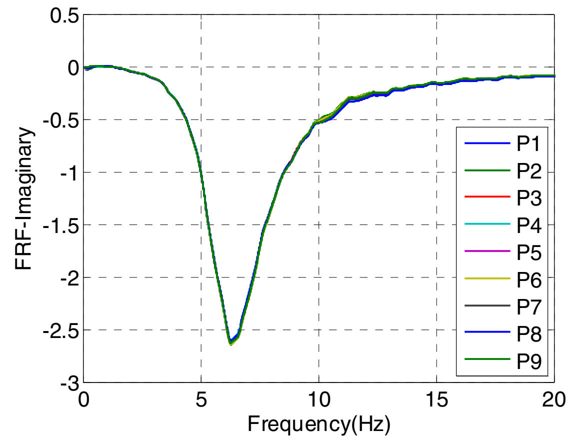

(b) Imaginary components - Test results

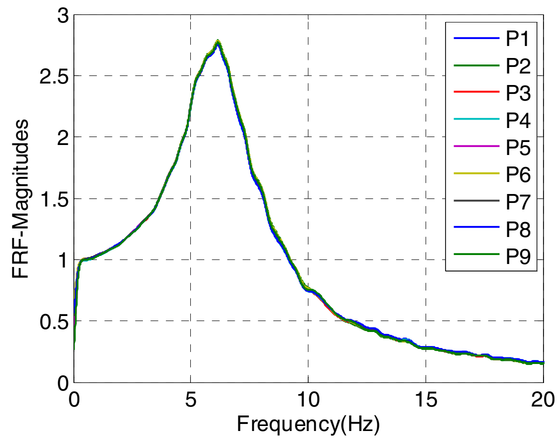

(c) Magnitudes - Test results

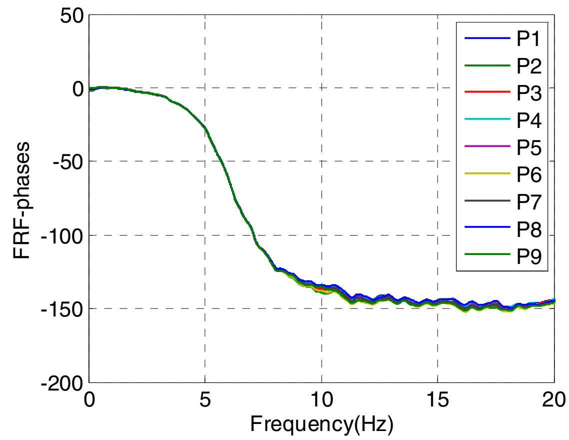

(d) Phases - Test results

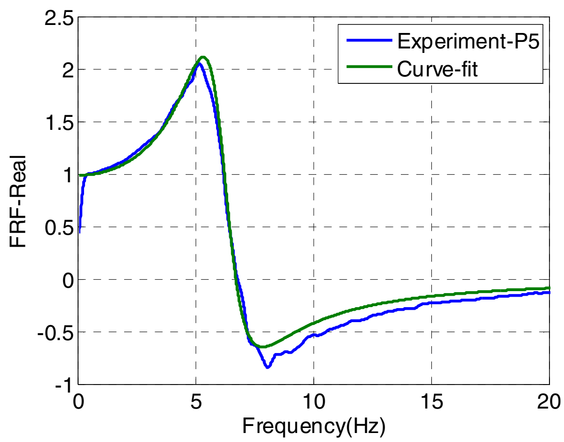

(e) Test result and Curve-fitting -Real

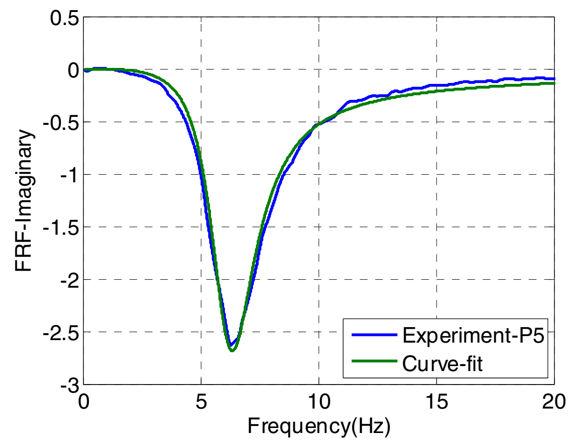

(f) Test result and Curve-fitting - Imaginary

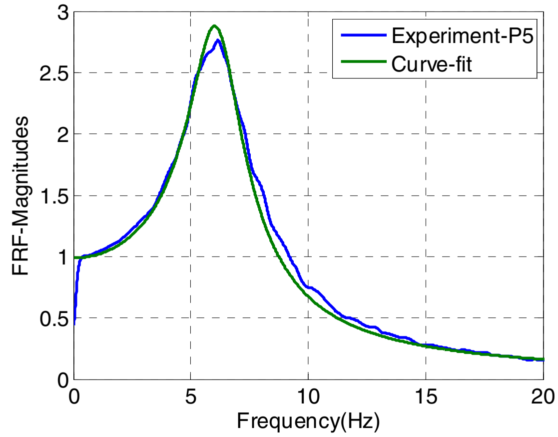

(g) Test result and Curve-fitting –Magn.

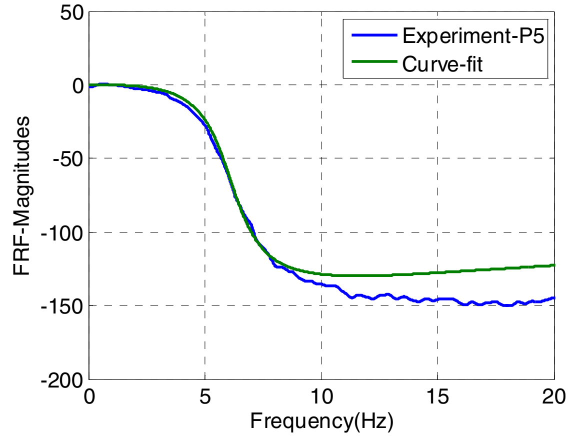

(h) Test result and Curve-fitting –Phases

Figure C-19 Phase 2, EW, Initial

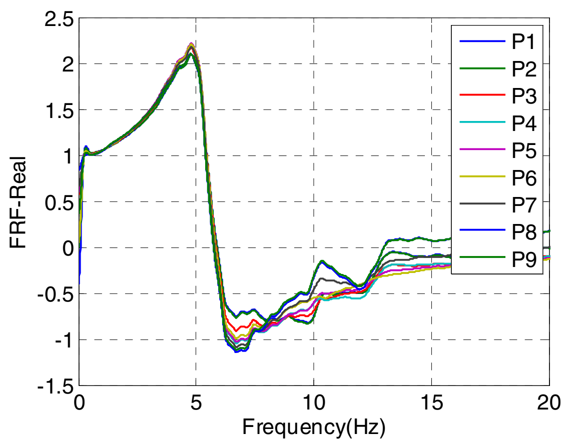

(a) Real components - Test results

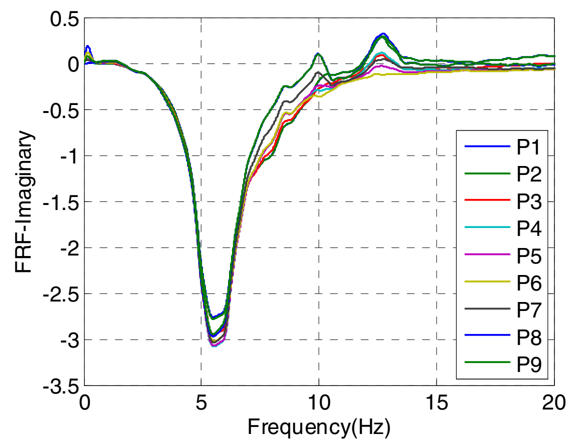

(b) Imaginary components - Test results

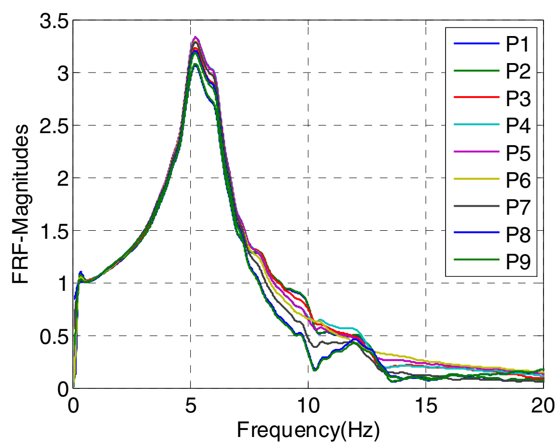

(c) Magnitudes - Test results

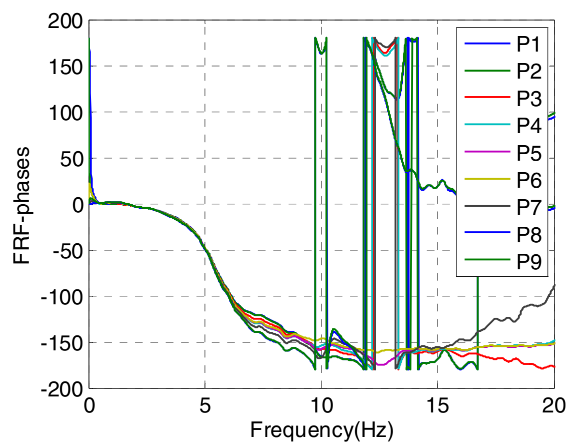

(d) Phases - Test results

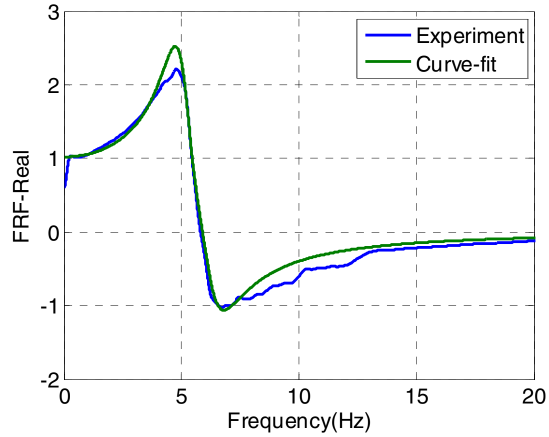

(e) Test result and Curve-fitting -Real

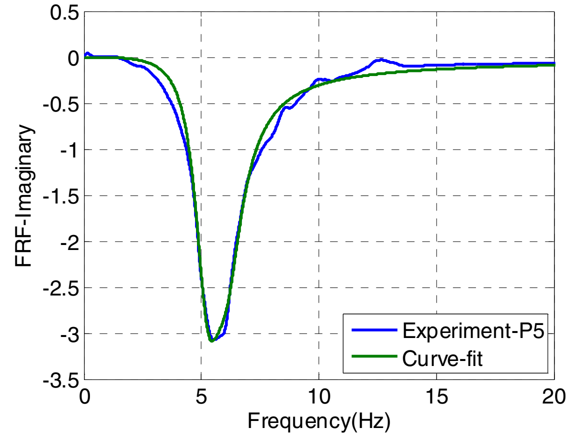

(f) Test result and Curve-fitting - Imaginary

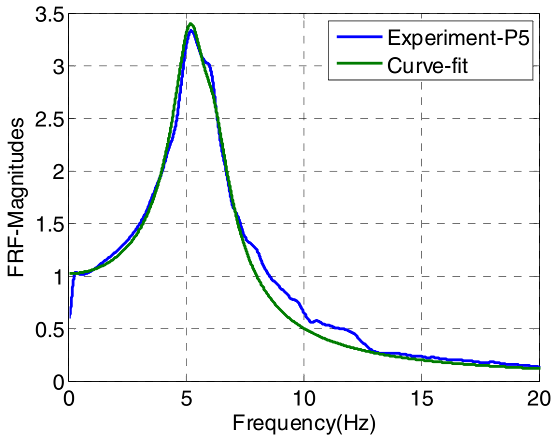

(g) Test result and Curve-fitting –Magn.

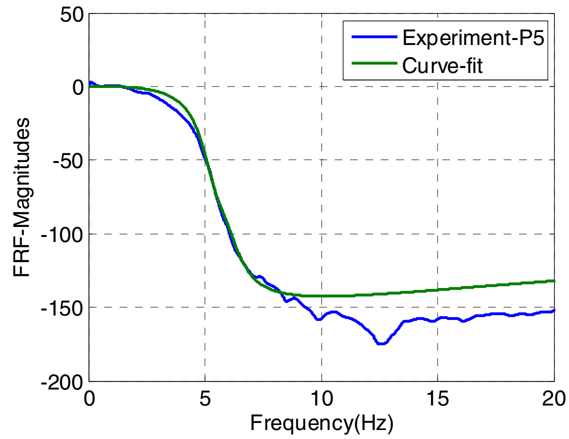

(h) Test result and Curve-fitting –Phases

Figure C-20 Phase 2, NS, Initial

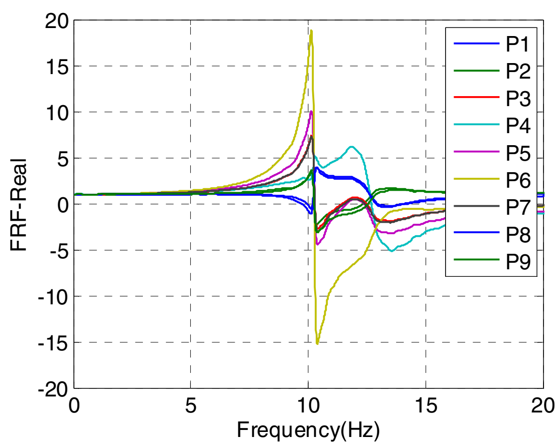

(a) Real components - Test results

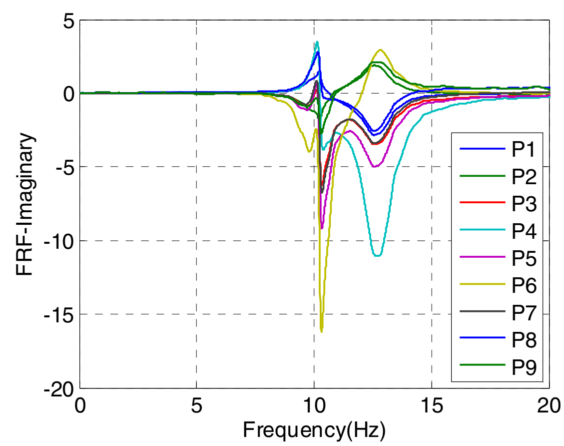

(b) Imaginary components - Test results

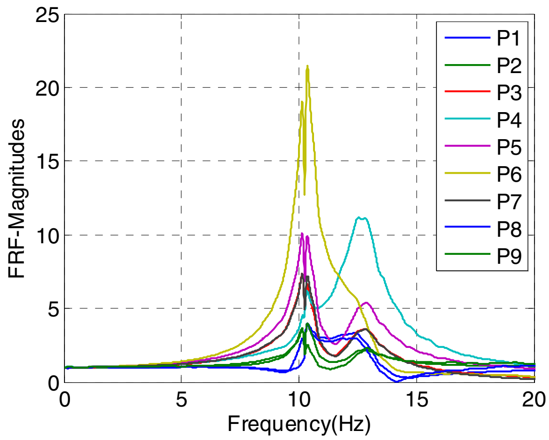

(c) Magnitudes - Test results

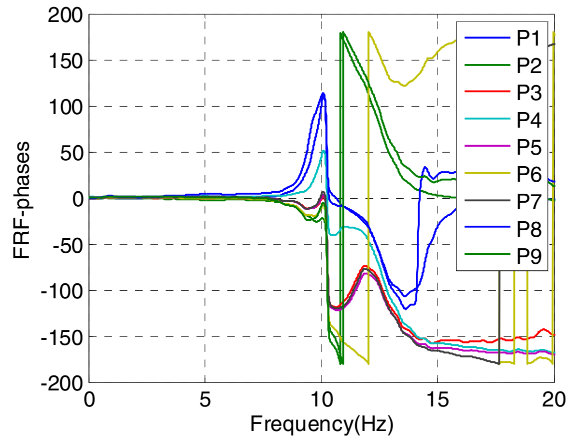

(d) Phases - Test results

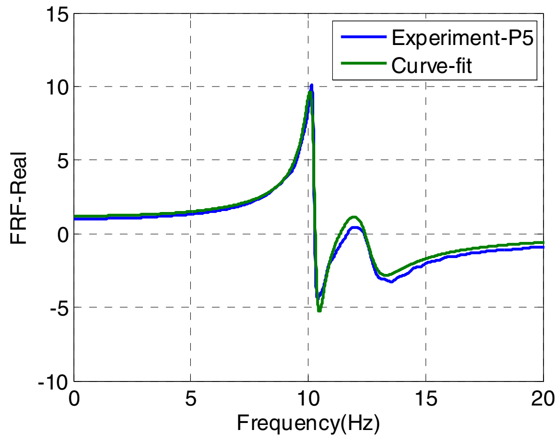

(e) Test result and Curve-fitting -Real

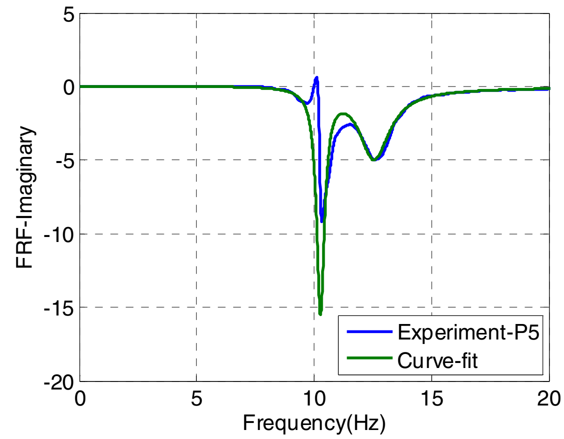

(f) Test result and Curve-fitting - Imaginary

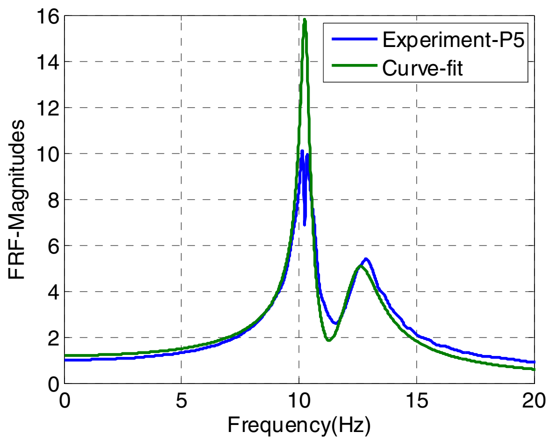

(g) Test result and Curve-fitting –Magn.

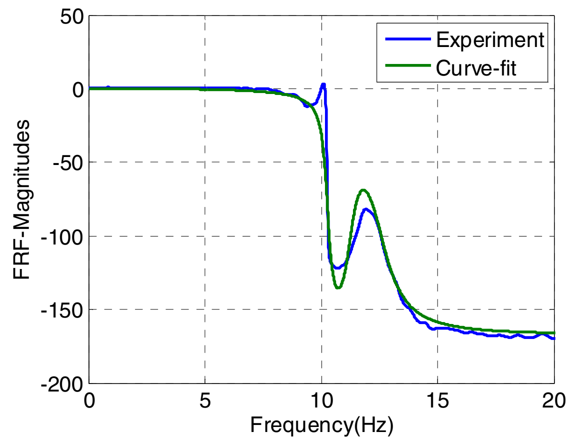

(h) Test result and Curve-fitting –Phases

Figure C-21 Phase 2, UD, Initial

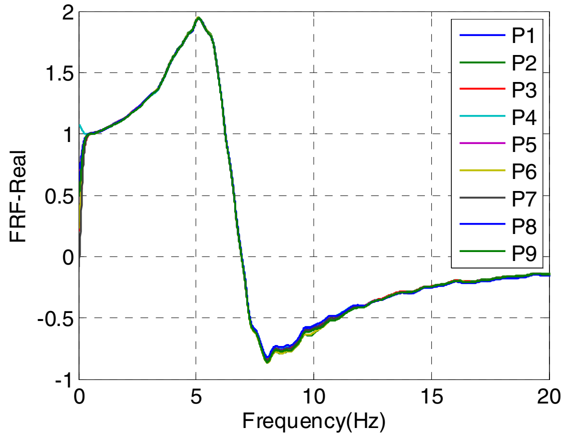

(a) Real components - Test results

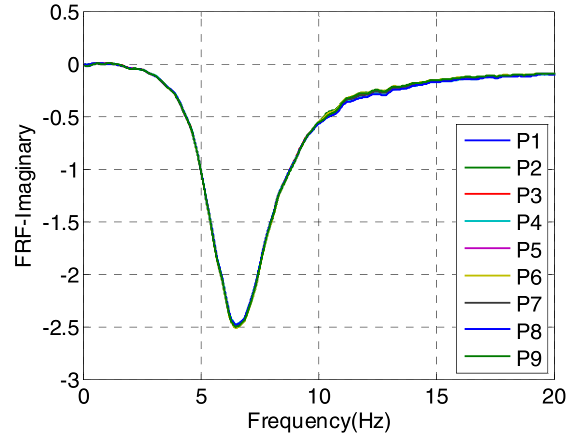

(b) Imaginary components - Test results

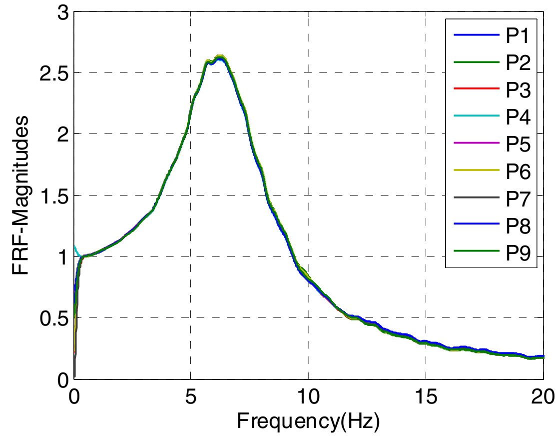

(c) Magnitudes - Test results

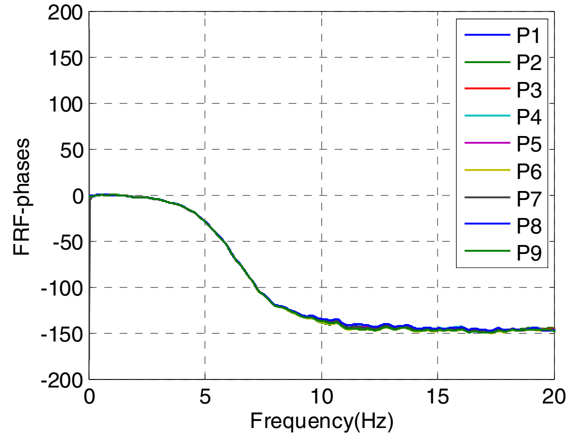

(d) Phases - Test results

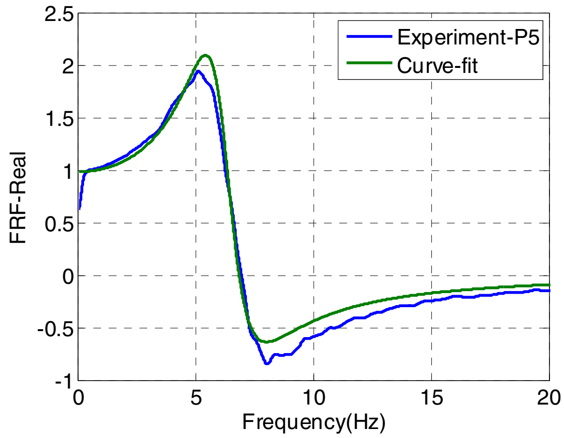

(e) Test result and Curve-fitting -Real

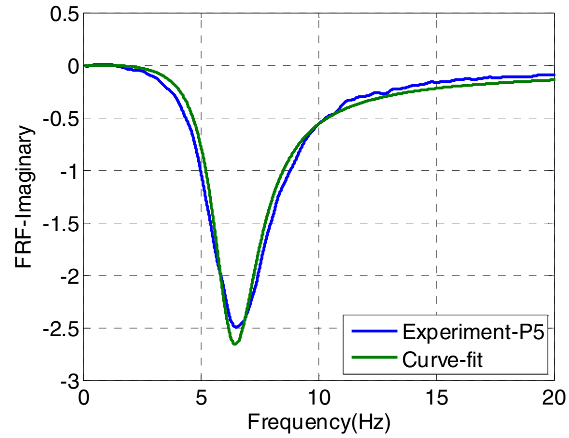

(f) Test result and Curve-fitting - Imaginary

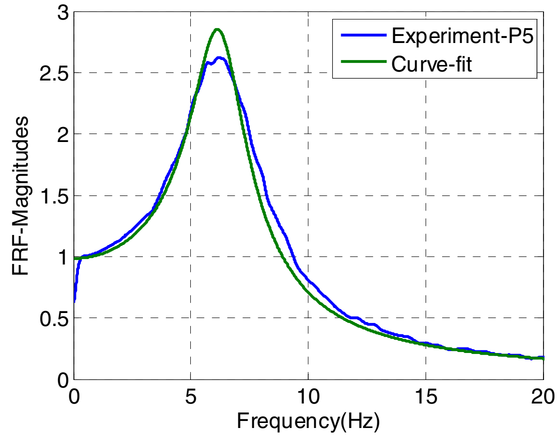

(g) Test result and Curve-fitting –Magn.

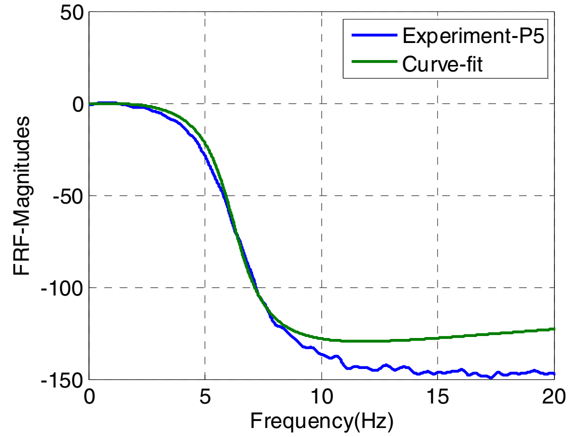

(h) Test result and Curve-fitting –Phases

Figure C-22 Phase 2, EW, After EL

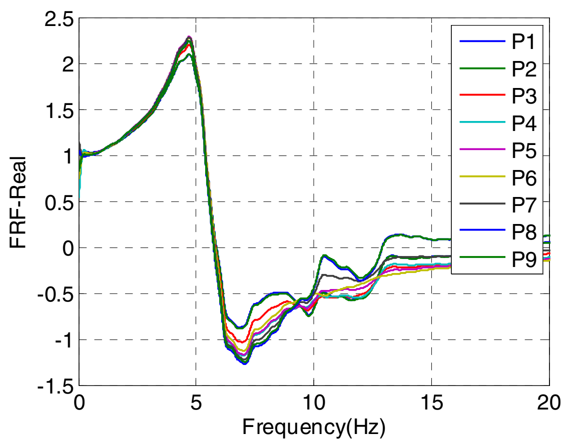

(a) Real components - Test results

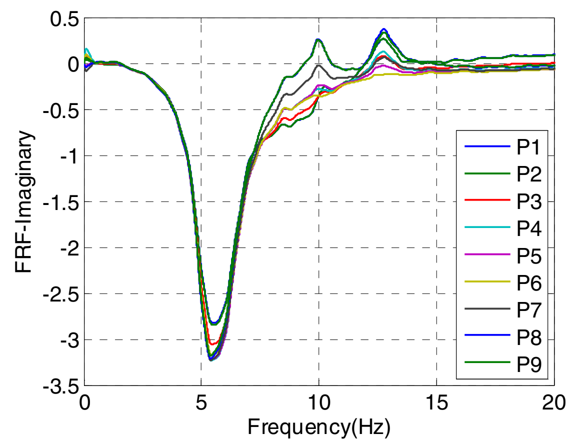

(b) Imaginary components - Test results

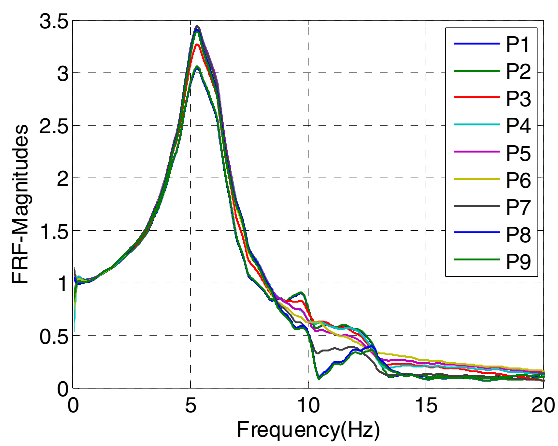

(c) Magnitudes - Test results

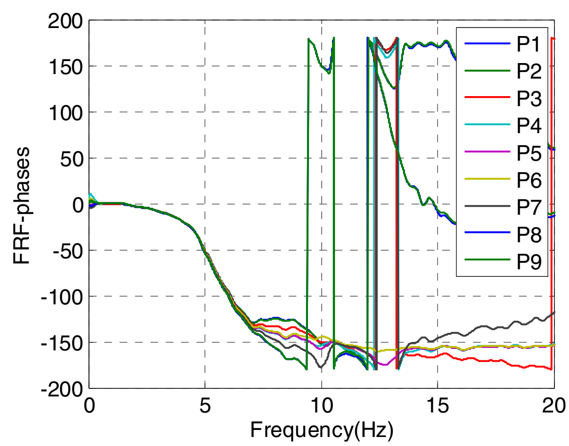

(d) Phases - Test results

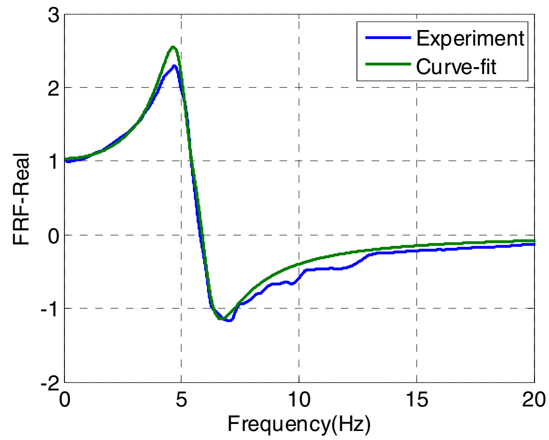

(e) Test result and Curve-fitting -Real

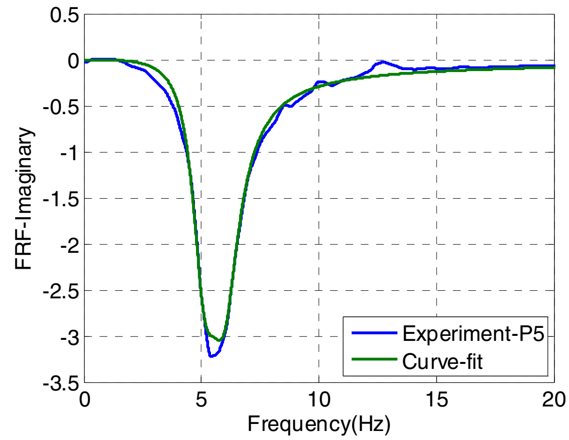

(f) Test result and Curve-fitting - Imaginary

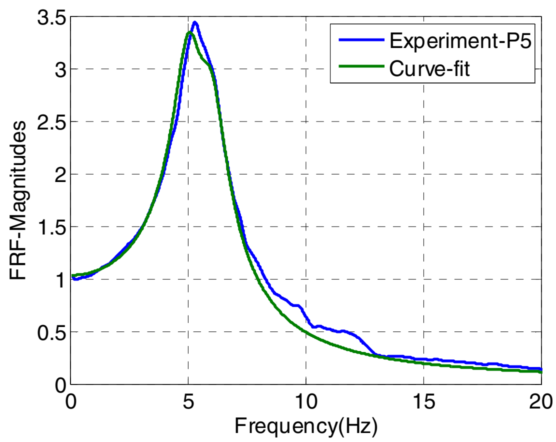

(g) Test result and Curve-fitting –Magn.

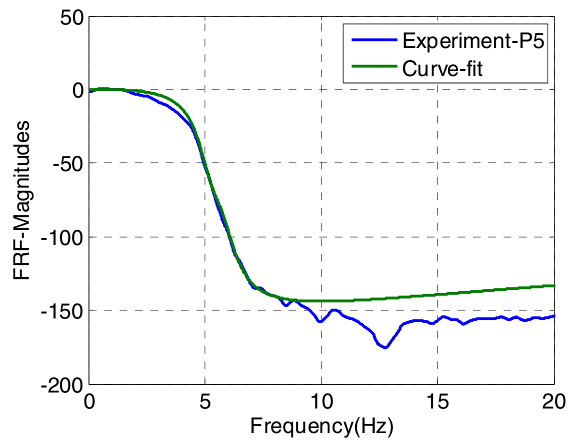

(h) Test result and Curve-fitting –Phases

Figure C-23 Phase 2, NS, After EL

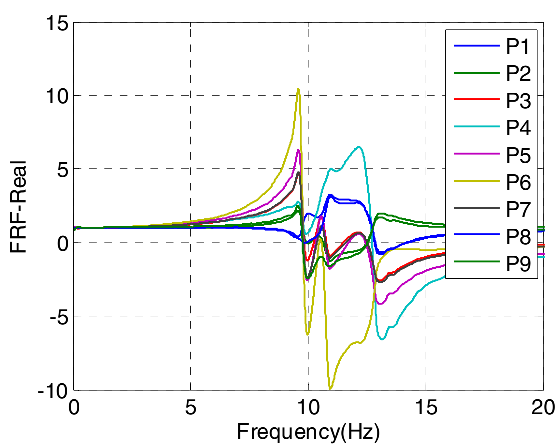

(a) Real components - Test results

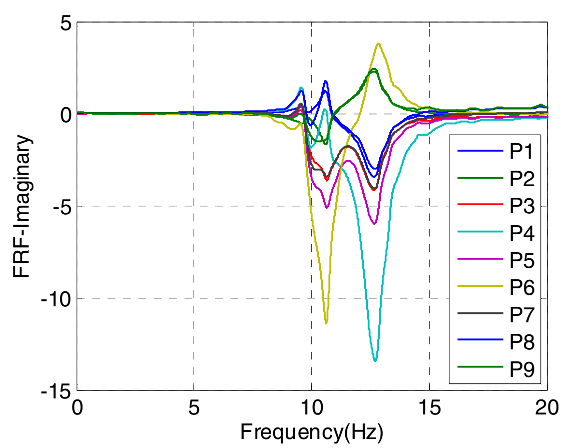

(b) Imaginary components - Test results

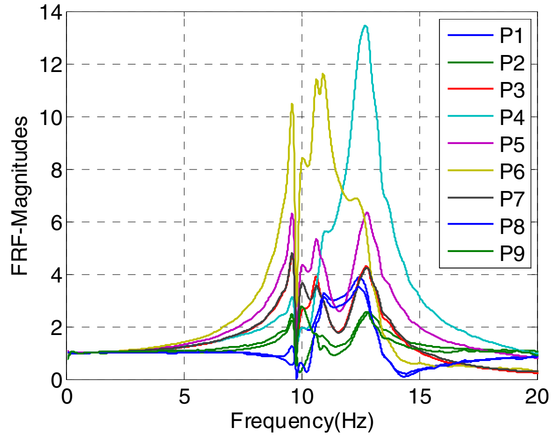

(c) Magnitudes - Test results

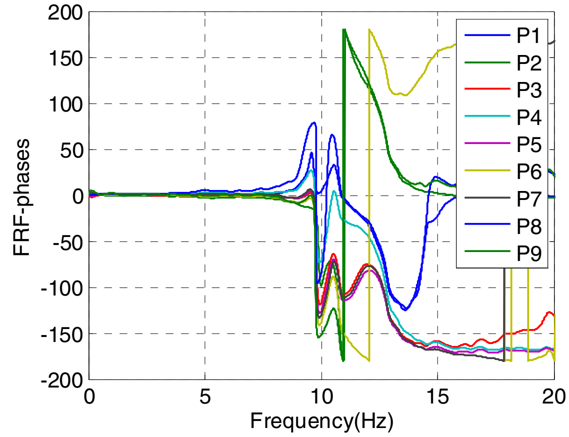

(d) Phases - Test results

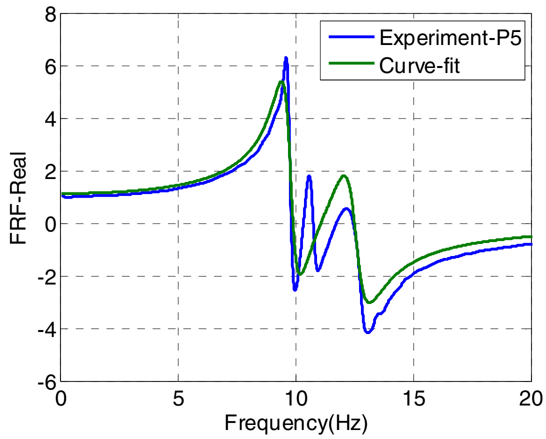

(e) Test result and Curve-fitting -Real

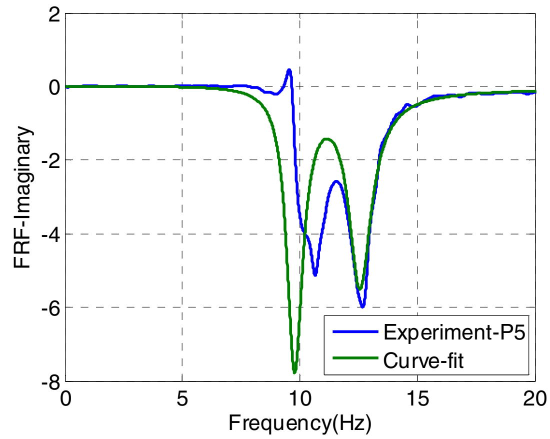

(f) Test result and Curve-fitting - Imaginary

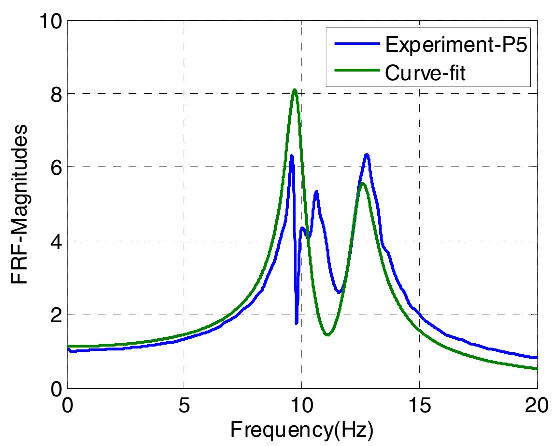

(g) Test result and Curve-fitting –Magn.

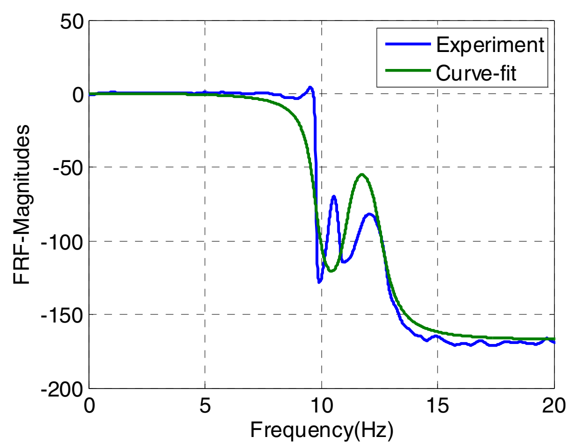

(h) Test result and Curve-fitting –Phases

Figure C-24 Phase 2, UD, After EL

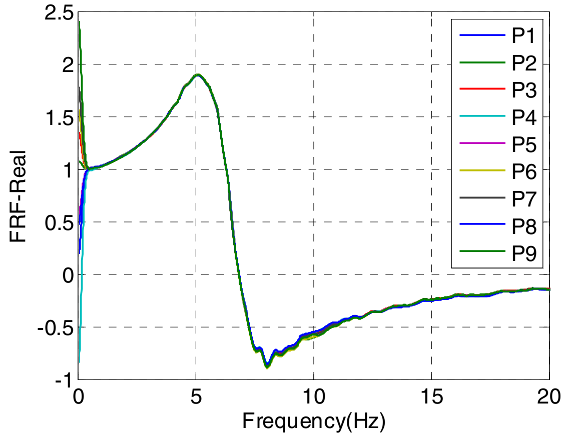

(a) Real components - Test results

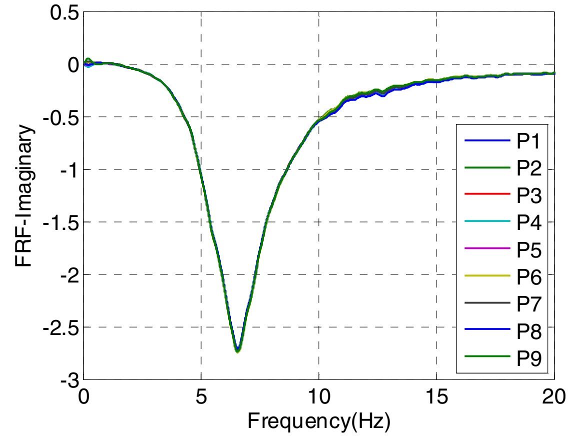

(b) Imaginary components - Test results

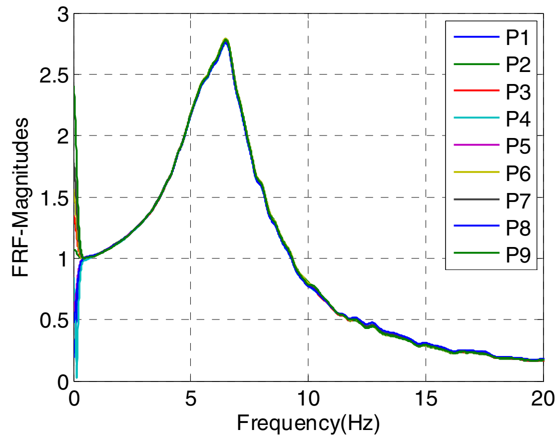

(c) Magnitudes - Test results

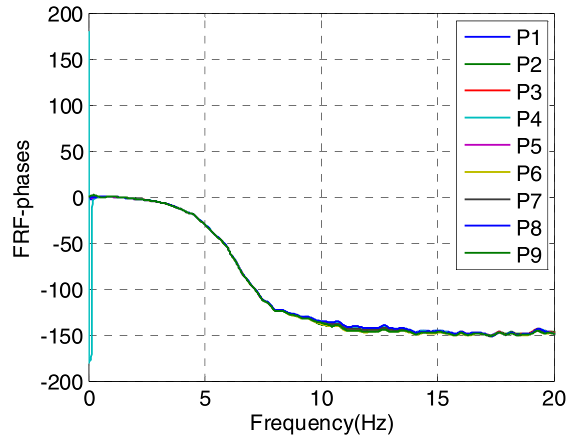

(d) Phases - Test results

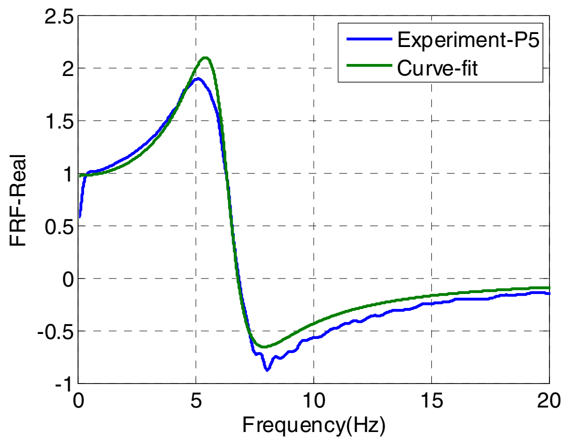

(e) Test result and Curve-fitting -Real

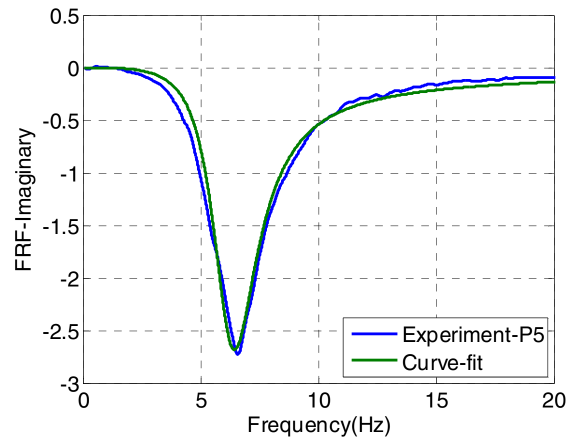

(f) Test result and Curve-fitting - Imaginary

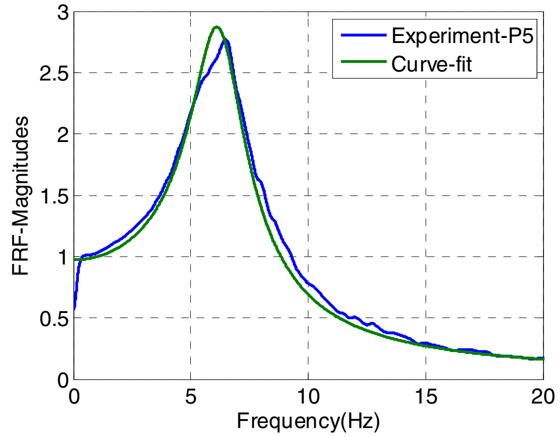

(g) Test result and Curve-fitting –Magn.

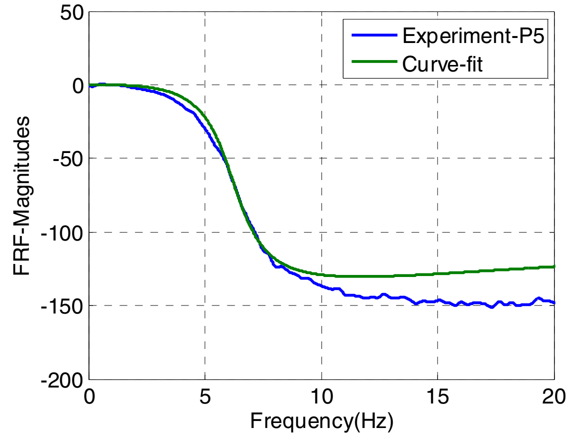

(h) Test result and Curve-fitting –Phases

Figure C-25 Phase 2, EW, After DE

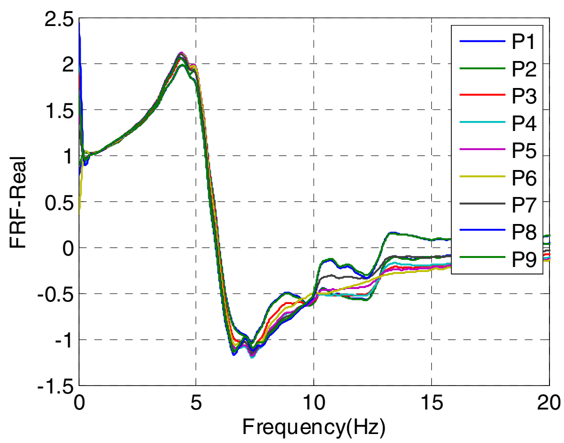

(a) Real components - Test results

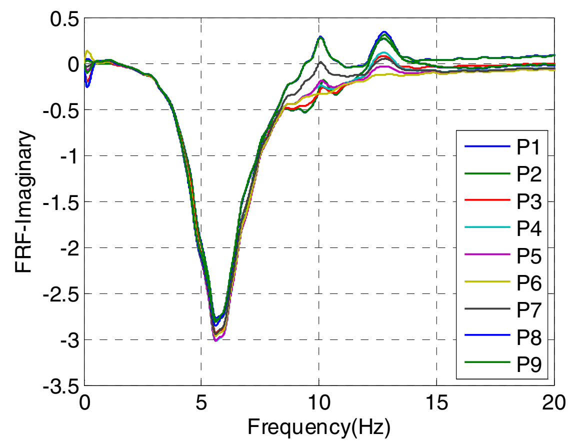

(b) Imaginary components - Test results

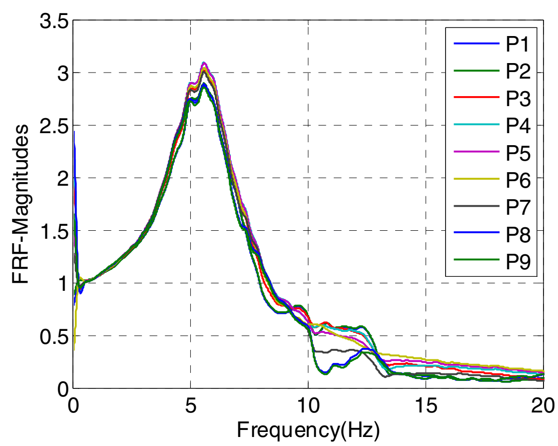

(c) Magnitudes - Test results

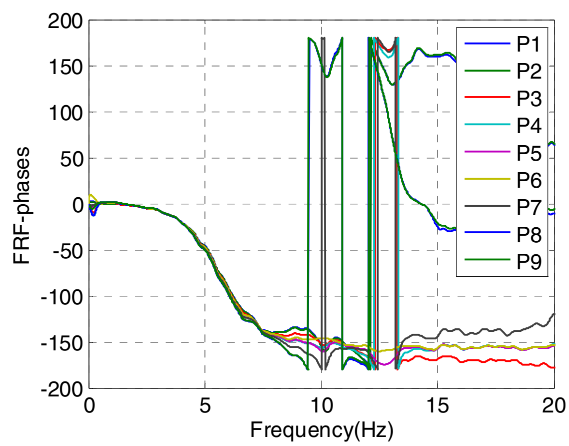

(d) Phases - Test results

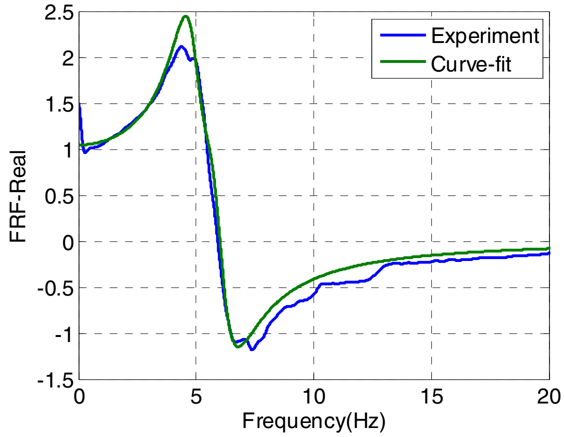

(e) Test result and Curve-fitting -Real

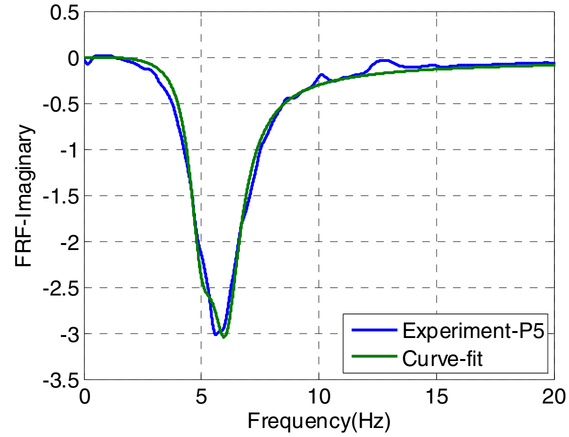

(f) Test result and Curve-fitting - Imaginary

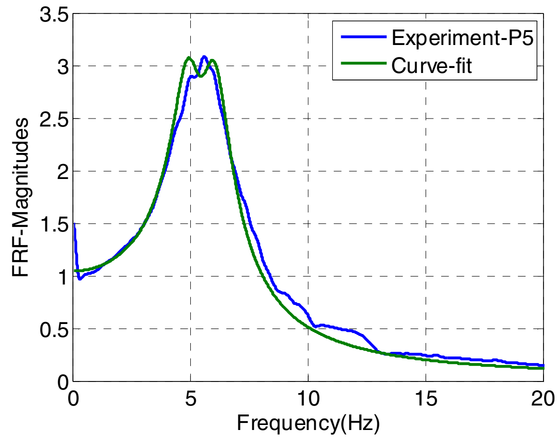

(g) Test result and Curve-fitting –Magn.

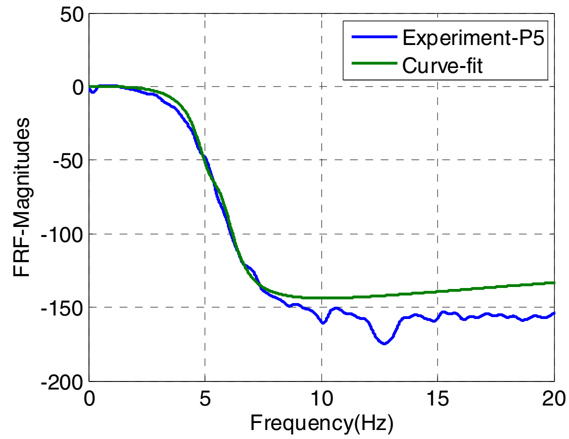

(h) Test result and Curve-fitting –Phases

Figure C-26 Phase 2, NS, After DE

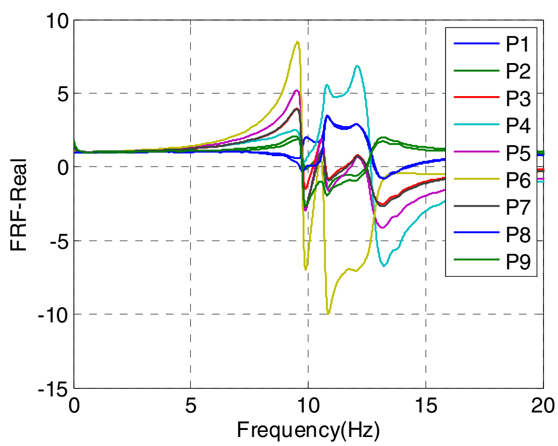

(a) Real components - Test results

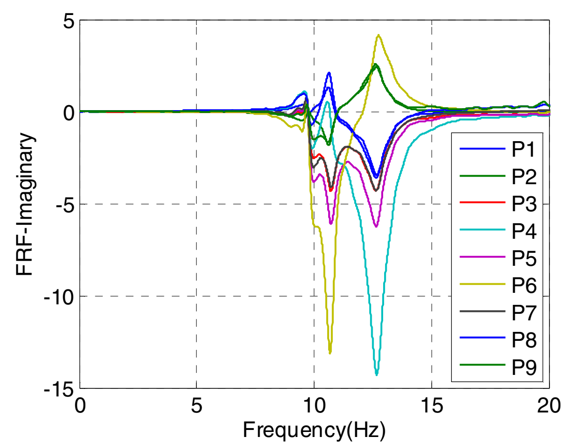

(b) Imaginary components - Test results

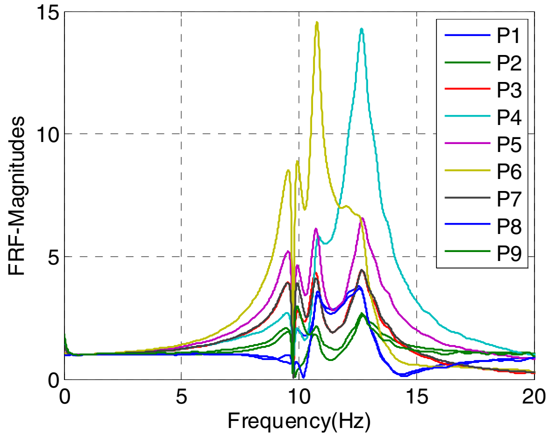

(c) Magnitudes - Test results

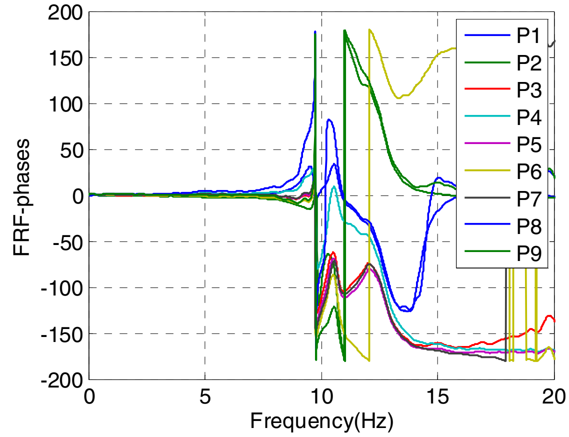

(d) Phases - Test results

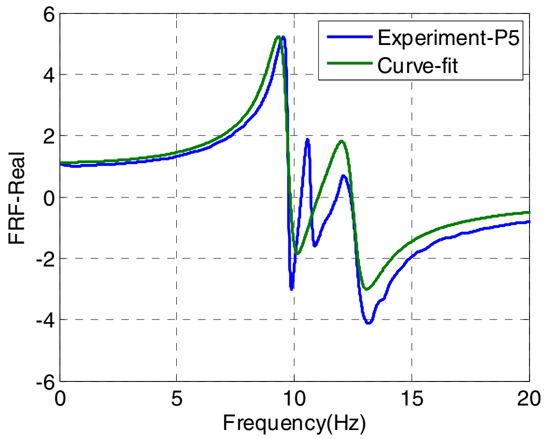

(e) Test result and Curve-fitting -Real

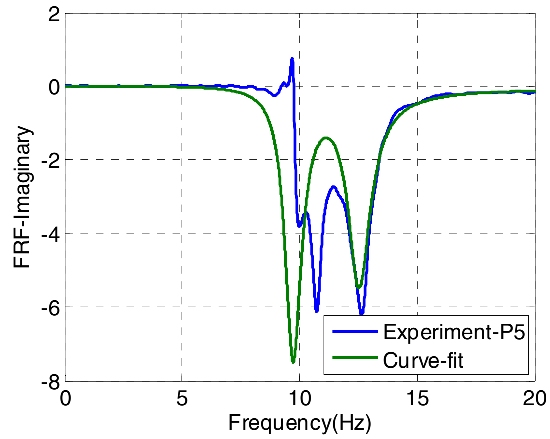

(f) Test result and Curve-fitting - Imaginary

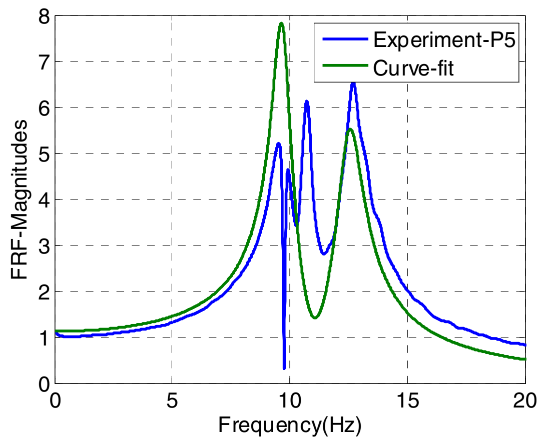

(g) Test result and Curve-fitting –Magn.

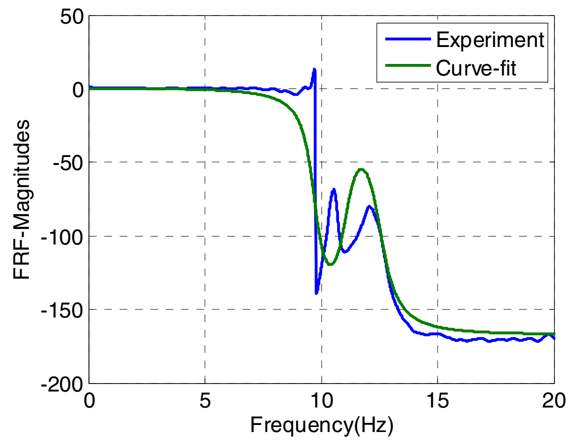

(h) Test result and Curve-fitting –Phases

Figure C-27 Phase 2, UD, After DE

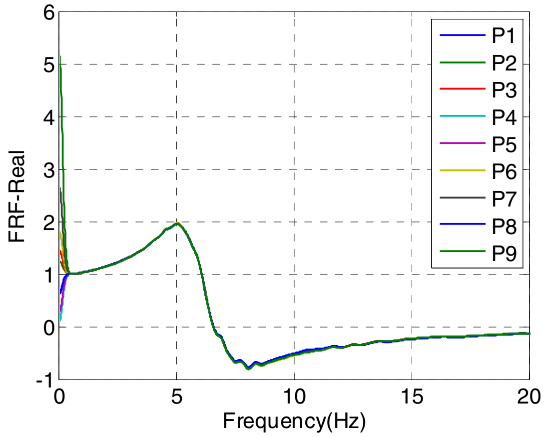

(a) Real components - Test results

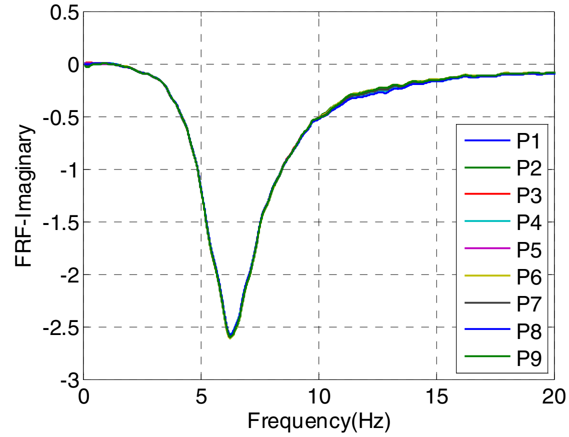

(b) Imaginary components - Test results

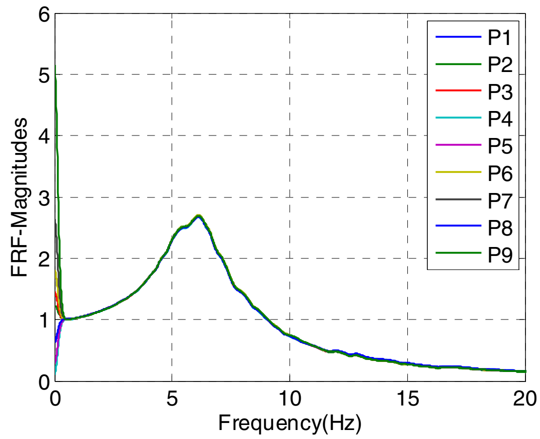

(c) Magnitudes - Test results

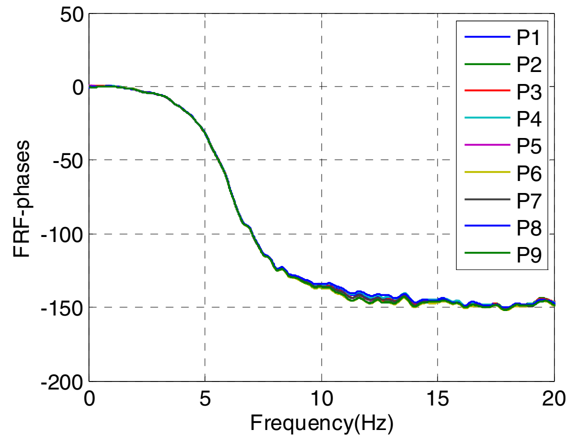

(d) Phases - Test results

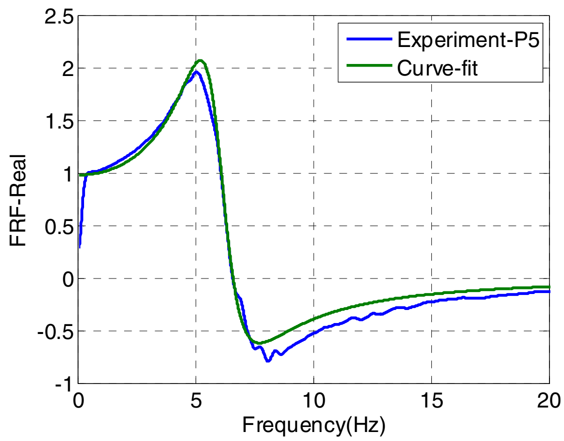

(e) Test result and Curve-fitting -Real

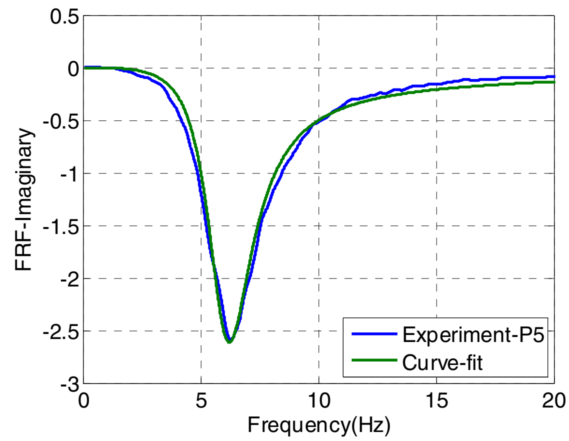

(f) Test result and Curve-fitting - Imaginary

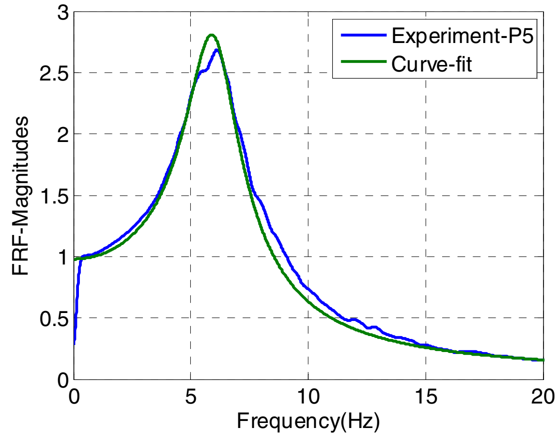

(g) Test result and Curve-fitting –Magn.

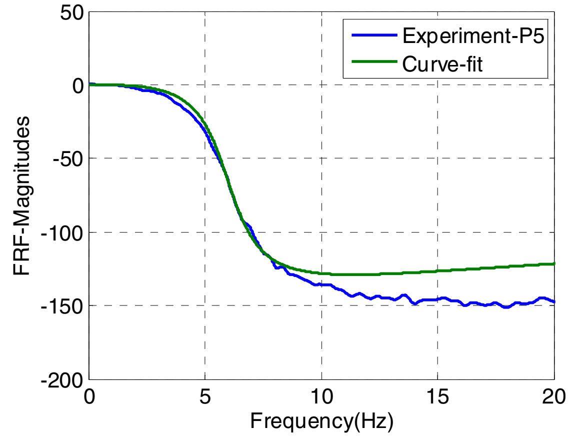

(h) Test result and Curve-fitting –Phases

Figure C-28 Phase 2, EW, After MCE

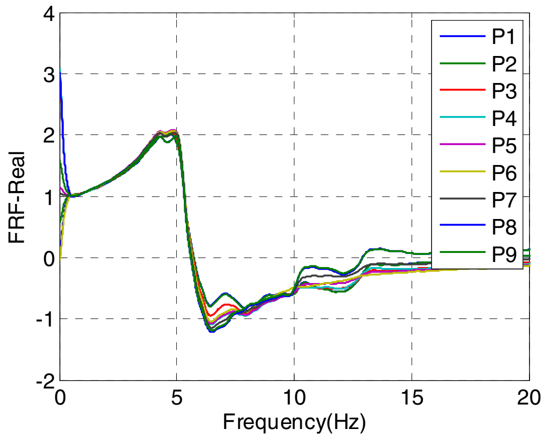

(a) Real components - Test results

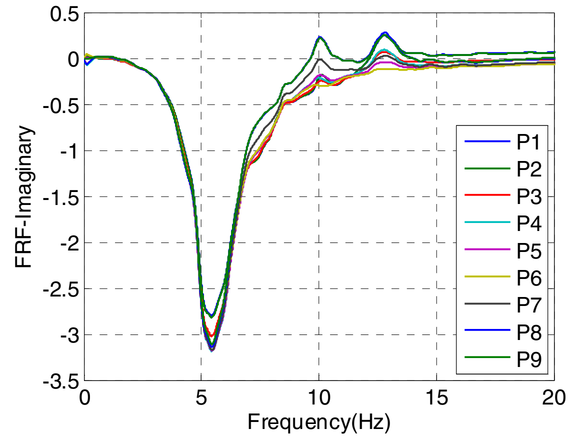

(b) Imaginary components - Test results

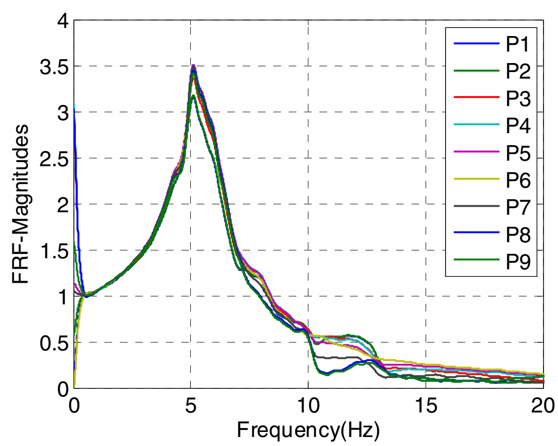

(c) Magnitudes - Test results

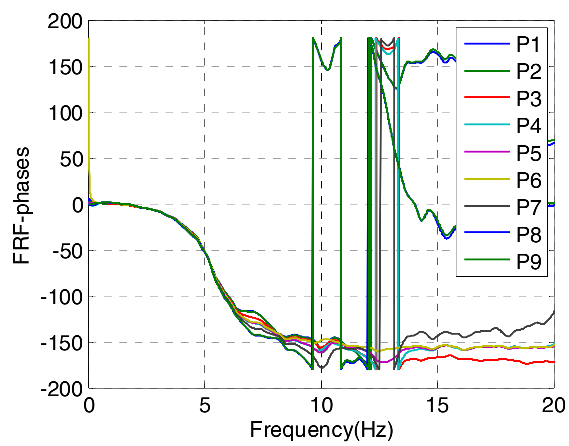

(d) Phases - Test results

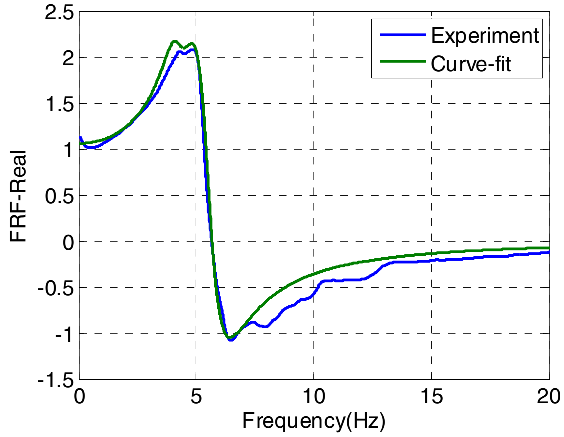

(e) Test result and Curve-fitting -Real

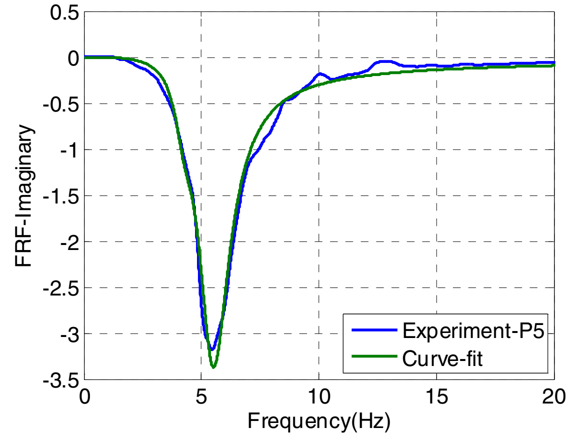

(f) Test result and Curve-fitting - Imaginary

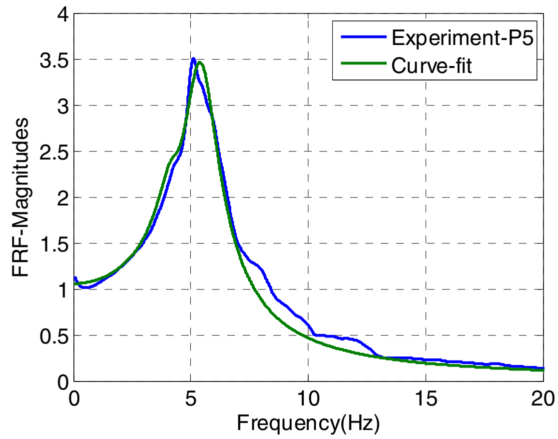

(g) Test result and Curve-fitting –Magn.

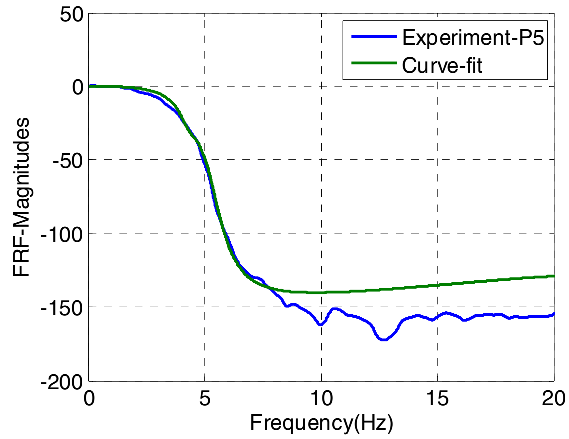

(h) Test result and Curve-fitting –Phases

Figure C-29 Phase 2, NS, After MCE

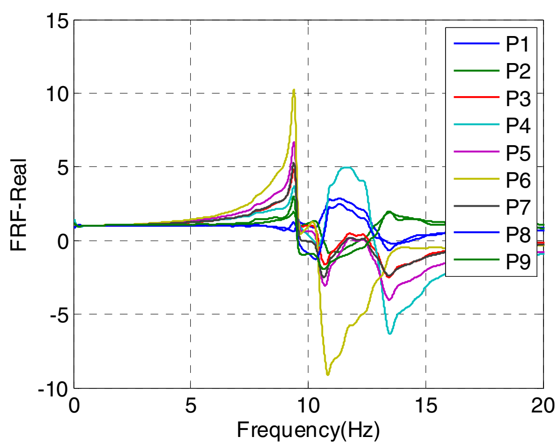

(a) Real components - Test results

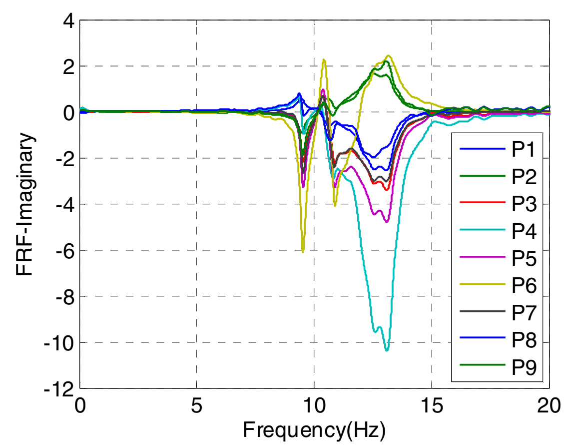

(b) Imaginary components - Test results

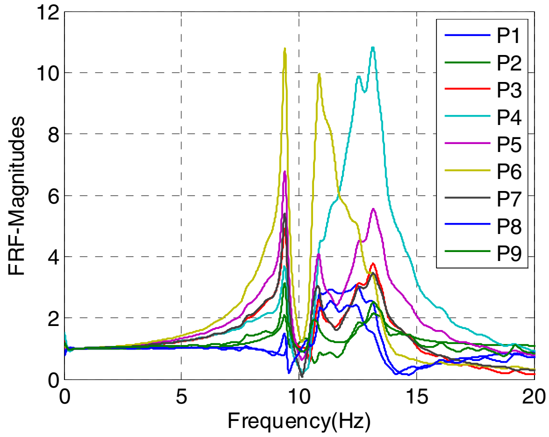

(c) Magnitudes - Test results

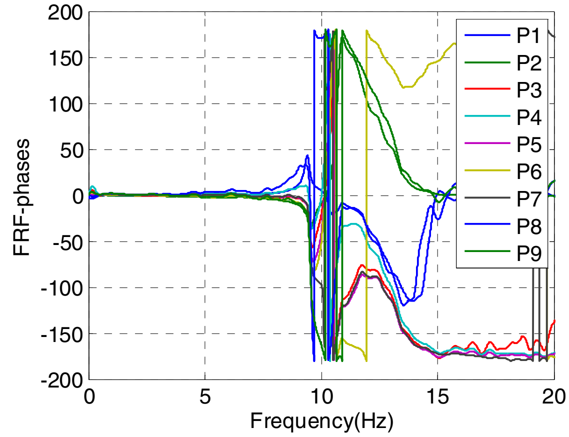

(d) Phases - Test results

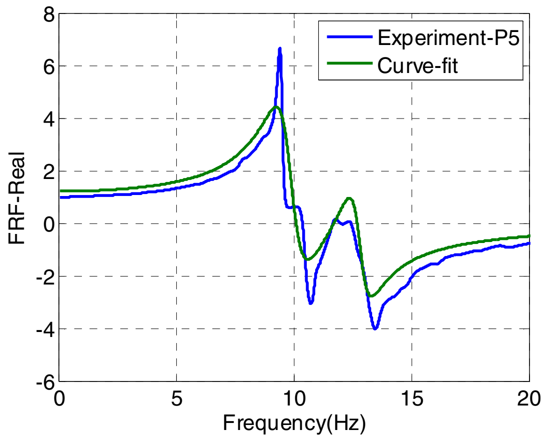

(e) Test result and Curve-fitting -Real

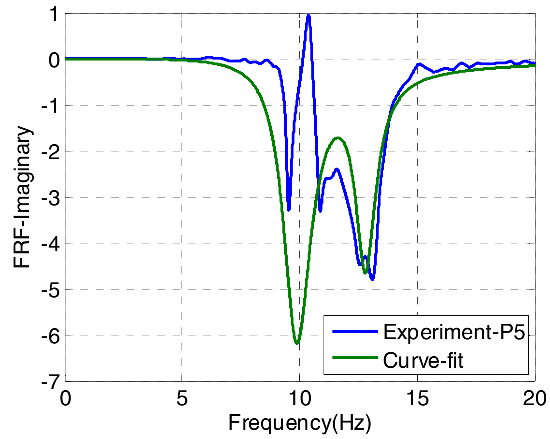

(f) Test result and Curve-fitting - Imaginary

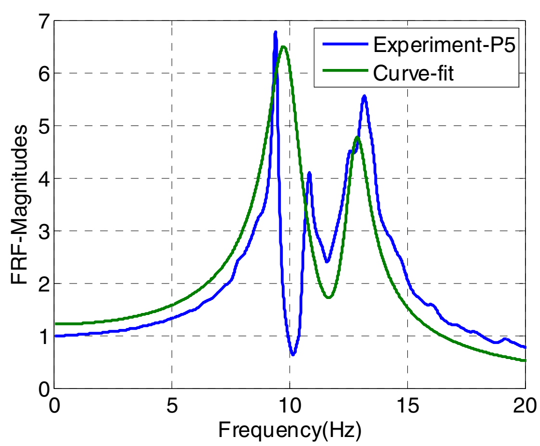

(g) Test result and Curve-fitting –Magn.

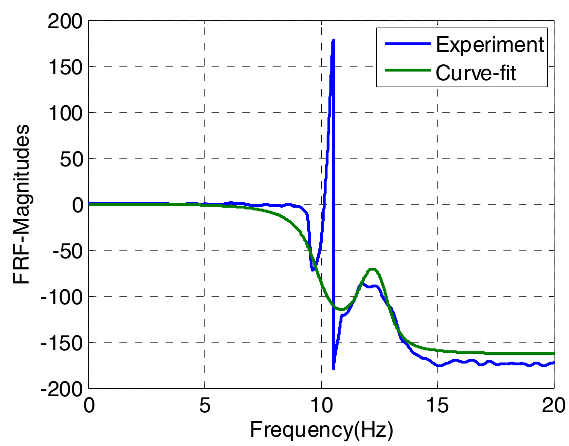

(h) Test result and Curve-fitting –Phases

Figure C-30 Phase 2, UD, After MCE

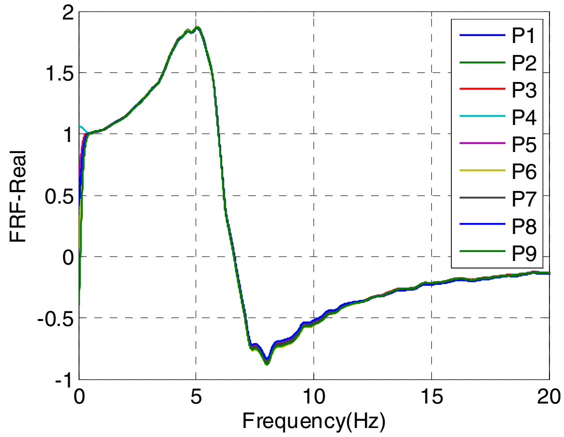

(a) Real components - Test results

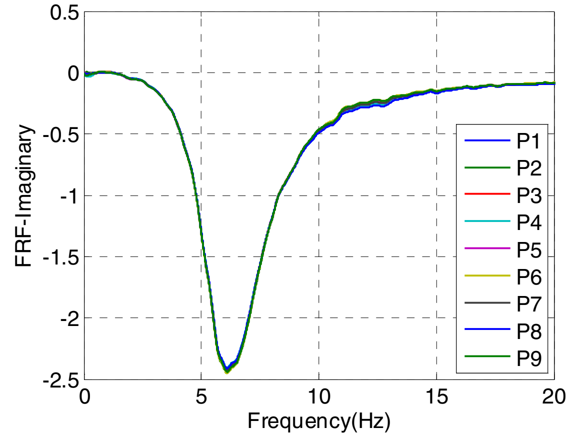

(b) Imaginary components - Test results

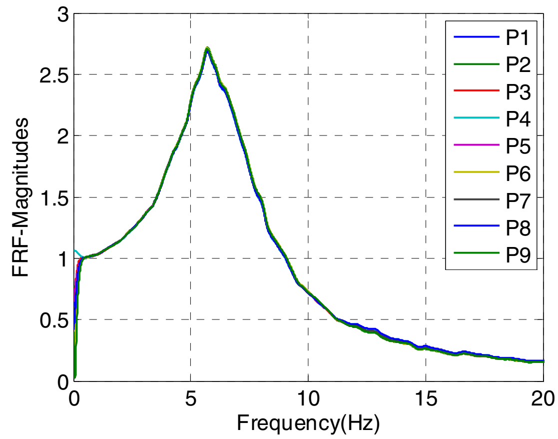

(c) Magnitudes - Test results

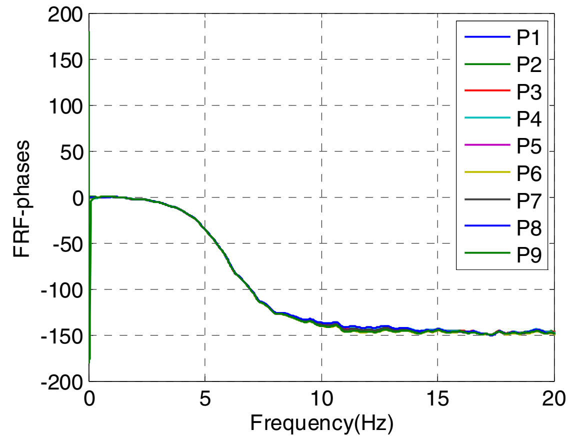

(d) Phases - Test results

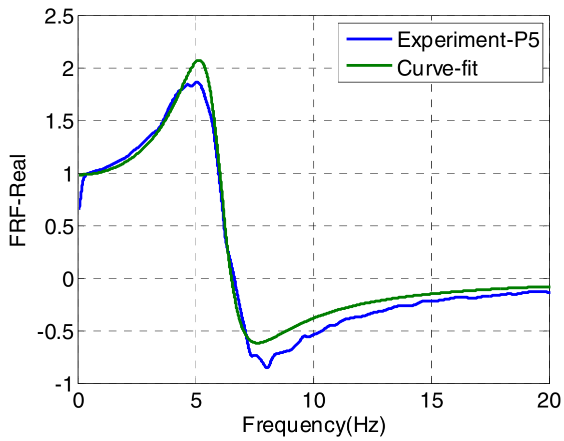

(e) Test result and Curve-fitting -Real

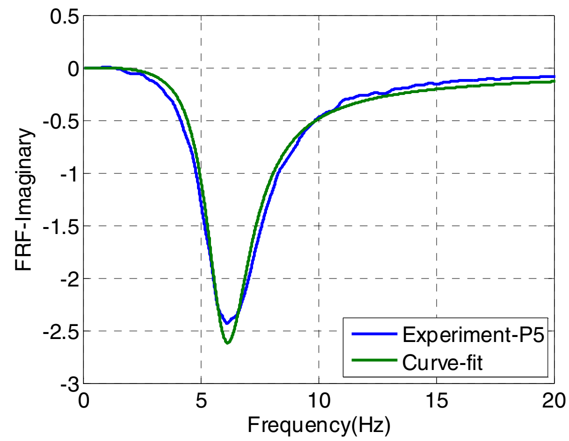

(f) Test result and Curve-fitting - Imaginary

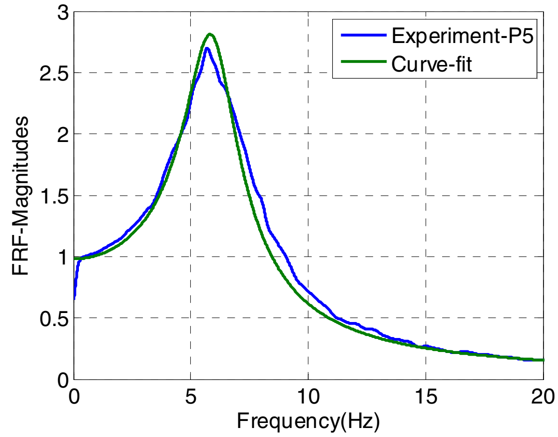

(g) Test result and Curve-fitting –Magn.

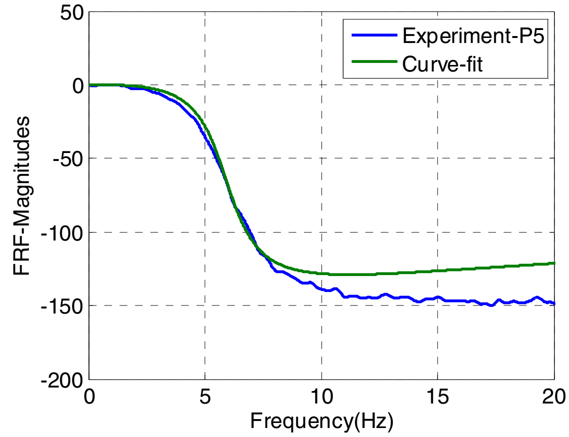

(h) Test result and Curve-fitting –Phases

Figure C-31 Phase 2, EW, After DE2

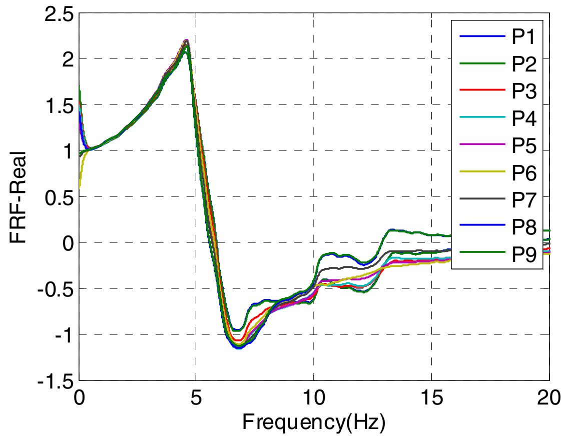

(a) Real components - Test results

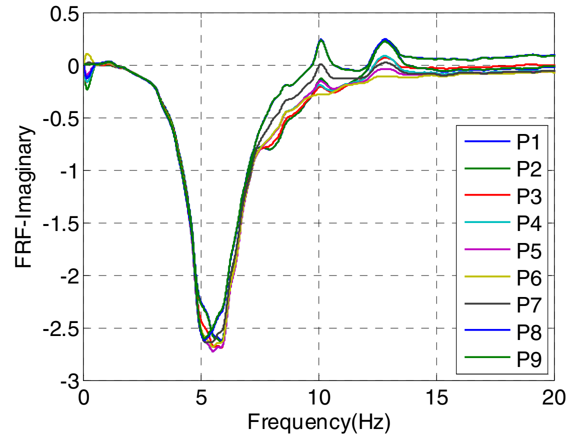

(b) Imaginary components - Test results

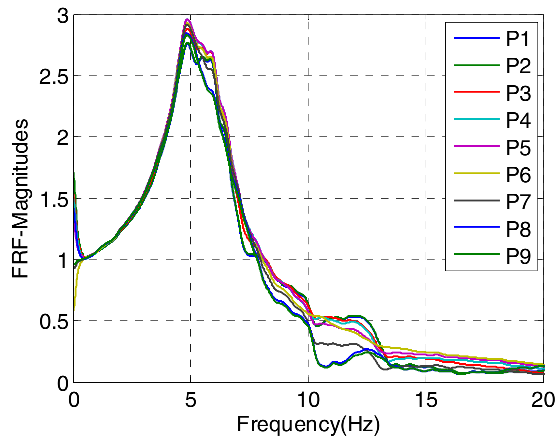

(c) Magnitudes - Test results

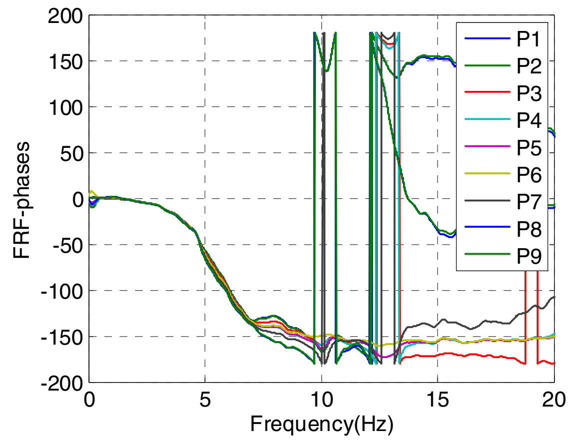

(d) Phases - Test results

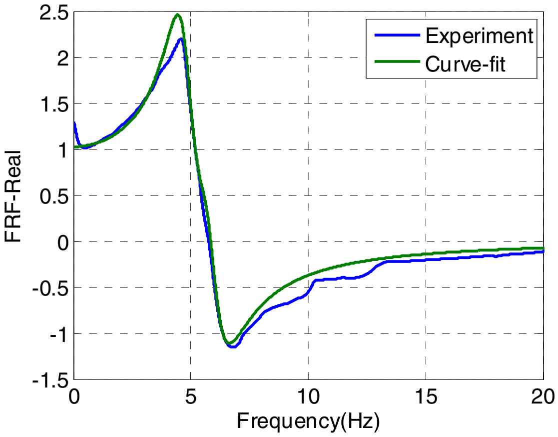

(e) Test result and Curve-fitting -Real

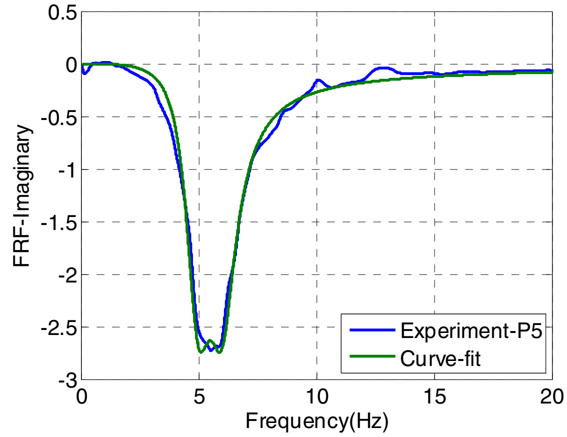

(f) Test result and Curve-fitting - Imaginary

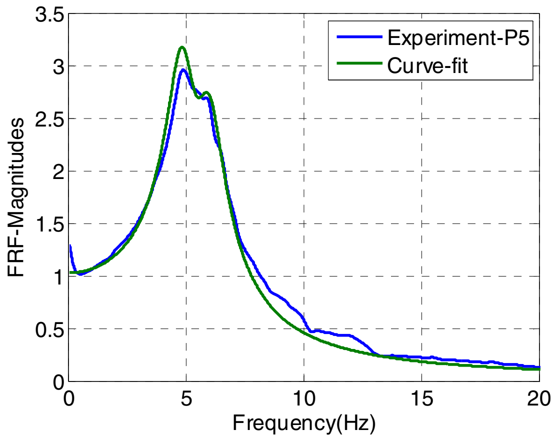

(g) Test result and Curve-fitting –Magn.

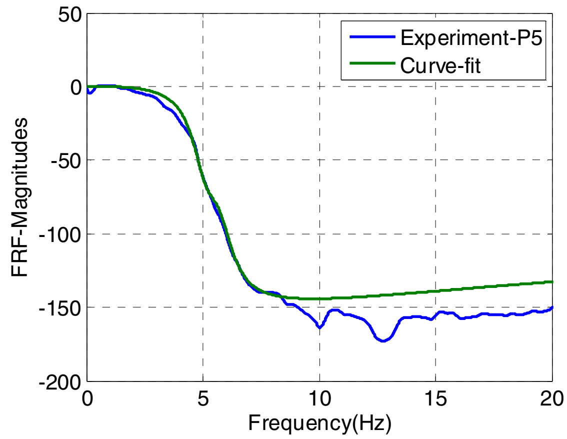

(h) Test result and Curve-fitting –Phases

Figure C-32 Phase 2, NS, After DE2

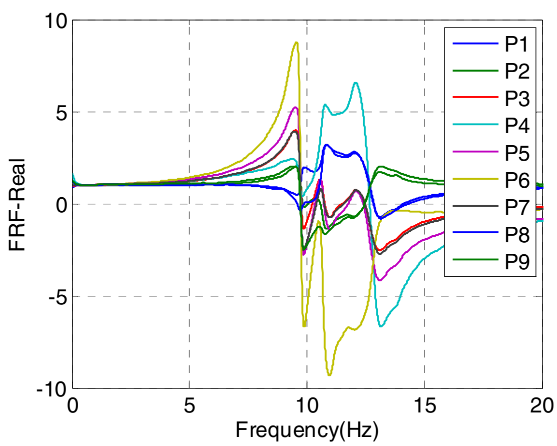

(a) Real components - Test results

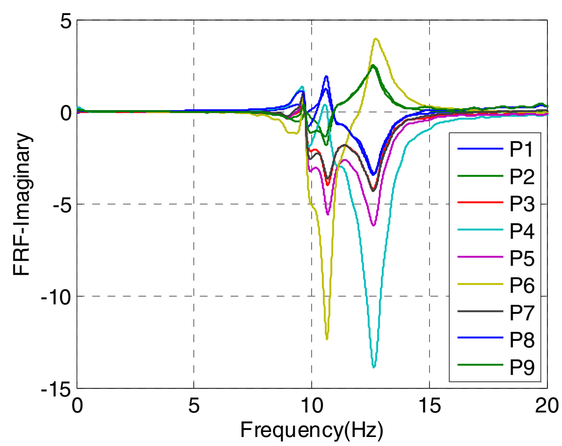

(b) Imaginary components - Test results

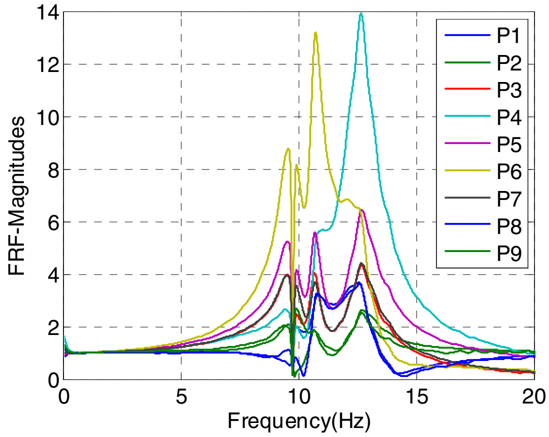

(c) Magnitudes - Test results

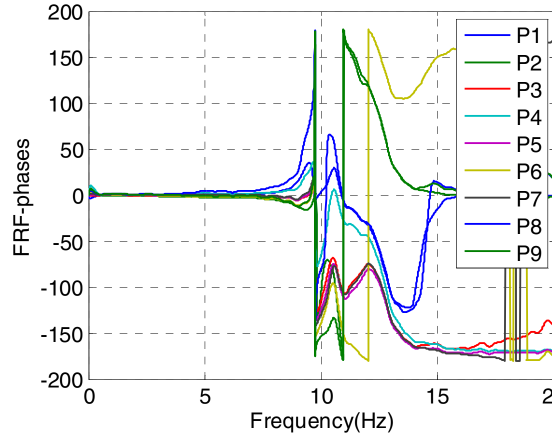

(d) Phases - Test results

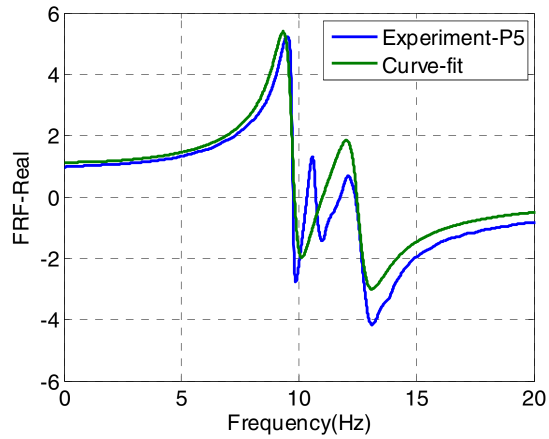

(e) Test result and Curve-fitting -Real

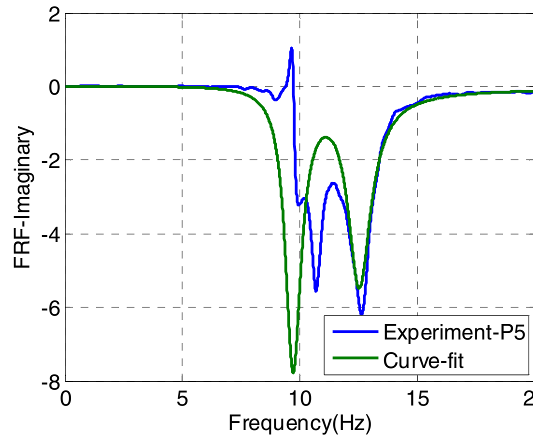

(f) Test result and Curve-fitting - Imaginary

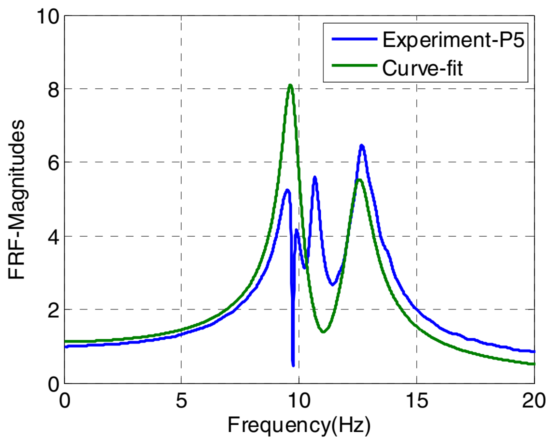

(g) Test result and Curve-fitting –Magn.

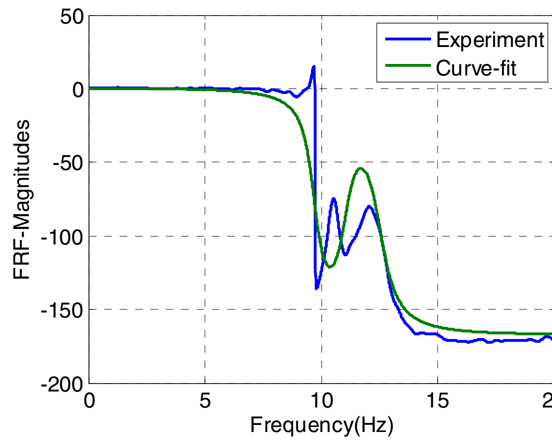

(h) Test result and Curve-fitting –Phases

Figure C-33 Phase 2, UD, After DE2

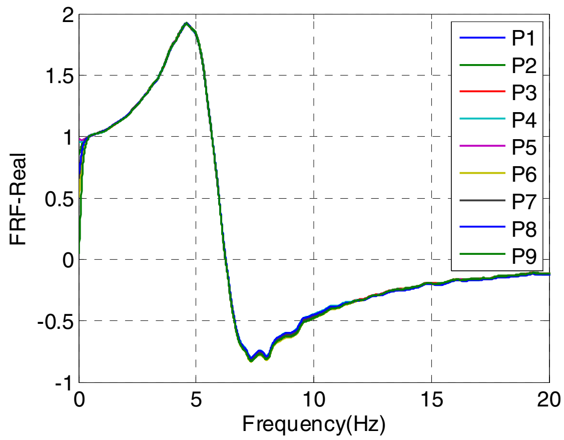

(a) Real components - Test results

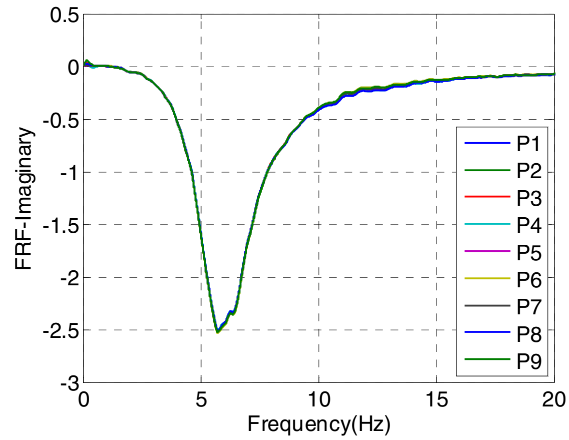

(b) Imaginary components - Test results

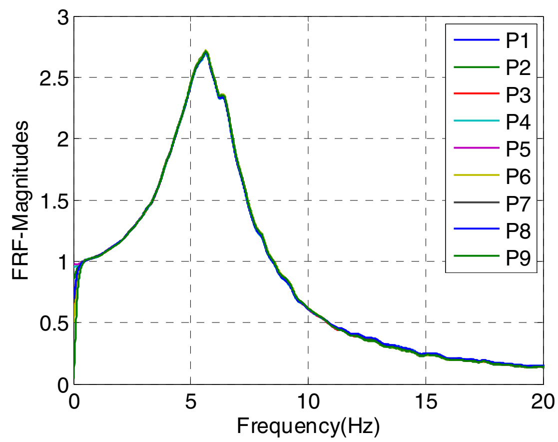

(c) Magnitudes - Test results

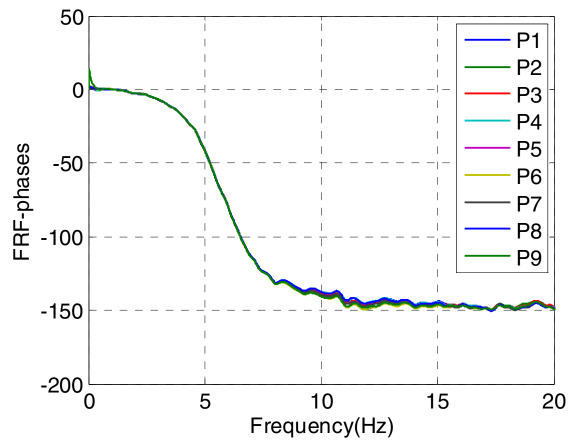

(d) Phases - Test results

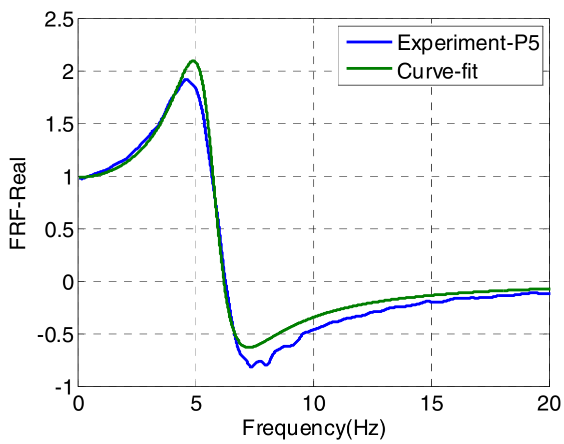

(e) Test result and Curve-fitting -Real

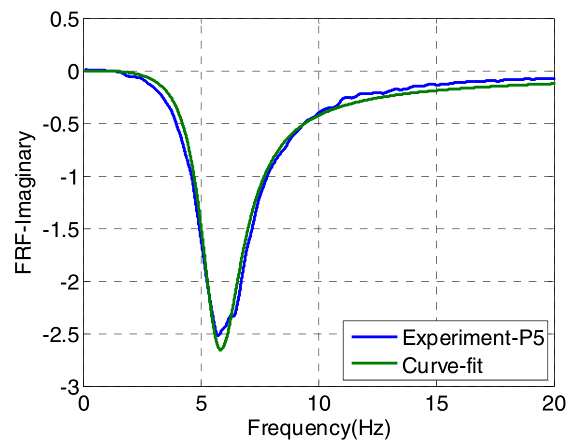

(f) Test result and Curve-fitting - Imaginary

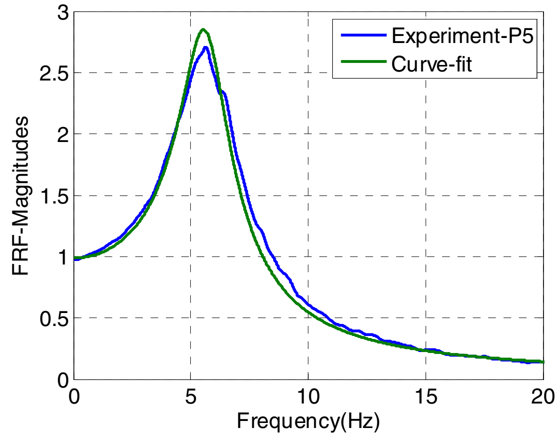

(g) Test result and Curve-fitting –Magn.

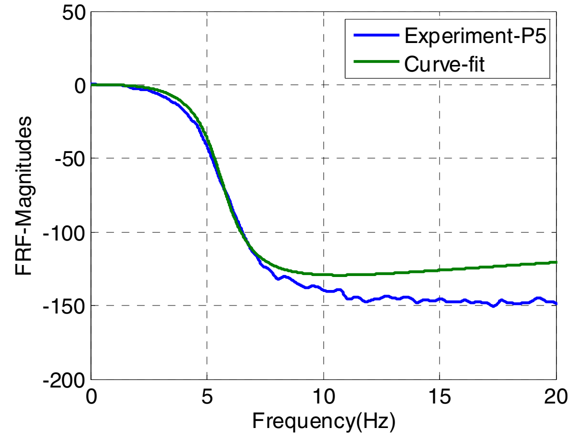

(h) Test result and Curve-fitting –Phases

Figure C-34 Phase 2, EW, After MAX

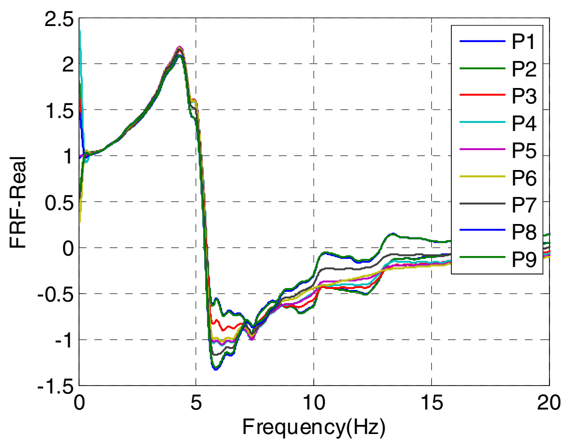

(a) Real components - Test results

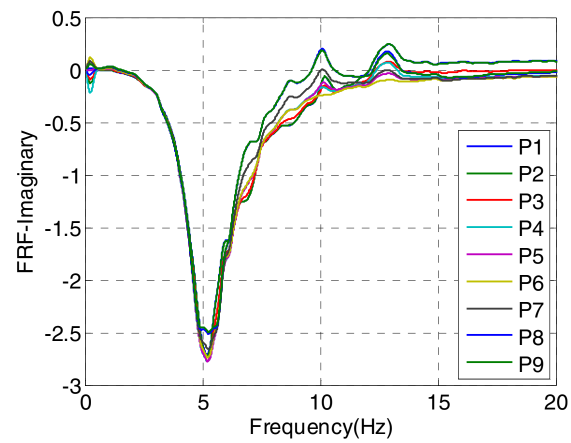

(b) Imaginary components - Test results

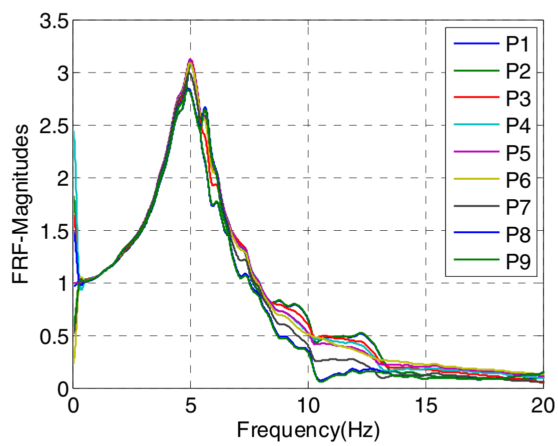

(c) Magnitudes - Test results

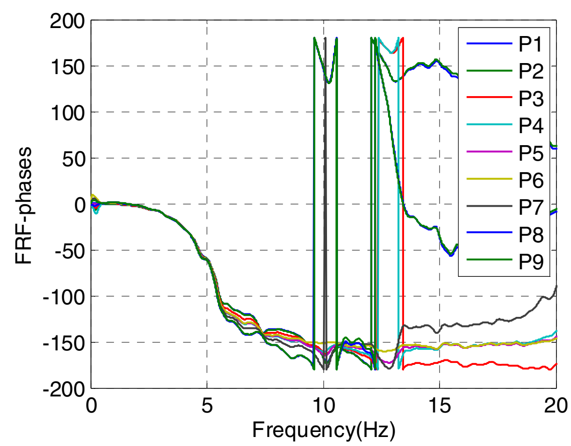

(d) Phases - Test results

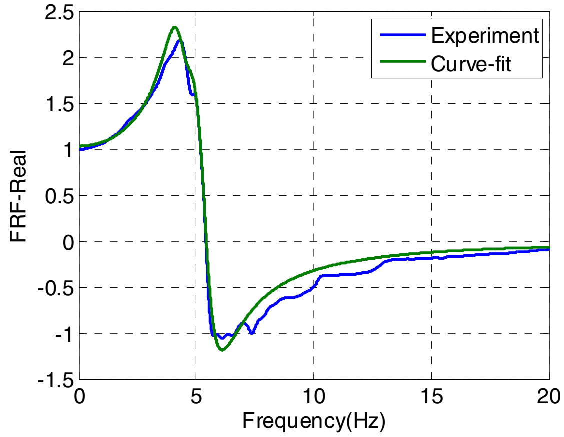

(e) Test result and Curve-fitting -Real

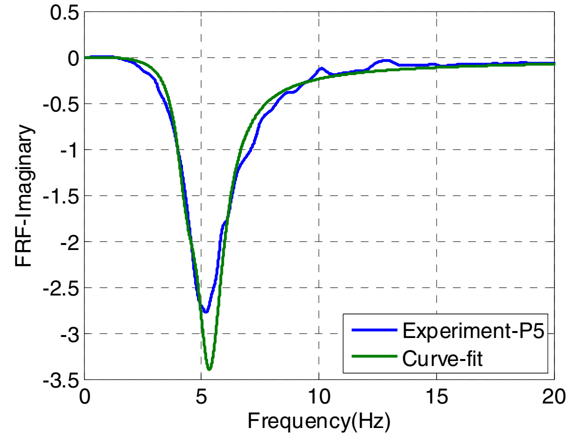

(f) Test result and Curve-fitting - Imaginary

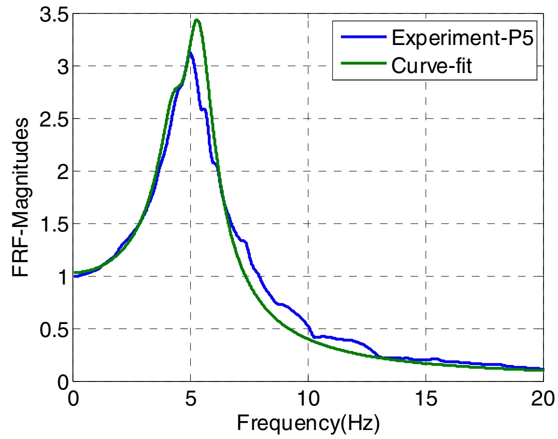

(g) Test result and Curve-fitting –Magn.

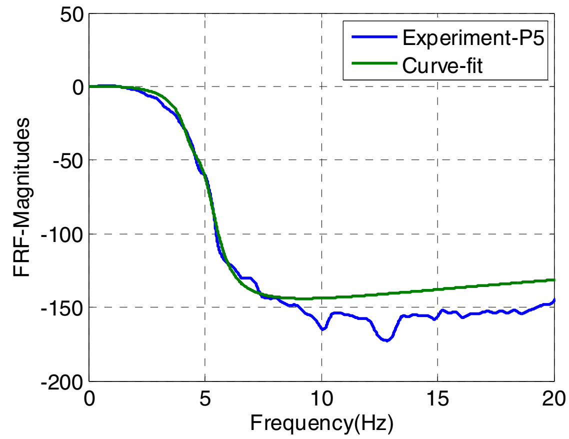

(h) Test result and Curve-fitting –Phases

Figure C-35 Phase 2, NS, After MAX

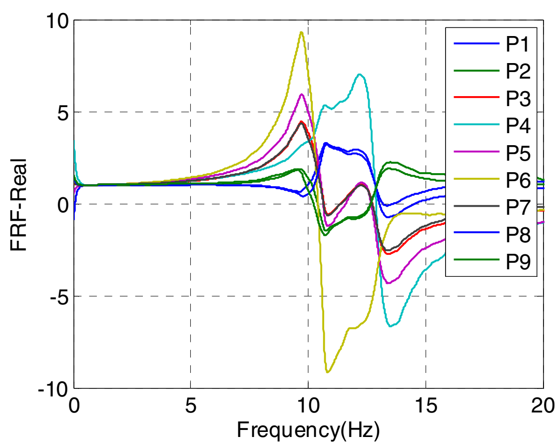

(a) Real components - Test results

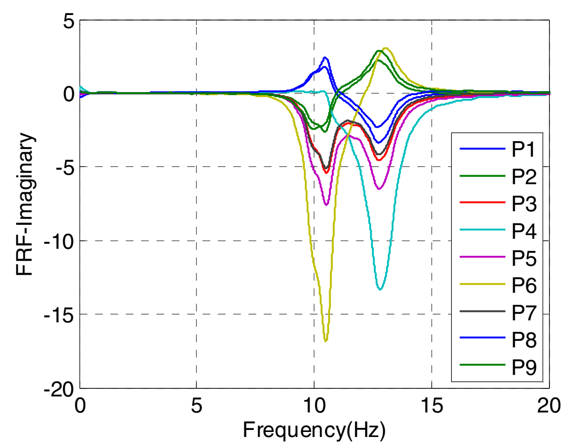

(b) Imaginary components - Test results

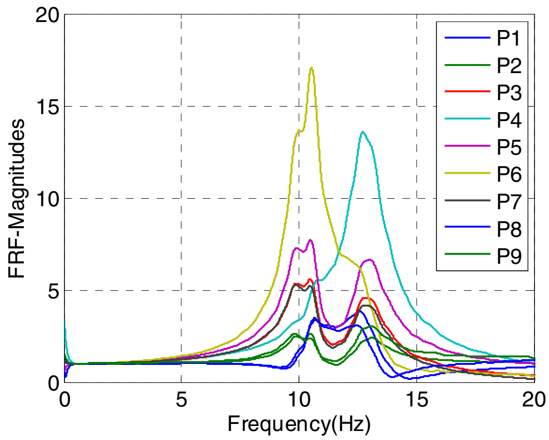

(c) Magnitudes - Test results

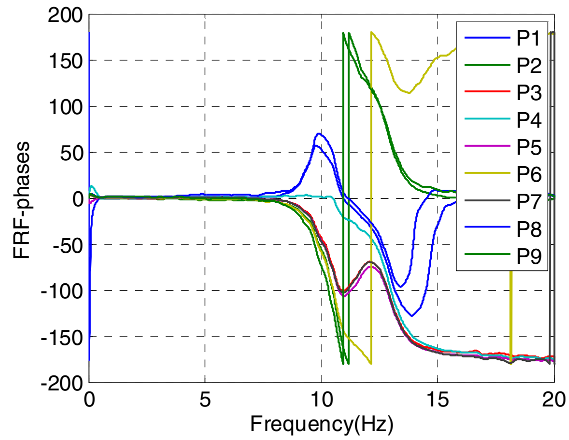

(d) Phases - Test results

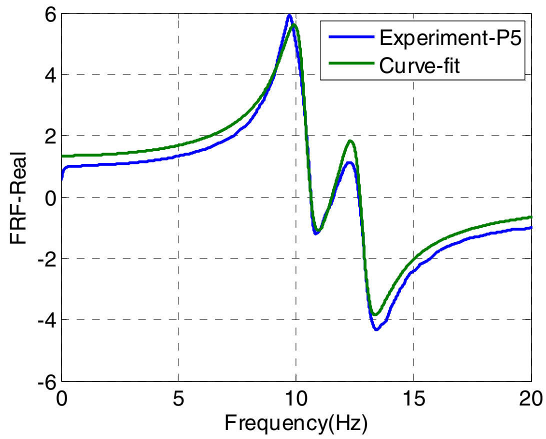

(e) Test result and Curve-fitting -Real

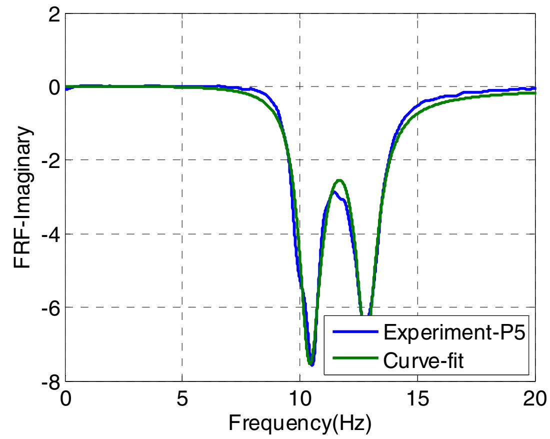

(f) Test result and Curve-fitting - Imaginary

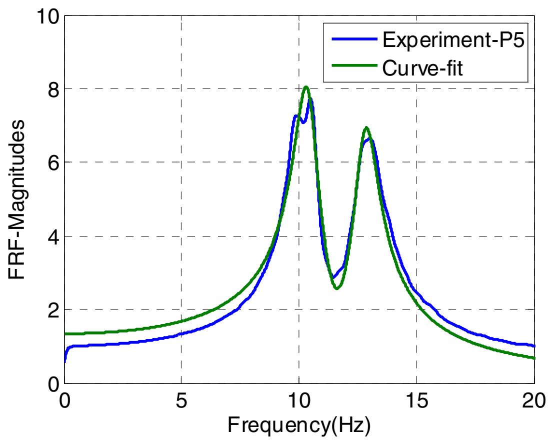

(g) Test result and Curve-fitting –Magn.

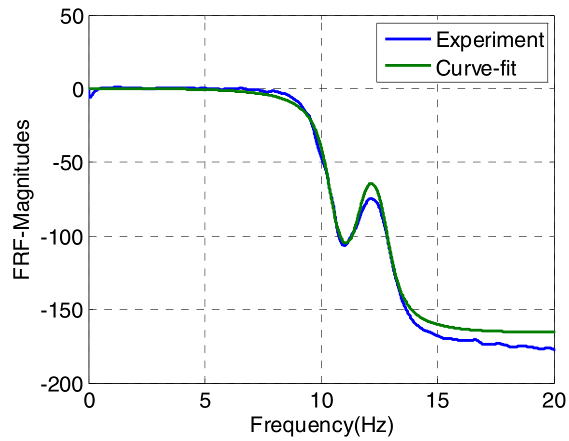

(h) Test result and Curve-fitting –Phases

Figure C-36 Phase 2, UD, After MAX

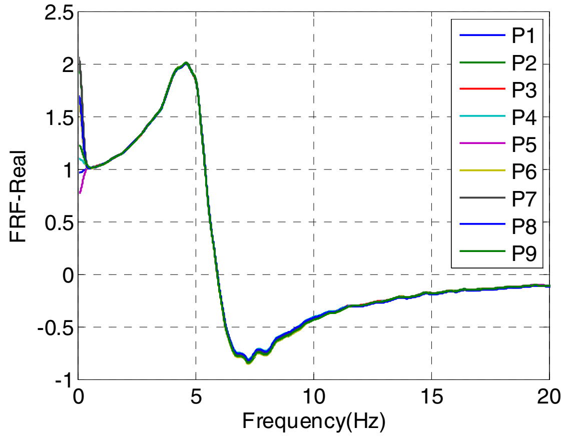

(a) Real components - Test results

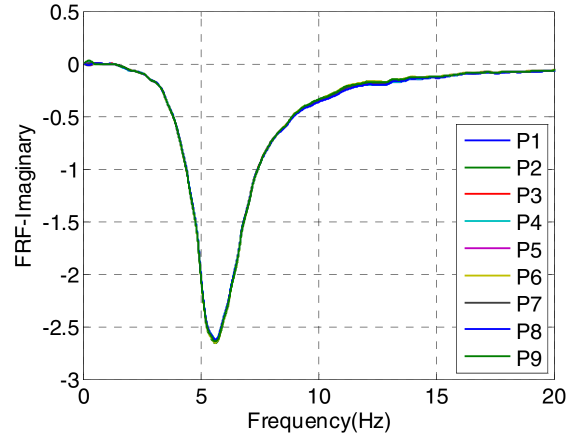

(b) Imaginary components - Test results

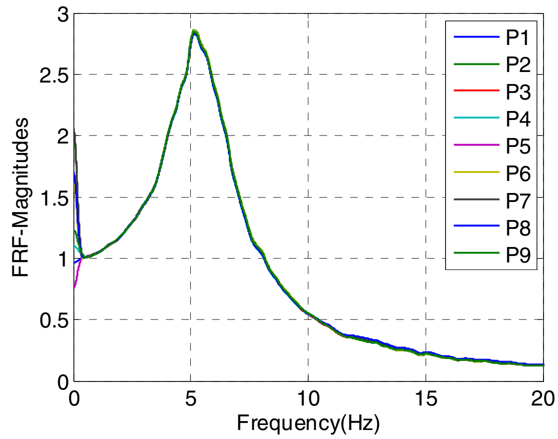

(c) Magnitudes - Test results

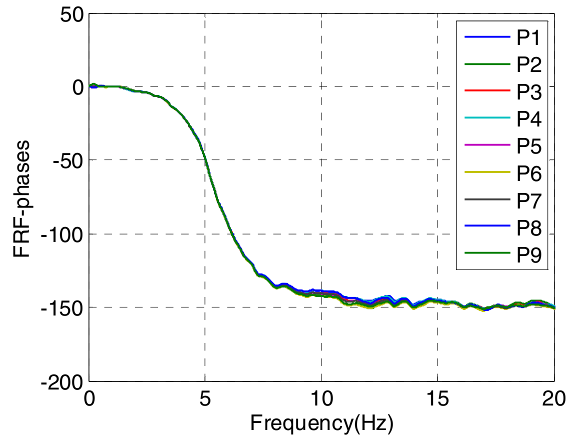

(d) Phases - Test results

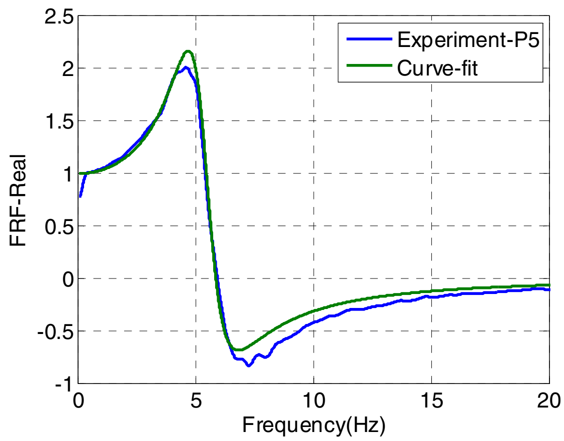

(e) Test result and Curve-fitting -Real

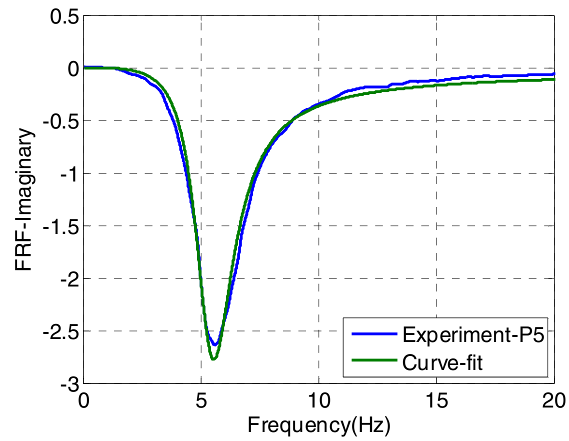

(f) Test result and Curve-fitting - Imaginary

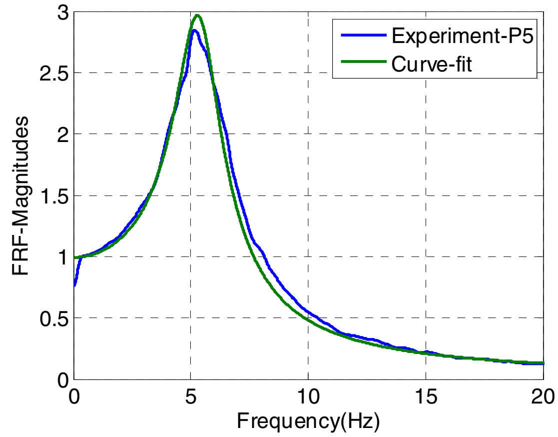

(g) Test result and Curve-fitting –Magn.

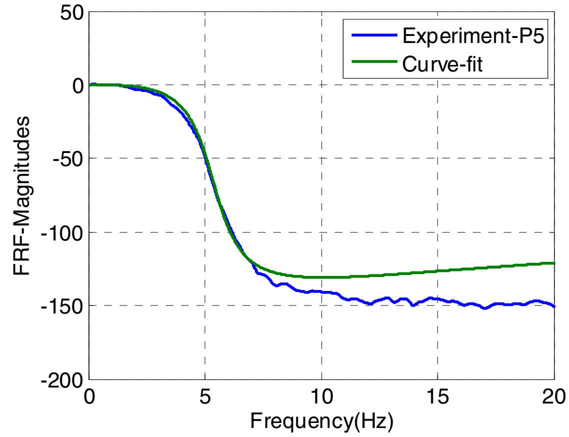

(h) Test result and Curve-fitting –Phases

Figure C-37 Phase 2, EW, After MAX*1.2

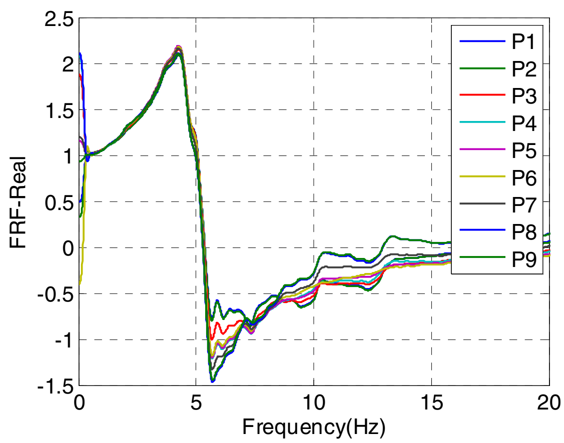

(a) Real components - Test results

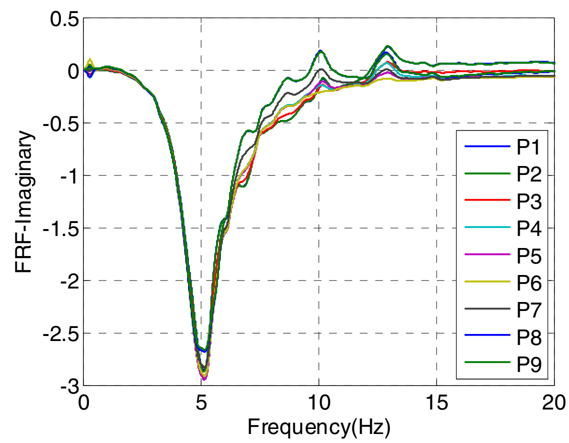

(b) Imaginary components - Test results

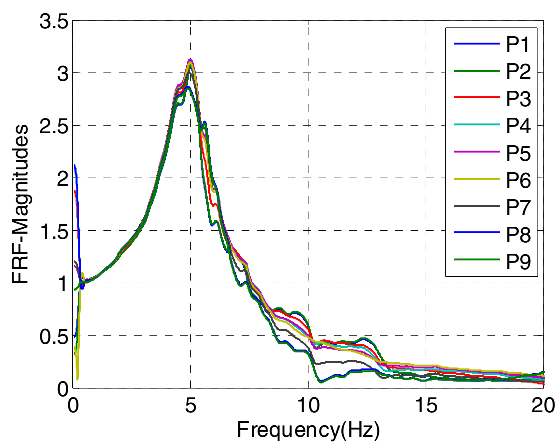

(c) Magnitudes - Test results

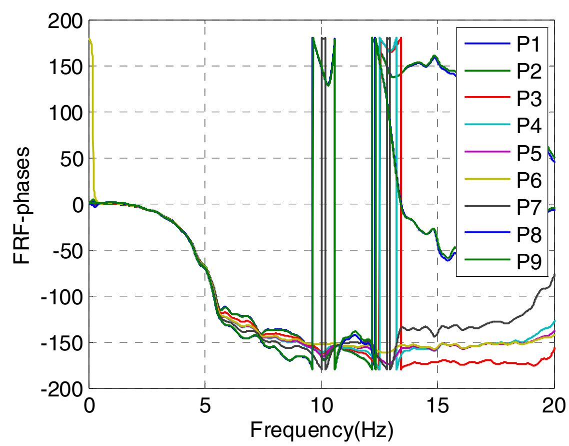

(d) Phases - Test results

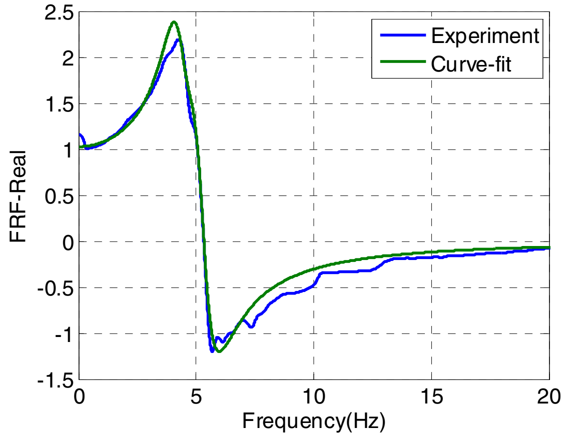

(e) Test result and Curve-fitting -Real

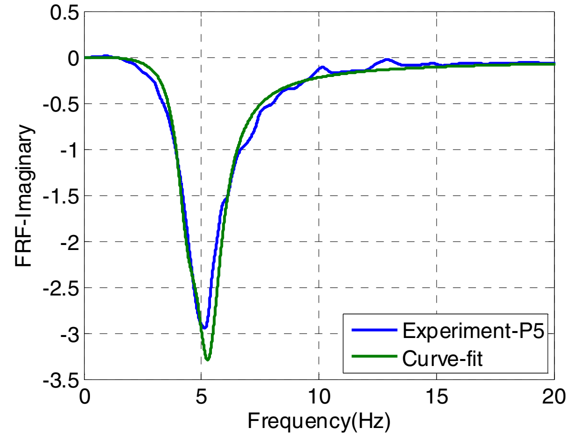

(f) Test result and Curve-fitting - Imaginary

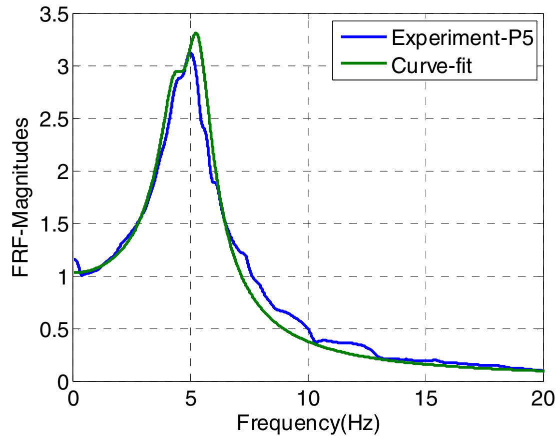

(g) Test result and Curve-fitting –Magn.

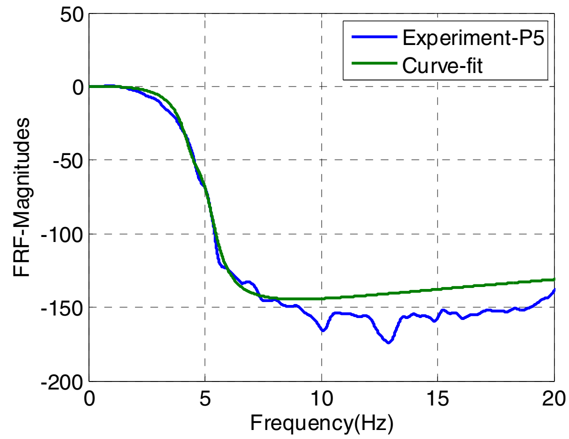

(h) Test result and Curve-fitting –Phases

Figure C-38 Phase 2, NS, After MAX*1.2

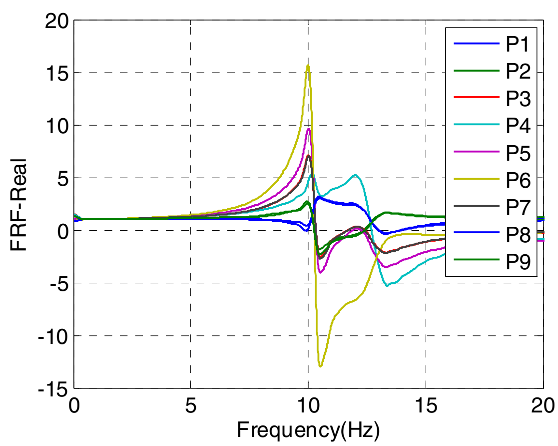

(a) Real components - Test results

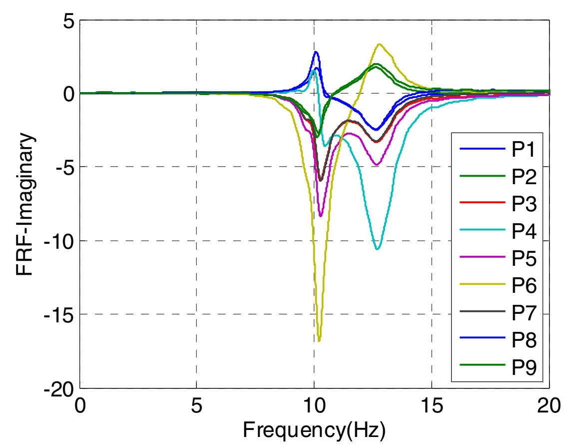

(b) Imaginary components - Test results

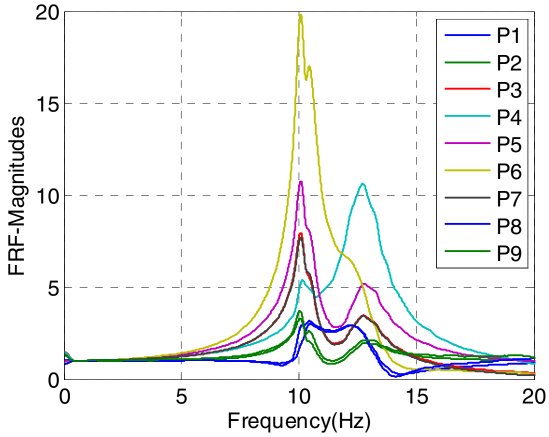

(c) Magnitudes - Test results

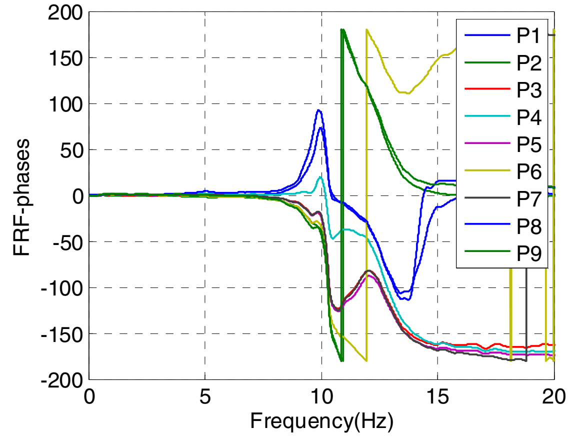

(d) Phases - Test results

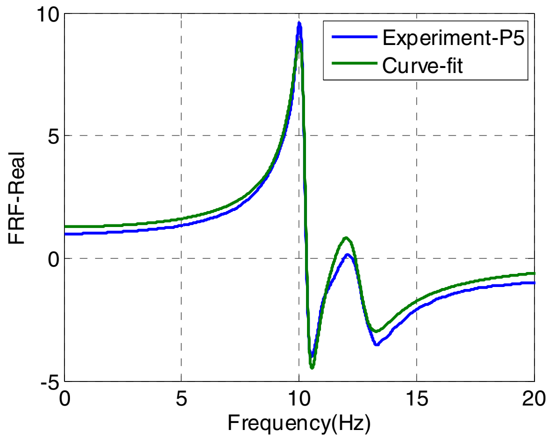

(e) Test result and Curve-fitting -Real

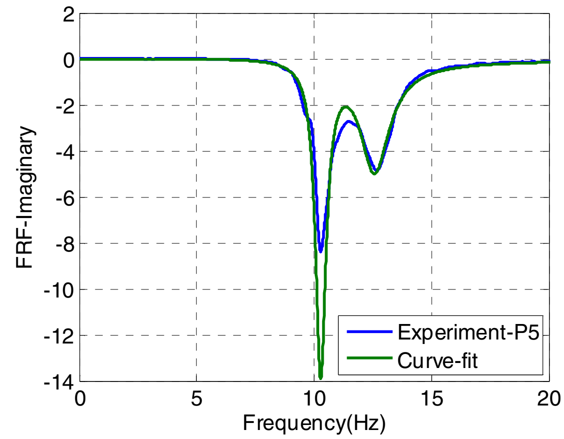

(f) Test result and Curve-fitting - Imaginary

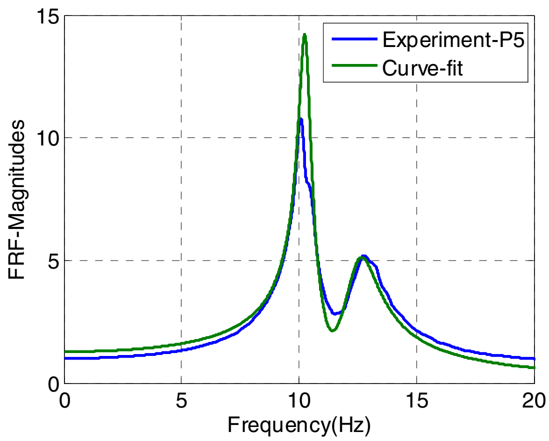

(g) Test result and Curve-fitting –Magn.

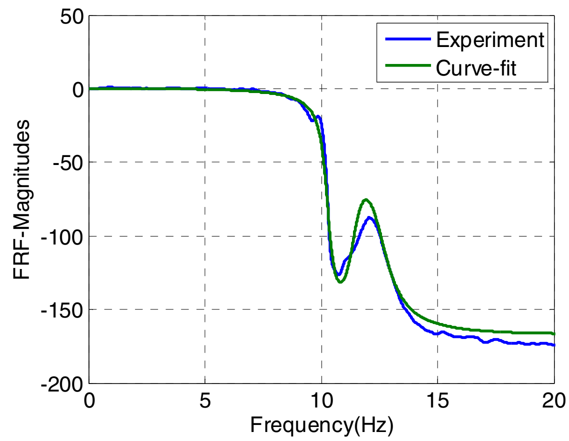

(h) Test result and Curve-fitting –Phases

Figure C-39 Phase 2, UD, After MAX*1.2

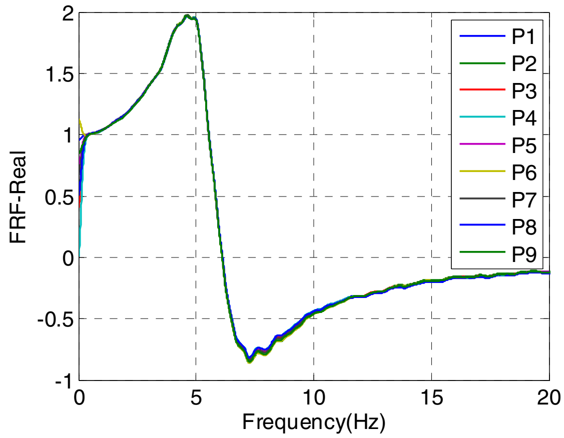

(a) Real components - Test results

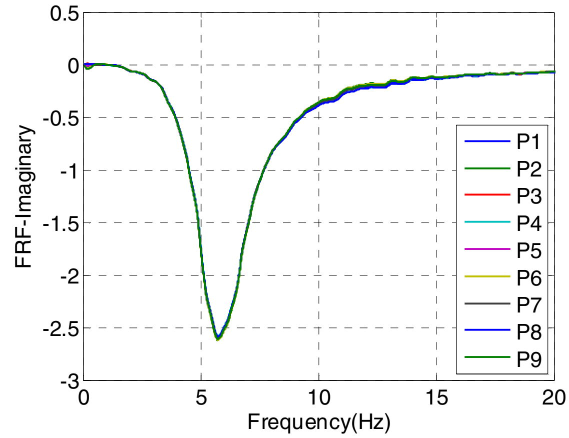

(b) Imaginary components - Test results

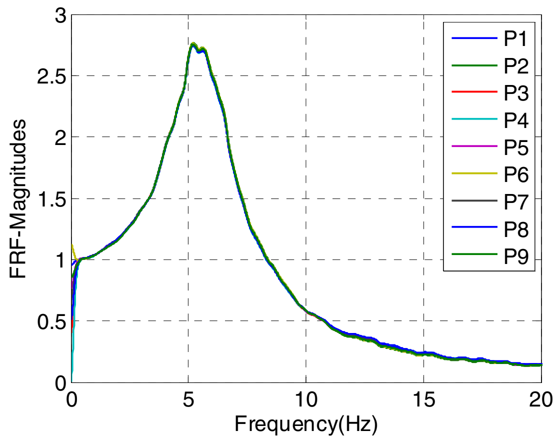

(c) Magnitudes - Test results

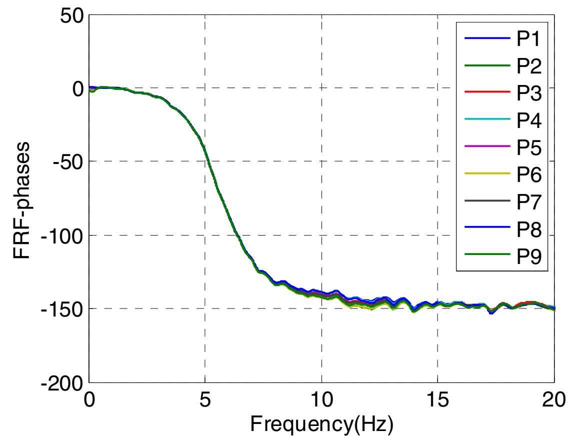

(d) Phases - Test results

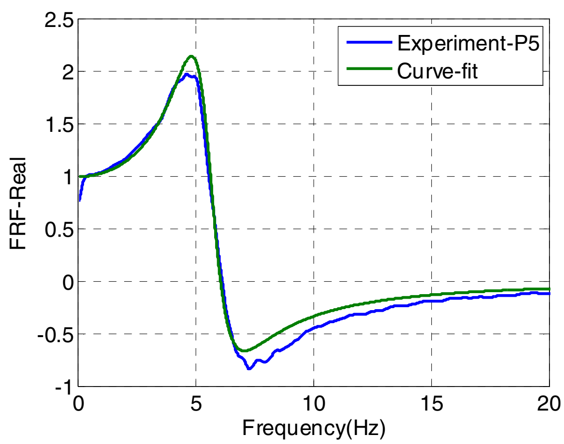

(e) Test result and Curve-fitting -Real

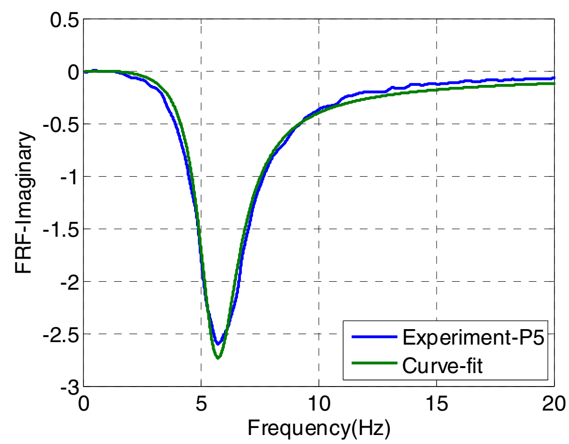

(f) Test result and Curve-fitting - Imaginary

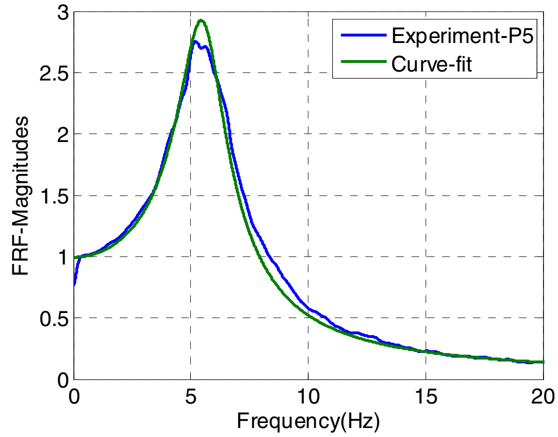

(g) Test result and Curve-fitting –Magn.

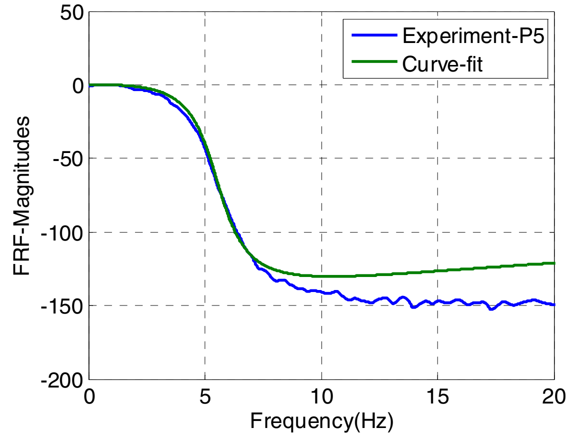

(h) Test result and Curve-fitting –Phases

Figure C-40 Phase 3, EW, After Max

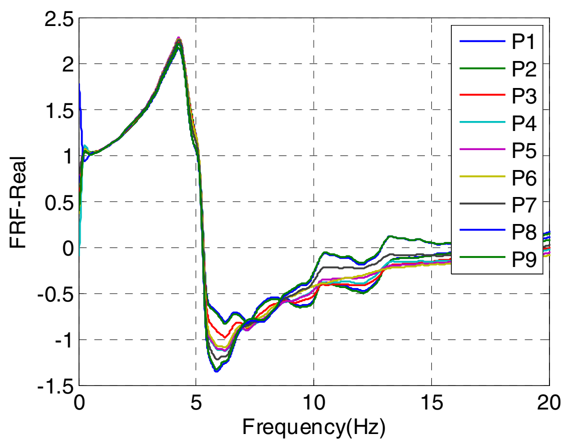

(a) Real components - Test results

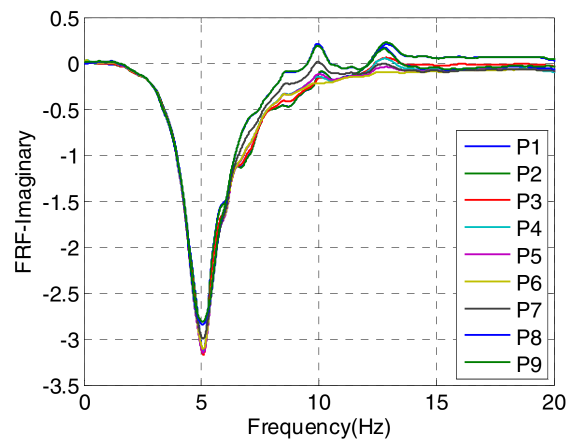

(b) Imaginary components - Test results

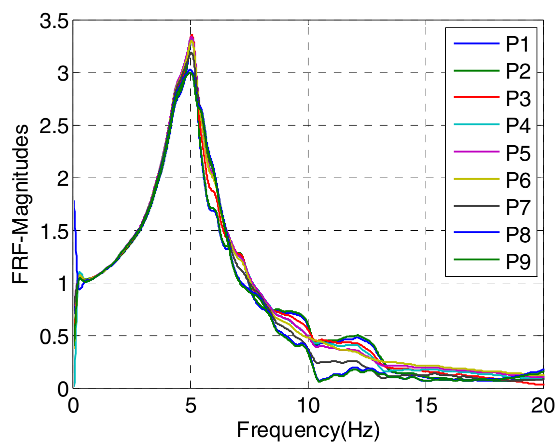

(c) Magnitudes - Test results

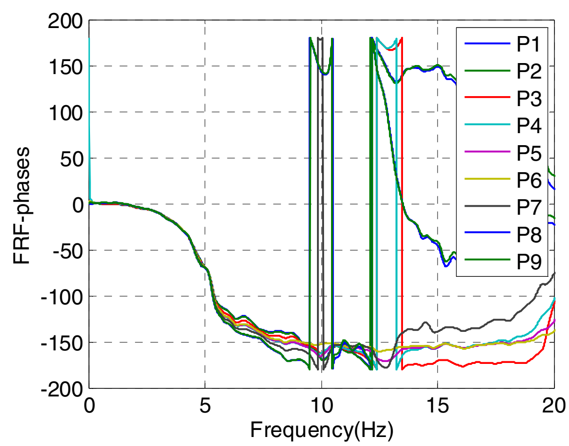

(d) Phases - Test results

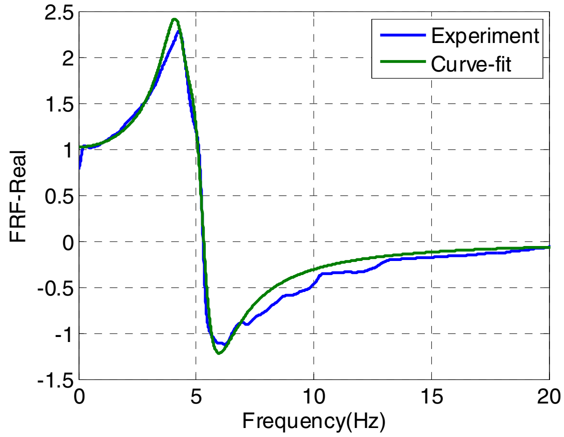

(e) Test result and Curve-fitting -Real

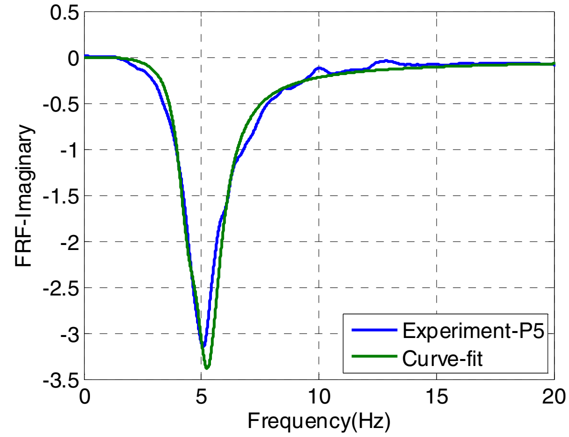

(f) Test result and Curve-fitting - Imaginary

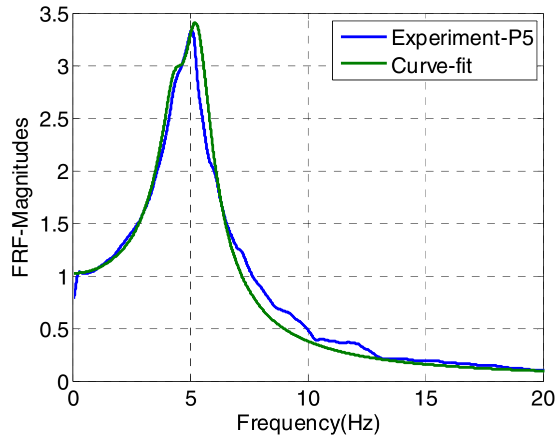

(g) Test result and Curve-fitting –Magn.

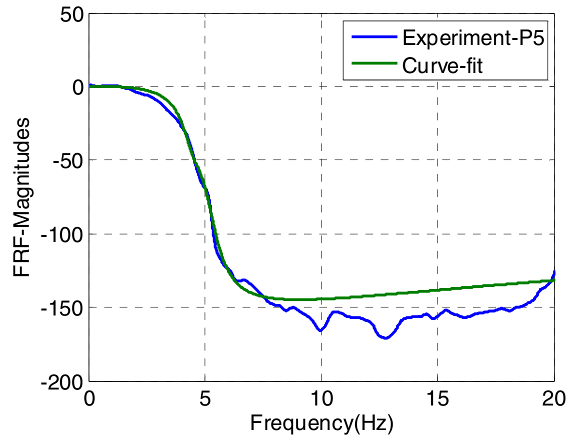

(h) Test result and Curve-fitting –Phases

Figure C-41 Phase 3, NS, After Max

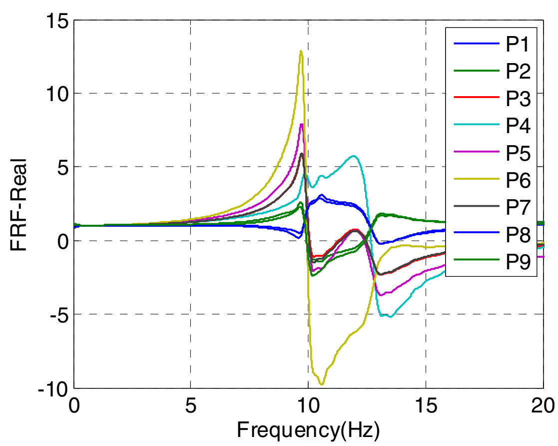

(a) Real components - Test results

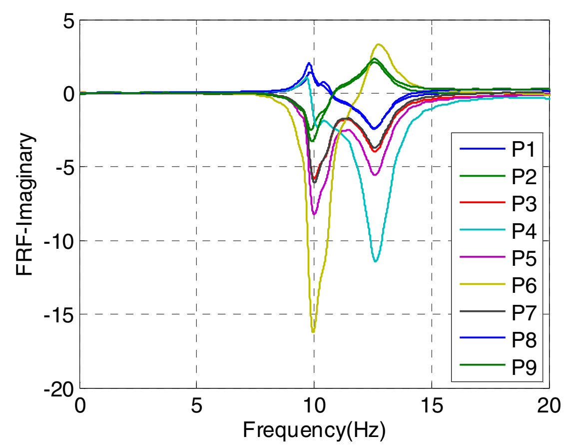

(b) Imaginary components - Test results

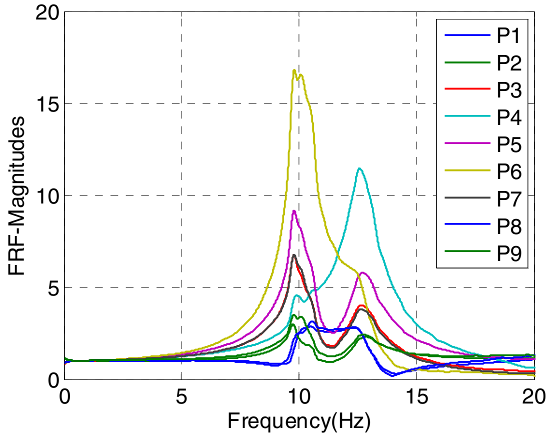

(c) Magnitudes - Test results

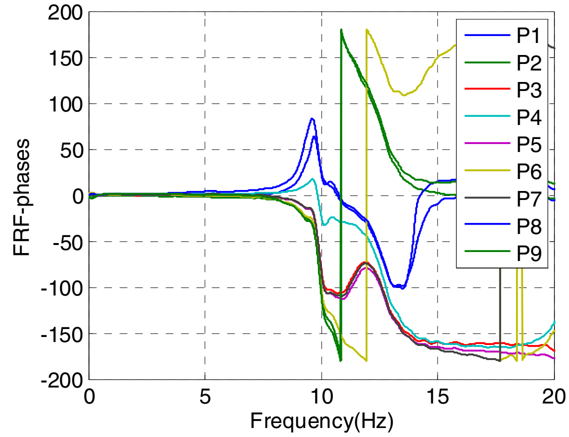

(d) Phases - Test results

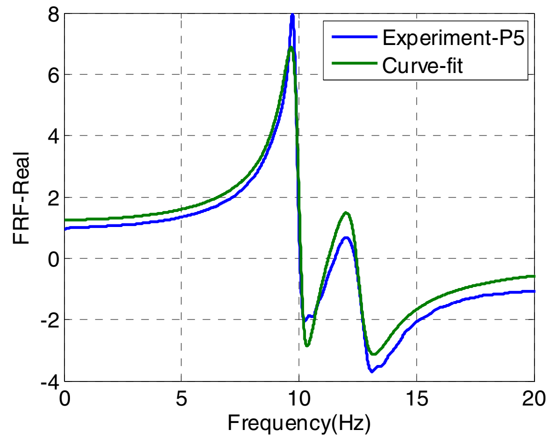

(e) Test result and Curve-fitting -Real

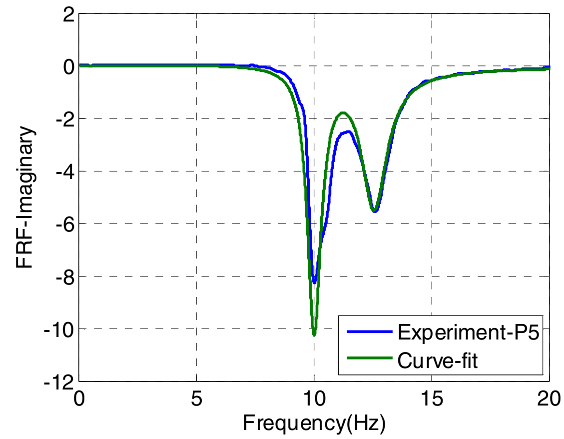

(f) Test result and Curve-fitting - Imaginary

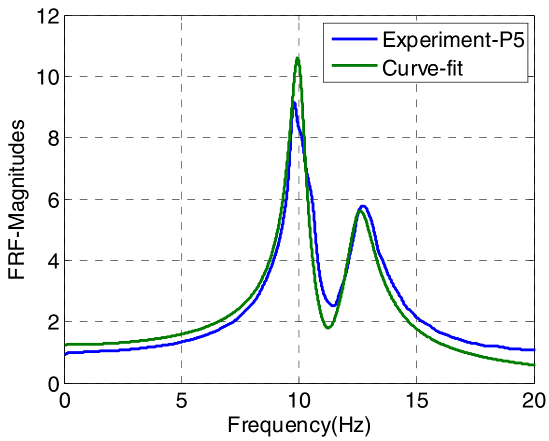

(g) Test result and Curve-fitting –Magn.

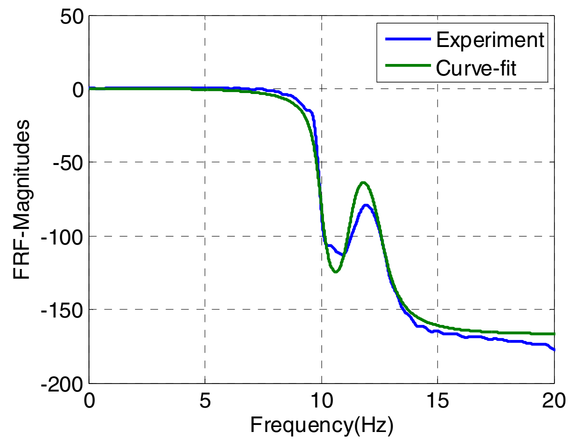

(h) Test result and Curve-fitting –Phases

Figure C-42 Phase 3, UD, After Max

APPENDIX D

MAXIMUM STRAIN IN THE SESIMIC TESTS

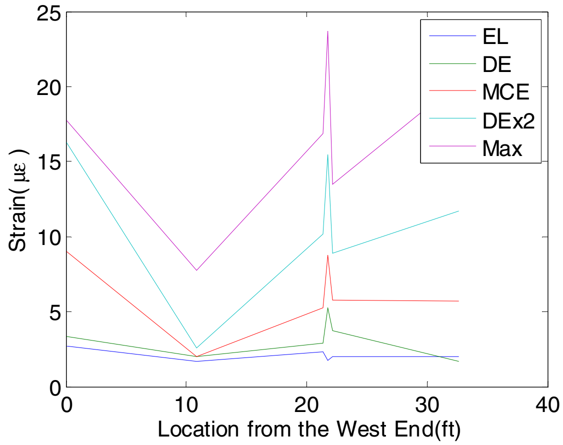

(a) Far 1 Strain in the Deck-bulb-Tee girder

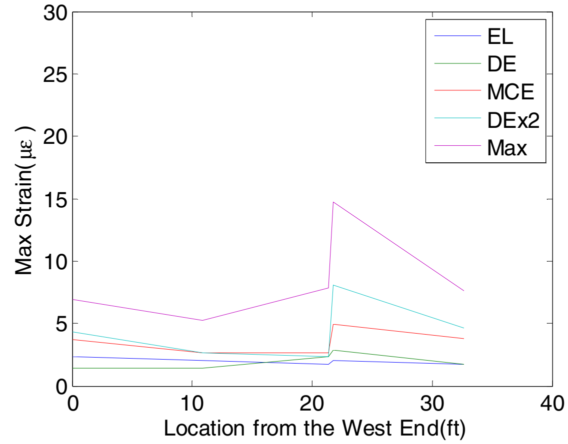

(b) Far 1 Strain in the UHPC Connection

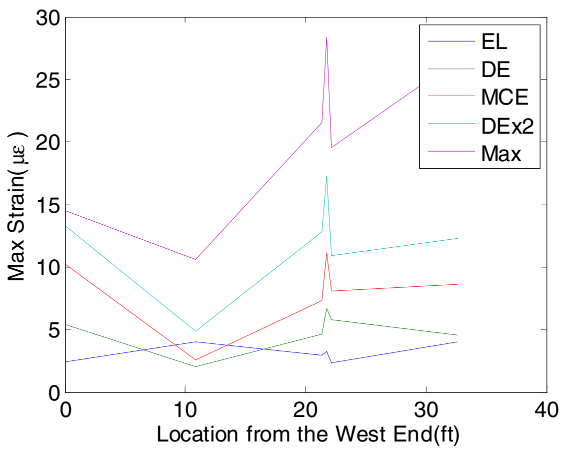

(c) Far 2 Strain in the Deck-bulb-Tee girder

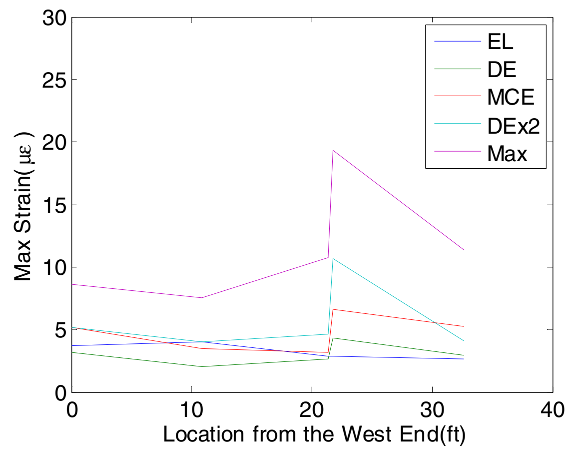

(d) Far 2 Strain in the UHPC Connection

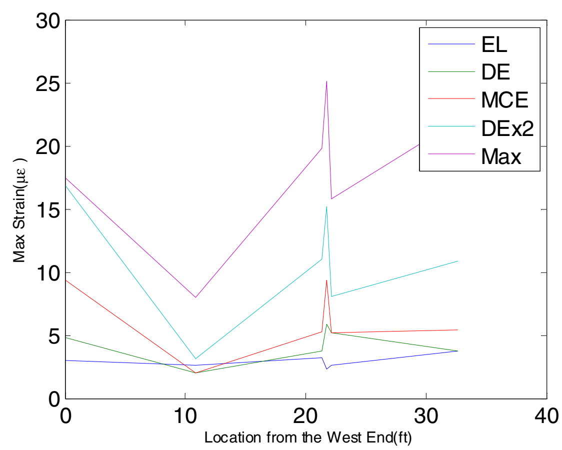

(e) Far 3 Strain in the Deck-bulb-Tee girder

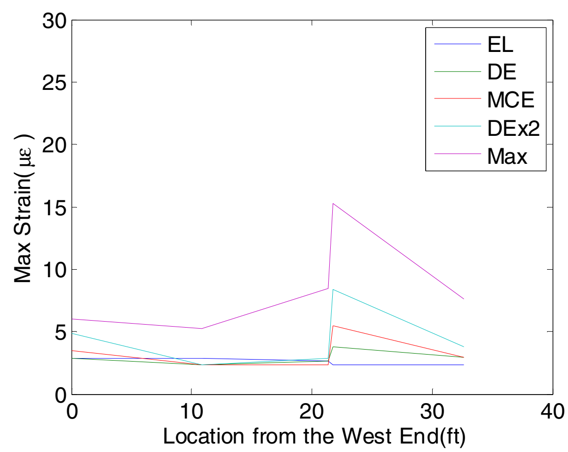

(f) Far 3 Strain in the UHPC Connection

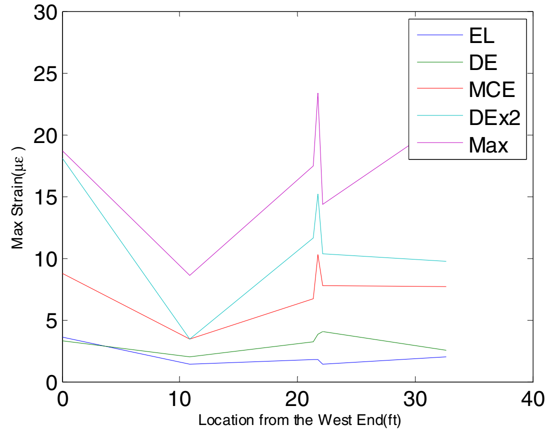

(g) Far 4 Strain in the Deck-bulb-Tee girder

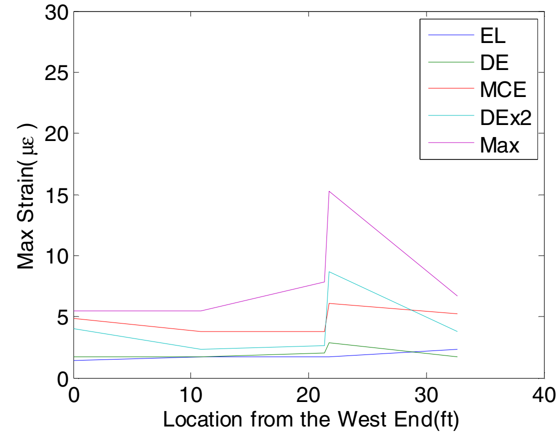

(h) Far 4 Strain in the UHPC Connection

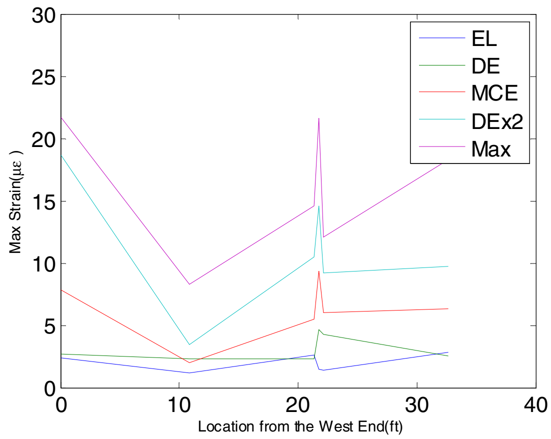

(i) Far 5 Strain in the Deck-bulb-Tee girder

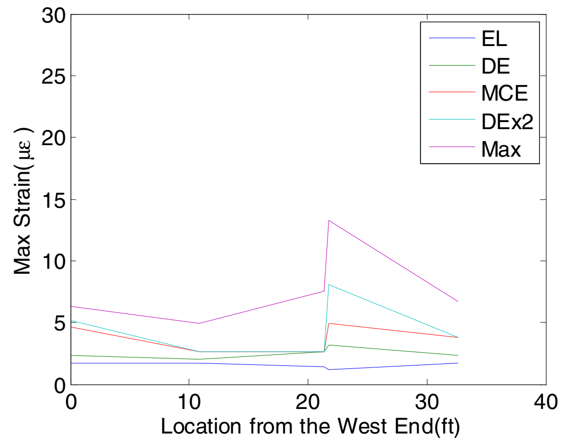

(j) Far 5 Strain in the UHPC Connection

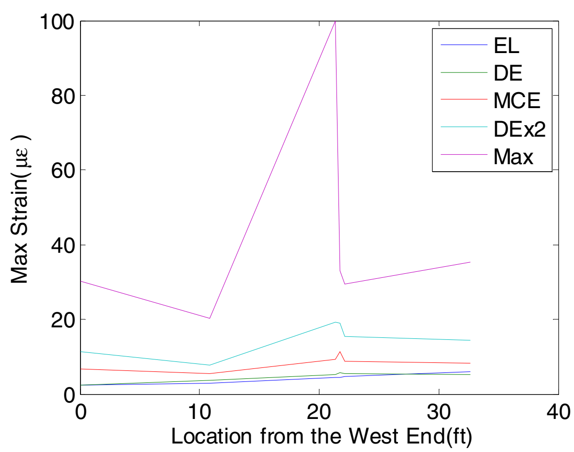

(k) Near 1 Strain in the Deck-bulb-Tee girder

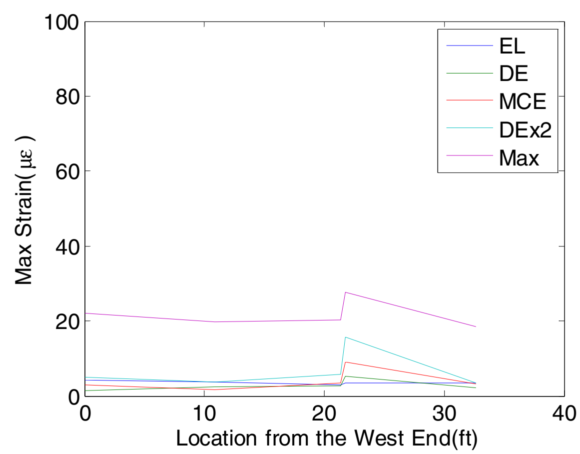

(l) Near 1 Strain in the UHPC Connection

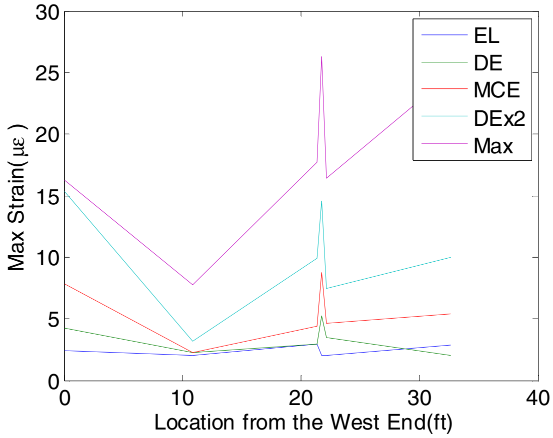

(m) Near 2 Strain in the Deck-bulb-Tee girder

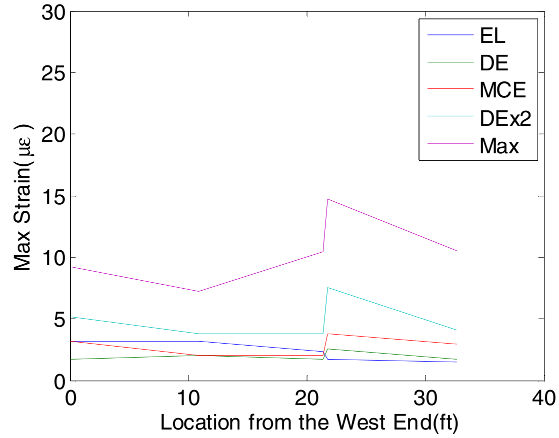

(n) Near 2 Strain in the UHPC Connection

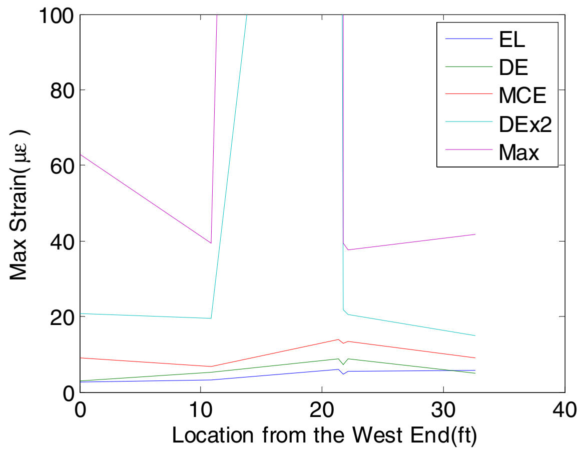

(o) Near 3 Strain in the Deck-bulb-Tee girder*(1400)

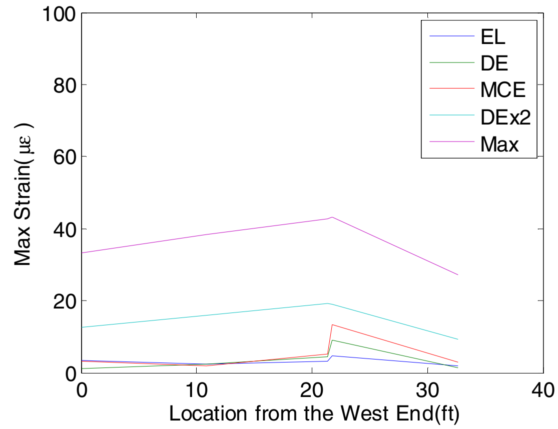

(p) Near 3 Strain in the UHPC Connection

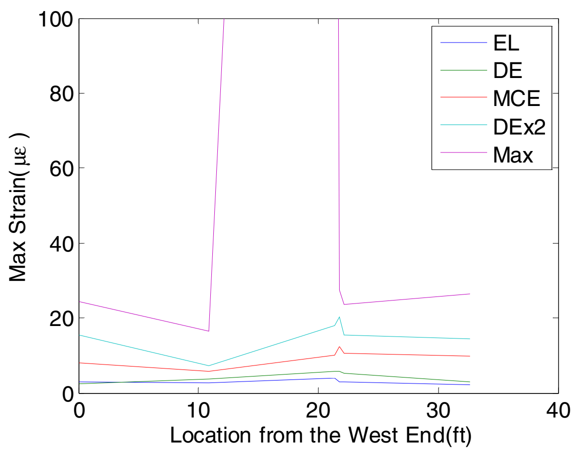

(q) Near 4 Strain in the Deck-bulb-Tee girder*(700)

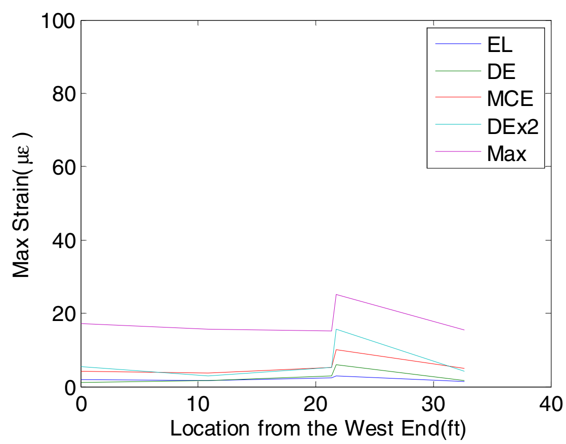

(r) Near 4 Strain in the UHPC Connection

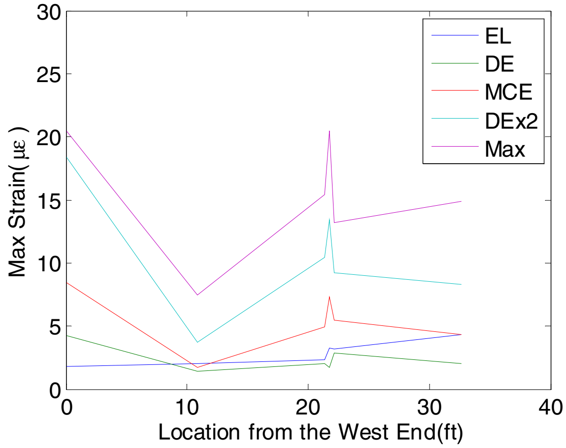

(s) Near 5 Strain in the Deck-bulb-Tee girder

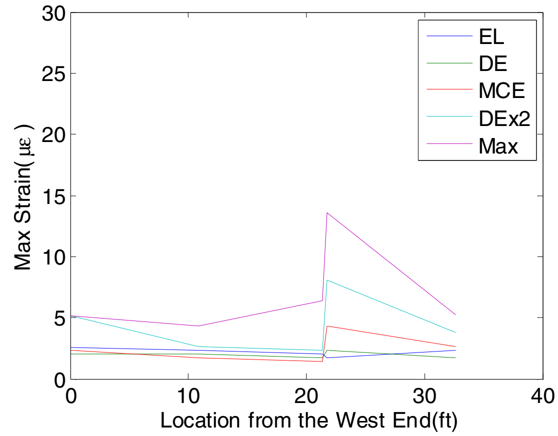

(t) Near 5 Strain in the UHPC Connection

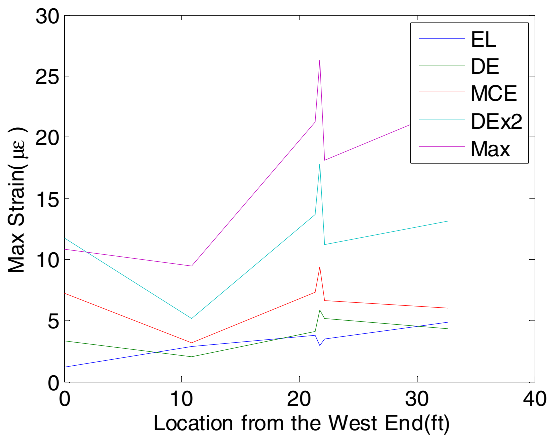

(u) Near 6 Strain in the Deck-bulb-Tee girder

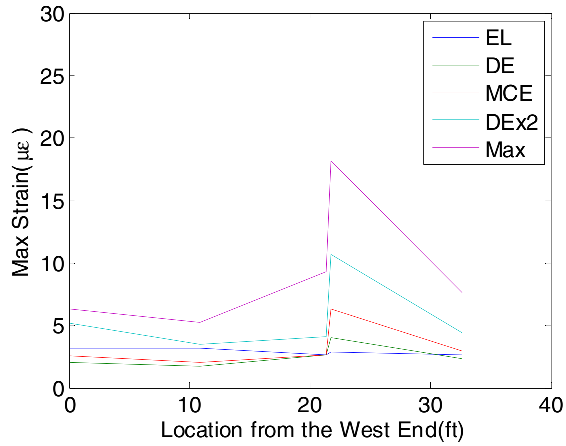

(v) Near 6 Strain in the UHPC Connection

Figure D-1 Phase 1, Strain along the longitudinal direction

(*Note: two results generated a very high value of strain in the Deck-bulb-tee girder deck flange, but the strain in the UHPC connection remained in a very low range of under 30).

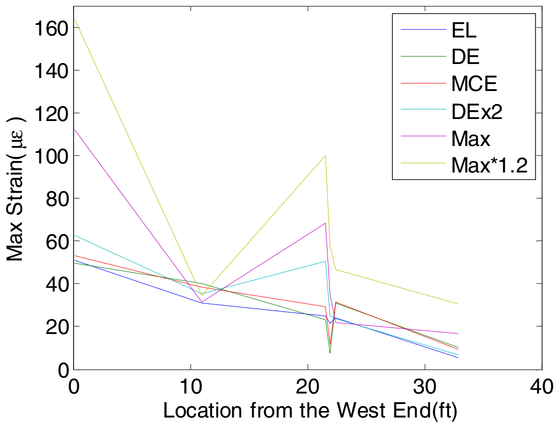

(a) Far 1 Strain in the Deck-bulb-Tee girder

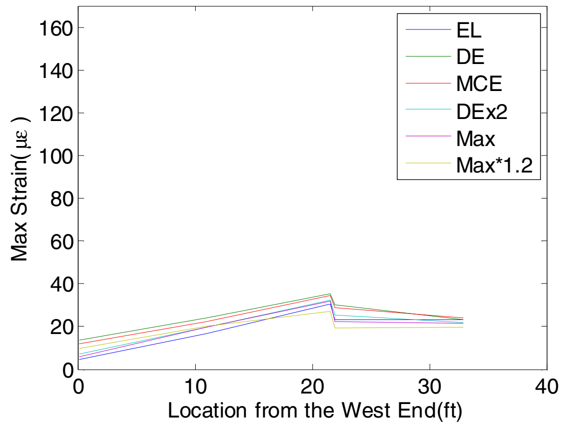

(b) Far 1 Strain in the UHPC Connection

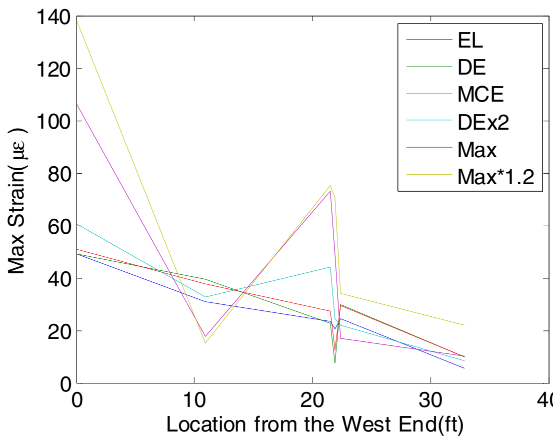

(c) Far 2 Strain in the Deck-bulb-Tee girder

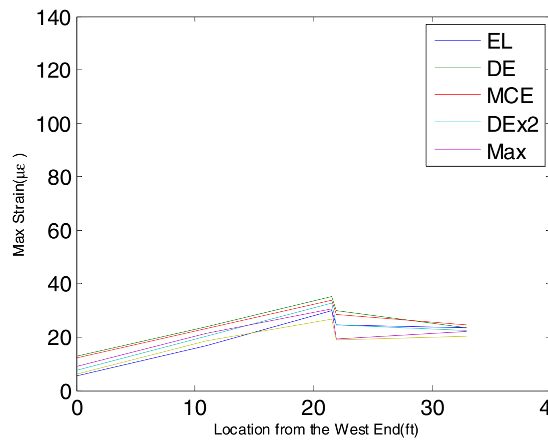

(d) Far 2 Strain in the UHPC Connection

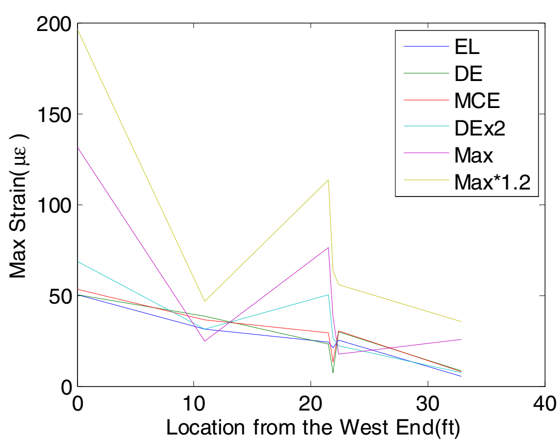

(e) Far 3 Strain in the Deck-bulb-Tee girder

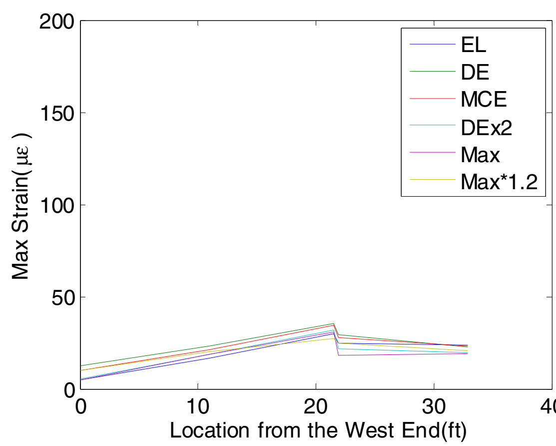

(f) Far 3 Strain in the UHPC Connection

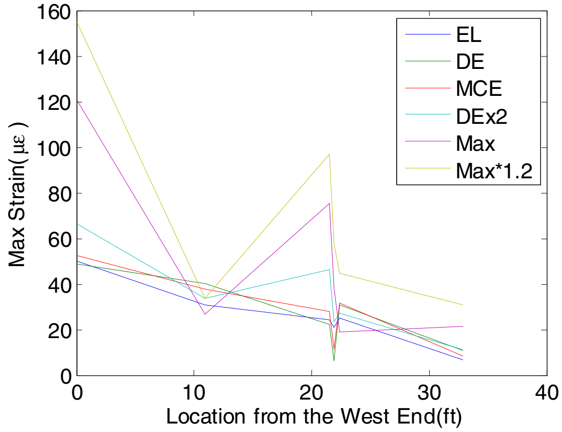

(g) Far 4 Strain in the Deck-bulb-Tee girder

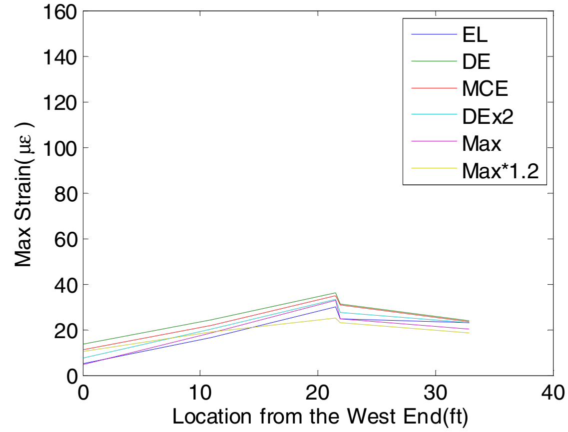

(h) Far 4 Strain in the UHPC Connection

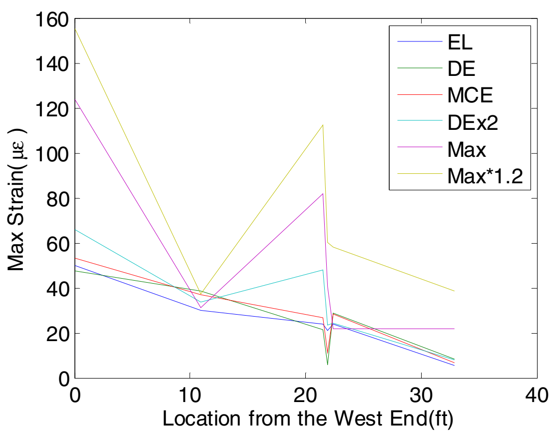

(i) Far 5 Strain in the Deck-bulb-Tee girder

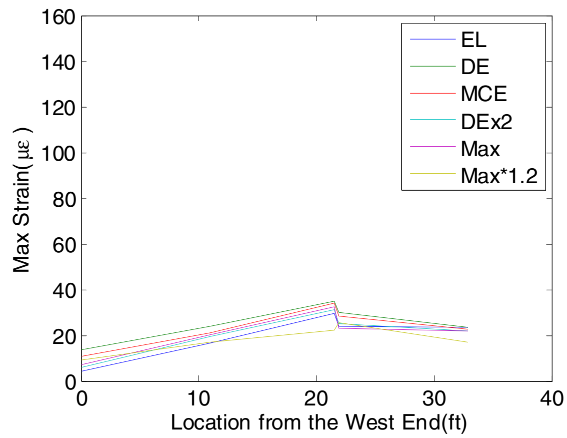

(j) Far 5 Strain in the UHPC Connection

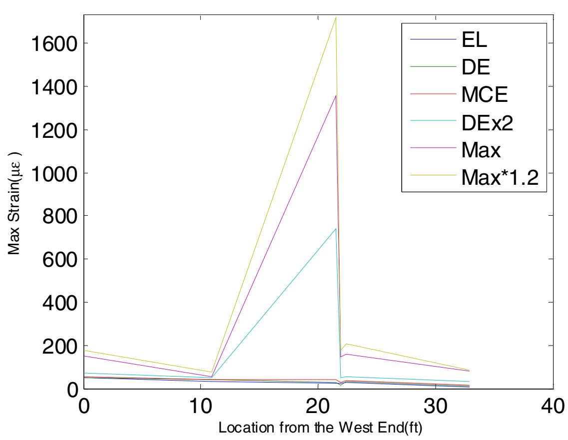

(k) Near 1 Strain in the Deck-bulb-Tee girder*(1600)

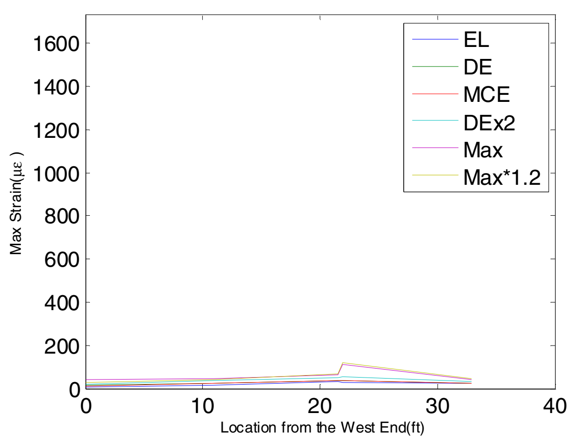

(l) Near 1 Strain in the UHPC Connection

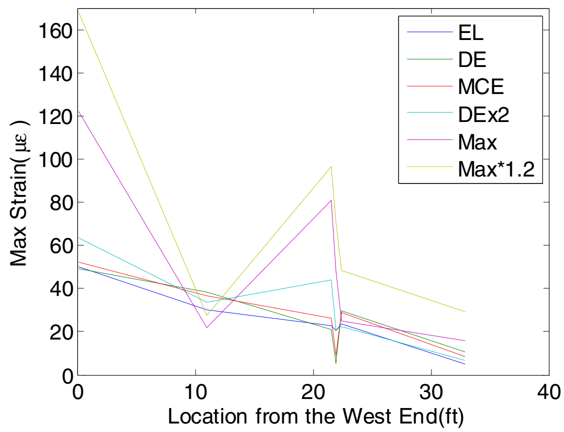

(m) Near 2 Strain in the Deck-bulb-Tee girder

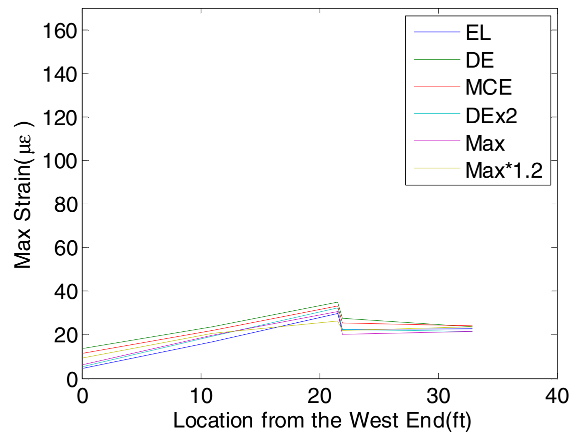

(n) Near 2 Strain in the UHPC Connection

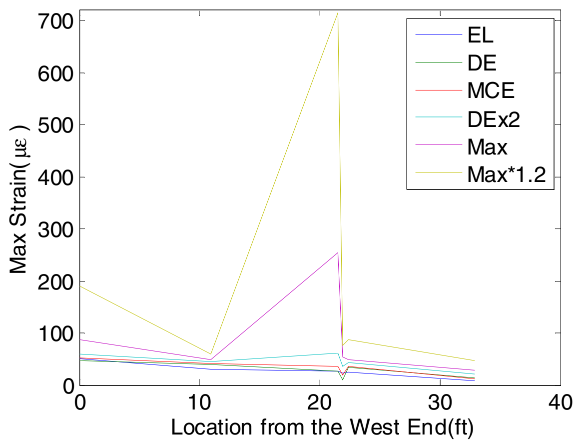

(o) Near 3 Strain in the Deck-bulb-Tee girder*(700)

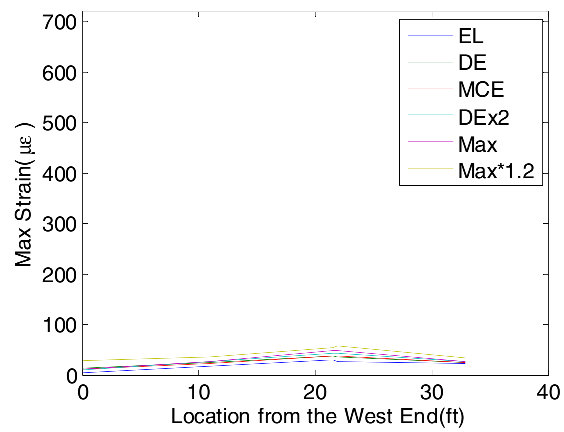

(p) Near 3 Strain in the UHPC Connection

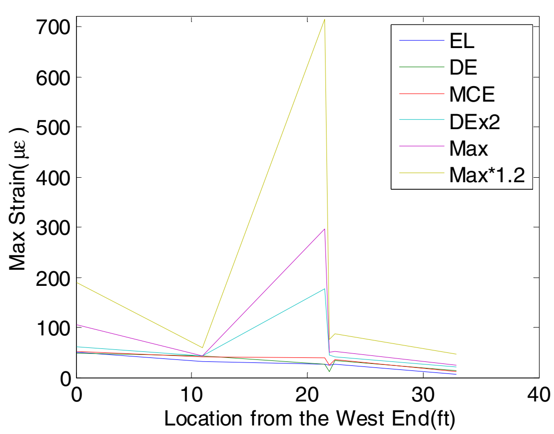

(q) Near 4 Strain in the Deck-bulb-Tee girder*(700)

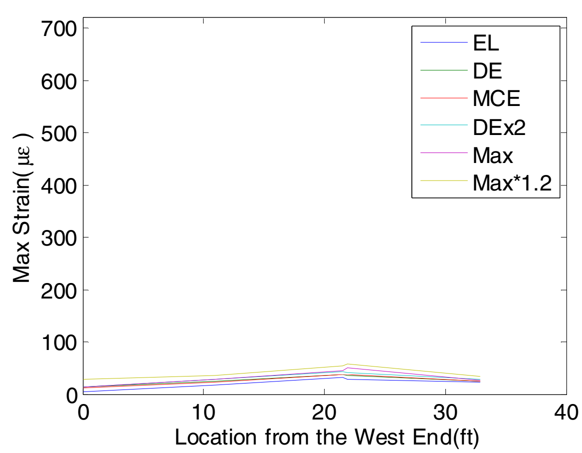

(r) Near 4 Strain in the UHPC Connection

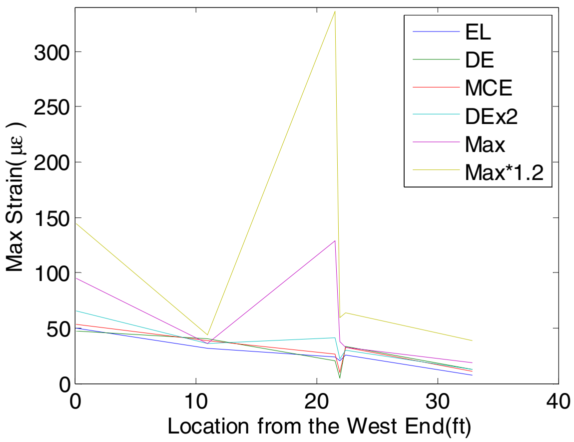

(s) Near 5 Strain in the Deck-bulb-Tee girder

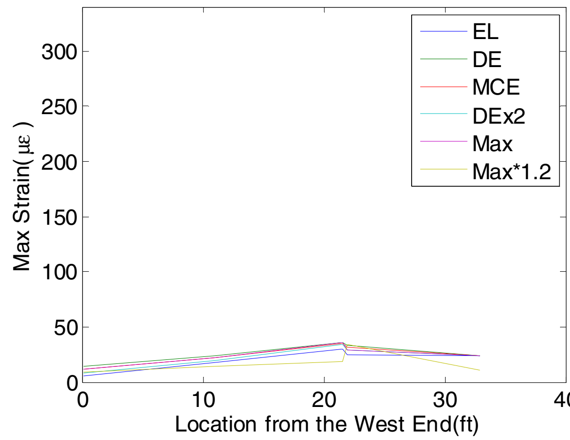

(t) Near 5 Strain in the UHPC Connection

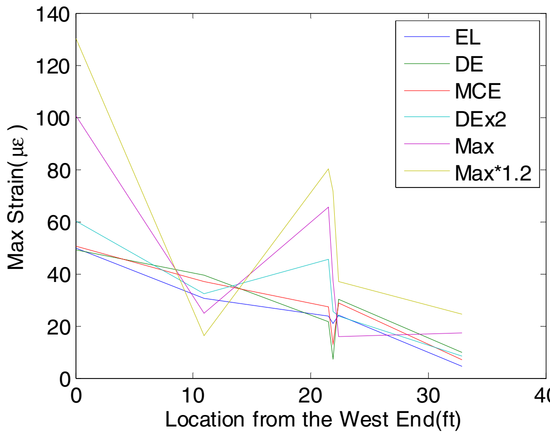

(u) Near 6 Strain in the Deck-bulb-Tee girder

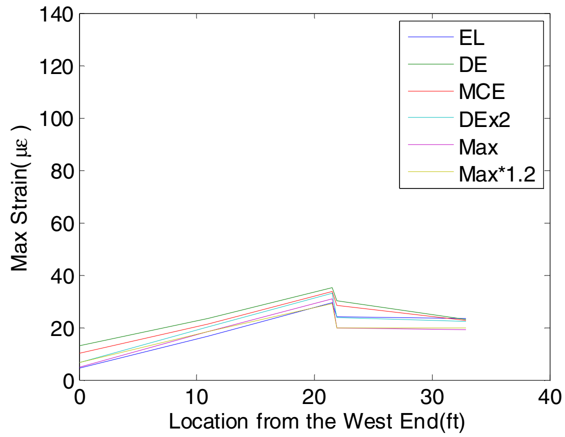

(v) Near 6 Strain in the UHPC Connection

Figure D-2 Phase 2, Strain along the longitudinal direction

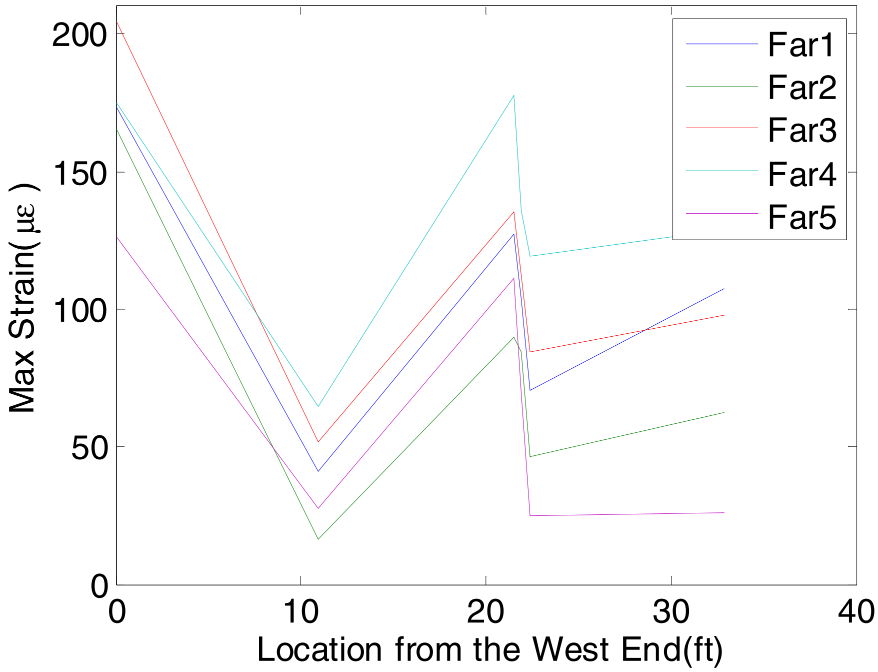

(a) Far 1-5 Strain in the Deck-bulb-Tee girder

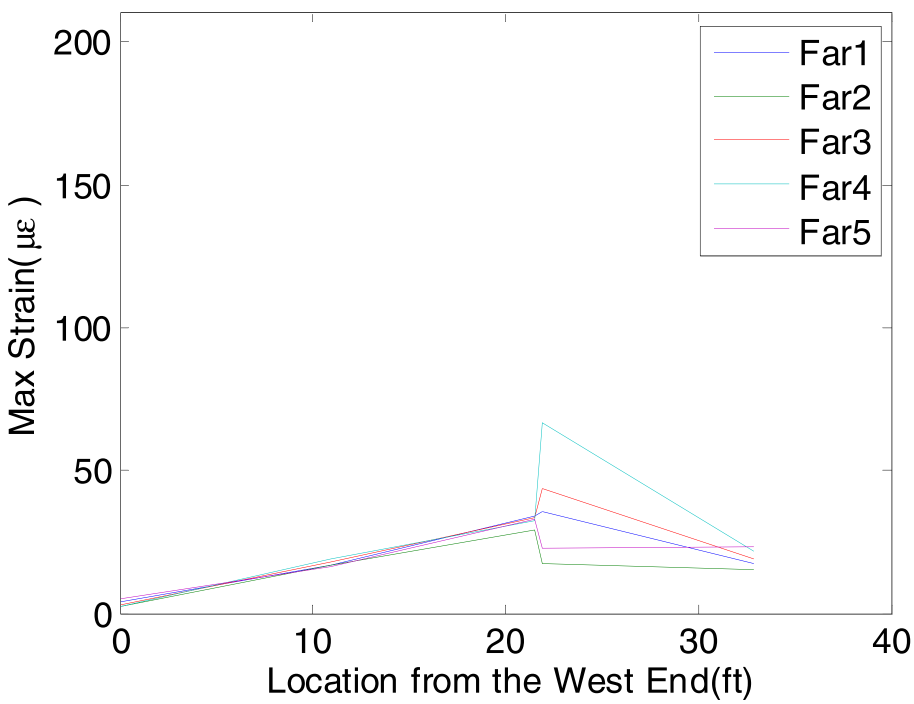

(b) Far 1-5 Strain in the UHPC Connection

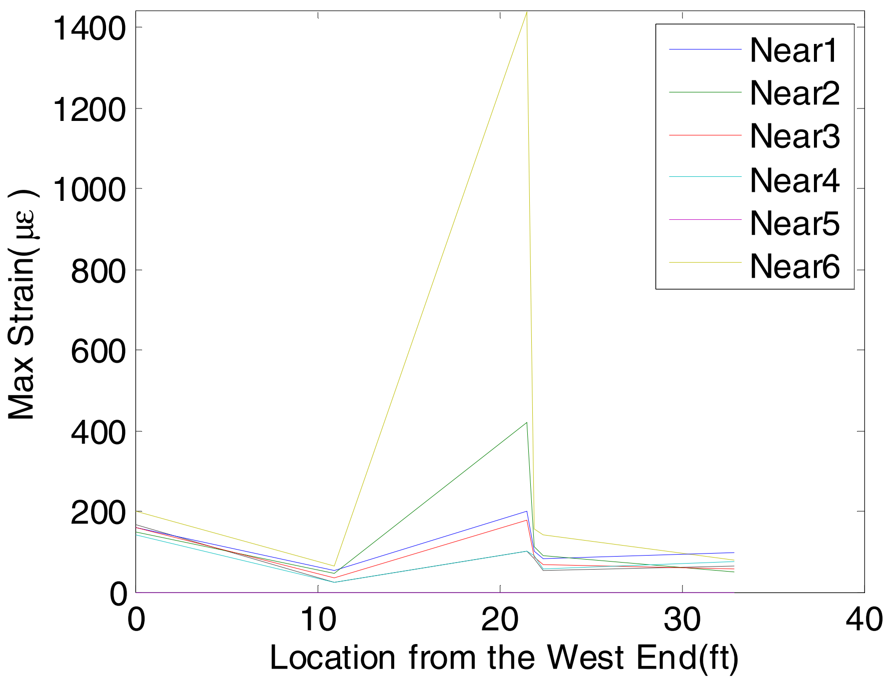

(c) Near 1-6 Strain in the Deck-bulb-Tee girder

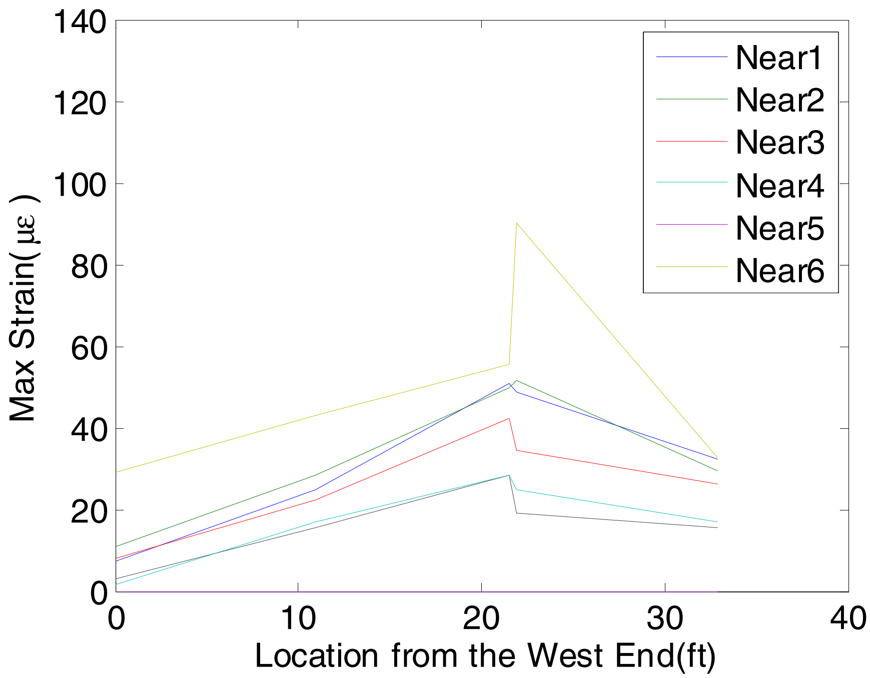

(c) Near 1-6 Strain in the UHPC Connection

Figure D-3 Phase 3 Strain comparison on the girder and UHPC

MCEER Technical Reports

MCEER publishes technical reports on a variety of subjects written by authors funded through MCEER. These reports are available from both MCEER Publications and the National Technical Information Service (NTIS). Requests for reports should be directed to MCEER Publications, MCEER, University at Buffalo, State University of New York, 133A Ketter Hall, Buffalo, New York 14260. Reports can also be requested through NTIS, P.O. Box 1425, Springfield, Virginia 22151. NTIS accession numbers are shown in parenthesis, if available.

NCEER-87-0001 "First-Year Program in Research, Education and Technology Transfer," 3/5/87, (PB88-134275, A04, MF-A01).

NCEER-87-0002 "Experimental Evaluation of Instantaneous Optimal Algorithms for Structural Control," by R.C. Lin, T.T. Soong and A.M. Reinhorn, 4/20/87, (PB88-134341, A04, MF-A01).

NCEER-87-0003 "Experimentation Using the Earthquake Simulation Facilities at University at Buffalo," by A.M. Reinhorn and R.L. Ketter, not available.

NCEER-87-0004 "The System Characteristics and Performance of a Shaking Table," by J.S. Hwang, K.C. Chang and G.C. Lee, 6/1/87, (PB88-134259, A03, MF-A01). This report is available only through NTIS (see address given above).

NCEER-87-0005 "A Finite Element Formulation for Nonlinear Viscoplastic Material Using a Q Model," by O. Gyebi and G. Dasgupta, 11/2/87, (PB88-213764, A08, MF-A01).

NCEER-87-0006 "Symbolic Manipulation Program (SMP) - Algebraic Codes for Two and Three Dimensional Finite Element Formulations," by X. Lee and G. Dasgupta, 11/9/87, (PB88-218522, A05, MF-A01).

NCEER-87-0007 "Instantaneous Optimal Control Laws for Tall Buildings Under Seismic Excitations," by J.N. Yang, A. Akbarpour and P. Ghaemmaghami, 6/10/87, (PB88-134333, A06, MF-A01). This report is only available through NTIS (see address given above).

NCEER-87-0008 "IDARC: Inelastic Damage Analysis of Reinforced Concrete Frame - Shear-Wall Structures," by Y.J. Park, A.M. Reinhorn and S.K. Kunnath, 7/20/87, (PB88-134325, A09, MF-A01). This report is only available through NTIS (see address given above).

NCEER-87-0009 "Liquefaction Potential for New York State: A Preliminary Report on Sites in Manhattan and Buffalo," by M. Budhu, V. Vijayakumar, R.F. Giese and L. Baumgras, 8/31/87, (PB88-163704, A03, MF-A01). This report is available only through NTIS (see address given above).

NCEER-87-0010 "Vertical and Torsional Vibration of Foundations in Inhomogeneous Media," by A.S. Veletsos and K.W. Dotson, 6/1/87, (PB88-134291, A03, MF-A01). This report is only available through NTIS (see address given above).

NCEER-87-0011 "Seismic Probabilistic Risk Assessment and Seismic Margins Studies for Nuclear Power Plants," by Howard H.M. Hwang, 6/15/87, (PB88-134267, A03, MF-A01). This report is only available through NTIS (see address given above).

NCEER-87-0012 "Parametric Studies of Frequency Response of Secondary Systems Under Ground-Acceleration Excitations," by Y. Yong and Y.K. Lin, 6/10/87, (PB88-134309, A03, MF-A01). This report is only available through NTIS (see address given above).

NCEER-87-0013 "Frequency Response of Secondary Systems Under Seismic Excitation," by J.A. HoLung, J. Cai and Y.K. Lin, 7/31/87, (PB88-134317, A05, MF-A01). This report is only available through NTIS (see address given above).

NCEER-87-0014 "Modelling Earthquake Ground Motions in Seismically Active Regions Using Parametric Time Series Methods," by G.W. Ellis and A.S. Cakmak, 8/25/87, (PB88-134283, A08, MF-A01). This report is only available through NTIS (see address given above).

NCEER-87-0015 "Detection and Assessment of Seismic Structural Damage," by E. DiPasquale and A.S. Cakmak, 8/25/87, (PB88-163712, A05, MF-A01). This report is only available through NTIS (see address given above).

NCEER-87-0016 "Pipeline Experiment at Parkfield, California," by J. Isenberg and E. Richardson, 9/15/87, (PB88-163720, A03, MF-A01). This report is available only through NTIS (see address given above).

NCEER-87-0017 "Digital Simulation of Seismic Ground Motion," by M. Shinozuka, G. Deodatis and T. Harada, 8/31/87, (PB88-155197, A04, MF-A01). This report is available only through NTIS (see address given above).

NCEER-87-0018 "Practical Considerations for Structural Control: System Uncertainty, System Time Delay and Truncation of Small Control Forces," J.N. Yang and A. Akbarpour, 8/10/87, (PB88-163738, A08, MF-A01). This report is only available through NTIS (see address given above).

NCEER-87-0019 "Modal Analysis of Nonclassically Damped Structural Systems Using Canonical Transformation," by J.N. Yang, S. Sarkani and F.X. Long, 9/27/87, (PB88-187851, A04, MF-A01).

NCEER-87-0020 "A Nonstationary Solution in Random Vibration Theory," by J.R. Red-Horse and P.D. Spanos, 11/3/87, (PB88-163746, A03, MF-A01).

NCEER-87-0021 "Horizontal Impedances for Radially Inhomogeneous Viscoelastic Soil Layers," by A.S. Veletsos and K.W. Dotson, 10/15/87, (PB88-150859, A04, MF-A01).

NCEER-87-0022 "Seismic Damage Assessment of Reinforced Concrete Members," by Y.S. Chung, C. Meyer and M. Shinozuka, 10/9/87, (PB88-150867, A05, MF-A01). This report is available only through NTIS (see address given above).

NCEER-87-0023 "Active Structural Control in Civil Engineering," by T.T. Soong, 11/11/87, (PB88-187778, A03, MF-A01).

NCEER-87-0024 "Vertical and Torsional Impedances for Radially Inhomogeneous Viscoelastic Soil Layers," by K.W. Dotson and A.S. Veletsos, 12/87, (PB88-187786, A03, MF-A01).

NCEER-87-0025 "Proceedings from the Symposium on Seismic Hazards, Ground Motions, Soil-Liquefaction and Engineering Practice in Eastern North America," October 20-22, 1987, edited by K.H. Jacob, 12/87, (PB88-188115, A23, MF-A01). This report is available only through NTIS (see address given above).

NCEER-87-0026 "Report on the Whittier-Narrows, California, Earthquake of October 1, 1987," by J. Pantelic and A. Reinhorn, 11/87, (PB88-187752, A03, MF-A01). This report is available only through NTIS (see address given above).

NCEER-87-0027 "Design of a Modular Program for Transient Nonlinear Analysis of Large 3-D Building Structures," by S. Srivastav and J.F. Abel, 12/30/87, (PB88-187950, A05, MF-A01). This report is only available through NTIS (see address given above).

NCEER-87-0028 "Second-Year Program in Research, Education and Technology Transfer," 3/8/88, (PB88-219480, A04, MF-A01).

NCEER-88-0001 "Workshop on Seismic Computer Analysis and Design of Buildings With Interactive Graphics," by W. McGuire, J.F. Abel and C.H. Conley, 1/18/88, (PB88-187760, A03, MF-A01). This report is only available through NTIS (see address given above).

NCEER-88-0002 "Optimal Control of Nonlinear Flexible Structures," by J.N. Yang, F.X. Long and D. Wong, 1/22/88, (PB88-213772, A06, MF-A01).

NCEER-88-0003 "Substructuring Techniques in the Time Domain for Primary-Secondary Structural Systems," by G.D. Manolis and G. Juhn, 2/10/88, (PB88-213780, A04, MF-A01).

NCEER-88-0004 "Iterative Seismic Analysis of Primary-Secondary Systems," by A. Singhal, L.D. Lutes and P.D. Spanos, 2/23/88, (PB88-213798, A04, MF-A01).

NCEER-88-0005 "Stochastic Finite Element Expansion for Random Media," by P.D. Spanos and R. Ghanem, 3/14/88, (PB88-213806, A03, MF-A01).

NCEER-88-0006 "Combining Structural Optimization and Structural Control," by F.Y. Cheng and C.P. Pantelides, 1/10/88, (PB88-213814, A05, MF-A01).

NCEER-88-0007 "Seismic Performance Assessment of Code-Designed Structures," by H.H-M. Hwang, J-W. Jaw and H-J. Shau, 3/20/88, (PB88-219423, A04, MF-A01). This report is only available through NTIS (see address given above).

NCEER-88-0008 "Reliability Analysis of Code-Designed Structures Under Natural Hazards," by H.H-M. Hwang, H. Ushiba and M. Shinozuka, 2/29/88, (PB88-229471, A07, MF-A01). This report is only available through NTIS (see address given above).

NCEER-88-0009 "Seismic Fragility Analysis of Shear Wall Structures," by J-W Jaw and H.H-M. Hwang, 4/30/88, (PB89-102867, A04, MF-A01).

NCEER-88-0010 "Base Isolation of a Multi-Story Building Under a Harmonic Ground Motion - A Comparison of Performances of Various Systems," by F-G Fan, G. Ahmadi and I.G. Tadjbakhsh, 5/18/88, (PB89-122238, A06, MF-A01). This report is only available through NTIS (see address given above).

NCEER-88-0011 "Seismic Floor Response Spectra for a Combined System by Green's Functions," by F.M. Lavelle, L.A. Bergman and P.D. Spanos, 5/1/88, (PB89-102875, A03, MF-A01).

NCEER-88-0012 "A New Solution Technique for Randomly Excited Hysteretic Structures," by G.Q. Cai and Y.K. Lin, 5/16/88, (PB89-102883, A03, MF-A01).

NCEER-88-0013 "A Study of Radiation Damping and Soil-Structure Interaction Effects in the Centrifuge," by K. Weissman, supervised by J.H. Prevost, 5/24/88, (PB89-144703, A06, MF-A01).

NCEER-88-0014 "Parameter Identification and Implementation of a Kinematic Plasticity Model for Frictional Soils," by J.H. Prevost and D.V. Griffiths, not available.

NCEER-88-0015 "Two- and Three- Dimensional Dynamic Finite Element Analyses of the Long Valley Dam," by D.V. Griffiths and J.H. Prevost, 6/17/88, (PB89-144711, A04, MF-A01).

NCEER-88-0016 "Damage Assessment of Reinforced Concrete Structures in Eastern United States," by A.M. Reinhorn, M.J. Seidel, S.K. Kunnath and Y.J. Park, 6/15/88, (PB89-122220, A04, MF-A01). This report is only available through NTIS (see address given above).

NCEER-88-0017 "Dynamic Compliance of Vertically Loaded Strip Foundations in Multilayered Viscoelastic Soils," by S. Ahmad and A.S.M. Israil, 6/17/88, (PB89-102891, A04, MF-A01).

NCEER-88-0018 "An Experimental Study of Seismic Structural Response With Added Viscoelastic Dampers," by R.C. Lin, Z. Liang, T.T. Soong and R.H. Zhang, 6/30/88, (PB89-122212, A05, MF-A01). This report is available only through NTIS (see address given above).

NCEER-88-0019 "Experimental Investigation of Primary - Secondary System Interaction," by G.D. Manolis, G. Juhn and A.M. Reinhorn, 5/27/88, (PB89-122204, A04, MF-A01).

NCEER-88-0020 "A Response Spectrum Approach For Analysis of Nonclassically Damped Structures," by J.N. Yang, S. Sarkani and F.X. Long, 4/22/88, (PB89-102909, A04, MF-A01).

NCEER-88-0021 "Seismic Interaction of Structures and Soils: Stochastic Approach," by A.S. Veletsos and A.M. Prasad, 7/21/88, (PB89-122196, A04, MF-A01). This report is only available through NTIS (see address given above).

NCEER-88-0022 "Identification of the Serviceability Limit State and Detection of Seismic Structural Damage," by E. DiPasquale and A.S. Cakmak, 6/15/88, (PB89-122188, A05, MF-A01). This report is available only through NTIS (see address given above).

NCEER-88-0023 "Multi-Hazard Risk Analysis: Case of a Simple Offshore Structure," by B.K. Bhartia and E.H. Vanmarcke, 7/21/88, (PB89-145213, A05, MF-A01).

NCEER-88-0024 "Automated Seismic Design of Reinforced Concrete Buildings," by Y.S. Chung, C. Meyer and M. Shinozuka, 7/5/88, (PB89-122170, A06, MF-A01). This report is available only through NTIS (see address given above).

NCEER-88-0025 "Experimental Study of Active Control of MDOF Structures Under Seismic Excitations," by L.L. Chung, R.C. Lin, T.T. Soong and A.M. Reinhorn, 7/10/88, (PB89-122600, A04, MF-A01).

NCEER-88-0026 "Earthquake Simulation Tests of a Low-Rise Metal Structure," by J.S. Hwang, K.C. Chang, G.C. Lee and R.L. Ketter, 8/1/88, (PB89-102917, A04, MF-A01).

NCEER-88-0027 "Systems Study of Urban Response and Reconstruction Due to Catastrophic Earthquakes," by F. Kozin and H.K. Zhou, 9/22/88, (PB90-162348, A04, MF-A01).

NCEER-88-0028 "Seismic Fragility Analysis of Plane Frame Structures," by H.H-M. Hwang and Y.K. Low, 7/31/88, (PB89-131445, A06, MF-A01).

NCEER-88-0029 "Response Analysis of Stochastic Structures," by A. Kardara, C. Bucher and M. Shinozuka, 9/22/88, (PB89-174429, A04, MF-A01).

NCEER-88-0030 "Nonnormal Accelerations Due to Yielding in a Primary Structure," by D.C.K. Chen and L.D. Lutes, 9/19/88, (PB89-131437, A04, MF-A01).

NCEER-88-0031 "Design Approaches for Soil-Structure Interaction," by A.S. Veletsos, A.M. Prasad and Y. Tang, 12/30/88, (PB89-174437, A03, MF-A01). This report is available only through NTIS (see address given above).

NCEER-88-0032 "A Re-evaluation of Design Spectra for Seismic Damage Control," by C.J. Turkstra and A.G. Tallin, 11/7/88, (PB89-145221, A05, MF-A01).

NCEER-88-0033 "The Behavior and Design of Noncontact Lap Splices Subjected to Repeated Inelastic Tensile Loading," by V.E. Sagan, P. Gergely and R.N. White, 12/8/88, (PB89-163737, A08, MF-A01).

NCEER-88-0034 "Seismic Response of Pile Foundations," by S.M. Mamoon, P.K. Banerjee and S. Ahmad, 11/1/88, (PB89-145239, A04, MF-A01).

NCEER-88-0035 "Modeling of R/C Building Structures With Flexible Floor Diaphragms (IDARC2)," by A.M. Reinhorn, S.K. Kunnath and N. Panahshahi, 9/7/88, (PB89-207153, A07, MF-A01).

NCEER-88-0036 "Solution of the Dam-Reservoir Interaction Problem Using a Combination of FEM, BEM with Particular Integrals, Modal Analysis, and Substructuring," by C-S. Tsai, G.C. Lee and R.L. Ketter, 12/31/88, (PB89-207146, A04, MF-A01).

NCEER-88-0037 "Optimal Placement of Actuators for Structural Control," by F.Y. Cheng and C.P. Pantelides, 8/15/88, (PB89-162846, A05, MF-A01).

NCEER-88-0038 "Teflon Bearings in Aseismic Base Isolation: Experimental Studies and Mathematical Modeling," by A. Mokha, M.C. Constantinou and A.M. Reinhorn, 12/5/88, (PB89-218457, A10, MF-A01). This report is available only through NTIS (see address given above).

NCEER-88-0039 "Seismic Behavior of Flat Slab High-Rise Buildings in the New York City Area," by P. Weidlinger and M. Ettouney, 10/15/88, (PB90-145681, A04, MF-A01).

NCEER-88-0040 "Evaluation of the Earthquake Resistance of Existing Buildings in New York City," by P. Weidlinger and M. Ettouney, 10/15/88, not available.

NCEER-88-0041 "Small-Scale Modeling Techniques for Reinforced Concrete Structures Subjected to Seismic Loads," by W. Kim, A. El-Attar and R.N. White, 11/22/88, (PB89-189625, A05, MF-A01).

NCEER-88-0042 "Modeling Strong Ground Motion from Multiple Event Earthquakes," by G.W. Ellis and A.S. Cakmak, 10/15/88, (PB89-174445, A03, MF-A01).

NCEER-88-0043 "Nonstationary Models of Seismic Ground Acceleration," by M. Grigoriu, S.E. Ruiz and E. Rosenblueth, 7/15/88, (PB89-189617, A04, MF-A01).

NCEER-88-0044 "SARCF User's Guide: Seismic Analysis of Reinforced Concrete Frames," by Y.S. Chung, C. Meyer and M. Shinozuka, 11/9/88, (PB89-174452, A08, MF-A01).

NCEER-88-0045 "First Expert Panel Meeting on Disaster Research and Planning," edited by J. Pantelic and J. Stoyle, 9/15/88, (PB89-174460, A05, MF-A01).

NCEER-88-0046 "Preliminary Studies of the Effect of Degrading Infill Walls on the Nonlinear Seismic Response of Steel Frames," by C.Z. Chrysostomou, P. Gergely and J.F. Abel, 12/19/88, (PB89-208383, A05, MF-A01).

NCEER-88-0047 "Reinforced Concrete Frame Component Testing Facility - Design, Construction, Instrumentation and Operation," by S.P. Pessiki, C. Conley, T. Bond, P. Gergely and R.N. White, 12/16/88, (PB89-174478, A04, MF-A01).

NCEER-89-0001 "Effects of Protective Cushion and Soil Compliancy on the Response of Equipment Within a Seismically Excited Building," by J.A. HoLung, 2/16/89, (PB89-207179, A04, MF-A01).

NCEER-89-0002 "Statistical Evaluation of Response Modification Factors for Reinforced Concrete Structures," by H.H-M. Hwang and J-W. Jaw, 2/17/89, (PB89-207187, A05, MF-A01).

NCEER-89-0003 "Hysteretic Columns Under Random Excitation," by G-Q. Cai and Y.K. Lin, 1/9/89, (PB89-196513, A03, MF-A01).

NCEER-89-0004 "Experimental Study of `Elephant Foot Bulge' Instability of Thin-Walled Metal Tanks," by Z-H. Jia and R.L. Ketter, 2/22/89, (PB89-207195, A03, MF-A01).

NCEER-89-0005 "Experiment on Performance of Buried Pipelines Across San Andreas Fault," by J. Isenberg, E. Richardson and T.D. O'Rourke, 3/10/89, (PB89-218440, A04, MF-A01). This report is available only through NTIS (see address given above).

NCEER-89-0006 "A Knowledge-Based Approach to Structural Design of Earthquake-Resistant Buildings," by M. Subramani, P. Gergely, C.H. Conley, J.F. Abel and A.H. Zaghw, 1/15/89, (PB89-218465, A06, MF-A01).

NCEER-89-0007 "Liquefaction Hazards and Their Effects on Buried Pipelines," by T.D. O'Rourke and P.A. Lane, 2/1/89, (PB89-218481, A09, MF-A01).

NCEER-89-0008 "Fundamentals of System Identification in Structural Dynamics," by H. Imai, C-B. Yun, O. Maruyama and M. Shinozuka, 1/26/89, (PB89-207211, A04, MF-A01).

NCEER-89-0009 "Effects of the 1985 Michoacan Earthquake on Water Systems and Other Buried Lifelines in Mexico," by A.G. Ayala and M.J. O'Rourke, 3/8/89, (PB89-207229, A06, MF-A01).

NCEER-89-R010 "NCEER Bibliography of Earthquake Education Materials," by K.E.K. Ross, Second Revision, 9/1/89, (PB90-125352, A05, MF-A01). This report is replaced by NCEER-92-0018.

NCEER-89-0011 "Inelastic Three-Dimensional Response Analysis of Reinforced Concrete Building Structures (IDARC-3D), Part I - Modeling," by S.K. Kunnath and A.M. Reinhorn, 4/17/89, (PB90-114612, A07, MF-A01). This report is available only through NTIS (see address given above).

NCEER-89-0012 "Recommended Modifications to ATC-14," by C.D. Poland and J.O. Malley, 4/12/89, (PB90-108648, A15, MF-A01).

NCEER-89-0013 "Repair and Strengthening of Beam-to-Column Connections Subjected to Earthquake Loading," by M. Corazao and A.J. Durrani, 2/28/89, (PB90-109885, A06, MF-A01).

NCEER-89-0014 "Program EXKAL2 for Identification of Structural Dynamic Systems," by O. Maruyama, C-B. Yun, M. Hoshiya and M. Shinozuka, 5/19/89, (PB90-109877, A09, MF-A01).

NCEER-89-0015 "Response of Frames With Bolted Semi-Rigid Connections, Part I - Experimental Study and Analytical Predictions," by P.J. DiCorso, A.M. Reinhorn, J.R. Dickerson, J.B. Radziminski and W.L. Harper, 6/1/89, not available.

NCEER-89-0016 "ARMA Monte Carlo Simulation in Probabilistic Structural Analysis," by P.D. Spanos and M.P. Mignolet, 7/10/89, (PB90-109893, A03, MF-A01).

NCEER-89-P017 "Preliminary Proceedings from the Conference on Disaster Preparedness - The Place of Earthquake Education in Our Schools," Edited by K.E.K. Ross, 6/23/89, (PB90-108606, A03, MF-A01).

NCEER-89-0017 "Proceedings from the Conference on Disaster Preparedness - The Place of Earthquake Education in Our Schools," Edited by K.E.K. Ross, 12/31/89, (PB90-207895, A012, MF-A02). This report is available only through NTIS (see address given above).

NCEER-89-0018 "Multidimensional Models of Hysteretic Material Behavior for Vibration Analysis of Shape Memory Energy Absorbing Devices, by E.J. Graesser and F.A. Cozzarelli, 6/7/89, (PB90-164146, A04, MF-A01).

NCEER-89-0019 "Nonlinear Dynamic Analysis of Three-Dimensional Base Isolated Structures (3D-BASIS)," by S. Nagarajaiah, A.M. Reinhorn and M.C. Constantinou, 8/3/89, (PB90-161936, A06, MF-A01). This report has been replaced by NCEER-93-0011.

NCEER-89-0020 "Structural Control Considering Time-Rate of Control Forces and Control Rate Constraints," by F.Y. Cheng and C.P. Pantelides, 8/3/89, (PB90-120445, A04, MF-A01).

NCEER-89-0021 "Subsurface Conditions of Memphis and Shelby County," by K.W. Ng, T-S. Chang and H-H.M. Hwang, 7/26/89, (PB90-120437, A03, MF-A01).

NCEER-89-0022 "Seismic Wave Propagation Effects on Straight Jointed Buried Pipelines," by K. Elhmadi and M.J. O'Rourke, 8/24/89, (PB90-162322, A10, MF-A02).

NCEER-89-0023 "Workshop on Serviceability Analysis of Water Delivery Systems," edited by M. Grigoriu, 3/6/89, (PB90-127424, A03, MF-A01).

NCEER-89-0024 "Shaking Table Study of a 1/5 Scale Steel Frame Composed of Tapered Members," by K.C. Chang, J.S. Hwang and G.C. Lee, 9/18/89, (PB90-160169, A04, MF-A01).

NCEER-89-0025 "DYNA1D: A Computer Program for Nonlinear Seismic Site Response Analysis - Technical Documentation," by Jean H. Prevost, 9/14/89, (PB90-161944, A07, MF-A01). This report is available only through NTIS (see address given above).

NCEER-89-0026 "1:4 Scale Model Studies of Active Tendon Systems and Active Mass Dampers for Aseismic Protection," by A.M. Reinhorn, T.T. Soong, R.C. Lin, Y.P. Yang, Y. Fukao, H. Abe and M. Nakai, 9/15/89, (PB90-173246, A10, MF-A02). This report is available only through NTIS (see address given above).

NCEER-89-0027 "Scattering of Waves by Inclusions in a Nonhomogeneous Elastic Half Space Solved by Boundary Element Methods," by P.K. Hadley, A. Askar and A.S. Cakmak, 6/15/89, (PB90-145699, A07, MF-A01).

NCEER-89-0028 "Statistical Evaluation of Deflection Amplification Factors for Reinforced Concrete Structures," by H.H.M. Hwang, J-W. Jaw and A.L. Ch'ng, 8/31/89, (PB90-164633, A05, MF-A01).

NCEER-89-0029 "Bedrock Accelerations in Memphis Area Due to Large New Madrid Earthquakes," by H.H.M. Hwang, C.H.S. Chen and G. Yu, 11/7/89, (PB90-162330, A04, MF-A01).

NCEER-89-0030 "Seismic Behavior and Response Sensitivity of Secondary Structural Systems," by Y.Q. Chen and T.T. Soong, 10/23/89, (PB90-164658, A08, MF-A01).

NCEER-89-0031 "Random Vibration and Reliability Analysis of Primary-Secondary Structural Systems," by Y. Ibrahim, M. Grigoriu and T.T. Soong, 11/10/89, (PB90-161951, A04, MF-A01).

NCEER-89-0032 "Proceedings from the Second U.S. - Japan Workshop on Liquefaction, Large Ground Deformation and Their Effects on Lifelines, September 26-29, 1989," Edited by T.D. O'Rourke and M. Hamada, 12/1/89, (PB90-209388, A22, MF-A03).

NCEER-89-0033 "Deterministic Model for Seismic Damage Evaluation of Reinforced Concrete Structures," by J.M. Bracci, A.M. Reinhorn, J.B. Mander and S.K. Kunnath, 9/27/89, (PB91-108803, A06, MF-A01).

NCEER-89-0034 "On the Relation Between Local and Global Damage Indices," by E. DiPasquale and A.S. Cakmak, 8/15/89, (PB90-173865, A05, MF-A01).

NCEER-89-0035 "Cyclic Undrained Behavior of Nonplastic and Low Plasticity Silts," by A.J. Walker and H.E. Stewart, 7/26/89, (PB90-183518, A10, MF-A01).

NCEER-89-0036 "Liquefaction Potential of Surficial Deposits in the City of Buffalo, New York," by M. Budhu, R. Giese and L. Baumgrass, 1/17/89, (PB90-208455, A04, MF-A01).

NCEER-89-0037 "A Deterministic Assessment of Effects of Ground Motion Incoherence," by A.S. Veletsos and Y. Tang, 7/15/89, (PB90-164294, A03, MF-A01).

NCEER-89-0038 "Workshop on Ground Motion Parameters for Seismic Hazard Mapping," July 17-18, 1989, edited by R.V. Whitman, 12/1/89, (PB90-173923, A04, MF-A01).

NCEER-89-0039 "Seismic Effects on Elevated Transit Lines of the New York City Transit Authority," by C.J. Costantino, C.A. Miller and E. Heymsfield, 12/26/89, (PB90-207887, A06, MF-A01).

NCEER-89-0040 "Centrifugal Modeling of Dynamic Soil-Structure Interaction," by K. Weissman, Supervised by J.H. Prevost, 5/10/89, (PB90-207879, A07, MF-A01).

NCEER-89-0041 "Linearized Identification of Buildings With Cores for Seismic Vulnerability Assessment," by I-K. Ho and A.E. Aktan, 11/1/89, (PB90-251943, A07, MF-A01).

NCEER-90-0001 "Geotechnical and Lifeline Aspects of the October 17, 1989 Loma Prieta Earthquake in San Francisco," by T.D. O'Rourke, H.E. Stewart, F.T. Blackburn and T.S. Dickerman, 1/90, (PB90-208596, A05, MF-A01).

NCEER-90-0002 "Nonnormal Secondary Response Due to Yielding in a Primary Structure," by D.C.K. Chen and L.D. Lutes, 2/28/90, (PB90-251976, A07, MF-A01).

NCEER-90-0003 "Earthquake Education Materials for Grades K-12," by K.E.K. Ross, 4/16/90, (PB91-251984, A05, MF-A05). This report has been replaced by NCEER-92-0018.

NCEER-90-0004 "Catalog of Strong Motion Stations in Eastern North America," by R.W. Busby, 4/3/90, (PB90-251984, A05, MF-A01).

NCEER-90-0005 "NCEER Strong-Motion Data Base: A User Manual for the GeoBase Release (Version 1.0 for the Sun3)," by P. Friberg and K. Jacob, 3/31/90 (PB90-258062, A04, MF-A01).

NCEER-90-0006 "Seismic Hazard Along a Crude Oil Pipeline in the Event of an 1811-1812 Type New Madrid Earthquake," by H.H.M. Hwang and C-H.S. Chen, 4/16/90, (PB90-258054, A04, MF-A01).

NCEER-90-0007 "Site-Specific Response Spectra for Memphis Sheahan Pumping Station," by H.H.M. Hwang and C.S. Lee, 5/15/90, (PB91-108811, A05, MF-A01).

NCEER-90-0008 "Pilot Study on Seismic Vulnerability of Crude Oil Transmission Systems," by T. Ariman, R. Dobry, M. Grigoriu, F. Kozin, M. O'Rourke, T. O'Rourke and M. Shinozuka, 5/25/90, (PB91-108837, A06, MF-A01).

NCEER-90-0009 "A Program to Generate Site Dependent Time Histories: EQGEN," by G.W. Ellis, M. Srinivasan and A.S. Cakmak, 1/30/90, (PB91-108829, A04, MF-A01).

NCEER-90-0010 "Active Isolation for Seismic Protection of Operating Rooms," by M.E. Talbott, Supervised by M. Shinozuka, 6/8/9, (PB91-110205, A05, MF-A01).

NCEER-90-0011 "Program LINEARID for Identification of Linear Structural Dynamic Systems," by C-B. Yun and M. Shinozuka, 6/25/90, (PB91-110312, A08, MF-A01).

NCEER-90-0012 "Two-Dimensional Two-Phase Elasto-Plastic Seismic Response of Earth Dams," by A.N. Yiagos, Supervised by J.H. Prevost, 6/20/90, (PB91-110197, A13, MF-A02).

NCEER-90-0013 "Secondary Systems in Base-Isolated Structures: Experimental Investigation, Stochastic Response and Stochastic Sensitivity," by G.D. Manolis, G. Juhn, M.C. Constantinou and A.M. Reinhorn, 7/1/90, (PB91-110320, A08, MF-A01).

NCEER-90-0014 "Seismic Behavior of Lightly-Reinforced Concrete Column and Beam-Column Joint Details," by S.P. Pessiki, C.H. Conley, P. Gergely and R.N. White, 8/22/90, (PB91-108795, A11, MF-A02).

NCEER-90-0015 "Two Hybrid Control Systems for Building Structures Under Strong Earthquakes," by J.N. Yang and A. Danielians, 6/29/90, (PB91-125393, A04, MF-A01).

NCEER-90-0016 "Instantaneous Optimal Control with Acceleration and Velocity Feedback," by J.N. Yang and Z. Li, 6/29/90, (PB91-125401, A03, MF-A01).

NCEER-90-0017 "Reconnaissance Report on the Northern Iran Earthquake of June 21, 1990," by M. Mehrain, 10/4/90, (PB91-125377, A03, MF-A01).

NCEER-90-0018 "Evaluation of Liquefaction Potential in Memphis and Shelby County," by T.S. Chang, P.S. Tang, C.S. Lee and H. Hwang, 8/10/90, (PB91-125427, A09, MF-A01).

NCEER-90-0019 "Experimental and Analytical Study of a Combined Sliding Disc Bearing and Helical Steel Spring Isolation System," by M.C. Constantinou, A.S. Mokha and A.M. Reinhorn, 10/4/90, (PB91-125385, A06, MF-A01). This report is available only through NTIS (see address given above).

NCEER-90-0020 "Experimental Study and Analytical Prediction of Earthquake Response of a Sliding Isolation System with a Spherical Surface," by A.S. Mokha, M.C. Constantinou and A.M. Reinhorn, 10/11/90, (PB91-125419, A05, MF-A01).

NCEER-90-0021 "Dynamic Interaction Factors for Floating Pile Groups," by G. Gazetas, K. Fan, A. Kaynia and E. Kausel, 9/10/90, (PB91-170381, A05, MF-A01).

NCEER-90-0022 "Evaluation of Seismic Damage Indices for Reinforced Concrete Structures," by S. Rodriguez-Gomez and A.S. Cakmak, 9/30/90, PB91-171322, A06, MF-A01).

NCEER-90-0023 "Study of Site Response at a Selected Memphis Site," by H. Desai, S. Ahmad, E.S. Gazetas and M.R. Oh, 10/11/90, (PB91-196857, A03, MF-A01).

NCEER-90-0024 "A User's Guide to Strongmo: Version 1.0 of NCEER's Strong-Motion Data Access Tool for PCs and Terminals," by P.A. Friberg and C.A.T. Susch, 11/15/90, (PB91-171272, A03, MF-A01).

NCEER-90-0025 "A Three-Dimensional Analytical Study of Spatial Variability of Seismic Ground Motions," by L-L. Hong and A.H.-S. Ang, 10/30/90, (PB91-170399, A09, MF-A01).

NCEER-90-0026 "MUMOID User's Guide - A Program for the Identification of Modal Parameters," by S. Rodriguez-Gomez and E. DiPasquale, 9/30/90, (PB91-171298, A04, MF-A01).

NCEER-90-0027 "SARCF-II User's Guide - Seismic Analysis of Reinforced Concrete Frames," by S. Rodriguez-Gomez, Y.S. Chung and C. Meyer, 9/30/90, (PB91-171280, A05, MF-A01).

NCEER-90-0028 "Viscous Dampers: Testing, Modeling and Application in Vibration and Seismic Isolation," by N. Makris and M.C. Constantinou, 12/20/90 (PB91-190561, A06, MF-A01).

NCEER-90-0029 "Soil Effects on Earthquake Ground Motions in the Memphis Area," by H. Hwang, C.S. Lee, K.W. Ng and T.S. Chang, 8/2/90, (PB91-190751, A05, MF-A01).

NCEER-91-0001 "Proceedings from the Third Japan-U.S. Workshop on Earthquake Resistant Design of Lifeline Facilities and Countermeasures for Soil Liquefaction, December 17-19, 1990," edited by T.D. O'Rourke and M. Hamada, 2/1/91, (PB91-179259, A99, MF-A04).

NCEER-91-0002 "Physical Space Solutions of Non-Proportionally Damped Systems," by M. Tong, Z. Liang and G.C. Lee, 1/15/91, (PB91-179242, A04, MF-A01).

NCEER-91-0003 "Seismic Response of Single Piles and Pile Groups," by K. Fan and G. Gazetas, 1/10/91, (PB92-174994, A04, MF-A01).

NCEER-91-0004 "Damping of Structures: Part 1 - Theory of Complex Damping," by Z. Liang and G. Lee, 10/10/91, (PB92-197235, A12, MF-A03).

NCEER-91-0005 "3D-BASIS - Nonlinear Dynamic Analysis of Three Dimensional Base Isolated Structures: Part II," by S. Nagarajaiah, A.M. Reinhorn and M.C. Constantinou, 2/28/91, (PB91-190553, A07, MF-A01). This report has been replaced by NCEER-93-0011.

NCEER-91-0006 "A Multidimensional Hysteretic Model for Plasticity Deforming Metals in Energy Absorbing Devices," by E.J. Graesser and F.A. Cozzarelli, 4/9/91, (PB92-108364, A04, MF-A01).

NCEER-91-0007 "A Framework for Customizable Knowledge-Based Expert Systems with an Application to a KBES for Evaluating the Seismic Resistance of Existing Buildings," by E.G. Ibarra-Anaya and S.J. Fenves, 4/9/91, (PB91-210930, A08, MF-A01).

NCEER-91-0008 "Nonlinear Analysis of Steel Frames with Semi-Rigid Connections Using the Capacity Spectrum Method," by G.G. Deierlein, S-H. Hsieh, Y-J. Shen and J.F. Abel, 7/2/91, (PB92-113828, A05, MF-A01).

NCEER-91-0009 "Earthquake Education Materials for Grades K-12," by K.E.K. Ross, 4/30/91, (PB91-212142, A06, MF-A01). This report has been replaced by NCEER-92-0018.

NCEER-91-0010 "Phase Wave Velocities and Displacement Phase Differences in a Harmonically Oscillating Pile," by N. Makris and G. Gazetas, 7/8/91, (PB92-108356, A04, MF-A01).

NCEER-91-0011 "Dynamic Characteristics of a Full-Size Five-Story Steel Structure and a 2/5 Scale Model," by K.C. Chang, G.C. Yao, G.C. Lee, D.S. Hao and Y.C. Yeh," 7/2/91, (PB93-116648, A06, MF-A02).

NCEER-91-0012 "Seismic Response of a 2/5 Scale Steel Structure with Added Viscoelastic Dampers," by K.C. Chang, T.T. Soong, S-T. Oh and M.L. Lai, 5/17/91, (PB92-110816, A05, MF-A01).

NCEER-91-0013 "Earthquake Response of Retaining Walls; Full-Scale Testing and Computational Modeling," by S. Alampalli and A-W.M. Elgamal, 6/20/91, not available.

NCEER-91-0014 "3D-BASIS-M: Nonlinear Dynamic Analysis of Multiple Building Base Isolated Structures," by P.C. Tsopelas, S. Nagarajaiah, M.C. Constantinou and A.M. Reinhorn, 5/28/91, (PB92-113885, A09, MF-A02).

NCEER-91-0015 "Evaluation of SEAOC Design Requirements for Sliding Isolated Structures," by D. Theodossiou and M.C. Constantinou, 6/10/91, (PB92-114602, A11, MF-A03).

NCEER-91-0016 "Closed-Loop Modal Testing of a 27-Story Reinforced Concrete Flat Plate-Core Building," by H.R. Somaprasad, T. Toksoy, H. Yoshiyuki and A.E. Aktan, 7/15/91, (PB92-129980, A07, MF-A02).

NCEER-91-0017 "Shake Table Test of a 1/6 Scale Two-Story Lightly Reinforced Concrete Building," by A.G. El-Attar, R.N. White and P. Gergely, 2/28/91, (PB92-222447, A06, MF-A02).

NCEER-91-0018 "Shake Table Test of a 1/8 Scale Three-Story Lightly Reinforced Concrete Building," by A.G. El-Attar, R.N. White and P. Gergely, 2/28/91, (PB93-116630, A08, MF-A02).

NCEER-91-0019 "Transfer Functions for Rigid Rectangular Foundations," by A.S. Veletsos, A.M. Prasad and W.H. Wu, 7/31/91, not available.

NCEER-91-0020 "Hybrid Control of Seismic-Excited Nonlinear and Inelastic Structural Systems," by J.N. Yang, Z. Li and A. Danielians, 8/1/91, (PB92-143171, A06, MF-A02).

NCEER-91-0021 "The NCEER-91 Earthquake Catalog: Improved Intensity-Based Magnitudes and Recurrence Relations for U.S. Earthquakes East of New Madrid," by L. Seeber and J.G. Armbruster, 8/28/91, (PB92-176742, A06, MF-A02).

NCEER-91-0022 "Proceedings from the Implementation of Earthquake Planning and Education in Schools: The Need for Change - The Roles of the Changemakers," by K.E.K. Ross and F. Winslow, 7/23/91, (PB92-129998, A12, MF-A03).

NCEER-91-0023 "A Study of Reliability-Based Criteria for Seismic Design of Reinforced Concrete Frame Buildings," by H.H.M. Hwang and H-M. Hsu, 8/10/91, (PB92-140235, A09, MF-A02).

NCEER-91-0024 "Experimental Verification of a Number of Structural System Identification Algorithms," by R.G. Ghanem, H. Gavin and M. Shinozuka, 9/18/91, (PB92-176577, A18, MF-A04).

NCEER-91-0025 "Probabilistic Evaluation of Liquefaction Potential," by H.H.M. Hwang and C.S. Lee," 11/25/91, (PB92-143429, A05, MF-A01).

NCEER-91-0026 "Instantaneous Optimal Control for Linear, Nonlinear and Hysteretic Structures - Stable Controllers," by J.N. Yang and Z. Li, 11/15/91, (PB92-163807, A04, MF-A01).

NCEER-91-0027 "Experimental and Theoretical Study of a Sliding Isolation System for Bridges," by M.C. Constantinou, A. Kartoum, A.M. Reinhorn and P. Bradford, 11/15/91, (PB92-176973, A10, MF-A03).

NCEER-92-0001 "Case Studies of Liquefaction and Lifeline Performance During Past Earthquakes, Volume 1: Japanese Case Studies," Edited by M. Hamada and T. O'Rourke, 2/17/92, (PB92-197243, A18, MF-A04).

NCEER-92-0002 "Case Studies of Liquefaction and Lifeline Performance During Past Earthquakes, Volume 2: United States Case Studies," Edited by T. O'Rourke and M. Hamada, 2/17/92, (PB92-197250, A20, MF-A04).

NCEER-92-0003 "Issues in Earthquake Education," Edited by K. Ross, 2/3/92, (PB92-222389, A07, MF-A02).

NCEER-92-0004 "Proceedings from the First U.S. - Japan Workshop on Earthquake Protective Systems for Bridges," Edited by I.G. Buckle, 2/4/92, (PB94-142239, A99, MF-A06).

NCEER-92-0005 "Seismic Ground Motion from a Haskell-Type Source in a Multiple-Layered Half-Space," A.P. Theoharis, G. Deodatis and M. Shinozuka, 1/2/92, not available.

NCEER-92-0006 "Proceedings from the Site Effects Workshop," Edited by R. Whitman, 2/29/92, (PB92-197201, A04, MF-A01).

NCEER-92-0007 "Engineering Evaluation of Permanent Ground Deformations Due to Seismically-Induced Liquefaction," by M.H. Baziar, R. Dobry and A-W.M. Elgamal, 3/24/92, (PB92-222421, A13, MF-A03).

NCEER-92-0008 "A Procedure for the Seismic Evaluation of Buildings in the Central and Eastern United States," by C.D. Poland and J.O. Malley, 4/2/92, (PB92-222439, A20, MF-A04).

NCEER-92-0009 "Experimental and Analytical Study of a Hybrid Isolation System Using Friction Controllable Sliding Bearings," by M.Q. Feng, S. Fujii and M. Shinozuka, 5/15/92, (PB93-150282, A06, MF-A02).

NCEER-92-0010 "Seismic Resistance of Slab-Column Connections in Existing Non-Ductile Flat-Plate Buildings," by A.J. Durrani and Y. Du, 5/18/92, (PB93-116812, A06, MF-A02).

NCEER-92-0011 "The Hysteretic and Dynamic Behavior of Brick Masonry Walls Upgraded by Ferrocement Coatings Under Cyclic Loading and Strong Simulated Ground Motion," by H. Lee and S.P. Prawel, 5/11/92, not available.

NCEER-92-0012 "Study of Wire Rope Systems for Seismic Protection of Equipment in Buildings," by G.F. Demetriades, M.C. Constantinou and A.M. Reinhorn, 5/20/92, (PB93-116655, A08, MF-A02).

NCEER-92-0013 "Shape Memory Structural Dampers: Material Properties, Design and Seismic Testing," by P.R. Witting and F.A. Cozzarelli, 5/26/92, (PB93-116663, A05, MF-A01).

NCEER-92-0014 "Longitudinal Permanent Ground Deformation Effects on Buried Continuous Pipelines," by M.J. O'Rourke, and C. Nordberg, 6/15/92, (PB93-116671, A08, MF-A02).

NCEER-92-0015 "A Simulation Method for Stationary Gaussian Random Functions Based on the Sampling Theorem," by M. Grigoriu and S. Balopoulou, 6/11/92, (PB93-127496, A05, MF-A01).

NCEER-92-0016 "Gravity-Load-Designed Reinforced Concrete Buildings: Seismic Evaluation of Existing Construction and Detailing Strategies for Improved Seismic Resistance," by G.W. Hoffmann, S.K. Kunnath, A.M. Reinhorn and J.B. Mander, 7/15/92, (PB94-142007, A08, MF-A02).

NCEER-92-0017 "Observations on Water System and Pipeline Performance in the Limón Area of Costa Rica Due to the April 22, 1991 Earthquake," by M. O'Rourke and D. Ballantyne, 6/30/92, (PB93-126811, A06, MF-A02).

NCEER-92-0018 "Fourth Edition of Earthquake Education Materials for Grades K-12," Edited by K.E.K. Ross, 8/10/92, (PB93-114023, A07, MF-A02).

NCEER-92-0019 "Proceedings from the Fourth Japan-U.S. Workshop on Earthquake Resistant Design of Lifeline Facilities and Countermeasures for Soil Liquefaction," Edited by M. Hamada and T.D. O'Rourke, 8/12/92, (PB93-163939, A99, MF-E11).

NCEER-92-0020 "Active Bracing System: A Full Scale Implementation of Active Control," by A.M. Reinhorn, T.T. Soong, R.C. Lin, M.A. Riley, Y.P. Wang, S. Aizawa and M. Higashino, 8/14/92, (PB93-127512, A06, MF-A02).

NCEER-92-0021 "Empirical Analysis of Horizontal Ground Displacement Generated by Liquefaction-Induced Lateral Spreads," by S.F. Bartlett and T.L. Youd, 8/17/92, (PB93-188241, A06, MF-A02).

NCEER-92-0022 "IDARC Version 3.0: Inelastic Damage Analysis of Reinforced Concrete Structures," by S.K. Kunnath, A.M. Reinhorn and R.F. Lobo, 8/31/92, (PB93-227502, A07, MF-A02).

NCEER-92-0023 "A Semi-Empirical Analysis of Strong-Motion Peaks in Terms of Seismic Source, Propagation Path and Local Site Conditions, by M. Kamiyama, M.J. O'Rourke and R. Flores-Berrones, 9/9/92, (PB93-150266, A08, MF-A02).

NCEER-92-0024 "Seismic Behavior of Reinforced Concrete Frame Structures with Nonductile Details, Part I: Summary of Experimental Findings of Full Scale Beam-Column Joint Tests," by A. Beres, R.N. White and P. Gergely, 9/30/92, (PB93-227783, A05, MF-A01).

NCEER-92-0025 "Experimental Results of Repaired and Retrofitted Beam-Column Joint Tests in Lightly Reinforced Concrete Frame Buildings," by A. Beres, S. El-Borgi, R.N. White and P. Gergely, 10/29/92, (PB93-227791, A05, MF-A01).

NCEER-92-0026 "A Generalization of Optimal Control Theory: Linear and Nonlinear Structures," by J.N. Yang, Z. Li and S. Vongchavalitkul, 11/2/92, (PB93-188621, A05, MF-A01).

NCEER-92-0027 "Seismic Resistance of Reinforced Concrete Frame Structures Designed Only for Gravity Loads: Part I - Design and Properties of a One-Third Scale Model Structure," by J.M. Bracci, A.M. Reinhorn and J.B. Mander, 12/1/92, (PB94-104502, A08, MF-A02).

NCEER-92-0028 "Seismic Resistance of Reinforced Concrete Frame Structures Designed Only for Gravity Loads: Part II - Experimental Performance of Subassemblages," by L.E. Aycardi, J.B. Mander and A.M. Reinhorn, 12/1/92, (PB94-104510, A08, MF-A02).

NCEER-92-0029 "Seismic Resistance of Reinforced Concrete Frame Structures Designed Only for Gravity Loads: Part III - Experimental Performance and Analytical Study of a Structural Model," by J.M. Bracci, A.M. Reinhorn and J.B. Mander, 12/1/92, (PB93-227528, A09, MF-A01).

NCEER-92-0030 "Evaluation of Seismic Retrofit of Reinforced Concrete Frame Structures: Part I - Experimental Performance of Retrofitted Subassemblages," by D. Choudhuri, J.B. Mander and A.M. Reinhorn, 12/8/92, (PB93-198307, A07, MF-A02).

NCEER-92-0031 "Evaluation of Seismic Retrofit of Reinforced Concrete Frame Structures: Part II - Experimental Performance and Analytical Study of a Retrofitted Structural Model," by J.M. Bracci, A.M. Reinhorn and J.B. Mander, 12/8/92, (PB93-198315, A09, MF-A03).

NCEER-92-0032 "Experimental and Analytical Investigation of Seismic Response of Structures with Supplemental Fluid Viscous Dampers," by M.C. Constantinou and M.D. Symans, 12/21/92, (PB93-191435, A10, MF-A03). This report is available only through NTIS (see address given above).

NCEER-92-0033 "Reconnaissance Report on the Cairo, Egypt Earthquake of October 12, 1992," by M. Khater, 12/23/92, (PB93-188621, A03, MF-A01).

NCEER-92-0034 "Low-Level Dynamic Characteristics of Four Tall Flat-Plate Buildings in New York City," by H. Gavin, S. Yuan, J. Grossman, E. Pekelis and K. Jacob, 12/28/92, (PB93-188217, A07, MF-A02).

NCEER-93-0001 "An Experimental Study on the Seismic Performance of Brick-Infilled Steel Frames With and Without Retrofit," by J.B. Mander, B. Nair, K. Wojtkowski and J. Ma, 1/29/93, (PB93-227510, A07, MF-A02).

NCEER-93-0002 "Social Accounting for Disaster Preparedness and Recovery Planning," by S. Cole, E. Pantoja and V. Razak, 2/22/93, (PB94-142114, A12, MF-A03).

NCEER-93-0003 "Assessment of 1991 NEHRP Provisions for Nonstructural Components and Recommended Revisions," by T.T. Soong, G. Chen, Z. Wu, R-H. Zhang and M. Grigoriu, 3/1/93, (PB93-188639, A06, MF-A02).

NCEER-93-0004 "Evaluation of Static and Response Spectrum Analysis Procedures of SEAOC/UBC for Seismic Isolated Structures," by C.W. Winters and M.C. Constantinou, 3/23/93, (PB93-198299, A10, MF-A03).

NCEER-93-0005 "Earthquakes in the Northeast - Are We Ignoring the Hazard? A Workshop on Earthquake Science and Safety for Educators," edited by K.E.K. Ross, 4/2/93, (PB94-103066, A09, MF-A02).

NCEER-93-0006 "Inelastic Response of Reinforced Concrete Structures with Viscoelastic Braces," by R.F. Lobo, J.M. Bracci, K.L. Shen, A.M. Reinhorn and T.T. Soong, 4/5/93, (PB93-227486, A05, MF-A02).

NCEER-93-0007 "Seismic Testing of Installation Methods for Computers and Data Processing Equipment," by K. Kosar, T.T. Soong, K.L. Shen, J.A. HoLung and Y.K. Lin, 4/12/93, (PB93-198299, A07, MF-A02).

NCEER-93-0008 "Retrofit of Reinforced Concrete Frames Using Added Dampers," by A. Reinhorn, M. Constantinou and C. Li, not available.

NCEER-93-0009 "Seismic Behavior and Design Guidelines for Steel Frame Structures with Added Viscoelastic Dampers," by K.C. Chang, M.L. Lai, T.T. Soong, D.S. Hao and Y.C. Yeh, 5/1/93, (PB94-141959, A07, MF-A02).

NCEER-93-0010 "Seismic Performance of Shear-Critical Reinforced Concrete Bridge Piers," by J.B. Mander, S.M. Waheed, M.T.A. Chaudhary and S.S. Chen, 5/12/93, (PB93-227494, A08, MF-A02).

NCEER-93-0011 "3D-BASIS-TABS: Computer Program for Nonlinear Dynamic Analysis of Three Dimensional Base Isolated Structures," by S. Nagarajaiah, C. Li, A.M. Reinhorn and M.C. Constantinou, 8/2/93, (PB94-141819, A09, MF-A02).

NCEER-93-0012 "Effects of Hydrocarbon Spills from an Oil Pipeline Break on Ground Water," by O.J. Helweg and H.H.M. Hwang, 8/3/93, (PB94-141942, A06, MF-A02).

NCEER-93-0013 "Simplified Procedures for Seismic Design of Nonstructural Components and Assessment of Current Code Provisions," by M.P. Singh, L.E. Suarez, E.E. Matheu and G.O. Maldonado, 8/4/93, (PB94-141827, A09, MF-A02).

NCEER-93-0014 "An Energy Approach to Seismic Analysis and Design of Secondary Systems," by G. Chen and T.T. Soong, 8/6/93, (PB94-142767, A11, MF-A03).

NCEER-93-0015 "Proceedings from School Sites: Becoming Prepared for Earthquakes - Commemorating the Third Anniversary of the Loma Prieta Earthquake," Edited by F.E. Winslow and K.E.K. Ross, 8/16/93, (PB94-154275, A16, MF-A02).

NCEER-93-0016 "Reconnaissance Report of Damage to Historic Monuments in Cairo, Egypt Following the October 12, 1992 Dahshur Earthquake," by D. Sykora, D. Look, G. Croci, E. Karaesmen and E. Karaesmen, 8/19/93, (PB94-142221, A08, MF-A02).

NCEER-93-0017 "The Island of Guam Earthquake of August 8, 1993," by S.W. Swan and S.K. Harris, 9/30/93, (PB94-141843, A04, MF-A01).

NCEER-93-0018 "Engineering Aspects of the October 12, 1992 Egyptian Earthquake," by A.W. Elgamal, M. Amer, K. Adalier and A. Abul-Fadl, 10/7/93, (PB94-141983, A05, MF-A01).

NCEER-93-0019 "Development of an Earthquake Motion Simulator and its Application in Dynamic Centrifuge Testing," by I. Krstelj, Supervised by J.H. Prevost, 10/23/93, (PB94-181773, A-10, MF-A03).

NCEER-93-0020 "NCEER-Taisei Corporation Research Program on Sliding Seismic Isolation Systems for Bridges: Experimental and Analytical Study of a Friction Pendulum System (FPS)," by M.C. Constantinou, P. Tsopelas, Y-S. Kim and S. Okamoto, 11/1/93, (PB94-142775, A08, MF-A02).

NCEER-93-0021 "Finite Element Modeling of Elastomeric Seismic Isolation Bearings," by L.J. Billings, Supervised by R. Shepherd, 11/8/93, not available.

NCEER-93-0022 "Seismic Vulnerability of Equipment in Critical Facilities: Life-Safety and Operational Consequences," by K. Porter, G.S. Johnson, M.M. Zadeh, C. Scawthorn and S. Eder, 11/24/93, (PB94-181765, A16, MF-A03).

NCEER-93-0023 "Hokkaido Nansei-oki, Japan Earthquake of July 12, 1993, by P.I. Yanev and C.R. Scawthorn, 12/23/93, (PB94-181500, A07, MF-A01).

NCEER-94-0001 "An Evaluation of Seismic Serviceability of Water Supply Networks with Application to the San Francisco Auxiliary Water Supply System," by I. Markov, Supervised by M. Grigoriu and T. O'Rourke, 1/21/94, (PB94-204013, A07, MF-A02).

NCEER-94-0002 "NCEER-Taisei Corporation Research Program on Sliding Seismic Isolation Systems for Bridges: Experimental and Analytical Study of Systems Consisting of Sliding Bearings, Rubber Restoring Force Devices and Fluid Dampers," Volumes I and II, by P. Tsopelas, S. Okamoto, M.C. Constantinou, D. Ozaki and S. Fujii, 2/4/94, (PB94-181740, A09, MF-A02 and PB94-181757, A12, MF-A03).

NCEER-94-0003 "A Markov Model for Local and Global Damage Indices in Seismic Analysis," by S. Rahman and M. Grigoriu, 2/18/94, (PB94-206000, A12, MF-A03).

NCEER-94-0004 "Proceedings from the NCEER Workshop on Seismic Response of Masonry Infills," edited by D.P. Abrams, 3/1/94, (PB94-180783, A07, MF-A02).

NCEER-94-0005 "The Northridge, California Earthquake of January 17, 1994: General Reconnaissance Report," edited by J.D. Goltz, 3/11/94, (PB94-193943, A10, MF-A03).

NCEER-94-0006 "Seismic Energy Based Fatigue Damage Analysis of Bridge Columns: Part I - Evaluation of Seismic Capacity," by G.A. Chang and J.B. Mander, 3/14/94, (PB94-219185, A11, MF-A03).

NCEER-94-0007 "Seismic Isolation of Multi-Story Frame Structures Using Spherical Sliding Isolation Systems," by T.M. Al-Hussaini, V.A. Zayas and M.C. Constantinou, 3/17/94, (PB94-193745, A09, MF-A02).

NCEER-94-0008 "The Northridge, California Earthquake of January 17, 1994: Performance of Highway Bridges," edited by I.G. Buckle, 3/24/94, (PB94-193851, A06, MF-A02).

NCEER-94-0009 "Proceedings of the Third U.S.-Japan Workshop on Earthquake Protective Systems for Bridges," edited by I.G. Buckle and I. Friedland, 3/31/94, (PB94-195815, A99, MF-A06).

NCEER-94-0010 "3D-BASIS-ME: Computer Program for Nonlinear Dynamic Analysis of Seismically Isolated Single and Multiple Structures and Liquid Storage Tanks," by P.C. Tsopelas, M.C. Constantinou and A.M. Reinhorn, 4/12/94, (PB94-204922, A09, MF-A02).

NCEER-94-0011 "The Northridge, California Earthquake of January 17, 1994: Performance of Gas Transmission Pipelines," by T.D. O'Rourke and M.C. Palmer, 5/16/94, (PB94-204989, A05, MF-A01).

NCEER-94-0012 "Feasibility Study of Replacement Procedures and Earthquake Performance Related to Gas Transmission Pipelines," by T.D. O'Rourke and M.C. Palmer, 5/25/94, (PB94-206638, A09, MF-A02).

NCEER-94-0013 "Seismic Energy Based Fatigue Damage Analysis of Bridge Columns: Part II - Evaluation of Seismic Demand," by G.A. Chang and J.B. Mander, 6/1/94, (PB95-18106, A08, MF-A02).

NCEER-94-0014 "NCEER-Taisei Corporation Research Program on Sliding Seismic Isolation Systems for Bridges: Experimental and Analytical Study of a System Consisting of Sliding Bearings and Fluid Restoring Force/Damping Devices," by P. Tsopelas and M.C. Constantinou, 6/13/94, (PB94-219144, A10, MF-A03).

NCEER-94-0015 "Generation of Hazard-Consistent Fragility Curves for Seismic Loss Estimation Studies," by H. Hwang and J-R. Huo, 6/14/94, (PB95-181996, A09, MF-A02).

NCEER-94-0016 "Seismic Study of Building Frames with Added Energy-Absorbing Devices," by W.S. Pong, C.S. Tsai and G.C. Lee, 6/20/94, (PB94-219136, A10, A03).

NCEER-94-0017 "Sliding Mode Control for Seismic-Excited Linear and Nonlinear Civil Engineering Structures," by J. Yang, J. Wu, A. Agrawal and Z. Li, 6/21/94, (PB95-138483, A06, MF-A02).

NCEER-94-0018 "3D-BASIS-TABS Version 2.0: Computer Program for Nonlinear Dynamic Analysis of Three Dimensional Base Isolated Structures," by A.M. Reinhorn, S. Nagarajaiah, M.C. Constantinou, P. Tsopelas and R. Li, 6/22/94, (PB95-182176, A08, MF-A02).

NCEER-94-0019 "Proceedings of the International Workshop on Civil Infrastructure Systems: Application of Intelligent Systems and Advanced Materials on Bridge Systems," Edited by G.C. Lee and K.C. Chang, 7/18/94, (PB95-252474, A20, MF-A04).

NCEER-94-0020 "Study of Seismic Isolation Systems for Computer Floors," by V. Lambrou and M.C. Constantinou, 7/19/94, (PB95-138533, A10, MF-A03).

NCEER-94-0021 "Proceedings of the U.S.-Italian Workshop on Guidelines for Seismic Evaluation and Rehabilitation of Unreinforced Masonry Buildings," Edited by D.P. Abrams and G.M. Calvi, 7/20/94, (PB95-138749, A13, MF-A03).

NCEER-94-0022 "NCEER-Taisei Corporation Research Program on Sliding Seismic Isolation Systems for Bridges: Experimental and Analytical Study of a System Consisting of Lubricated PTFE Sliding Bearings and Mild Steel Dampers," by P. Tsopelas and M.C. Constantinou, 7/22/94, (PB95-182184, A08, MF-A02).

NCEER-94-0023 "Development of Reliability-Based Design Criteria for Buildings Under Seismic Load," by Y.K. Wen, H. Hwang and M. Shinozuka, 8/1/94, (PB95-211934, A08, MF-A02).

NCEER-94-0024 "Experimental Verification of Acceleration Feedback Control Strategies for an Active Tendon System," by S.J. Dyke, B.F. Spencer, Jr., P. Quast, M.K. Sain, D.C. Kaspari, Jr. and T.T. Soong, 8/29/94, (PB95-212320, A05, MF-A01).

NCEER-94-0025 "Seismic Retrofitting Manual for Highway Bridges," Edited by I.G. Buckle and I.F. Friedland, published by the Federal Highway Administration (PB95-212676, A15, MF-A03).

NCEER-94-0026 "Proceedings from the Fifth U.S.-Japan Workshop on Earthquake Resistant Design of Lifeline Facilities and Countermeasures Against Soil Liquefaction," Edited by T.D. O'Rourke and M. Hamada, 11/7/94, (PB95-220802, A99, MF-E08).

NCEER-95-0001 "Experimental and Analytical Investigation of Seismic Retrofit of Structures with Supplemental Damping: Part 1 - Fluid Viscous Damping Devices," by A.M. Reinhorn, C. Li and M.C. Constantinou, 1/3/95, (PB95-266599, A09, MF-A02).

NCEER-95-0002 "Experimental and Analytical Study of Low-Cycle Fatigue Behavior of Semi-Rigid Top-And-Seat Angle Connections," by G. Pekcan, J.B. Mander and S.S. Chen, 1/5/95, (PB95-220042, A07, MF-A02).

NCEER-95-0003 "NCEER-ATC Joint Study on Fragility of Buildings," by T. Anagnos, C. Rojahn and A.S. Kiremidjian, 1/20/95, (PB95-220026, A06, MF-A02).

NCEER-95-0004 "Nonlinear Control Algorithms for Peak Response Reduction," by Z. Wu, T.T. Soong, V. Gattulli and R.C. Lin, 2/16/95, (PB95-220349, A05, MF-A01).

NCEER-95-0005 "Pipeline Replacement Feasibility Study: A Methodology for Minimizing Seismic and Corrosion Risks to Underground Natural Gas Pipelines," by R.T. Eguchi, H.A. Seligson and D.G. Honegger, 3/2/95, (PB95-252326, A06, MF-A02).

NCEER-95-0006 "Evaluation of Seismic Performance of an 11-Story Frame Building During the 1994 Northridge Earthquake," by F. Naeim, R. DiSulio, K. Benuska, A. Reinhorn and C. Li, not available.

NCEER-95-0007 "Prioritization of Bridges for Seismic Retrofitting," by N. Basöz and A.S. Kiremidjian, 4/24/95, (PB95-252300, A08, MF-A02).

NCEER-95-0008 "Method for Developing Motion Damage Relationships for Reinforced Concrete Frames," by A. Singhal and A.S. Kiremidjian, 5/11/95, (PB95-266607, A06, MF-A02).

NCEER-95-0009 "Experimental and Analytical Investigation of Seismic Retrofit of Structures with Supplemental Damping: Part II - Friction Devices," by C. Li and A.M. Reinhorn, 7/6/95, (PB96-128087, A11, MF-A03).

NCEER-95-0010 "Experimental Performance and Analytical Study of a Non-Ductile Reinforced Concrete Frame Structure Retrofitted with Elastomeric Spring Dampers," by G. Pekcan, J.B. Mander and S.S. Chen, 7/14/95, (PB96-137161, A08, MF-A02).

NCEER-95-0011 "Development and Experimental Study of Semi-Active Fluid Damping Devices for Seismic Protection of Structures," by M.D. Symans and M.C. Constantinou, 8/3/95, (PB96-136940, A23, MF-A04).

NCEER-95-0012 "Real-Time Structural Parameter Modification (RSPM): Development of Innervated Structures," by Z. Liang, M. Tong and G.C. Lee, 4/11/95, (PB96-137153, A06, MF-A01).

NCEER-95-0013 "Experimental and Analytical Investigation of Seismic Retrofit of Structures with Supplemental Damping: Part III - Viscous Damping Walls," by A.M. Reinhorn and C. Li, 10/1/95, (PB96-176409, A11, MF-A03).

NCEER-95-0014 "Seismic Fragility Analysis of Equipment and Structures in a Memphis Electric Substation," by J-R. Huo and H.H.M. Hwang, 8/10/95, (PB96-128087, A09, MF-A02).

NCEER-95-0015 "The Hanshin-Awaji Earthquake of January 17, 1995: Performance of Lifelines," Edited by M. Shinozuka, 11/3/95, (PB96-176383, A15, MF-A03).

NCEER-95-0016 "Highway Culvert Performance During Earthquakes," by T.L. Youd and C.J. Beckman, available as NCEER-96-0015.

NCEER-95-0017 "The Hanshin-Awaji Earthquake of January 17, 1995: Performance of Highway Bridges," Edited by I.G. Buckle, 12/1/95, not available.

NCEER-95-0018 "Modeling of Masonry Infill Panels for Structural Analysis," by A.M. Reinhorn, A. Madan, R.E. Valles, Y. Reichmann and J.B. Mander, 12/8/95, (PB97-110886, MF-A01, A06).

NCEER-95-0019 "Optimal Polynomial Control for Linear and Nonlinear Structures," by A.K. Agrawal and J.N. Yang, 12/11/95, (PB96-168737, A07, MF-A02).

NCEER-95-0020 "Retrofit of Non-Ductile Reinforced Concrete Frames Using Friction Dampers," by R.S. Rao, P. Gergely and R.N. White, 12/22/95, (PB97-133508, A10, MF-A02).

NCEER-95-0021 "Parametric Results for Seismic Response of Pile-Supported Bridge Bents," by G. Mylonakis, A. Nikolaou and G. Gazetas, 12/22/95, (PB97-100242, A12, MF-A03).

NCEER-95-0022 "Kinematic Bending Moments in Seismically Stressed Piles," by A. Nikolaou, G. Mylonakis and G. Gazetas, 12/23/95, (PB97-113914, MF-A03, A13).

NCEER-96-0001 "Dynamic Response of Unreinforced Masonry Buildings with Flexible Diaphragms," by A.C. Costley and D.P. Abrams," 10/10/96, (PB97-133573, MF-A03, A15).

NCEER-96-0002 "State of the Art Review: Foundations and Retaining Structures," by I. Po Lam, not available.

NCEER-96-0003 "Ductility of Rectangular Reinforced Concrete Bridge Columns with Moderate Confinement," by N. Wehbe, M. Saiidi, D. Sanders and B. Douglas, 11/7/96, (PB97-133557, A06, MF-A02).

NCEER-96-0004 "Proceedings of the Long-Span Bridge Seismic Research Workshop," edited by I.G. Buckle and I.M. Friedland, not available.

NCEER-96-0005 "Establish Representative Pier Types for Comprehensive Study: Eastern United States," by J. Kulicki and Z. Prucz, 5/28/96, (PB98-119217, A07, MF-A02).

NCEER-96-0006 "Establish Representative Pier Types for Comprehensive Study: Western United States," by R. Imbsen, R.A. Schamber and T.A. Osterkamp, 5/28/96, (PB98-118607, A07, MF-A02).

NCEER-96-0007 "Nonlinear Control Techniques for Dynamical Systems with Uncertain Parameters," by R.G. Ghanem and M.I. Bujakov, 5/27/96, (PB97-100259, A17, MF-A03).

NCEER-96-0008 "Seismic Evaluation of a 30-Year Old Non-Ductile Highway Bridge Pier and Its Retrofit," by J.B. Mander, B. Mahmoodzadegan, S. Bhadra and S.S. Chen, 5/31/96, (PB97-110902, MF-A03, A10).

NCEER-96-0009 "Seismic Performance of a Model Reinforced Concrete Bridge Pier Before and After Retrofit," by J.B. Mander, J.H. Kim and C.A. Ligozio, 5/31/96, (PB97-110910, MF-A02, A10).

NCEER-96-0010 "IDARC2D Version 4.0: A Computer Program for the Inelastic Damage Analysis of Buildings," by R.E. Valles, A.M. Reinhorn, S.K. Kunnath, C. Li and A. Madan, 6/3/96, (PB97-100234, A17, MF-A03).

NCEER-96-0011 "Estimation of the Economic Impact of Multiple Lifeline Disruption: Memphis Light, Gas and Water Division Case Study," by S.E. Chang, H.A. Seligson and R.T. Eguchi, 8/16/96, (PB97-133490, A11, MF-A03).

NCEER-96-0012 "Proceedings from the Sixth Japan-U.S. Workshop on Earthquake Resistant Design of Lifeline Facilities and Countermeasures Against Soil Liquefaction, Edited by M. Hamada and T. O'Rourke, 9/11/96, (PB97-133581, A99, MF-A06).

NCEER-96-0013 "Chemical Hazards, Mitigation and Preparedness in Areas of High Seismic Risk: A Methodology for Estimating the Risk of Post-Earthquake Hazardous Materials Release," by H.A. Seligson, R.T. Eguchi, K.J. Tierney and K. Richmond, 11/7/96, (PB97-133565, MF-A02, A08).

NCEER-96-0014 "Response of Steel Bridge Bearings to Reversed Cyclic Loading," by J.B. Mander, D-K. Kim, S.S. Chen and G.J. Premus, 11/13/96, (PB97-140735, A12, MF-A03).

NCEER-96-0015 "Highway Culvert Performance During Past Earthquakes," by T.L. Youd and C.J. Beckman, 11/25/96, (PB97-133532, A06, MF-A01).

NCEER-97-0001 "Evaluation, Prevention and Mitigation of Pounding Effects in Building Structures," by R.E. Valles and A.M. Reinhorn, 2/20/97, (PB97-159552, A14, MF-A03).

NCEER-97-0002 "Seismic Design Criteria for Bridges and Other Highway Structures," by C. Rojahn, R. Mayes, D.G. Anderson, J. Clark, J.H. Hom, R.V. Nutt and M.J. O'Rourke, 4/30/97, (PB97-194658, A06, MF-A03).

NCEER-97-0003 "Proceedings of the U.S.-Italian Workshop on Seismic Evaluation and Retrofit," Edited by D.P. Abrams and G.M. Calvi, 3/19/97, (PB97-194666, A13, MF-A03).

NCEER-97-0004 "Investigation of Seismic Response of Buildings with Linear and Nonlinear Fluid Viscous Dampers," by A.A. Seleemah and M.C. Constantinou, 5/21/97, (PB98-109002, A15, MF-A03).

NCEER-97-0005 "Proceedings of the Workshop on Earthquake Engineering Frontiers in Transportation Facilities," edited by G.C. Lee and I.M. Friedland, 8/29/97, (PB98-128911, A25, MR-A04).

NCEER-97-0006 "Cumulative Seismic Damage of Reinforced Concrete Bridge Piers," by S.K. Kunnath, A. El-Bahy, A. Taylor and W. Stone, 9/2/97, (PB98-108814, A11, MF-A03).

NCEER-97-0007 "Structural Details to Accommodate Seismic Movements of Highway Bridges and Retaining Walls," by R.A. Imbsen, R.A. Schamber, E. Thorkildsen, A. Kartoum, B.T. Martin, T.N. Rosser and J.M. Kulicki, 9/3/97, (PB98-108996, A09, MF-A02).

NCEER-97-0008 "A Method for Earthquake Motion-Damage Relationships with Application to Reinforced Concrete Frames," by A. Singhal and A.S. Kiremidjian, 9/10/97, (PB98-108988, A13, MF-A03).

NCEER-97-0009 "Seismic Analysis and Design of Bridge Abutments Considering Sliding and Rotation," by K. Fishman and R. Richards, Jr., 9/15/97, (PB98-108897, A06, MF-A02).

NCEER-97-0010 "Proceedings of the FHWA/NCEER Workshop on the National Representation of Seismic Ground Motion for New and Existing Highway Facilities," edited by I.M. Friedland, M.S. Power and R.L. Mayes, 9/22/97, (PB98-128903, A21, MF-A04).

NCEER-97-0011 "Seismic Analysis for Design or Retrofit of Gravity Bridge Abutments," by K.L. Fishman, R. Richards, Jr. and R.C. Divito, 10/2/97, (PB98-128937, A08, MF-A02).

NCEER-97-0012 "Evaluation of Simplified Methods of Analysis for Yielding Structures," by P. Tsopelas, M.C. Constantinou, C.A. Kircher and A.S. Whittaker, 10/31/97, (PB98-128929, A10, MF-A03).

NCEER-97-0013 "Seismic Design of Bridge Columns Based on Control and Repairability of Damage," by C-T. Cheng and J.B. Mander, 12/8/97, (PB98-144249, A11, MF-A03).

NCEER-97-0014 "Seismic Resistance of Bridge Piers Based on Damage Avoidance Design," by J.B. Mander and C-T. Cheng, 12/10/97, (PB98-144223, A09, MF-A02).

NCEER-97-0015 "Seismic Response of Nominally Symmetric Systems with Strength Uncertainty," by S. Balopoulou and M. Grigoriu, 12/23/97, (PB98-153422, A11, MF-A03).

NCEER-97-0016 "Evaluation of Seismic Retrofit Methods for Reinforced Concrete Bridge Columns," by T.J. Wipf, F.W. Klaiber and F.M. Russo, 12/28/97, (PB98-144215, A12, MF-A03).

NCEER-97-0017 "Seismic Fragility of Existing Conventional Reinforced Concrete Highway Bridges," by C.L. Mullen and A.S. Cakmak, 12/30/97, (PB98-153406, A08, MF-A02).

NCEER-97-0018 "Loss Asssessment of Memphis Buildings," edited by D.P. Abrams and M. Shinozuka, 12/31/97, (PB98-144231, A13, MF-A03).

NCEER-97-0019 "Seismic Evaluation of Frames with Infill Walls Using Quasi-static Experiments," by K.M. Mosalam, R.N. White and P. Gergely, 12/31/97, (PB98-153455, A07, MF-A02).

NCEER-97-0020 "Seismic Evaluation of Frames with Infill Walls Using Pseudo-dynamic Experiments," by K.M. Mosalam, R.N. White and P. Gergely, 12/31/97, (PB98-153430, A07, MF-A02).

NCEER-97-0021 "Computational Strategies for Frames with Infill Walls: Discrete and Smeared Crack Analyses and Seismic Fragility," by K.M. Mosalam, R.N. White and P. Gergely, 12/31/97, (PB98-153414, A10, MF-A02).

NCEER-97-0022 "Proceedings of the NCEER Workshop on Evaluation of Liquefaction Resistance of Soils," edited by T.L. Youd and I.M. Idriss, 12/31/97, (PB98-155617, A15, MF-A03).

MCEER-98-0001 "Extraction of Nonlinear Hysteretic Properties of Seismically Isolated Bridges from Quick-Release Field Tests," by Q. Chen, B.M. Douglas, E.M. Maragakis and I.G. Buckle, 5/26/98, (PB99-118838, A06, MF-A01).

MCEER-98-0002 "Methodologies for Evaluating the Importance of Highway Bridges," by A. Thomas, S. Eshenaur and J. Kulicki, 5/29/98, (PB99-118846, A10, MF-A02).

MCEER-98-0003 "Capacity Design of Bridge Piers and the Analysis of Overstrength," by J.B. Mander, A. Dutta and P. Goel, 6/1/98, (PB99-118853, A09, MF-A02).

MCEER-98-0004 "Evaluation of Bridge Damage Data from the Loma Prieta and Northridge, California Earthquakes," by N. Basoz and A. Kiremidjian, 6/2/98, (PB99-118861, A15, MF-A03).

MCEER-98-0005 "Screening Guide for Rapid Assessment of Liquefaction Hazard at Highway Bridge Sites," by T. L. Youd, 6/16/98, (PB99-118879, A06, not available on microfiche).

MCEER-98-0006 "Structural Steel and Steel/Concrete Interface Details for Bridges," by P. Ritchie, N. Kauhl and J. Kulicki, 7/13/98, (PB99-118945, A06, MF-A01).

MCEER-98-0007 "Capacity Design and Fatigue Analysis of Confined Concrete Columns," by A. Dutta and J.B. Mander, 7/14/98, (PB99-118960, A14, MF-A03).

MCEER-98-0008 "Proceedings of the Workshop on Performance Criteria for Telecommunication Services Under Earthquake Conditions," edited by A.J. Schiff, 7/15/98, (PB99-118952, A08, MF-A02).

MCEER-98-0009 "Fatigue Analysis of Unconfined Concrete Columns," by J.B. Mander, A. Dutta and J.H. Kim, 9/12/98, (PB99-123655, A10, MF-A02).

MCEER-98-0010 "Centrifuge Modeling of Cyclic Lateral Response of Pile-Cap Systems and Seat-Type Abutments in Dry Sands," by A.D. Gadre and R. Dobry, 10/2/98, (PB99-123606, A13, MF-A03).

MCEER-98-0011 "IDARC-BRIDGE: A Computational Platform for Seismic Damage Assessment of Bridge Structures," by A.M. Reinhorn, V. Simeonov, G. Mylonakis and Y. Reichman, 10/2/98, (PB99-162919, A15, MF-A03).

MCEER-98-0012 "Experimental Investigation of the Dynamic Response of Two Bridges Before and After Retrofitting with Elastomeric Bearings," by D.A. Wendichansky, S.S. Chen and J.B. Mander, 10/2/98, (PB99-162927, A15, MF-A03).

MCEER-98-0013 "Design Procedures for Hinge Restrainers and Hinge Sear Width for Multiple-Frame Bridges," by R. Des Roches and G.L. Fenves, 11/3/98, (PB99-140477, A13, MF-A03).

MCEER-98-0014 "Response Modification Factors for Seismically Isolated Bridges," by M.C. Constantinou and J.K. Quarshie, 11/3/98, (PB99-140485, A14, MF-A03).

MCEER-98-0015 "Proceedings of the U.S.-Italy Workshop on Seismic Protective Systems for Bridges," edited by I.M. Friedland and M.C. Constantinou, 11/3/98, (PB2000-101711, A22, MF-A04).

MCEER-98-0016 "Appropriate Seismic Reliability for Critical Equipment Systems: Recommendations Based on Regional Analysis of Financial and Life Loss," by K. Porter, C. Scawthorn, C. Taylor and N. Blais, 11/10/98, (PB99-157265, A08, MF-A02).

MCEER-98-0017 "Proceedings of the U.S. Japan Joint Seminar on Civil Infrastructure Systems Research," edited by M. Shinozuka and A. Rose, 11/12/98, (PB99-156713, A16, MF-A03).

MCEER-98-0018 "Modeling of Pile Footings and Drilled Shafts for Seismic Design," by I. PoLam, M. Kapuskar and D. Chaudhuri, 12/21/98, (PB99-157257, A09, MF-A02).

MCEER-99-0001 "Seismic Evaluation of a Masonry Infilled Reinforced Concrete Frame by Pseudodynamic Testing," by S.G. Buonopane and R.N. White, 2/16/99, (PB99-162851, A09, MF-A02).

MCEER-99-0002 "Response History Analysis of Structures with Seismic Isolation and Energy Dissipation Systems: Verification Examples for Program SAP2000," by J. Scheller and M.C. Constantinou, 2/22/99, (PB99-162869, A08, MF-A02).

MCEER-99-0003 "Experimental Study on the Seismic Design and Retrofit of Bridge Columns Including Axial Load Effects," by A. Dutta, T. Kokorina and J.B. Mander, 2/22/99, (PB99-162877, A09, MF-A02).

MCEER-99-0004 "Experimental Study of Bridge Elastomeric and Other Isolation and Energy Dissipation Systems with Emphasis on Uplift Prevention and High Velocity Near-source Seismic Excitation," by A. Kasalanati and M. C. Constantinou, 2/26/99, (PB99-162885, A12, MF-A03).

MCEER-99-0005 "Truss Modeling of Reinforced Concrete Shear-flexure Behavior," by J.H. Kim and J.B. Mander, 3/8/99, (PB99-163693, A12, MF-A03).

MCEER-99-0006 "Experimental Investigation and Computational Modeling of Seismic Response of a 1:4 Scale Model Steel Structure with a Load Balancing Supplemental Damping System," by G. Pekcan, J.B. Mander and S.S. Chen, 4/2/99, (PB99-162893, A11, MF-A03).

MCEER-99-0007 "Effect of Vertical Ground Motions on the Structural Response of Highway Bridges," by M.R. Button, C.J. Cronin and R.L. Mayes, 4/10/99, (PB2000-101411, A10, MF-A03).

MCEER-99-0008 "Seismic Reliability Assessment of Critical Facilities: A Handbook, Supporting Documentation, and Model Code Provisions," by G.S. Johnson, R.E. Sheppard, M.D. Quilici, S.J. Eder and C.R. Scawthorn, 4/12/99, (PB2000-101701, A18, MF-A04).

MCEER-99-0009 "Impact Assessment of Selected MCEER Highway Project Research on the Seismic Design of Highway Structures," by C. Rojahn, R. Mayes, D.G. Anderson, J.H. Clark, D'Appolonia Engineering, S. Gloyd and R.V. Nutt, 4/14/99, (PB99-162901, A10, MF-A02).

MCEER-99-0010 "Site Factors and Site Categories in Seismic Codes," by R. Dobry, R. Ramos and M.S. Power, 7/19/99, (PB2000-101705, A08, MF-A02).

MCEER-99-0011 "Restrainer Design Procedures for Multi-Span Simply-Supported Bridges," by M.J. Randall, M. Saiidi, E. Maragakis and T. Isakovic, 7/20/99, (PB2000-101702, A10, MF-A02).

MCEER-99-0012 "Property Modification Factors for Seismic Isolation Bearings," by M.C. Constantinou, P. Tsopelas, A. Kasalanati and E. Wolff, 7/20/99, (PB2000-103387, A11, MF-A03).

MCEER-99-0013 "Critical Seismic Issues for Existing Steel Bridges," by P. Ritchie, N. Kauhl and J. Kulicki, 7/20/99, (PB2000-101697, A09, MF-A02).

MCEER-99-0014 "Nonstructural Damage Database," by A. Kao, T.T. Soong and A. Vender, 7/24/99, (PB2000-101407, A06, MF-A01).

MCEER-99-0015 "Guide to Remedial Measures for Liquefaction Mitigation at Existing Highway Bridge Sites," by H.G. Cooke and J. K. Mitchell, 7/26/99, (PB2000-101703, A11, MF-A03).

MCEER-99-0016 "Proceedings of the MCEER Workshop on Ground Motion Methodologies for the Eastern United States," edited by N. Abrahamson and A. Becker, 8/11/99, (PB2000-103385, A07, MF-A02).

MCEER-99-0017 "Quindío, Colombia Earthquake of January 25, 1999: Reconnaissance Report," by A.P. Asfura and P.J. Flores, 10/4/99, (PB2000-106893, A06, MF-A01).

MCEER-99-0018 "Hysteretic Models for Cyclic Behavior of Deteriorating Inelastic Structures," by M.V. Sivaselvan and A.M. Reinhorn, 11/5/99, (PB2000-103386, A08, MF-A02).

MCEER-99-0019 "Proceedings of the 7th U.S.- Japan Workshop on Earthquake Resistant Design of Lifeline Facilities and Countermeasures Against Soil Liquefaction," edited by T.D. O'Rourke, J.P. Bardet and M. Hamada, 11/19/99, (PB2000-103354, A99, MF-A06).

MCEER-99-0020 "Development of Measurement Capability for Micro-Vibration Evaluations with Application to Chip Fabrication Facilities," by G.C. Lee, Z. Liang, J.W. Song, J.D. Shen and W.C. Liu, 12/1/99, (PB2000-105993, A08, MF-A02).

MCEER-99-0021 "Design and Retrofit Methodology for Building Structures with Supplemental Energy Dissipating Systems," by G. Pekcan, J.B. Mander and S.S. Chen, 12/31/99, (PB2000-105994, A11, MF-A03).

MCEER-00-0001 "The Marmara, Turkey Earthquake of August 17, 1999: Reconnaissance Report," edited by C. Scawthorn; with major contributions by M. Bruneau, R. Eguchi, T. Holzer, G. Johnson, J. Mander, J. Mitchell, W. Mitchell, A. Papageorgiou, C. Scaethorn, and G. Webb, 3/23/00, (PB2000-106200, A11, MF-A03).

MCEER-00-0002 "Proceedings of the MCEER Workshop for Seismic Hazard Mitigation of Health Care Facilities," edited by G.C. Lee, M. Ettouney, M. Grigoriu, J. Hauer and J. Nigg, 3/29/00, (PB2000-106892, A08, MF-A02).

MCEER-00-0003 "The Chi-Chi, Taiwan Earthquake of September 21, 1999: Reconnaissance Report," edited by G.C. Lee and C.H. Loh, with major contributions by G.C. Lee, M. Bruneau, I.G. Buckle, S.E. Chang, P.J. Flores, T.D. O'Rourke, M. Shinozuka, T.T. Soong, C-H. Loh, K-C. Chang, Z-J. Chen, J-S. Hwang, M-L. Lin, G-Y. Liu, K-C. Tsai, G.C. Yao and C-L. Yen, 4/30/00, (PB2001-100980, A10, MF-A02).

MCEER-00-0004 "Seismic Retrofit of End-Sway Frames of Steel Deck-Truss Bridges with a Supplemental Tendon System: Experimental and Analytical Investigation," by G. Pekcan, J.B. Mander and S.S. Chen, 7/1/00, (PB2001-100982, A10, MF-A02).

MCEER-00-0005 "Sliding Fragility of Unrestrained Equipment in Critical Facilities," by W.H. Chong and T.T. Soong, 7/5/00, (PB2001-100983, A08, MF-A02).

MCEER-00-0006 "Seismic Response of Reinforced Concrete Bridge Pier Walls in the Weak Direction," by N. Abo-Shadi, M. Saiidi and D. Sanders, 7/17/00, (PB2001-100981, A17, MF-A03).

MCEER-00-0007 "Low-Cycle Fatigue Behavior of Longitudinal Reinforcement in Reinforced Concrete Bridge Columns," by J. Brown and S.K. Kunnath, 7/23/00, (PB2001-104392, A08, MF-A02).

MCEER-00-0008 "Soil Structure Interaction of Bridges for Seismic Analysis," I. PoLam and H. Law, 9/25/00, (PB2001-105397, A08, MF-A02).

MCEER-00-0009 "Proceedings of the First MCEER Workshop on Mitigation of Earthquake Disaster by Advanced Technologies (MEDAT-1), edited by M. Shinozuka, D.J. Inman and T.D. O'Rourke, 11/10/00, (PB2001-105399, A14, MF-A03).

MCEER-00-0010 "Development and Evaluation of Simplified Procedures for Analysis and Design of Buildings with Passive Energy Dissipation Systems, Revision 01," by O.M. Ramirez, M.C. Constantinou, C.A. Kircher, A.S. Whittaker, M.W. Johnson, J.D. Gomez and C. Chrysostomou, 11/16/01, (PB2001-105523, A23, MF-A04).

MCEER-00-0011 "Dynamic Soil-Foundation-Structure Interaction Analyses of Large Caissons," by C-Y. Chang, C-M. Mok, Z-L. Wang, R. Settgast, F. Waggoner, M.A. Ketchum, H.M. Gonnermann and C-C. Chin, 12/30/00, (PB2001-104373, A07, MF-A02).

MCEER-00-0012 "Experimental Evaluation of Seismic Performance of Bridge Restrainers," by A.G. Vlassis, E.M. Maragakis and M. Saiid Saiidi, 12/30/00, (PB2001-104354, A09, MF-A02).

MCEER-00-0013 "Effect of Spatial Variation of Ground Motion on Highway Structures," by M. Shinozuka, V. Saxena and G. Deodatis, 12/31/00, (PB2001-108755, A13, MF-A03).

MCEER-00-0014 "A Risk-Based Methodology for Assessing the Seismic Performance of Highway Systems," by S.D. Werner, C.E. Taylor, J.E. Moore, II, J.S. Walton and S. Cho, 12/31/00, (PB2001-108756, A14, MF-A03).

MCEER-01-0001 "Experimental Investigation of P-Delta Effects to Collapse During Earthquakes," by D. Vian and M. Bruneau, 6/25/01, (PB2002-100534, A17, MF-A03).

MCEER-01-0002 "Proceedings of the Second MCEER Workshop on Mitigation of Earthquake Disaster by Advanced Technologies (MEDAT-2)," edited by M. Bruneau and D.J. Inman, 7/23/01, (PB2002-100434, A16, MF-A03).

MCEER-01-0003 "Sensitivity Analysis of Dynamic Systems Subjected to Seismic Loads," by C. Roth and M. Grigoriu, 9/18/01, (PB2003-100884, A12, MF-A03).

MCEER-01-0004 "Overcoming Obstacles to Implementing Earthquake Hazard Mitigation Policies: Stage 1 Report," by D.J. Alesch and W.J. Petak, 12/17/01, (PB2002-107949, A07, MF-A02).

MCEER-01-0005 "Updating Real-Time Earthquake Loss Estimates: Methods, Problems and Insights," by C.E. Taylor, S.E. Chang and R.T. Eguchi, 12/17/01, (PB2002-107948, A05, MF-A01).

MCEER-01-0006 "Experimental Investigation and Retrofit of Steel Pile Foundations and Pile Bents Under Cyclic Lateral Loadings," by A. Shama, J. Mander, B. Blabac and S. Chen, 12/31/01, (PB2002-107950, A13, MF-A03).

MCEER-02-0001 "Assessment of Performance of Bolu Viaduct in the 1999 Duzce Earthquake in Turkey" by P.C. Roussis, M.C. Constantinou, M. Erdik, E. Durukal and M. Dicleli, 5/8/02, (PB2003-100883, A08, MF-A02).

MCEER-02-0002 "Seismic Behavior of Rail Counterweight Systems of Elevators in Buildings," by M.P. Singh, Rildova and L.E. Suarez, 5/27/02. (PB2003-100882, A11, MF-A03).

MCEER-02-0003 "Development of Analysis and Design Procedures for Spread Footings," by G. Mylonakis, G. Gazetas, S. Nikolaou and A. Chauncey, 10/02/02, (PB2004-101636, A13, MF-A03, CD-A13).

MCEER-02-0004 "Bare-Earth Algorithms for Use with SAR and LIDAR Digital Elevation Models," by C.K. Huyck, R.T. Eguchi and B. Houshmand, 10/16/02, (PB2004-101637, A07, CD-A07).

MCEER-02-0005 "Review of Energy Dissipation of Compression Members in Concentrically Braced Frames," by K.Lee and M. Bruneau, 10/18/02, (PB2004-101638, A10, CD-A10).

MCEER-03-0001 "Experimental Investigation of Light-Gauge Steel Plate Shear Walls for the Seismic Retrofit of Buildings" by J. Berman and M. Bruneau, 5/2/03, (PB2004-101622, A10, MF-A03, CD-A10).

MCEER-03-0002 "Statistical Analysis of Fragility Curves," by M. Shinozuka, M.Q. Feng, H. Kim, T. Uzawa and T. Ueda, 6/16/03, (PB2004-101849, A09, CD-A09).

MCEER-03-0003 "Proceedings of the Eighth U.S.-Japan Workshop on Earthquake Resistant Design f Lifeline Facilities and Countermeasures Against Liquefaction," edited by M. Hamada, J.P. Bardet and T.D. O'Rourke, 6/30/03, (PB2004-104386, A99, CD-A99).

MCEER-03-0004 "Proceedings of the PRC-US Workshop on Seismic Analysis and Design of Special Bridges," edited by L.C. Fan and G.C. Lee, 7/15/03, (PB2004-104387, A14, CD-A14).

MCEER-03-0005 "Urban Disaster Recovery: A Framework and Simulation Model," by S.B. Miles and S.E. Chang, 7/25/03, (PB2004-104388, A07, CD-A07).

MCEER-03-0006 "Behavior of Underground Piping Joints Due to Static and Dynamic Loading," by R.D. Meis, M. Maragakis and R. Siddharthan, 11/17/03, (PB2005-102194, A13, MF-A03, CD-A00).

MCEER-04-0001 "Experimental Study of Seismic Isolation Systems with Emphasis on Secondary System Response and Verification of Accuracy of Dynamic Response History Analysis Methods," by E. Wolff and M. Constantinou, 1/16/04 (PB2005-102195, A99, MF-E08, CD-A00).

MCEER-04-0002 "Tension, Compression and Cyclic Testing of Engineered Cementitious Composite Materials," by K. Kesner and S.L. Billington, 3/1/04, (PB2005-102196, A08, CD-A08).

MCEER-04-0003 "Cyclic Testing of Braces Laterally Restrained by Steel Studs to Enhance Performance During Earthquakes," by O.C. Celik, J.W. Berman and M. Bruneau, 3/16/04, (PB2005-102197, A13, MF-A03, CD-A00).

MCEER-04-0004 "Methodologies for Post Earthquake Building Damage Detection Using SAR and Optical Remote Sensing: Application to the August 17, 1999 Marmara, Turkey Earthquake," by C.K. Huyck, B.J. Adams, S. Cho, R.T. Eguchi, B. Mansouri and B. Houshmand, 6/15/04, (PB2005-104888, A10, CD-A00).

MCEER-04-0005 "Nonlinear Structural Analysis Towards Collapse Simulation: A Dynamical Systems Approach," by M.V. Sivaselvan and A.M. Reinhorn, 6/16/04, (PB2005-104889, A11, MF-A03, CD-A00).

MCEER-04-0006 "Proceedings of the Second PRC-US Workshop on Seismic Analysis and Design of Special Bridges," edited by G.C. Lee and L.C. Fan, 6/25/04, (PB2005-104890, A16, CD-A00).

MCEER-04-0007 "Seismic Vulnerability Evaluation of Axially Loaded Steel Built-up Laced Members," by K. Lee and M. Bruneau, 6/30/04, (PB2005-104891, A16, CD-A00).

MCEER-04-0008 "Evaluation of Accuracy of Simplified Methods of Analysis and Design of Buildings with Damping Systems for Near-Fault and for Soft-Soil Seismic Motions," by E.A. Pavlou and M.C. Constantinou, 8/16/04, (PB2005-104892, A08, MF-A02, CD-A00).

MCEER-04-0009 "Assessment of Geotechnical Issues in Acute Care Facilities in California," by M. Lew, T.D. O'Rourke, R. Dobry and M. Koch, 9/15/04, (PB2005-104893, A08, CD-A00).

MCEER-04-0010 "Scissor-Jack-Damper Energy Dissipation System," by A.N. Sigaher-Boyle and M.C. Constantinou, 12/1/04 (PB2005-108221).

MCEER-04-0011 "Seismic Retrofit of Bridge Steel Truss Piers Using a Controlled Rocking Approach," by M. Pollino and M. Bruneau, 12/20/04 (PB2006-105795).

MCEER-05-0001 "Experimental and Analytical Studies of Structures Seismically Isolated with an Uplift-Restraint Isolation System," by P.C. Roussis and M.C. Constantinou, 1/10/05 (PB2005-108222).

MCEER-05-0002 "A Versatile Experimentation Model for Study of Structures Near Collapse Applied to Seismic Evaluation of Irregular Structures," by D. Kusumastuti, A.M. Reinhorn and A. Rutenberg, 3/31/05 (PB2006-101523).

MCEER-05-0003 "Proceedings of the Third PRC-US Workshop on Seismic Analysis and Design of Special Bridges," edited by L.C. Fan and G.C. Lee, 4/20/05, (PB2006-105796).

MCEER-05-0004 "Approaches for the Seismic Retrofit of Braced Steel Bridge Piers and Proof-of-Concept Testing of an Eccentrically Braced Frame with Tubular Link," by J.W. Berman and M. Bruneau, 4/21/05 (PB2006-101524).

MCEER-05-0005 "Simulation of Strong Ground Motions for Seismic Fragility Evaluation of Nonstructural Components in Hospitals," by A. Wanitkorkul and A. Filiatrault, 5/26/05 (PB2006-500027).

MCEER-05-0006 "Seismic Safety in California Hospitals: Assessing an Attempt to Accelerate the Replacement or Seismic Retrofit of Older Hospital Facilities," by D.J. Alesch, L.A. Arendt and W.J. Petak, 6/6/05 (PB2006-105794).

MCEER-05-0007 "Development of Seismic Strengthening and Retrofit Strategies for Critical Facilities Using Engineered Cementitious Composite Materials," by K. Kesner and S.L. Billington, 8/29/05 (PB2006-111701).

MCEER-05-0008 "Experimental and Analytical Studies of Base Isolation Systems for Seismic Protection of Power Transformers," by N. Murota, M.Q. Feng and G-Y. Liu, 9/30/05 (PB2006-111702).

MCEER-05-0009 "3D-BASIS-ME-MB: Computer Program for Nonlinear Dynamic Analysis of Seismically Isolated Structures," by P.C. Tsopelas, P.C. Roussis, M.C. Constantinou, R. Buchanan and A.M. Reinhorn, 10/3/05 (PB2006-111703).

MCEER-05-0010 "Steel Plate Shear Walls for Seismic Design and Retrofit of Building Structures," by D. Vian and M. Bruneau, 12/15/05 (PB2006-111704).

MCEER-05-0011 "The Performance-Based Design Paradigm," by M.J. Astrella and A. Whittaker, 12/15/05 (PB2006-111705).

MCEER-06-0001 "Seismic Fragility of Suspended Ceiling Systems," H. Badillo-Almaraz, A.S. Whittaker, A.M. Reinhorn and G.P. Cimellaro, 2/4/06 (PB2006-111706).

MCEER-06-0002 "Multi-Dimensional Fragility of Structures," by G.P. Cimellaro, A.M. Reinhorn and M. Bruneau, 3/1/06 (PB2007-106974, A09, MF-A02, CD A00).

MCEER-06-0003 "Built-Up Shear Links as Energy Dissipators for Seismic Protection of Bridges," by P. Dusicka, A.M. Itani and I.G. Buckle, 3/15/06 (PB2006-111708).

MCEER-06-0004 "Analytical Investigation of the Structural Fuse Concept," by R.E. Vargas and M. Bruneau, 3/16/06 (PB2006-111709).

MCEER-06-0005 "Experimental Investigation of the Structural Fuse Concept," by R.E. Vargas and M. Bruneau, 3/17/06 (PB2006-111710).

MCEER-06-0006 "Further Development of Tubular Eccentrically Braced Frame Links for the Seismic Retrofit of Braced Steel Truss Bridge Piers," by J.W. Berman and M. Bruneau, 3/27/06 (PB2007-105147).

MCEER-06-0007 "REDARS Validation Report," by S. Cho, C.K. Huyck, S. Ghosh and R.T. Eguchi, 8/8/06 (PB2007-106983).

MCEER-06-0008 "Review of Current NDE Technologies for Post-Earthquake Assessment of Retrofitted Bridge Columns," by J.W. Song, Z. Liang and G.C. Lee, 8/21/06 (PB2007-106984).

MCEER-06-0009 "Liquefaction Remediation in Silty Soils Using Dynamic Compaction and Stone Columns," by S. Thevanayagam, G.R. Martin, R. Nashed, T. Shenthan, T. Kanagalingam and N. Ecemis, 8/28/06 (PB2007-106985).

MCEER-06-0010 "Conceptual Design and Experimental Investigation of Polymer Matrix Composite Infill Panels for Seismic Retrofitting," by W. Jung, M. Chiewanichakorn and A.J. Aref, 9/21/06 (PB2007-106986).

MCEER-06-0011 "A Study of the Coupled Horizontal-Vertical Behavior of Elastomeric and Lead-Rubber Seismic Isolation Bearings," by G.P. Warn and A.S. Whittaker, 9/22/06 (PB2007-108679).

MCEER-06-0012 "Proceedings of the Fourth PRC-US Workshop on Seismic Analysis and Design of Special Bridges: Advancing Bridge Technologies in Research, Design, Construction and Preservation," Edited by L.C. Fan, G.C. Lee and L. Ziang, 10/12/06 (PB2007-109042).

MCEER-06-0013 "Cyclic Response and Low Cycle Fatigue Characteristics of Plate Steels," by P. Dusicka, A.M. Itani and I.G. Buckle, 11/1/06 06 (PB2007-106987).

MCEER-06-0014 "Proceedings of the Second US-Taiwan Bridge Engineering Workshop," edited by W.P. Yen, J. Shen, J-Y. Chen and M. Wang, 11/15/06 (PB2008-500041).

MCEER-06-0015 "User Manual and Technical Documentation for the REDARS^{TM} Import Wizard," by S. Cho, S. Ghosh, C.K. Huyck and S.D. Werner, 11/30/06 (PB2007-114766).

MCEER-06-0016 "Hazard Mitigation Strategy and Monitoring Technologies for Urban and Infrastructure Public Buildings: Proceedings of the China-US Workshops," edited by X.Y. Zhou, A.L. Zhang, G.C. Lee and M. Tong, 12/12/06 (PB2008-500018).

MCEER-07-0001 "Static and Kinetic Coefficients of Friction for Rigid Blocks," by C. Kafali, S. Fathali, M. Grigoriu and A.S. Whittaker, 3/20/07 (PB2007-114767).

MCEER-07-0002 "Hazard Mitigation Investment Decision Making: Organizational Response to Legislative Mandate," by L.A. Arendt, D.J. Alesch and W.J. Petak, 4/9/07 (PB2007-114768).

MCEER-07-0003 "Seismic Behavior of Bidirectional-Resistant Ductile End Diaphragms with Unbonded Braces in Straight or Skewed Steel Bridges," by O. Celik and M. Bruneau, 4/11/07 (PB2008-105141).

MCEER-07-0004 "Modeling Pile Behavior in Large Pile Groups Under Lateral Loading," by A.M. Dodds and G.R. Martin, 4/16/07(PB2008-105142).

MCEER-07-0005 "Experimental Investigation of Blast Performance of Seismically Resistant Concrete-Filled Steel Tube Bridge Piers," by S. Fujikura, M. Bruneau and D. Lopez-Garcia, 4/20/07 (PB2008-105143).

MCEER-07-0006 "Seismic Analysis of Conventional and Isolated Liquefied Natural Gas Tanks Using Mechanical Analogs," by I.P. Christovasilis and A.S. Whittaker, 5/1/07, not available.

MCEER-07-0007 "Experimental Seismic Performance Evaluation of Isolation/Restraint Systems for Mechanical Equipment – Part 1: Heavy Equipment Study," by S. Fathali and A. Filiatrault, 6/6/07 (PB2008-105144).

MCEER-07-0008 "Seismic Vulnerability of Timber Bridges and Timber Substructures," by A.A. Sharma, J.B. Mander, I.M. Friedland and D.R. Allicock, 6/7/07 (PB2008-105145).

MCEER-07-0009 "Experimental and Analytical Study of the XY-Friction Pendulum (XY-FP) Bearing for Bridge Applications," by C.C. Marin-Artieda, A.S. Whittaker and M.C. Constantinou, 6/7/07 (PB2008-105191).

MCEER-07-0010 "Proceedings of the PRC-US Earthquake Engineering Forum for Young Researchers," Edited by G.C. Lee and X.Z. Qi, 6/8/07 (PB2008-500058).

MCEER-07-0011 "Design Recommendations for Perforated Steel Plate Shear Walls," by R. Purba and M. Bruneau, 6/18/07, (PB2008-105192).

MCEER-07-0012 "Performance of Seismic Isolation Hardware Under Service and Seismic Loading," by M.C. Constantinou, A.S. Whittaker, Y. Kalpakidis, D.M. Fenz and G.P. Warn, 8/27/07, (PB2008-105193).

MCEER-07-0013 "Experimental Evaluation of the Seismic Performance of Hospital Piping Subassemblies," by E.R. Goodwin, E. Maragakis and A.M. Itani, 9/4/07, (PB2008-105194).

MCEER-07-0014 "A Simulation Model of Urban Disaster Recovery and Resilience: Implementation for the 1994 Northridge Earthquake," by S. Miles and S.E. Chang, 9/7/07, (PB2008-106426).

MCEER-07-0015 "Statistical and Mechanistic Fragility Analysis of Concrete Bridges," by M. Shinozuka, S. Banerjee and S-H. Kim, 9/10/07, (PB2008-106427).

MCEER-07-0016 "Three-Dimensional Modeling of Inelastic Buckling in Frame Structures," by M. Schachter and AM. Reinhorn, 9/13/07, (PB2008-108125).

MCEER-07-0017 "Modeling of Seismic Wave Scattering on Pile Groups and Caissons," by I. Po Lam, H. Law and C.T. Yang, 9/17/07 (PB2008-108150).

MCEER-07-0018 "Bridge Foundations: Modeling Large Pile Groups and Caissons for Seismic Design," by I. Po Lam, H. Law and G.R. Martin (Coordinating Author), 12/1/07 (PB2008-111190).

MCEER-07-0019 "Principles and Performance of Roller Seismic Isolation Bearings for Highway Bridges," by G.C. Lee, Y.C. Ou, Z. Liang, T.C. Niu and J. Song, 12/10/07 (PB2009-110466).

MCEER-07-0020 "Centrifuge Modeling of Permeability and Pinning Reinforcement Effects on Pile Response to Lateral Spreading," by L.L Gonzalez-Lagos, T. Abdoun and R. Dobry, 12/10/07 (PB2008-111191).

MCEER-07-0021 "Damage to the Highway System from the Pisco, Perú Earthquake of August 15, 2007," by J.S. O'Connor, L. Mesa and M. Nykamp, 12/10/07, (PB2008-108126).

MCEER-07-0022 "Experimental Seismic Performance Evaluation of Isolation/Restraint Systems for Mechanical Equipment – Part 2: Light Equipment Study," by S. Fathali and A. Filiatrault, 12/13/07 (PB2008-111192).

MCEER-07-0023 "Fragility Considerations in Highway Bridge Design," by M. Shinozuka, S. Banerjee and S.H. Kim, 12/14/07 (PB2008-111193).

MCEER-07-0024 “Performance Estimates for Seismically Isolated Bridges,” by G.P. Warn and A.S. Whittaker, 12/30/07 (PB2008-112230).

MCEER-08-0001 “Seismic Performance of Steel Girder Bridge Superstructures with Conventional Cross Frames,” by L.P. Carden, A.M. Itani and I.G. Buckle, 1/7/08, (PB2008-112231).

MCEER-08-0002 “Seismic Performance of Steel Girder Bridge Superstructures with Ductile End Cross Frames with Seismic Isolators,” by L.P. Carden, A.M. Itani and I.G. Buckle, 1/7/08 (PB2008-112232).

MCEER-08-0003 “Analytical and Experimental Investigation of a Controlled Rocking Approach for Seismic Protection of Bridge Steel Truss Piers,” by M. Pollino and M. Bruneau, 1/21/08 (PB2008-112233).

MCEER-08-0004 “Linking Lifeline Infrastructure Performance and Community Disaster Resilience: Models and Multi-Stakeholder Processes,” by S.E. Chang, C. Pasion, K. Tatebe and R. Ahmad, 3/3/08 (PB2008-112234).

MCEER-08-0005 “Modal Analysis of Generally Damped Linear Structures Subjected to Seismic Excitations,” by J. Song, Y-L. Chu, Z. Liang and G.C. Lee, 3/4/08 (PB2009-102311).

MCEER-08-0006 “System Performance Under Multi-Hazard Environments,” by C. Kafali and M. Grigoriu, 3/4/08 (PB2008-112235).

MCEER-08-0007 “Mechanical Behavior of Multi-Spherical Sliding Bearings,” by D.M. Fenz and M.C. Constantinou, 3/6/08 (PB2008-112236).

MCEER-08-0008 “Post-Earthquake Restoration of the Los Angeles Water Supply System,” by T.H.P. Tabucchi and R.A. Davidson, 3/7/08 (PB2008-112237).

MCEER-08-0009 “Fragility Analysis of Water Supply Systems,” by A. Jacobson and M. Grigoriu, 3/10/08 (PB2009-105545).

MCEER-08-0010 “Experimental Investigation of Full-Scale Two-Story Steel Plate Shear Walls with Reduced Beam Section Connections,” by B. Qu, M. Bruneau, C-H. Lin and K-C. Tsai, 3/17/08 (PB2009-106368).

MCEER-08-0011 “Seismic Evaluation and Rehabilitation of Critical Components of Electrical Power Systems,” S. Ersoy, B. Feizi, A. Ashrafi and M. Ala Saadeghvaziri, 3/17/08 (PB2009-105546).

MCEER-08-0012 “Seismic Behavior and Design of Boundary Frame Members of Steel Plate Shear Walls,” by B. Qu and M. Bruneau, 4/26/08 . (PB2009-106744).

MCEER-08-0013 “Development and Appraisal of a Numerical Cyclic Loading Protocol for Quantifying Building System Performance,” by A. Filiatrault, A. Wanitkorkul and M. Constantinou, 4/27/08 (PB2009-107906).

MCEER-08-0014 “Structural and Nonstructural Earthquake Design: The Challenge of Integrating Specialty Areas in Designing Complex, Critical Facilities,” by W.J. Petak and D.J. Alesch, 4/30/08 (PB2009-107907).

MCEER-08-0015 “Seismic Performance Evaluation of Water Systems,” by Y. Wang and T.D. O’Rourke, 5/5/08 (PB2009-107908).

MCEER-08-0016 “Seismic Response Modeling of Water Supply Systems,” by P. Shi and T.D. O’Rourke, 5/5/08 (PB2009-107910).

MCEER-08-0017 “Numerical and Experimental Studies of Self-Centering Post-Tensioned Steel Frames,” by D. Wang and A. Filiatrault, 5/12/08 (PB2009-110479).

MCEER-08-0018 “Development, Implementation and Verification of Dynamic Analysis Models for Multi-Spherical Sliding Bearings,” by D.M. Fenz and M.C. Constantinou, 8/15/08 (PB2009-107911).

MCEER-08-0019 “Performance Assessment of Conventional and Base Isolated Nuclear Power Plants for Earthquake Blast Loadings,” by Y.N. Huang, A.S. Whittaker and N. Luco, 10/28/08 (PB2009-107912).

MCEER-08-0020 "Remote Sensing for Resilient Multi-Hazard Disaster Response – Volume I: Introduction to Damage Assessment Methodologies," by B.J. Adams and R.T. Eguchi, 11/17/08 (PB2010-102695).

MCEER-08-0021 "Remote Sensing for Resilient Multi-Hazard Disaster Response – Volume II: Counting the Number of Collapsed Buildings Using an Object-Oriented Analysis: Case Study of the 2003 Bam Earthquake," by L. Gusella, C.K. Huyck and B.J. Adams, 11/17/08 (PB2010-100925).

MCEER-08-0022 "Remote Sensing for Resilient Multi-Hazard Disaster Response – Volume III: Multi-Sensor Image Fusion Techniques for Robust Neighborhood-Scale Urban Damage Assessment," by B.J. Adams and A. McMillan, 11/17/08 (PB2010-100926).

MCEER-08-0023 "Remote Sensing for Resilient Multi-Hazard Disaster Response – Volume IV: A Study of Multi-Temporal and Multi-Resolution SAR Imagery for Post-Katrina Flood Monitoring in New Orleans," by A. McMillan, J.G. Morley, B.J. Adams and S. Chesworth, 11/17/08 (PB2010-100927).

MCEER-08-0024 "Remote Sensing for Resilient Multi-Hazard Disaster Response – Volume V: Integration of Remote Sensing Imagery and VIEWS^{TM} Field Data for Post-Hurricane Charley Building Damage Assessment," by J.A. Womble, K. Mehta and B.J. Adams, 11/17/08 (PB2009-115532).

MCEER-08-0025 "Building Inventory Compilation for Disaster Management: Application of Remote Sensing and Statistical Modeling," by P. Sarabandi, A.S. Kiremidjian, R.T. Eguchi and B. J. Adams, 11/20/08 (PB2009-110484).

MCEER-08-0026 "New Experimental Capabilities and Loading Protocols for Seismic Qualification and Fragility Assessment of Nonstructural Systems," by R. Retamales, G. Mosqueda, A. Filiatrault and A. Reinhorn, 11/24/08 (PB2009-110485).

MCEER-08-0027 "Effects of Heating and Load History on the Behavior of Lead-Rubber Bearings," by I.V. Kalpakidis and M.C. Constantinou, 12/1/08 (PB2009-115533).

MCEER-08-0028 "Experimental and Analytical Investigation of Blast Performance of Seismically Resistant Bridge Piers," by S.Fujikura and M. Bruneau, 12/8/08 (PB2009-115534).

MCEER-08-0029 "Evolutionary Methodology for Aseismic Decision Support," by Y. Hu and G. Dargush, 12/15/08.

MCEER-08-0030 "Development of a Steel Plate Shear Wall Bridge Pier System Conceived from a Multi-Hazard Perspective," by D. Keller and M. Bruneau, 12/19/08 (PB2010-102696).

MCEER-09-0001 "Modal Analysis of Arbitrarily Damped Three-Dimensional Linear Structures Subjected to Seismic Excitations," by Y.L. Chu, J. Song and G.C. Lee, 1/31/09 (PB2010-100922).

MCEER-09-0002 "Air-Blast Effects on Structural Shapes," by G. Ballantyne, A.S. Whittaker, A.J. Aref and G.F. Dargush, 2/2/09 (PB2010-102697).

MCEER-09-0003 "Water Supply Performance During Earthquakes and Extreme Events," by A.L. Bonneau and T.D. O'Rourke, 2/16/09 (PB2010-100923).

MCEER-09-0004 "Generalized Linear (Mixed) Models of Post-Earthquake Ignitions," by R.A. Davidson, 7/20/09 (PB2010-102698).

MCEER-09-0005 "Seismic Testing of a Full-Scale Two-Story Light-Frame Wood Building: NEESWood Benchmark Test," by I.P. Christovasilis, A. Filiatrault and A. Wanitkorkul, 7/22/09 (PB2012-102401).

MCEER-09-0006 "IDARC2D Version 7.0: A Program for the Inelastic Damage Analysis of Structures," by A.M. Reinhorn, H. Roh, M. Sivaselvan, S.K. Kunnath, R.E. Valles, A. Madan, C. Li, R. Lobo and Y.J. Park, 7/28/09 (PB2010-103199).

MCEER-09-0007 "Enhancements to Hospital Resiliency: Improving Emergency Planning for and Response to Hurricanes," by D.B. Hess and L.A. Arendt, 7/30/09 (PB2010-100924).

MCEER-09-0008 "Assessment of Base-Isolated Nuclear Structures for Design and Beyond-Design Basis Earthquake Shaking," by Y.N. Huang, A.S. Whittaker, R.P. Kennedy and R.L. Mayes, 8/20/09 (PB2010-102699).

MCEER-09-0009 "Quantification of Disaster Resilience of Health Care Facilities," by G.P. Cimellaro, C. Fumo, A.M Reinhorn and M. Bruneau, 9/14/09 (PB2010-105384).

MCEER-09-0010 "Performance-Based Assessment and Design of Squat Reinforced Concrete Shear Walls," by C.K. Gulec and A.S. Whittaker, 9/15/09 (PB2010-102700).

MCEER-09-0011 "Proceedings of the Fourth US-Taiwan Bridge Engineering Workshop," edited by W.P. Yen, J.J. Shen, T.M. Lee and R.B. Zheng, 10/27/09 (PB2010-500009).

MCEER-09-0012 "Proceedings of the Special International Workshop on Seismic Connection Details for Segmental Bridge Construction," edited by W. Phillip Yen and George C. Lee, 12/21/09 (PB2012-102402).

MCEER-10-0001 "Direct Displacement Procedure for Performance-Based Seismic Design of Multistory Woodframe Structures," by W. Pang and D. Rosowsky, 4/26/10 (PB2012-102403).

MCEER-10-0002 "Simplified Direct Displacement Design of Six-Story NEESWood Capstone Building and Pre-Test Seismic Performance Assessment," by W. Pang, D. Rosowsky, J. van de Lindt and S. Pei, 5/28/10 (PB2012-102404).

MCEER-10-0003 "Integration of Seismic Protection Systems in Performance-Based Seismic Design of Woodframed Structures," by J.K. Shinde and M.D. Symans, 6/18/10 (PB2012-102405).

MCEER-10-0004 "Modeling and Seismic Evaluation of Nonstructural Components: Testing Frame for Experimental Evaluation of Suspended Ceiling Systems," by A.M. Reinhorn, K.P. Ryu and G. Maddaloni, 6/30/10 (PB2012-102406).

MCEER-10-0005 "Analytical Development and Experimental Validation of a Structural-Fuse Bridge Pier Concept," by S. El-Bahey and M. Bruneau, 10/1/10 (PB2012-102407).

MCEER-10-0006 "A Framework for Defining and Measuring Resilience at the Community Scale: The PEOPLES Resilience Framework," by C.S. Renschler, A.E. Frazier, L.A. Arendt, G.P. Cimellaro, A.M. Reinhorn and M. Bruneau, 10/8/10 (PB2012-102408).

MCEER-10-0007 "Impact of Horizontal Boundary Elements Design on Seismic Behavior of Steel Plate Shear Walls," by R. Purba and M. Bruneau, 11/14/10 (PB2012-102409).

MCEER-10-0008 "Seismic Testing of a Full-Scale Mid-Rise Building: The NEESWood Capstone Test," by S. Pei, J.W. van de Lindt, S.E. Pryor, H. Shimizu, H. Isoda and D.R. Rammer, 12/1/10 (PB2012-102410).

MCEER-10-0009 "Modeling the Effects of Detonations of High Explosives to Inform Blast-Resistant Design," by P. Sherkar, A.S. Whittaker and A.J. Aref, 12/1/10 (PB2012-102411).

MCEER-10-0010 "L'Aquila Earthquake of April 6, 2009 in Italy: Rebuilding a Resilient City to Withstand Multiple Hazards," by G.P. Cimellaro, I.P. Christovasilis, A.M. Reinhorn, A. De Stefano and T. Kirova, 12/29/10.

MCEER-11-0001 "Numerical and Experimental Investigation of the Seismic Response of Light-Frame Wood Structures," by I.P. Christovasilis and A. Filiatrault, 8/8/11 (PB2012-102412).

MCEER-11-0002 "Seismic Design and Analysis of a Precast Segmental Concrete Bridge Model," by M. Anagnostopoulou, A. Filiatrault and A. Aref, 9/15/11.

MCEER-11-0003 'Proceedings of the Workshop on Improving Earthquake Response of Substation Equipment," Edited by A.M. Reinhorn, 9/19/11 (PB2012-102413).

MCEER-11-0004 "LRFD-Based Analysis and Design Procedures for Bridge Bearings and Seismic Isolators," by M.C. Constantinou, I. Kalpakidis, A. Filiatrault and R.A. Ecker Lay, 9/26/11.

MCEER-11-0005 "Experimental Seismic Evaluation, Model Parameterization, and Effects of Cold-Formed Steel-Framed Gypsum Partition Walls on the Seismic Performance of an Essential Facility," by R. Davies, R. Retamales, G. Mosqueda and A. Filiatrault, 10/12/11.

MCEER-11-0006 "Modeling and Seismic Performance Evaluation of High Voltage Transformers and Bushings," by A.M. Reinhorn, K. Oikonomou, H. Roh, A. Schiff and L. Kempner, Jr., 10/3/11.

MCEER-11-0007 "Extreme Load Combinations: A Survey of State Bridge Engineers," by G.C. Lee, Z. Liang, J.J. Shen and J.S. O'Connor, 10/14/11.

MCEER-12-0001 "Simplified Analysis Procedures in Support of Performance Based Seismic Design," by Y.N. Huang and A.S. Whittaker.

MCEER-12-0002 "Seismic Protection of Electrical Transformer Bushing Systems by Stiffening Techniques," by M. Koliou, A. Filiatrault, A.M. Reinhorn and N. Oliveto, 6/1/12.

MCEER-12-0003 "Post-Earthquake Bridge Inspection Guidelines," by J.S. O'Connor and S. Alampalli, 6/8/12.

MCEER-12-0004 "Integrated Design Methodology for Isolated Floor Systems in Single-Degree-of-Freedom Structural Fuse Systems," by S. Cui, M. Bruneau and M.C. Constantinou, 6/13/12.

MCEER-12-0005 "Characterizing the Rotational Components of Earthquake Ground Motion," by D. Basu, A.S. Whittaker and M.C. Constantinou, 6/15/12.

MCEER-12-0006 "Bayesian Fragility for Nonstructural Systems," by C.H. Lee and M.D. Grigoriu, 9/12/12.

MCEER-12-0007 "A Numerical Model for Capturing the In-Plane Seismic Response of Interior Metal Stud Partition Walls," by R.L. Wood and T.C. Hutchinson, 9/12/12.

MCEER-12-0008 "Assessment of Floor Accelerations in Yielding Buildings," by J.D. Wieser, G. Pekcan, A.E. Zaghi, A.M. Itani and E. Maragakis, 10/5/12.

MCEER-13-0001 "Experimental Seismic Study of Pressurized Fire Sprinkler Piping Systems," by Y. Tian, A. Filiatrault and G. Mosqueda, 4/8/13.

MCEER-13-0002 "Enhancing Resource Coordination for Multi-Modal Evacuation Planning," by D.B. Hess, B.W. Conley and C.M. Farrell, 2/8/13.

MCEER-13-0003 "Seismic Response of Base Isolated Buildings Considering Pounding to Moat Walls," by A. Masroor and G. Mosqueda, 2/26/13.

MCEER-13-0004 "Seismic Response Control of Structures Using a Novel Adaptive Passive Negative Stiffness Device," by D.T.R. Pasala, A.A. Sarlis, S. Nagarajaiah, A.M. Reinhorn, M.C. Constantinou and D.P. Taylor, 6/10/13.

MCEER-13-0005 "Negative Stiffness Device for Seismic Protection of Structures," by A.A. Sarlis, D.T.R. Pasala, M.C. Constantinou, A.M. Reinhorn, S. Nagarajaiah and D.P. Taylor, 6/12/13.

MCEER-13-0006 "Emilia Earthquake of May 20, 2012 in Northern Italy: Rebuilding a Resilient Community to Withstand Multiple Hazards," by G.P. Cimellaro, M. Chiriatti, A.M. Reinhorn and L. Tirca, June 30, 2013.

MCEER-13-0007 "Precast Concrete Segmental Components and Systems for Accelerated Bridge Construction in Seismic Regions," by A.J. Aref, G.C. Lee, Y.C. Ou and P. Sideris, with contributions from K.C. Chang, S. Chen, A. Filiatrault and Y. Zhou, June 13, 2013.

MCEER-13-0008 "A Study of U.S. Bridge Failures (1980-2012)," by G.C. Lee, S.B. Mohan, C. Huang and B.N. Fard, June 15, 2013.

MCEER-13-0009 "Development of a Database Framework for Modeling Damaged Bridges," by G.C. Lee, J.C. Qi and C. Huang, June 16, 2013.

MCEER-13-0010 “Model of Triple Friction Pendulum Bearing for General Geometric and Frictional Parameters and for Uplift Conditions,” by A.A. Sarlis and M.C. Constantinou, July 1, 2013.

MCEER-13-0011 “Shake Table Testing of Triple Friction Pendulum Isolators under Extreme Conditions,” by A.A. Sarlis, M.C. Constantinou and A.M. Reinhorn, July 2, 2013.

MCEER-13-0012 “Theoretical Framework for the Development of MH-LRFD,” by G.C. Lee (coordinating author), H.A Capers, Jr., C. Huang, J.M. Kulicki, Z. Liang, T. Murphy, J.J.D. Shen, M. Shinozuka and P.W.H. Yen, July 31, 2013.

MCEER-13-0013 “Seismic Protection of Highway Bridges with Negative Stiffness Devices,” by N.K. Attary, M.D. Symans, S. Nagarajaiah, A.M. Reinhorn, M.C. Constantinou, A.A. Sarlis, D.T.R. Pasala, and D.P. Taylor, July 31, 2013.

MCEER-14-0001 “Simplified Seismic Collapse Capacity-Based Evaluation and Design of Frame Buildings with and without Supplemental Damping Systems,” by M. Hamidia, A. Filiatrault, and A. Aref, May 19, 2014.

MCEER-14-0007 “Seismic Performance Evaluation of Precast Girders with Field-Cast Ultra High Performance Concrete (UHPC) Connections,” by G.C. Lee, C. Huang, J. Song, and J. S. O’Connor, July 31, 2014.

MCEER

EARTHQUAKE ENGINEERING TO EXTREME EVENTS

University at Buffalo, The State University of New York
133A Ketter Hall ▪ Buffalo, New York 14260-4300
Phone: (716) 645-3391 ▪ Fax: (716) 645-3399
Email: *mceer@buffalo.edu* ▪ Web: *http://mceer.buffalo.edu*

University at Buffalo *The State University of New York*

ISSN 1520-295X